# Analysis and Design of Stable and Optimal Energy Management Strategies for Hybrid Electric Vehicles

Dissertation

Presented in Partial Fulfillment of the Requirements for the Degree Doctor of Philosophy in the Graduate School of The Ohio State University

By

Balaji Sampathnarayanan, B.Tech., M.S

Graduate Program in Electrical and Computer Engineering

The Ohio State University

2013

Dissertation Committee:

Professor Giorgio Rizzoni, Advisor

Professor Steve Yurkovich

Professor Vadim Utkin

Professor Yann Guezennec

Dr. Simona Onori

# Abstract

The ubiquitous influence of fossil fuels in driving the world economy and the imperative need to reduce dependence of transportation on these fuels, has brought about a decade of research on alternative propulsion systems. Of the several alternative propulsion systems, hybrid electric vehicles (HEVs) are seen as an important short-term solution. In the most generic sense, a HEV consists of a battery and one or more electric machines in addition to the engine powered by petroleum/diesel. Depending on the vehicle architecture, the additional degree of freedom in selecting the amount of energy supplied by the primary and the secondary source of energy is a challenging control and optimization problem. The energy management strategy in a HEV aims at finding the optimal distribution of energy between the battery and the fuel to satisfy the requested power from the driver. Different energy management strategies have been developed both by the industry and the academia and they can be classified into *non-realizable* and *realizable* energy management strategies based on the amount of information required for real-time implementation. Traditionally, the non-realizable strategies formulate the energy management problem as a constrained optimal control problem of minimizing a performance index over a finite time interval under operational constraints. These strategies provide the global optimal solution and are used as benchmark solutions for comparative analysis of strategies. The realizable strategies in the literature have been primarily developed for implementation in real vehicles and have been shown to produce results similar to the global optimal solution. In spite of the

extensive amount of research on both non-realizable and realizable energy management strategies, there are many shortcomings in the literature which have been addressed in this dissertation.

The energy management problem of finding the optimal split between the different sources of energy in a charge-sustaining pre-transmission parallel HEV, ensuring stability and optimality with respect to a performance objective, is addressed in this dissertation. The dissertation develops a generic stability and optimality framework within which energy management strategies can be analyzed and designed. The energy management problem is cast in the form of a nonlinear optimal regulation (with disturbance rejection) problem and a control Lyapunov function is used to design the control law. A series of theorems ensuring optimality and asymptotic stability of the energy management strategy are proposed and proved. The theorems use an appropriate Willans line model of the engine fuel consumption rate and a zero-*th* order model of the battery state of charge/energy dynamics. The sufficient conditions for optimality and stability are used to derive an analytical expression for the control law as a function of the battery state of charge/state of energy error, engine fuel consumption model and battery model parameters.

In this dissertation, several non-realizable and realizable energy management strategies are developed and implemented in the backward and forward vehicle simulators. The optimal control law (OCL) proposed in this dissertation is compared against dynamic programming (DP) and a version of equivalent consumption minimization strategy (ECMS) based on Pontryagin's minimum principle. The OCL strategy is further modified to develop a realizable strategy (called real-time OCL) and its performance is compared with an adaptive version of ECMS using a forward vehicle simulator. Throughout the dissertation, the performance of the proposed strategy is evaluated against the global optimal

solution from DP. The significant contribution of the dissertation is in developing and easy to implement strategy that has very less calibration effort. Though the framework and the strategy has been presented for a pre-transmission parallel HEV, it is scalable to different vehicle architectures and component sizes. The dissertation also presents a comprehensive comparison of the different proposed and developed energy management strategies.

To my parents for their unconditional love and encouragement over the years

# Acknowledgments

There have been several inspiring individuals in my life I would like to acknowledge. My interest in control systems and mathematics are a direct result of the interesting discussions and lectures given by Professor J. Prakash and Professor P. Kanagasabapathy. My desire to do a PhD is heavily inspired by my first mentor Professor G. Kannaian and I cannot thank him enough for the values he has taught me.

I would like to thank Professor Stephen Yurkovich for his guidance and support throughout the five and half years of my doctoral research. He has been an inspiring mentor, advisor and a role model for me in dealing with difficult situations. I would also like to thank Dr.Simona Onori for her valuable comments, discussions, ideas and guidance that helped me throughout my PhD. I thank Professor Giorgio Rizzoni for accepting to be my advisor and providing his insightful comments to improve the dissertation. I am also indebted to the CAR(OSU)-Cummins project which sponsored a good amount of my PhD research. During my stay at the Center for Automotive Research, I have been lucky to enjoy the company of great students and researchers and I would like to thank them all.

The fun times I had during my PhD have always been with my best friends at OSU. Specifically, Rajagopalan, Hari, Mrk, Mappi, Viggu (tennis buddy), Bharath, Kasi, Anusha, Ketaki, Sudha, Prabhu, Madhu, Vijay, JK, Athreya and many more. I would like to thank them all for the fun and crazy times we have shared.

Finally. I would like to acknowledge the unconditional love and support from my parents during all these years. They have been my first role models in pursuit of excellence and knowledge. During the final year of my PhD, my wife has been a tremendous support and encouragement for me to keep going and run the last mile. I think that my parents and my wife deserve a PhD too, because I have talked so much about it with them.

# Vita

## Fields of Study

Major Field: Electrical and Computer Engineering

# Table of Contents

# List of Tables

# List of Figures

# List of Symbols

$\alpha$      Normalized acceleration command

$\beta$      Normalized brake pedal command

$\dot{m}_f$      Fuel consumption rate of engine [kg/s]

$\dot{SOC}$      Battery state of charge dynamics [1/s]

$\eta$      Efficiency [-]

$\eta_{batt}$      Battery efficiency [-]

$\eta_{em}$      Electric machine efficiency [-]

$\eta_{gen}$      Electric generator efficiency [-]

$\eta_{mot}$      Electric motor efficiency [-]

$\eta_{trans}$      Transmission efficiency [-]

$\omega$      Rotational speed [rad/s]

$\omega_{gb,in}$      Gearbox rotational speed (input) [rad/s]

$\omega_{gb,out}$      Gearbox rotational speed (output)[rad/s]

$\omega_{gb}$      Gearbox rotational speed [rad/s]

$\omega_{gen}$     Electric generator rotational speed [rad/s]

$\omega_{ice,idle}$  Engine rotational speed (idle) [rad/s]

$\omega_{ice,max}$  Engine rotational speed (maximum) [rad/s]

$\omega_{ice,opt}$  Engine optimal rotational speed [rad/s]

$\omega_{ice}$     Engine rotational speed [rad/s]

$\omega_{mot}$     Electric motor rotational speed [rad/s]

$\rho_a$       Density of air [kg/$m^3$]

$\theta$        Road grade [rad]

$A_f$        Frontal area of the vehicle [$m^2$]

$Accel$  Vehicle Acceleration [m/$s^2$]

$C$         Clutch status (OPEN/CLOSE) [-]

$C_d$        Coefficient of drag [-]

$C_r$        Coefficient of rolling resistance [-]

$E$         Engine status (ON/OFF) [-]

$e_{ij}, \; i, j \; = \; 0, \; 1, \; 2$  Willans line coefficients [-]

$f_{em}$       Nonlinear mapping of electric machine torque and speed [-]

$f_{ice}$       Nonlinear mapping of engine torque and speed [-]

$F_{load}$     Load Force [N]

$f_{SOC}$   Nonlinear mapping of battery state of charge and battery power [-]

$F_{trac}$   Traction Force [N]

$g$   Acceleration due to gravity [kg/m$s^2$]

$Gear$   Gear number [-]

$I$   Battery current [A]

$I_{batt}$   Battery current [A]

$J_{ice}$   Engine inertia [$\frac{kg \cdot m^2}{rad^2}$]

$K_D$   Derivative gain

$K_I$   Integral gain

$K_P$   Proportional gain

$M$   Mass [kg]

$P$   Power [W]

$P_{accelec}$   Electrical accessory power [W]

$P_{accmech}$   Mechanical accessory power [W]

$P_{batt}$   Battery power [W]

$P_{gb}$   Gearbox (input) power [W]

$P_{gen,e}$   Electric generator electrical power [W]

$P_{gen,m}$   Electric generator mechanical power [W]

$P_{ice}$     Engine power [W]

$P_{in}$     Engine power input [W]

$p_i,\ i = 0, 1, \cdots , 6$   Known constants [kg/J]

$P_{mot,e}$   Electric motor electrical power [W]

$P_{mot,m}$   Electric motor mechanical power [W]

$P_{out}$     Engine power output [W]

$P_{req}$     Requested power [W]

$Q_{LHV}$   Lower heating calorific value of diesel [kJ/kg]

$Q_{max}$   Battery charge capacity (maximum) [Ah]

$R$       Gear ratio [-]

$R_{eq}$     Battery equivalent resistance [ohm]

$SOC$   Battery state of charge [-]

$SOE$   Battery state of energy

$T$       Torque [Nm]

$T_{accmech}$   Mechanical accessory torque [Nm]

$T_{em,max}$   Electric machine torque (maximum)[Nm]

$T_{em,min}$   Electric machine torque (minimum) [Nm]

$T_{gb,in}$   Gearbox torque (input) [Nm]

$T_{gb,out}$  Gearbox torque (output) [Nm]

$T_{gb}$  Gearbox torque [Nm]

$T_{gen}$  Electric generator torque [Nm]

$T_{ice,dmd}$  Engine torque (demand) [Nm]

$T_{ice,max}$  Engine torque (maximum) [Nm]

$T_{ice}$  Engine torque [Nm]

$T_{load}$  Engine load torque [Nm]

$T_{mot}$  Electric motor torque [Nm]

$u$  Error in vehicle velocity [m/s]

$V_{act}$  Actual vehicle velocity [m/s]

$V_{des}$  Desired vehicle velocity [m/s]

$V_L$  Battery terminal voltage [V]

$V_{oc}$  Battery open-circuit voltage [V]

$y$  Output of the driver model [-]

# Chapter 1: Introduction

The enormous amount of development over the last century, brought about by the industrial revolution to mankind cannot be overemphasized. The revolution brought about a huge impact in the way mankind saw energy resources and its utilization. The total primary energy supply (TPES) necessary to fuel the industrial revolution and the development that followed, has been met by the different fuel resources available in the world. As seen from Fig. 1.1, oil and coal have been the primary fuel sources during the past three decades, in spite of the availability of different fuels. During the past few years, there has been a high surge in using other types of fuel such as natural gas, water, nuclear and bio-fuels. Though the alternative fuel sources have been growing at a staggering pace, their combined contribution is only 40% of the total TPES in 2009. Thus oil will continue to be one of the primary sources of energy that will drive the economic and industrial development throughout the world. Nevertheless the amount of oil reserves in the world has been estimated to be a finite amount and though there have been several discoveries of oil reserves throughout the world, the amount of oil produced has been estimated to fall drastically in the next decade. Fig. 1.2 shows that the amount of crude oil produced from the available (and to be explored) fields throughout the world is on a steep decline. Such a decrease in the amount of oil available poses numerous techincal challenges in finding and using alternative fuels such as natural gas, nuclear, biofuels, hydro, etc.
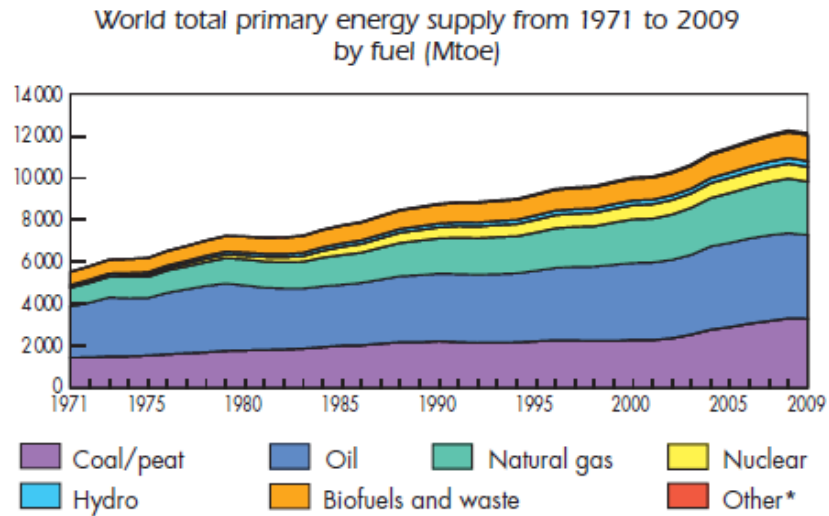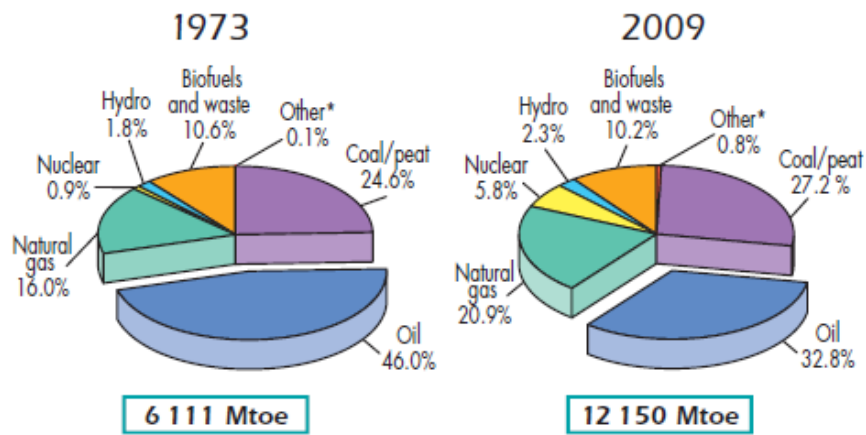
Figure 1.1: World TPES by fuel (Mtoe) (1971 - 2009) and fuel shares of TPES (1973 - 2009) [Source: Key world energy statistics, 2011]
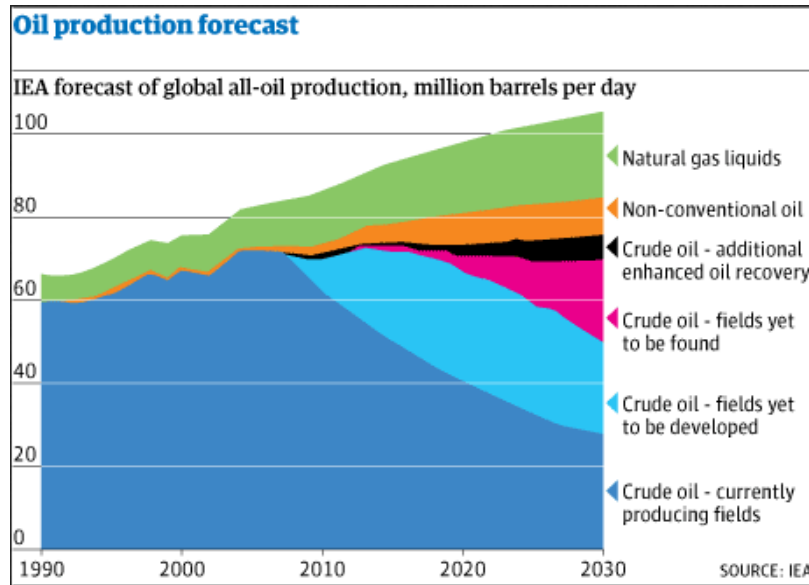
Figure 1.2: Oil production forecast throughout the world [Source: International Energy Agency, 2012]
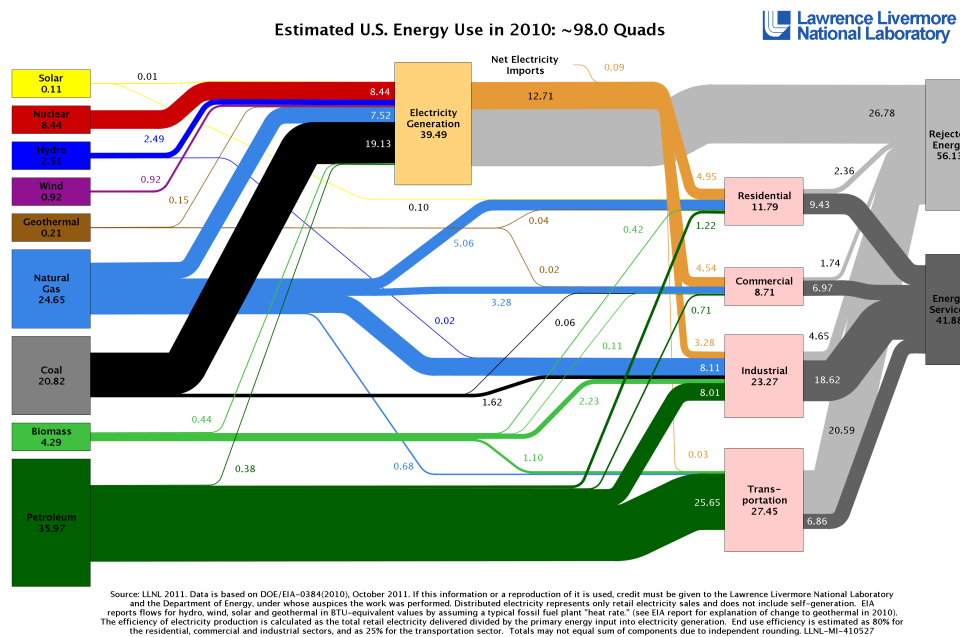


Figure 1.3: Estimated U.S. energy use in 2010 (A quad is $1.05510^{18}$ joules) [Source: Lawrence Livermoore National Laboratory and International energy agency, 2011]
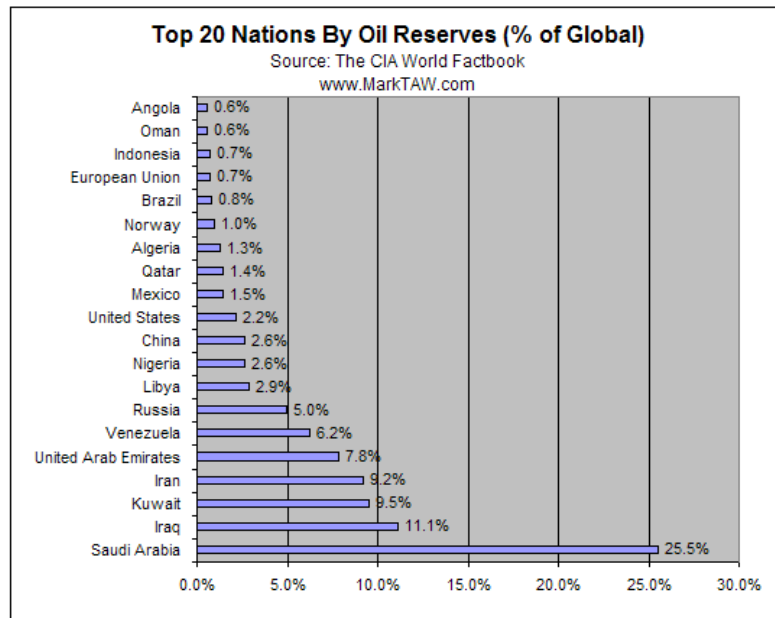
Figure 1.4: Top 20 nations by oil reserve as percentage of global reserves [Source: The CIA World Factbook]
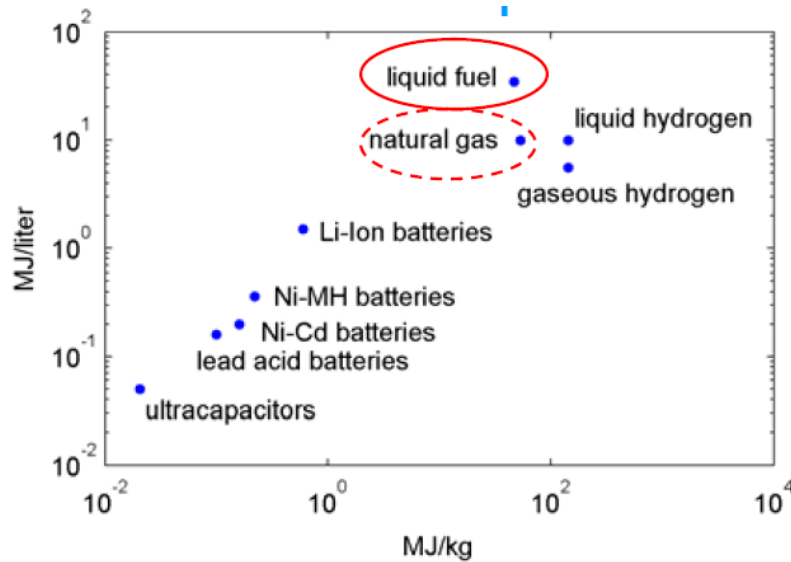


Figure 1.5: Comparison of fuel energy sources for transportation[Source: International Energy Agency, 2012]

Throughout the world, the ability to transport from one place to another has been the backbone of the industrial revolution. In the United States, the transportation sector is the major consumer of oil (primarily in the form of petroleum and diesel) as seen from Fig. 1.3. Although there are alternative sources of energy like electricity, natural gas, biomass, wind, solar, etc., they account for less than 3% of the amount of energy obtained from petroleum products to drive the transportation sector. Approximately 62% of the petroleum used in the U.S. is imported, and it is used almost exclusively for transportation and the situation is predicted to get worse during the next few years (Fig. 1.4). Thus, the imperative need to reduce the dependence of transportation systems on fossil fuels and the ever-tightening emission regulations for all types of vehicles, has forced researchers to study alternative propulsion systems. This surge brought about a decade of research on alternative propulsion systems based on energy storage devices like batteries, fuel cells, flywheels, etc. Because of the energy density, the liquid fuel (gasoline and diesel) has been the primary fuel energy sources for transportation (see Fig. 1.5). Unlike the alternative propulsion systems such as all-electric vehicles, fuel cell vehicles, natural gas powered vehicles which are prospective long term solutions to completely eliminate the dependence on fossil fuels, hybrid electric vehicles (HEVs) are the most common and popular short-term solution to the problem.

In general, a hybrid electric vehicle (HEV) is comprised of an electric propulsion system consisting of a battery pack and an electric machine. Depending on the vehicle architecture and the degree of hybridization of a conventional vehicle (only one energy source, namely fuel), a HEV offers the following features that can help reduce fuel consumption and emissions:

- **Idle-off capability:** Depending on the degree of hybridization and the HEV architecture, the engine in a generic HEV can be switched off whenever the vehicle is stopped. This is very useful in avoiding idle speed operation whenever possible and thus reducing the fuel consumption and emissions. For example, if the vehicle is stopped at a traffic light, depending on the accessory load, the engine can be turned off and the all-electric propulsion of the HEV can be used.

- **Regenerative braking:** In a conventional vehicle, the kinetic energy stored in the vehicle while accelerating is released as heat during braking events. This kinetic energy can be recovered using the electric motor and the battery in a HEV. This is possible because the electric machine is a reversible energy conversion device and can be also used as a generator to recharge the battery. The capability of the HEV to perform regenerating braking is one of the important benefits and is therefore used in all types of HEV.

- **Power assist:** In addition to supplying the requested power from the driver, the electric machine and battery can be used to add extra power/torque to the wheels depending on the HEV architecture.

- **Engine downsizing capability:** Because there is a battery and an electric machine, the engine need not be designed depending on the maximum power/torque request to be supplied by the vehicle and therefore smaller engine can be used at its most efficient region and the electric machine can be used to supply the remaining power/torque.

- **Electric-only drive capability:** Based on the HEV architecture and the degree of hybridization, the engine can be completely turned off and an all-electric propulsion

can be used to propel the vehicle. This capability of the vehicle helps using the engine at its most efficient region and therefore reducing fuel consumption and emissions.

These capabilities account for the attributed savings on fuel consumption and emissions with respect to the conventional vehicle. Unlike a conventional vehicle, the additional degree of freedom presents a challenging optimization problem. The objective of the energy management strategy in a HEV is to find the optimal torque/power split between the primary and secondary energy sources that minimizes a given objective function over an entire driving cycle. The minimization can be performed with respect to several objectives such as fuel consumption, emissions, battery aging, etc., or a combination of these objectives satisfying several operational constraints. The different capabilities of the HEV can be utilized to its maximum potential only with an effective energy management strategy. The design, development and implementation of the energy management strategy form a substantial part of the research done in the industry and academia.

From the time the first hybrid vehicle was developed in 1898 by Porsche, there have been several prototypes developed by different companies. The most successful, mass produced HEV is the Toyota Prius designed and developed by Toyota Motor Company. The first generation of Prius was commercially available by 2000 and it was a huge commercial success. Since then, there have been several commercially available HEVs produced by all the major vehicle manufacturers.

## 1.1 Literature Review

The energy management problem, by its very nature, is a constrained optimization problem, where the objective function (3.1) is minimized under system dynamics, instantaneous (local) and integral (global) constraints on the state and control variables. In addition to

the extensive amount of research performed by the industry to design and develop energy management strategies for commercial HEVs, the energy management problem in a charge-sustaining HEV has been studied in the literature for over a decade [1, 2, 3, 4, 5]. They can be classified into several categories depending on several factors. The following classification based on the amount of information necessary to implement the strategy in a real vehicle is used throughout this dissertation; an energy management strategy can be categorized as follows:

1. **Non-realizable Strategy:** A non-realizable strategy requires complete *a priori* knowledge of the driving cycle in order to solve the energy management problem and therefore cannot be implemented in a real vehicle. Dynamic programming, Pontryagin's minimum principle and certain versions of equivalent consumption minimization strategy are examples of non-realizable strategies.

2. **Realizable Strategy:** A realizable strategy does not require complete knowledge of the driving cycle to solve the energy management problem and therefore can be implemented in a real vehicle. Adaptive versions of equivalent consumption minimization strategy, rule based strategies and stochastic dynamic programming are in this category.

### 1.1.1  Non-realizable Energy Management Strategies

The first category of strategy requires the complete *a priori* knowledge of the driving cycle and involves the use of classical optimal control techniques guaranteeing global/local optimality of the solution. These strategies assume the knowledge of the past, present and future values of the variables involved in optimization. Thus in a sense, these control algorithms perform global optimization to minimize fuel consumption over a driving cycle,

assuming that the driving cycle is known *a priori*. This strong assumption renders the control law unrealizable in a real vehicle. Dynamic Programming (DP), Pontryagin's Minimum Principle (PMP) and a few versions of equivalent consumption minimization strategy (ECMS) are in this category.

DP assumes *a priori* knowledge of the driving cycle and solves the problem backwards in time, considering all possible power split choices at each instant. Because DP guarantees the global optimal solution according to Bellman's principle of optimality, it has been used as a benchmark solution in the HEV energy management literature [3, 6, 7, 8, 9].

PMP formulates and minimizes a Hamiltonian function (a function of the instantaneous cost and the state constraint) at each instant to obtain the optimal solution [10, 11, 12, 13, 14]. PMP gives only the necessary conditions (not sufficient) that must be satisfied by any global optimal solution (known as *extremal* solutions). For charge-sustaining HEVs, the uniqueness of the optimal solution facilitates the use of PMP to find the global optimal solution [13, 14].

The basic idea of ECMS is to reformulate the global optimization problem into a local optimization problem with tuning parameters. The ECMS takes into account that for a charge sustaining hybrid, the energy used to drive the vehicle comes eventually from the fuel stored in the vehicle which means the battery power must be replenished [15]. The method has been shown to produce fuel economy improvements, but the equivalence factors (tuning parameters) that allow for the transformation of electrical energy into future fuel consumption must be determined with optimization techniques, and are dependent on driving cycles. The papers [13, 16, 17] establish the equivalence of ECMS and PMP which ensures that under certain conditions, the local optimal solution derived from ECMS based on PMP can guarantee global optimality of the solution. Thus ECMS developed from PMP

9

cannot be implemented in a real vehicle because it requires complete knowledge of the driving cycle to ensure optimality.

## 1.1.2 Realizable Energy Management Strategies

The second category of strategies assume knowledge only of the past and present values of the variables involved in optimization and therefore can be implemented in a real-vehicle. Because the strategies are not typically based on solving the global optimization problem and are developed with the primary objective of realizability, they do not necessarily guarantee optimality. A few versions of ECMS, several adaptive energy management strategies and rule based strategies are in this category.

A few earlier versions of ECMS [15] developed based on engineering intuition have been shown to be realizable strategies. The strategy was developed and implemented in a real vehicle during the *Future Truck Competition* [18] giving 50% more fuel economy than the stock rule based strategy in the vehicle. The papers [19, 20] design and develop the first version of ECMS implemented in a vehicle and formalizes the concept of equivalent consumption minimization. The results clearly indicate such a method can give very good results, but the optimal equivalence factor, which depends on the driving cycle, must be determined *a priori* using optimization techniques. The strategy was initially developed using engineering common sense to be implemented in a real vehicle, but to guarantee any kind of optimality, the strategy requires complete knowledge of the driving cycles to tune the equivalence factors. Another version of ECMS called the *box-ECMS* has been implemented in the *ChallengeX Competition* as shown in [21]. Yet another version of ECMS accounting for the drivability constriants has been designed and implemented for the *EcoCAR Competition* (see [22] for more details).

10

A specific version of adaptive ECMS that has been implemented in a real vehicle adapts the tuning parameters of ECMS by predicting the driving cycle and using a look-up table to find the optimal value for the driving condition [23, 24, 25]. Because the strategy adapts the equivalence factor depending on the real world driving conditions, they are realizable in a real vehicle. A different version of adaptive ECMS as proposed in [26, 27, 28] adapts the tuning parameter using the correlation between equivalence factor and battery state of charge. Based on the driving condition experienced by the vehicle, the equivalence factor is adapted using a simple adaptation law depending on the deviation of the battery SOC from its reference value. These versions of adaptive ECMS clearly can be implemented in a real vehicle because they do not require the equivalence factors to be optimized for each driving cycle.

Heuristic rule based strategies based on rules developed using engineering intuition to explicitly distribute the power between the two energy sources on board have also been very popular. They have been studied for a long time now because of their simplicity in real-time implementation [29, 30, 31, 32]. The heuristic rule based strategies are the most common energy management strategies implemented in commercially available HEVs. Moreover, these rules can also be derived from the global optimal solution from DP [33].

There have also been other realizable energy management strategies which assume the knowledge of only the past and present values of the variables in optimization and which predict the future values of these variables. For example, model predictive control and stochastic dynamic programming are in this category. Model predictive control uses a model to predict the system behavior over a prediction horizon and the solution is obtained by minimizing an objective function over the prediction horizon. The papers [8, 34, 35, 36, 37, 38] deal with model predictive control as applied to HEVs.

Stochastic dynamic programming uses a Markov chain model to predict the power request based on an extensive amount of driving cycle data and has been applied to HEVs in [39, 40, 41, 42, 43, 44]. A comprehensive comparison of different types of energy management strategies (both realizable and non-realizable) for HEVs appears in [17].

## 1.2 Motivation

The following shortcomings in the HEV literature motivate the main contributions of the dissertation:

- Because the non-realizable strategies that are based on classical optimal control techniques (DP, PMP) require *a priori* knowledge of the driving cycle, the strategies cannot be implemented in a real vehicle. Both DP and PMP are used only as benchmark solutions to perform comparative analysis of other implementable energy management strategies.

- Other non-realizable strategies like ECMS that transform the global optimization problem into a local optimization problem cannot be implemented in a real vehicle, because the optimality of ECMS for a driving cycle depends on the optimal equivalence factor for that driving cycle [17, 26]. Moreover ECMS involves minimization at each instant, which requires significant computational power on board and the strategy must be tuned for the intended driving conditions to perform close to the optimal solution.

- The adaptive energy management strategies, which adapt one or more calibration parameters depending on the driving condition, cannot guarantee optimality of the solution. Though these strategies are very useful in performing close to the global

optimal solution from DP, they will always give sub-optimal results because any vehicle is subjected to a multitude of driving conditions other than the standard driving conditions.

- Though rule based energy management strategies are relatively easy to develop and implement in a real vehicle, a significant amount of calibration effort is required to improve performance over a driving cycle. Furthermore these strategies cannot guarantee optimality because they are developed from heuristic rules based on engineering common sense.

Though there have been several non-realizable and realizable energy management strategies proposed in the literature, there has not been a mathematically rigorous treatment of the design of *optimal* energy management strategies that can be implemented in a real vehicle. Furthermore, there has not been a stability framework within which stable and optimal energy management strategies can be designed. Such a framework is considered herein which facilitates the definition of stability in charge sustaining HEVs and utilizes the theoretical results in nonlinear optimal regulation theory to analyze and design energy management strategies. In order to develop the framework, the theoretical results published in the area of nonlinear optimal regulation theory is used. Linear-quadratic control theory has been developed extensively over the past century; extension to nonlinear control has broadened the effectiveness of such techniques. Because nonlinear controllers can effectively model the nonlinearities in the system and hence perform better than linear controllers for nonlinear systems, it is not surprising that significant effort has been devoted to developing the theory of nonlinear optimal regulation [45, 46, 47]. The papers [48, 49] serve as a tutorial exposition of a framework for nonlinear optimal regulation in feedback control problems involving non quadratic cost functionals. The main contribution here is in developing a

13

useful mathematically rigorous framework, and the goal is in developing an energy management strategy that can be easily implemented in a real-vehicle while assuring stability and optimality.

## 1.3 Organization

The dissertation is organized as follows:

- Chapter 2 describes the HEV architecture along with the simulation environment used to develop, test and simulate the energy management strategies proposed in the dissertation. The forward and backward vehicle simulator along with the component models are explained in this chapter. The simulation environment described in this chapter is used throughout the dissertation to implement the energy management strategies;

- Chapter 3 formulates the energy management problem in a pre-transmission parallel HEV and then applies optimal control techniques such as DP and PMP to solve the problem. The chapter first develops the global optimal solution from DP, then formulates a version of ECMS based on PMP and then implements these strategies in a backward vehicle simulator. Based on ECMS, an adaptive version of ECMS that can be implemented in a real vehicle is proposed and implemented. The adaptive ECMS is evaluated against DP over several repetitions of the driving cycle to evaluate the performance of the strategy.

- Chapter 4 describes the significant contributions of the dissertation. The chapter defines the stability and optimality framework which is used to cast the energy management problem as a nonlinear optimal regulation problem. A series of results on

applying the nonlinear optimal regulation to solve the energy management problem in a charge-sustaining HEV is proposed and then used to derive a closed-form expression for the optimal control law (OCL). The strategy is then implemented using a backward simulator and compared with the DP solution.

- Chapter 5 describes an extensive comparison of the various strategies developed in the dissertation by implementing them using a forward vehicle simulator. The calibration effort and performance of both the non-realizable (DP, ECMS, OCL) and realizable strategies (AECMS, real-time OCL) are compared.

- Chapter 6 provides a comprehensive description of the contributions made by the individual chapters in the dissertation and the major contributions of the dissertation to the HEV literature.

# Chapter 2: HEV Modeling and Simulation

The chapter describes the methodology used to model the various components of a generic HEV. Two of the most popular HEV architectures are chosen. The chapter also describes the two main approaches used in building a HEV simulator, forward and backward. Both the simulators are used in the remainder of this dissertation to design, analyze and test several energy management strategies.

## 2.1  Vehicle Architecture

In general, a HEV consists of several energy sources and energy converters. Unlike a conventional vehicle which uses an engine (with fuel as the only source of energy) to propel the vehicle, a HEV utilizes both the engine and an electric machine powered by a battery. Depending on the arrangement of the engine, electric machine, battery and transmission, HEVs can be classified into different types as follows:

- Series: This type of HEV uses only the electric motor to drive the wheels. The engine-generator set and the battery are connected in series to propel the vehicle. In a series HEV, the electrical power from the battery and the engine-generator set is summed electrically to satisfy the power/torque request at thw wheels. There have been several commercially successful heavy-duty series HEVs such as the UPS series hybrid pick-up truck and series hybrid buses by Designline.

- Parallel: The engine and the electric motor are connected in parallel to drive the wheels. Depending on the position of the electric motor and engine, these vehicles are further classified as pre-transmission and post-transmission parallel HEVs. Here the mechanical power from the engine and the electric machine is summed mechanically to propel the vehicle. Honda Insight, Civic Hybrid, Accord Hybrid and Chevy Malibu Hybrid are some of the very popular parallel HEVs.

- Series-Parallel: This type of HEV consists of more than one electric machine connected with the engine either mechanically or electrically. The simplest version of a series-parallel HEV consists of a clutch connecting the engine to the transmission. The power-split hybrid is the most popular series-parallel HEV, consisting of a planetary gear set combining all the energy conversion devices. The power from the engine and the electric machines can be summed either mechanically or electrically. Toyota Prius, Chevy Volt, GM 2-Mode Hybrid and GM Tahoe Hybrid are popular examples of the power-split series-parallel HEVs.

From the different types of HEVs described in the literature [50, 2, 51], the pre-transmission parallel HEV architecture has been selected and is used throughout this dissertation to simulate and evaluate the performance of the proposed energy management strategies. The vehicle architecture selected for modeling and simulation is described in detail in the following sections.

### 2.1.1 Pre-transmission Parallel HEV

The power flow in a pre-transmission parallel HEV is shown in Fig. 2.1. The sign convention adopted throughout the dissertation is as follows:
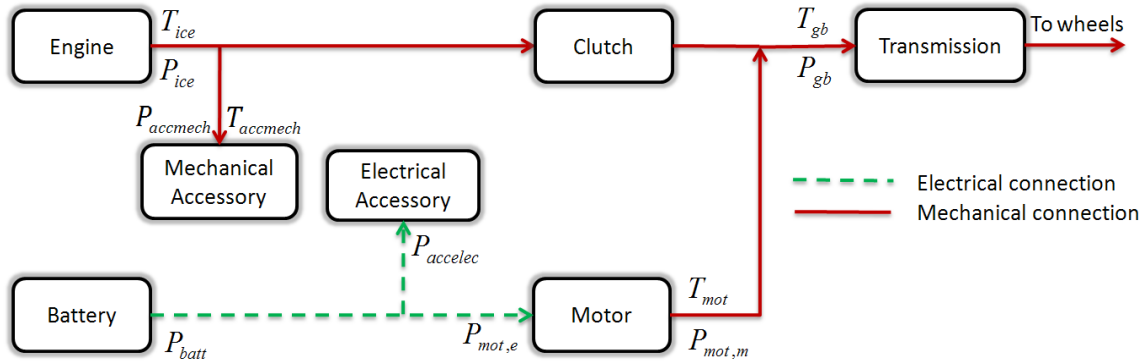
Figure 2.1: Power flow diagram of pre-transmission parallel HEV

- Electric machine power, torque and current are positive when the machines operate in motoring mode;

- Accessory torque and power are positive when the accessories are being driven;

- Engine torque is positive when it is motoring;

- Battery current and power are considered positive when the battery is discharged and vice-versa.

In Fig. 2.1, direction of the arrows indicate the positive sign convention. The dotted lines represent the electric connection between components while the solid lines show direct mechanical coupling. It is assumed that the mechanical accessory loads include only engine accessories, while the main secondary loads such as air conditioning, brake compressor, etc., are powered electrically from the main electric bus. The engine is connected in parallel with the electric motor and the battery pack and can be engaged or disengaged from the transmission (and wheels) using a clutch. The vehicle can operate in three different modes depending on the status of the engine (on/off), clutch (open/close) and the gearbox.
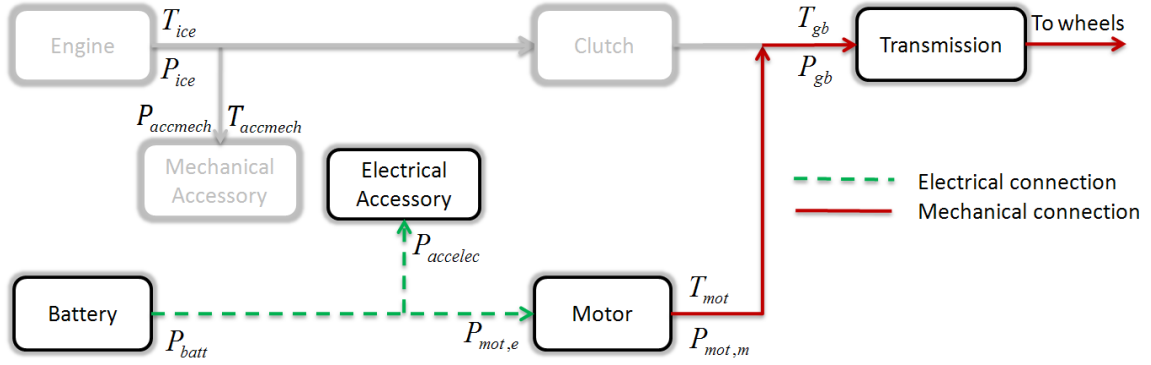
Figure 2.2: Power flow diagram of pre-transmission parallel HEV: Electric Mode

**Electric Mode**

With the clutch open, the vehicle uses only the battery and electric motor for propulsion. The engine can be switched off because it is completely disconnected from the wheels. This vehicle mode (shown in Fig. 2.2) does not involve any optimization as the electric motor is the only propulsion device. The torque/power requested by the driver at the wheels is satisfied using the battery and electric motor. The torque/power balance equations that must be satisfied at each instant are

$$
\begin{cases}
T_{mot}(t) = T_{gb}(t), \\
P_{batt}(t) = P_{mot,e}(t) + P_{accelec}(t), \\
\omega_{mot}(t) = \omega_{gb}(t),
\end{cases}
\tag{2.1}
$$

where $T_{gb}, \omega_{gb}$ represent the instantaneous gearbox torque and speed; $T_{mot}, \omega_{mot}$ represent the instantaneous electric motor and speed; $P_{accelec}$ represents the instantaneous electrical accessory power; $P_{batt}$ represents the instantaneous battery power and $P_{mot,e}$ represents the instantaneous electrical power at input/output terminals of the electric motor.
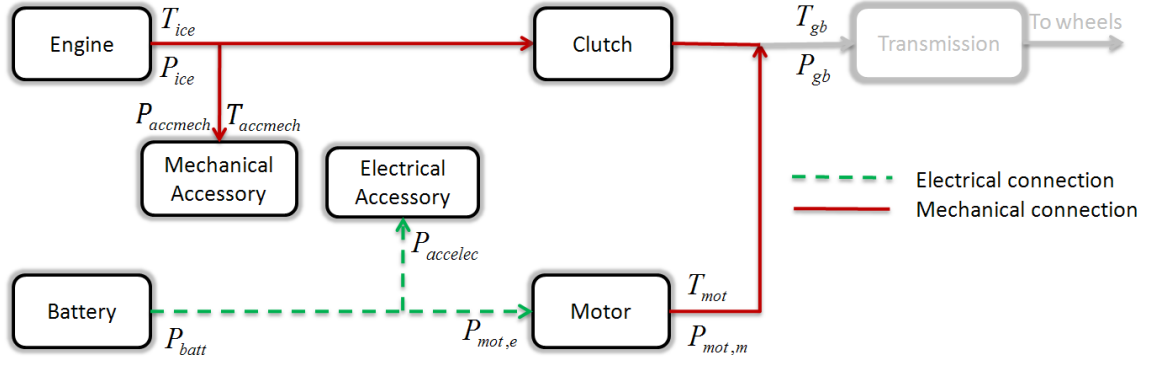
Figure 2.3: Power flow diagram of pre-transmission parallel HEV: Parallel Mode in neutral gear

**Parallel Mode in neutral gear**

In this mode of operation, shown in Fig. 2.3, the clutch is closed and the gearbox is in neutral position. The vehicle is assumed to be at stand still without any traction power required at the wheels. Although both the devices are connected to the transmission, because the gear is in neutral condition, the engine can be operated at any desired speed. This mode of operation mimics the real world situation of the vehicle being stopped at a traffic signal. The engine is kept on and used in conjunction with the battery and electric motor to charge/discharge the battery. Because the vehicle is stopped, the gearbox torque requested by the driver is zero. The torque/power balance equations that must be satisfied at each instant are

$$\begin{cases} T_{mot}(t) + T_{ice}(t) = T_{accmech}(t), \\ P_{batt}(t) = P_{mot,e}(t) + P_{accelec}(t), \\ \omega_{mot}(t) = \omega_{ice}(t) = \omega_{ice,opt}(t), \end{cases} \qquad (2.2)$$

where $T_{ice}, \omega_{ice}$ represent the instantaneous engine torque and speed; $T_{accmech}$ represents the instantaneous mechanical accessory torque and $\omega_{ice,opt}$ represents the instantaneous optimal engine speed selected based on the maximum efficiency operating line of the engine
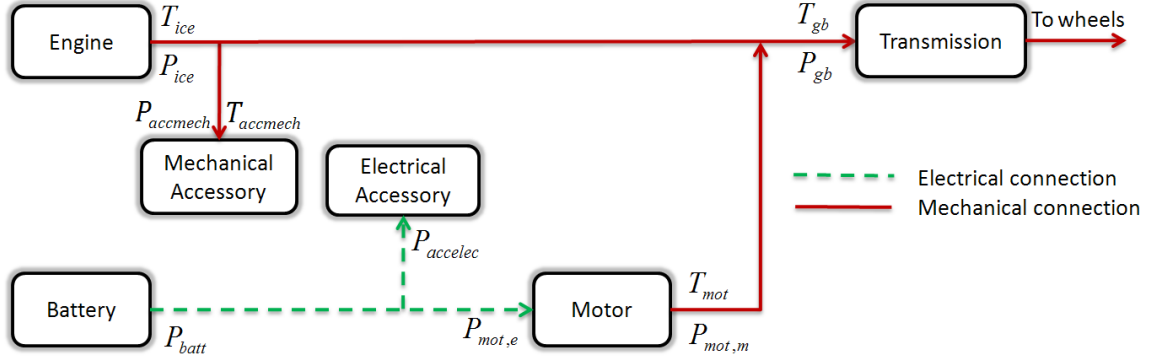
Figure 2.4: Power flow diagram of pre-transmission parallel HEV: Parallel Mode

(explained in Section 2.2.1) . Assuming a constant efficiency for the electric motor ($\eta_{mot}$), the engine power ($P_{ice}$) can be represented as a function of battery power ($P_{batt}$), electrical ($P_{accelec}$) and mechanical ($P_{accmech}$) accessory power as

$$P_{ice}(t) = \frac{1}{\eta_{mot}} P_{accelec}(t) + P_{accmech}(t) - \eta_{mot} P_{batt}(t). \tag{2.3}$$

**Parallel Mode**

With the clutch closed, the parallel mode of operation (Fig. 2.4) uses both the devices ($mot$,$ice$) to propel the vehicle with their speeds directly determined by the vehicle velocity. The torque/power requested by the driver is supplied by the parallel configuration. Unlike the parallel mode in neutral gear, in this mode of operation the gear position is determined using a gear ratio map dependent on vehicle velocity and acceleration. The only degree of freedom available in this mode is the engine torque ($T_{ice}$) or electric machine torque ($T_{mot}$). The torque/power balance equations that must be satisfied at each instant are

$$\begin{cases} T_{mot}(t) + T_{ice}(t) = T_{gb}(t) + T_{accmech}(t), \\ P_{batt}(t) = P_{mot,e}(t) + P_{accelec}(t), \\ \omega_{mot}(t) = \omega_{ice}(t) = \omega_{gb}(t). \end{cases} \tag{2.4}$$

Assuming a constant efficiency for the electric motor ($\eta_{mot}$), the battery power ($P_{batt}$) can be represented as a function of engine power ($P_{ice}$) and the requested power ($P_{req}$) as

$$\begin{cases} P_{batt}(t) = -\frac{1}{\eta_{mot}} P_{ice}(t) + \frac{1}{\eta_{mot}} P_{req}(t), \\ P_{req}(t) = P_{gb}(t) + \frac{1}{\eta_{mot}} P_{accelec}(t) + P_{accmech}(t). \end{cases} \tag{2.5}$$

## 2.2 Simulation Environment

Table 2.1: Vehicle characteristics

| Characteristic | Pre-Transmission Parallel HEV |
|---|---|
| Vehicle mass | 19878 kg |
| Engine capacity | 6.7 L Diesel |
| Engine power | 194 kW |
| Motor power | 100 kW (continuous) 200 kW (peak) |
| Battery energy capacity | 7.5 kWh (27 MJ) |
| Electrical Accessory | 7 kW |
| Mechanical Accessory | 4 kW |

This section describes the simulation environment that has been used to implement and compare the different energy management strategies designed and presented in this dissertation. The pre-transmission parallel HEV (Fig. 2.1) is modeled in MATLAB/Simulink environment and the vehicle characteristics are shown in Table 2.1. In order to study the performance of an energy management strategy, any HEV can be simulated using either a forward or backward approach [52, 53, 54, 55, 56, 57]. These longitudinal quasi-static vehicle simulators use stationary input/output maps (with and without inertial dynamics) to model the various components of the vehicle. Because the simulators are primarily used to compare the performance of different energy management strategies, in terms of
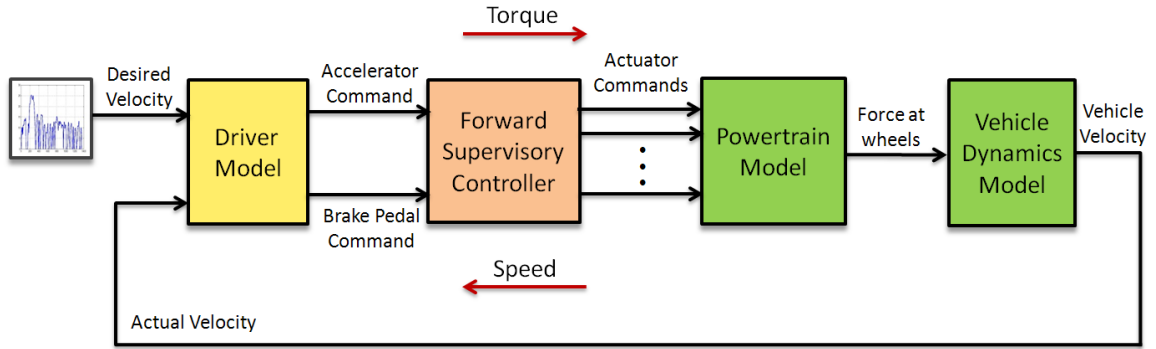
Figure 2.5: Information flow in forward vehicle simulator

steady state variables such as battery state of charge, fuel consumption over a driving cycle, etc., the level of complexity attained using stationary maps is sufficient. The different approaches used in simulating the vehicle are driven by the intended purpose of the simulator and the available computational capability.

Table 2.2: Forward and Backward Vehicle Simulator

| Component | Forward Simulator | Backward Simulator |
|---|---|---|
| Vehicle dynamics | All powertrain inertias considered | All powertrain inertias considered |
| Engine model | First order dynamics+fuel consumption map | Stationary fuel consumption map |
| Engine starter | Electrical cranking | Instantaneous power on |
| Electric machine | Stationary map | Stationary map |
| Battery model | Circuit model | Stationary map |
| Clutch dynamics | Slip dynamics | Instantaneous engagement |

### 2.2.1 Forward Vehicle Simulator

The forward vehicle simulator is a longitudinal and quasi-static simulator with standard representation of road load based on inertial, rolling and aerodynamic resistances. It is called a forward simulator because the torque/speed signals are propagated to/from different components of the vehicle. The information flow in a generic forward vehicle simulator is shown in Fig. 2.5. Based on the vehicle velocity profile to be followed, a simple PID based driver model generates acceleration and brake pedal commands (much like a real driver). The powertrain controller block receives the accelerator and brake pedal commands from the driver model and decides the optimal torque/power split between the sources available. The component torque/power requests are used by the powertrain model to calculate the force at the wheels. Because the forward simulator is primarily used in the analysis of energy management strategies, all the components are modeled using quasi-static map based models with the most relevant dynamics described in Table 2.2. This simulator is used to perform the following tasks:

1. Simulation of vehicle system behavior over different driving cycles;

2. Evaluation of instantaneous and cumulative fuel consumption and battery state of charge;

3. Possibility of evaluating effects of vehicle and drivetrain design parameters;

4. Possibility of testing and optimizing energy management strategies.

The various components of a forward vehicle simulator are described in detail with the corresponding input and output signals.
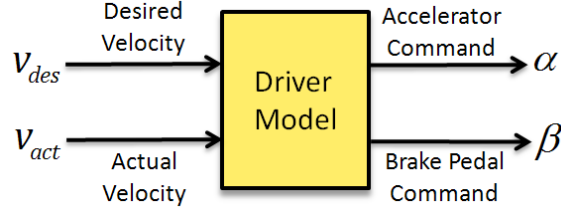
Figure 2.6: Driver Model

**Driver Model**

The PID based driver model, depicted in Fig. 2.6 and used in the forward vehicle simulator accepts the desired and actual vehicle velocity as inputs. Depending on the error in velocity, it calculates the accelerator and brake pedal commands. The equations governing the driver model can be expressed as

$$
\begin{cases}
u(t) = V_{des}(t) - V_{act}(t), \\
y(t) = K_P u(t) + K_I \int u(t) dt + K_D \frac{du(t)}{dt}, \\
\alpha(t) = y(t) \quad \forall y(t) > 0, \\
\beta(t) = y(t) \quad \forall y(t) \leq 0,
\end{cases}
\tag{2.6}
$$

where $u$ represents the error in velocity, $V_{des}$ represents the desired vehicle velocity, $V_{act}$ represents the actual vehicle velocity, $y$ represents the output of the PID controller, $K_P, K_I, K_D$ represent the proportional, integral and derivative constants respectively and $\alpha, \beta$ represent the normalized acceleration and brake pedal commands.

**Forward Supervisory Controller**

Unlike a conventional vehicle, the performance of a generic HEV strongly depends on the supervisory controller. The name "supervisory controller" is used because in addition to the lower-level component controllers, there is an extra layer of hierarchical control which decides the vehicle mode of operation and the torque/power split between the different
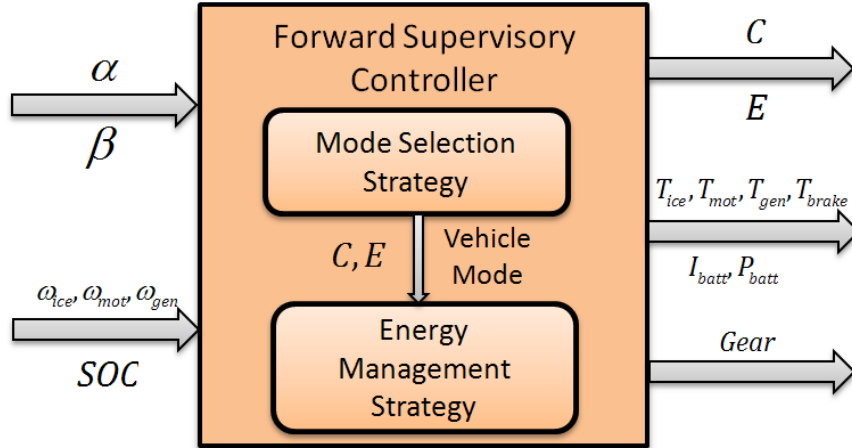
Figure 2.7: Forward Supervisory Controller

energy sources. Here the controller block accepts the accelerator and brake pedal commands as inputs and calculates the engine ON/OFF state, the clutch OPEN/CLOSE state and the torque/power/current of the powertrain components (engine, electric machine, battery, etc.). Fig. 2.7, shows a hierarchical control structure used in the development of the supervisory controller. It consists of a mode selection strategy and an energy management strategy. The mode selection strategy decides the vehicle mode of operation by selecting the engine and clutch states using a set of well-defined rules. In general, these rules can either be derived from engineering common sense [29, 30, 31] or from dynamic programming [33]. For each of the vehicle modes, the energy management strategy calculates the optimal torque/power split between the engine, electric machine and battery. The energy management strategies (ECMS, Adaptive ECMS, Optimal control law) proposed in this dissertation (Section 3.3, 3.4, 4.4) are implemented in this part of the supervisory controller.
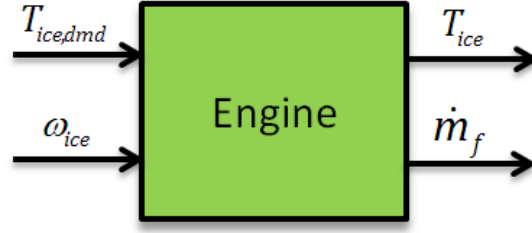
Figure 2.8: Powertrain Model: Engine

**Powertrain Model**

The powertrain model block used in the forward vehicle simulator accepts the actuator commands from the supervisory controller and calculates the force required at the wheels to satisfy the desired velocity. The model block consists of the engine, electric machine, battery and the transmission models.

**Engine Model**: The engine model (Fig. 2.8) uses a quasi-static fuel consumption map with first order inertial dynamics for the engine. Depending on the instantaneous torque demand and engine speed, the engine torque and the fuel consumed are calculated using

$$\begin{cases} T_{ice}(t) = \min(T_{ice,dmd}(t), T_{ice,max}(\omega_{ice}(t))(t)), \\ \dot{m}_f(t) = f_{ice}(T_{ice}(t), \omega_{ice}(t)), \\ J_{ice}\frac{d\omega_{ice}}{dt} = T_{ice}(t) - T_{load}(t). \end{cases} \tag{2.7}$$

where $T_{ice,dmd}$ represents the demanded engine torque, $T_{ice,max}$ represents the maximum engine torque, $\dot{m}_f$ denotes the fuel consumption rate of the engine, $J_{ice}$ denotes the inertia of the engine, $f_{ice}$ represents the nonlinear mapping relating the engine torque, speed and fuel consumption rate and $T_{load}$ represents the engine load torque.

The fuel consumption map of the engine used in this dissertation is shown in Fig. 2.9. The engine fuel consumption rate can be expressed as a function of the engine torque/power
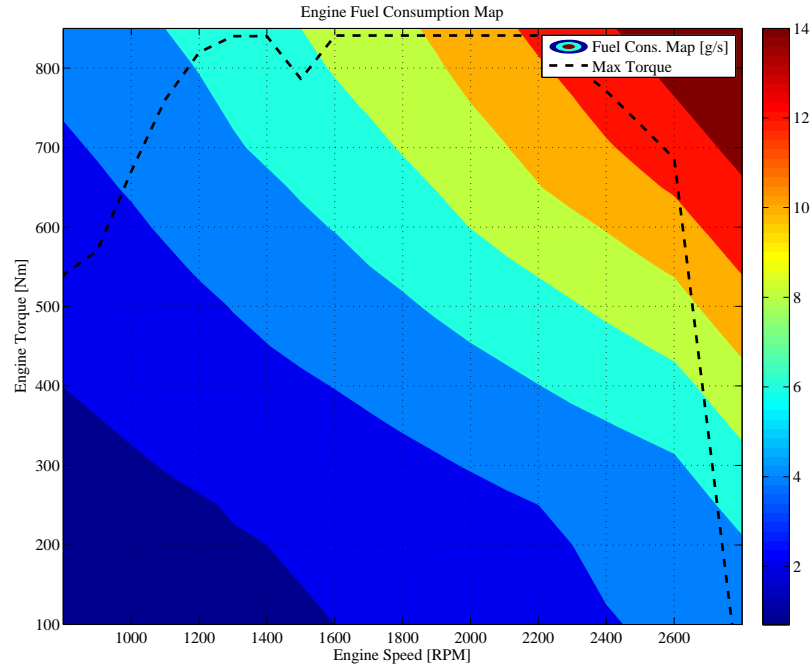
Figure 2.9: Fuel Consumption Map of 6.7L Diesel Engine
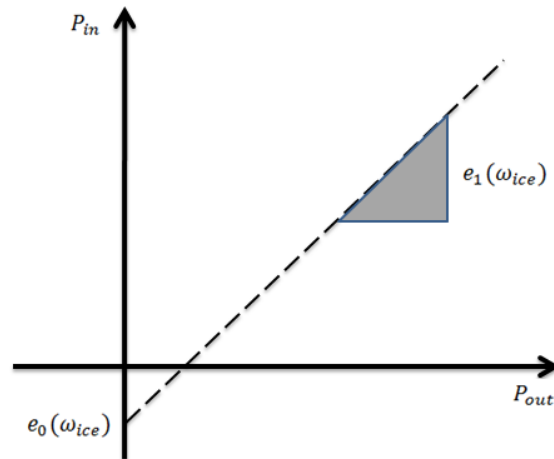


Figure 2.10: Illustration of Willans line model for engine
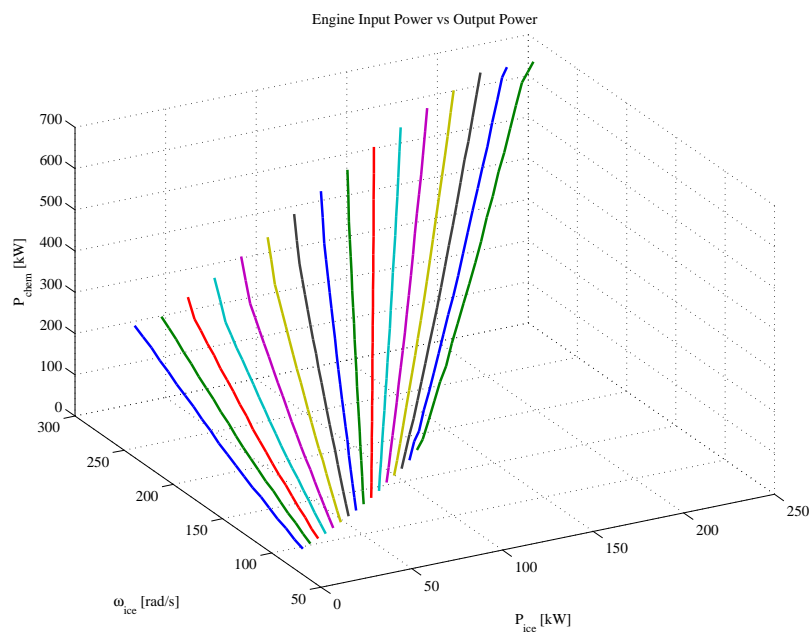
Figure 2.11: Willans line model: engine output power vs input power
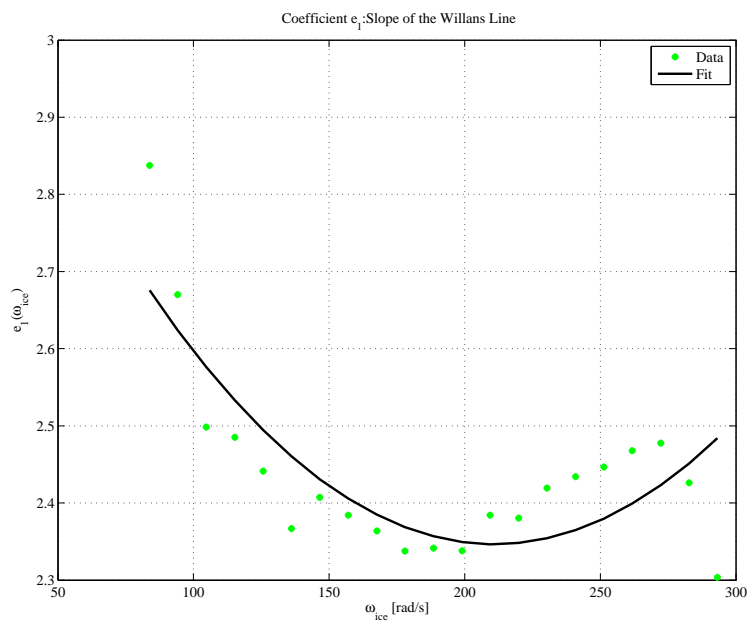


Figure 2.12: Quadratic fit for slope of Willans line model
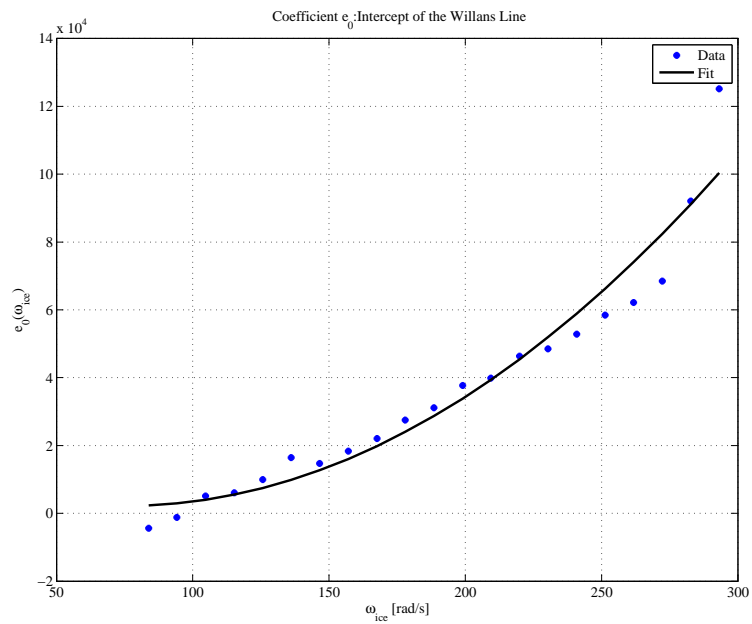
Figure 2.13: Quadratic fit for intercept of Willans line model
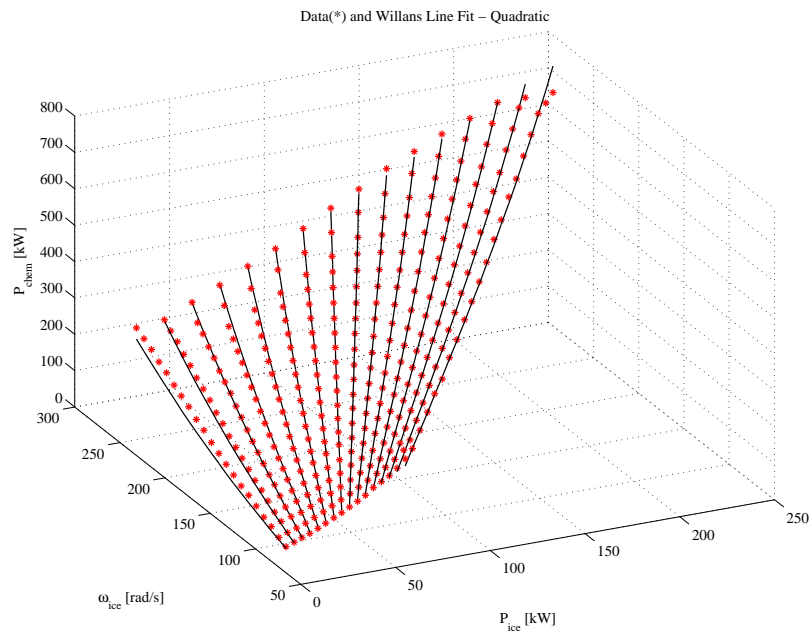


Figure 2.14: Effectiveness of Willans line model

and speed using an appropriate Willans line model [2, 58, 17]. In general, for any energy conversion device, the efficiency of the device can be modeled by representing the input power as an affine function of the output power and losses (Fig. 2.10). For the engine considered in this dissertation, the plot between the input and the output power is shown in Fig. 2.11. Here, at a given engine speed, the output power ($P_{ice}$) can be written as an affine function of the input chemical power ($P_{chem}$). The slope and intercept of each of the Willans lines can be expressed a polynomial function (Fig. 2.12 and Fig. 2.13) of the engine speed, by

$$
\begin{cases}
P_{in}(t) = e_0(\omega_{ice}(t)) + e_1(\omega_{ice}(t))P_{out}(t), \\
e_0(\omega_{ice}(t)) = e_{00} + e_{01}\omega_{ice}(t) + e_{02}\omega_{ice}^2(t), \\
e_1(\omega_{ice}(t)) = e_{10} + e_{11}\omega_{ice}(t) + e_{12}\omega_{ice}^2(t),
\end{cases}
\tag{2.8}
$$

where $e_{ij}$, $i, j = 0, 1, 2$ are Willans line coefficients, $P_{in} = P_{chem} = \dot{m}_f Q_{LHV}$ ($Q_{LHV}$ is the lower heating calorific value of diesel in $kJ/kg$) is the chemical power input to the engine and $P_{out} = P_{ice} = T_{ice}\omega_{ice}$ is the engine power output. Given the engine torque $T_{ice}$ and speed $\omega_{ice}$, the fuel consumption rate can be written as

$$
\dot{m}_f(t) = \frac{1}{Q_{LHV}}[e_0(\omega_{ice}(t)) + e_1(\omega_{ice}(t))P_{ice}(t)].
\tag{2.9}
$$

The effectiveness of the Willans line model in approximating the fuel consumption rate of the engine is shown in Fig. 2.14.

Depending on the vehicle mode of operation, the fuel consumption rate can also be expressed as a function of the engine power $P_{ice}$.

In the parallel mode of operation (Fig. 2.4), engine and electric motor speed are directly determined from the vehicle speed. The fuel consumption rate model can be written as

$$
\dot{m}_f(t) = \frac{1}{Q_{LHV}}[e_0(\omega_{gb}(t)) + e_1(\omega_{gb}(t))P_{ice}(t)].
\tag{2.10}
$$

Depending on the control input chosen, the fuel consumption rate can be expressed as a function of the control input using (2.5). Under the assumption that the slope and intercept of the Willans line model are independent of the engine speed, the fuel consumption rate can be expressed as an affine function of engine power $P_{ice}$ in the manner

$$\dot{m}_f(t) = p_2 + p_3 P_{ice}(t), \tag{2.11}$$

where $p_2, p_3$ are known constants calculated from (2.10). The constants $p_0, p_1, p_2, p_3$ were calculated and used depending on the vehicle mode of operation. The fuel consumption rate can also be expressed as a function of the battery power ($P_{batt}$) and the power requested at the gearbox ($P_{req}$) by substituting (2.5) on (2.11) to get,

$$\dot{m}_f(t) = p_4 + p_5 P_{batt}(t) + p_6 P_{req}(t), \tag{2.12}$$

where $p_4, p_5, p_6$ are known constants.

If the engine speed $\omega_{ice}$ can be chosen independent of the vehicle speed, it can be operated in its most efficient region. The *optimal* engine speed ($\omega_{ice,opt}$) can be calculated by minimizing the chemical power $P_{chem}$ as

$$\begin{cases} \frac{\partial P_{chem}}{\partial \omega_{ice}} = 0 \;\Rightarrow\; \omega_{ice,opt} = -\frac{1}{2}\frac{e_{01}+e_{11}P_{ice}}{e_{02}+e_{12}P_{ice}}, \\ \frac{\partial^2 P_{chem}}{\partial \omega_{ice}^2} > 0, \\ \omega_{ice} \in [\omega_{ice,idle}, \omega_{ice,max}], \end{cases} \tag{2.13}$$

where $\omega_{ice,idle}, \omega_{ice,max}$ represent the idle and maximum speed of the engine. The fuel consumption rate can be expressed as an affine function (Fig. 2.15) of $P_{ice}$ alone, as

$$\dot{m}_f(t) = m_0 + m_1 P_{ice}(t) \tag{2.14}$$

where $m_0$ and $m_1$ are known constants obtained from (2.9) and (2.13). Moreover, because $P_{ice}$ is a function of the control input $P_{batt}$ as given by (2.3), ultimately the fuel consumption
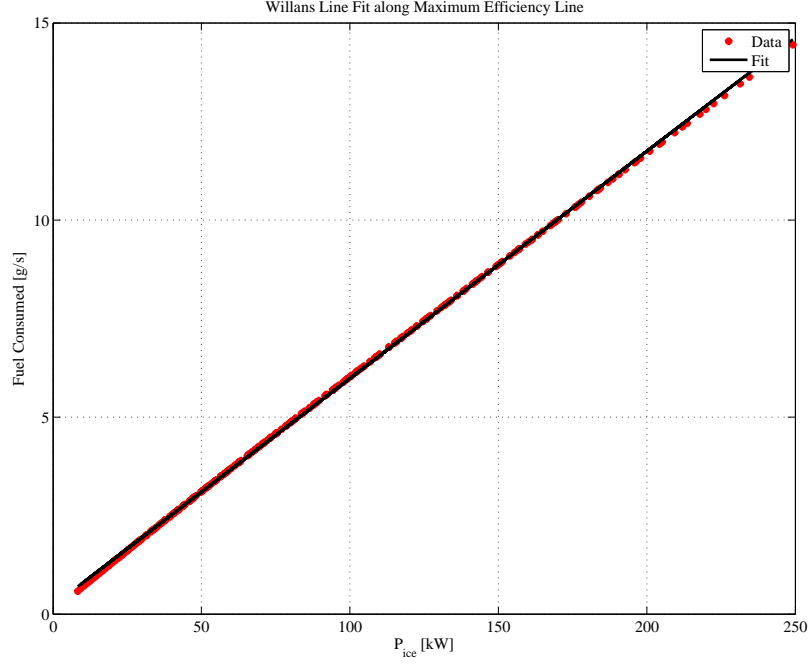
Figure 2.15: Willans line model with engine operating at maximum efficiency

rate $\dot{m}_f(t)$ can be expressed as a direct function of the control input, $P_{batt}$, i.e.,

$$\dot{m}_f(t) \quad = \quad p_0 + p_1 P_{batt}(t), \tag{2.15}$$

through coefficients $p_0, p_1$ expressed as follows:

$$\begin{cases} p_0 = m_0 + m_1 \left( P_{accmech} + \frac{1}{\eta_{mot}} P_{accelec} \right), \\ p_1 = -m_1 \eta_{mot}. \end{cases} \tag{2.16}$$

**Electric machine Model**: The electric machine model depicted in Fig. 2.16, uses a quasi-static efficiency map (Fig. 2.17) to calculate the electrical power. The usage of the efficiency map depends on the mode (motoring mode/generating mode) of usage of the electric machine. The speed of the electric machine and the torque demand are the inputs to the block. Based on these inputs, the torque and power at the output are calculated, using

$$\begin{cases} T_{em} = \max(\min(T_{em,dmd}(t), T_{em,max}(\omega_{em})(t)), T_{em,min}(\omega_{em})(t)), \\ \eta_{em} = f_{em}(T_{em}(t), \omega_{em}(t)), \end{cases} \tag{2.17}$$

33

Figure 2.16: Powertrain Model: Electric Machine

where $T_{em}, \omega_{em}$ represent the electric machine torque and speed, $T_{em,dmd}$ represent the demanded electric machine torque, $T_{em,min}, T_{em,max}$ denote the minimum and maximum electric machine torques, $f_{em}$ represents the nonlinear mapping of the efficiency of electric machine and $\eta_{em}$ denotes the efficiency of the electric machine.

**Battery Model**: The battery model (Fig. 2.18) used in the forward vehicle simulator is usually a circuit based $n^{th}$ order model. The battery state of charge (SOC) is the scalar state variable of the energy management problem whose dynamics can be expressed as

$$S\dot{O}C(t) = -\eta_{batt}\frac{I(t)}{Q_{max}} \tag{2.18}$$

where $\eta_{batt}$ represents the Coulombic efficiency [51], $I(t)$ represents the current flowing in (negative) and out (positive) of the battery and $Q_{max}$ the maximum battery charge capacity. Numerous battery models have been developed in HEV literature depending on the intended level of accuracy. However, the energy management problem places more importance on the efficiency and losses in the battery pack, which allows the use of a zero-*th* order equivalent circuit based model shown in Fig. 2.19. Depending on the order of the electric circuit based model, there are several parameters that must be characterized.
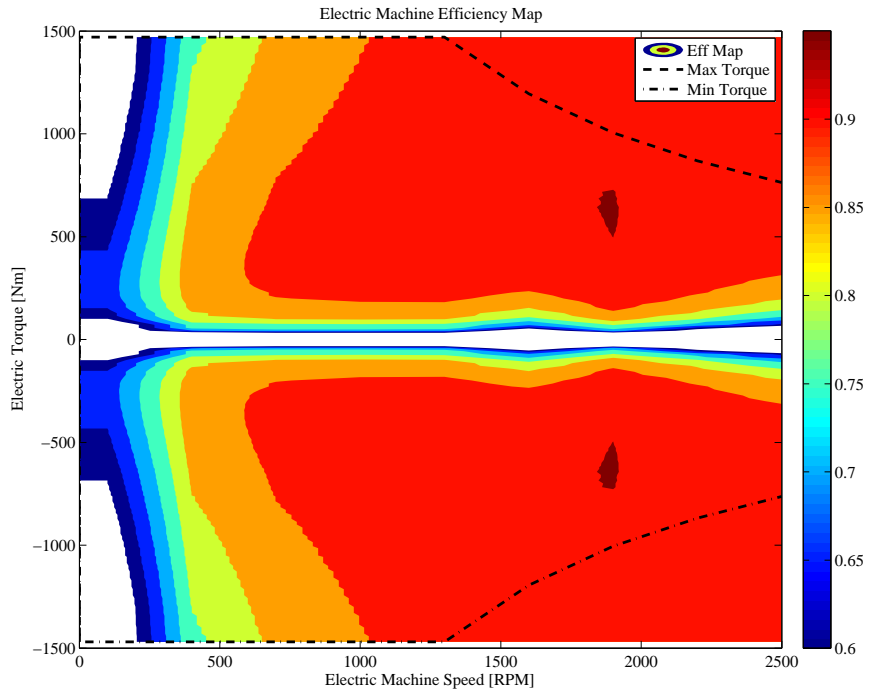
Figure 2.17: Electric Machine Efficiency Map
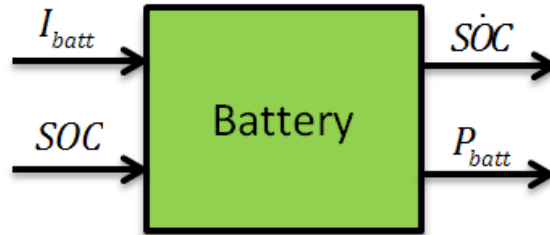


Figure 2.18: Powertrain Model: Battery
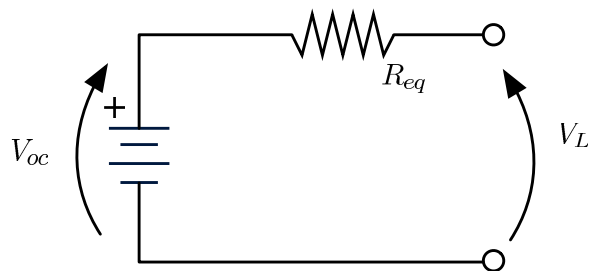


Figure 2.19: Zero-*th* order electrical circuit model of the battery

The parameters of the zero-*th* battery model are, the equivalent resistance $(R_{eq})$[1] and the open circuit voltage $(V_{oc})$[2]. In general, these parameters depend on several factors such as, state of charge and temperature. Typically, in a charge-sustaining HEV, the battery is used only over a limited range of SOC (typically between 0.5-0.8). It is well known that over this range of SOC operation, the model parameters $(R_{eq}, V_{oc})$ do not vary significantly as a function of SOC. Therefore, they are assumed to be known constants in this work. Moreover, in this study, the effect of temperature on battery parameters have not been considered, leaving the investigation on temperature dependent parameters to future studies. With reference to the zero-*th* order equivalent circuit model in Fig. 2.19, the voltage at the battery pack terminals is given by

$$V_L(t) = V_{oc} - I(t)R_{eq}, \tag{2.19}$$

where $V_L(t)$ is the instantaneous terminal voltage. Multiplying (2.19) by current $I(t)$ on both sides, battery power $P_{batt}$ is expressed as,

$$P_{batt}(t) = V_L(t)I(t) = V_{oc}I(t) - I^2(t)R_{eq}. \tag{2.20}$$

Solving the algebraic quadratic equation (2.20), the battery current $I(t)$ is expressed as a function of $P_{batt}$ as:

$$I(t) = \frac{V_{oc} - \sqrt{(V_{oc})^2 - 4R_{eq}P_{batt}(t)}}{2R_{eq}}. \tag{2.21}$$

This result can then be substituted into the definition of $\dot{SOC}(t)$ generating the nonlinear mapping

$$\dot{SOC}(t) = -\eta_{batt}\frac{V_{oc} - \sqrt{(V_{oc})^2 - 4R_{eq}P_{batt}(t)}}{2R_{eq}Q_{max}} = f_{SOC}(SOC(t), P_{batt}(t)) \tag{2.22}$$

---

[1]The equivalent resistance of a zero-*th* circuit model is a single lumped resistance of the battery pack estimated from experimental data [59].

[2]The open circuit voltage is the output voltage of the battery pack when it is not loaded and it is usually determined from experimental data [59].

Figure 2.20: Powertrain Model: Transmission

**Transmission Model**: The transmission model (Fig. 2.18) uses a stationary gear ratio map (Table 2.3) to determine the torque and speed at the output of the transmission expressed as,

$$\begin{cases} T_{gb,out} = \eta_{trans} * R * T_{gb,in}, \\ \omega_{gb,out} = \omega_{gb,in} * R. \end{cases} \quad (2.23)$$

where $T_{gb,in}, T_{gb,out}$ represent the gearbox input and output torque, $\eta_{trans}$ represents the efficiency of the transmission and $R$ represents the gear ratio.

Table 2.3: Transmission Characteristics

| Gear Number | $1^{st}$ | $2^{nd}$ | $3^{rd}$ | $4^{th}$ | $5^{th}$ | $6^{th}$ |
|---|---|---|---|---|---|---|
| Ratio (R) | 3.49 | 1.86 | 1.41 | 1 | 0.75 | 0.65 |

**Vehicle Dynamics Model**: The vehicle dynamics model (Fig. 2.21) calculates the vehicle velocity, given the force at the wheels at each instant. The inertial, aerodynamic and rolling resistance losses are taken into account and the following equations are used:

$$\begin{cases} F_{load} = \frac{1}{2}\rho_a C_d A_f V_{act}^2 + MgC_r \cos\theta + Mg\sin\theta, \\ (M + M_r)\frac{dV_{act}}{dt} = F_{trac} - F_{load}, \end{cases} \quad (2.24)$$
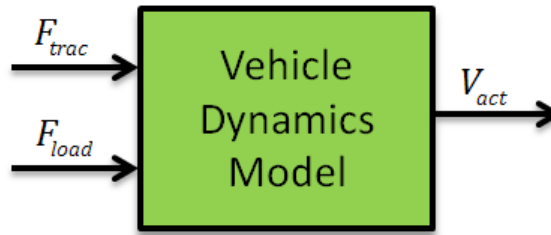
Figure 2.21: Powertrain Model: Vehicle Dynamics
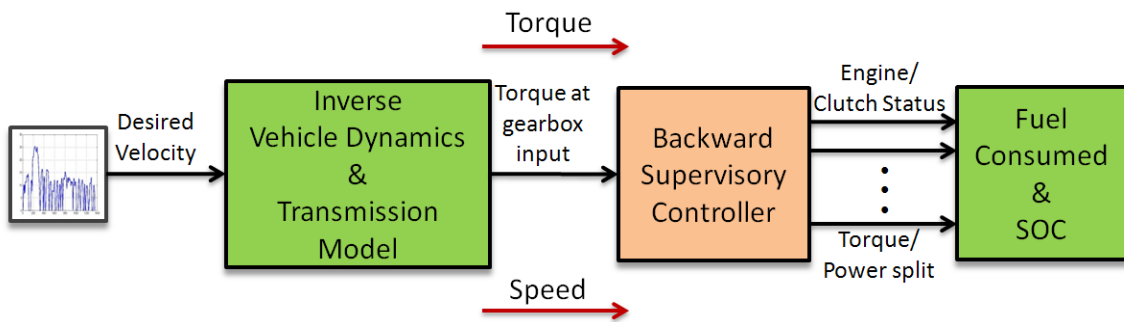


Figure 2.22: Information flow in backward vehicle simulator

where $F_{load}, F_{trac}$ represent the road load force and the tractive force at the wheels, $\rho_a$ represents the density of air, $C_d, C_r$ are the coefficient of drag and rolling resistance respectively, $A_f$ denotes the frontal area of the vehicle, $\theta$ represents the road grade, $M, M_r$ represent the given mass and effective mass of the vehicle and $g$ the acceleration due to gravity.

## 2.2.2  Backward Vehicle Simulator

In order to compare the performance of the proposed control law with the optimal global solution obtained from dynamic programming, a backward vehicle simulator is used. The

information flow in a backward simulator is shown in Fig. 2.22. The torque required at the wheels and subsequently the torque/speed required from the components is calculated with the assumption that the vehicle follows the desired velocity trajectory. The optimization algorithm decides the optimal component torques/power from the devices depending on the torque required at the wheels. The simulator primarily uses simplified quasi-static map based models for all the components. Unlike the forward simulator, the backward simulator, models all its components using stationary maps as shown in Table 2.2. The simulator is used to perform the following tasks:

1. Evaluation of instantaneous and cumulative fuel consumption and battery state of charge;

2. Obtain DP solution to the energy management problem in HEV;

3. Possibility of testing the effect of state and control input discretization levels on DP solutions.

The different blocks in a backward simulator are described in detail in the following sub-sections.

**Inverse Vehicle Dynamics and Transmission Model**

The inverse vehicle dynamics and transmission block (Fig. 2.23) accepts the desired vehicle velocity and acceleration as inputs and calculates the torque required at the gearbox in order to follow that velocity profile.
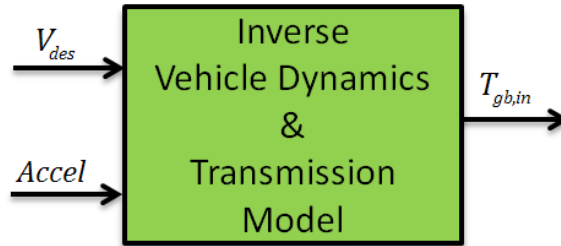
Figure 2.23: Inverse Vehicle Dynamics and Transmission Model
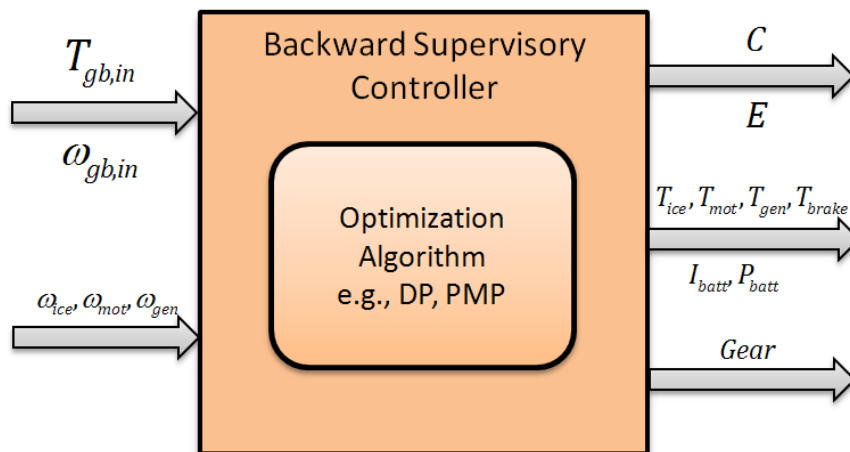


Figure 2.24: Backward Supervisory Controller
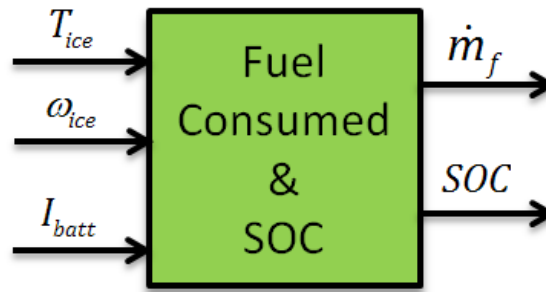
Figure 2.25: Fuel Consumption and SOC

**Backward Supervisory Controller**

The backward supervisory controller (Fig. 2.24) used in a backward vehicle simulator is typically an optimization algorithm that gives benchmark solution to the energy management problem. It accepts the torque required at the gearbox as the input and decides both the vehicle mode of operation and optimal torque/power split between the engine and the electric machine.

**Fuel Consumption and SOC**

The fuel consumed over the driving cycle and battery SOC (Fig. 2.25) is calculated using simple stationary maps as described in Section 2.2.1.

## 2.3 Conclusion

The pre-transmission parallel HEV explained in this chapter will be the vehicle architecture over which several energy management strategies will be tested. Both the forward and backward vehicle simulators are used to compare and benchmark different energy management strategies. The energy management strategies (Chapter 3) have been implemented

in both backward and forward vehicle simulators for the vehicle architecture described in this chapter. The stability and optimality framework developed in Chapter 4, uses the drivability constraints described in this chapter.

## Chapter 3: Energy Management Strategies for HEVs

In this chapter, we formulate the optimal control problem in a pre-transmission parallel HEV and develop different energy management strategies to solve the optimal control problem. In order to compare and evaluate the performance of energy management strategies, the global optimal solution from dynamic programming (DP) is used. The DP algorithm is used to solve the optimal control problem in a charge-sustaining HEV and implements the algorithm in a backward vehicle simulator using an open-source MATLAB DP code [60]. The equivalent consumption minimization strategy (ECMS) derived from the necessary conditions of optimality given by Pontryagin's Minimum Principle (PMP) is formulated and compared with DP. The strategy is implemented in a backward vehicle simulator and is compared against the benchmark solution obtained from DP. An adaptive version of ECMS is proposed, formulated and compared against DP.

## 3.1 Objective of the Energy Management Strategy

A generic HEV, regardless of the architecture considered, has two energy sources on board that can supply the torque/power requested by the driver. Unlike a conventional vehicle, the additional degree of freedom presents a challenging optimization problem. The objective of the energy management strategy in a HEV is to find the optimal torque/power split between the primary (fuel) and secondary (battery) energy sources that minimizes a

given objective function over an entire driving cycle. In general, the minimization can be performed with respect to several objectives, such as fuel consumption, emissions, battery aging, etc., or a combination of these objectives [61], [5]. Throughout the dissertation, we consider the problem of minimizing the total mass of fuel, $m_f$ [g] during a driving cycle, or equivalently, minimize the following cost $J$:

$$J = \int_{t_0}^{t_f} \dot{m}_f(u(t))dt \tag{3.1}$$

where $\dot{m}_f$ is the instantaneous fuel consumption rate expressed in [g/s], $u(t)$ is the control input, and $t_f - t_0$ is the length of the driving cycle. The energy management problem, by its very nature, is a constrained optimization problem, where the objective function (3.1) is minimized under system dynamics, instantaneous (local) and integral (global) constraints on the state and control variables, as outlined in the following.

- **System dynamics:** Because the energy management problem in a HEV involves finding the steady-state optimal torque/power split between the engine and electric motor, quasi-static vehicle simulators are used. The vehicle simulators can be either forward (Fig. 2.5) or backward (Fig. 2.22) in its approach. Thus the battery state of charge (SOC) is the scalar state variable of the energy management problem and is predicted using a zero-*th* order model as shown in Fig. 2.19. Based on this battery model, the battery SOC dynamics is expressed as

$$\dot{SOC}(t) = f_{SOC}(SOC(t), P_{batt}(t)) \tag{3.2}$$

where $f_{SOC}$ is the nonlinear mapping derived using the circuit based model shown in (2.22). The battery SOC and battery power are the state variables and control input of the energy management problem, respectively.

44

- **Integral constraint:** In a charge sustaining HEV, the net energy from the battery is zero over a given driving cycle, which means that the SOC at the end of the driving cycle is desired to be the same as that in the beginning of the driving cycle, or

$$SOC(t_f) = SOC(t_0), \tag{3.3}$$

where $SOC(t_0), SOC(t_f)$ represent the battery SOC at the beginning and end of the driving cycle. Even though this is not considered as a hard constraint in a real HEV, it is mathematically convenient to assume that the state variable must satisfy the constraint for any driving cycle.

- **Instantaneous constraints:** Similar to the integral constraint (3.3) on battery SOC, there are instantaneous constraints imposed on the state and control variables. These constraints mostly concern physical operation limits, such as the maximum engine torque and speed, the maximum motor power/torque and the battery SOC. The instantaneous constraints for a pre-transmission parallel HEV powertrain shown in Fig. 2.1 are

$$\begin{cases} P_{batt,min} \leq P_{batt}(t) \leq P_{batt,max}, \\ SOC_{min} \leq SOC(t) \leq SOC_{max}, \\ T_{x,min} \leq T_x(t) \leq T_{x,max} \qquad \forall t \in [t_0, t_f] \\ P_{x,min} \leq P_x(t) \leq P_{x,max}, \\ \omega_{x,min} \leq \omega_x(t) \leq \omega_{x,max}, \ x = ice, \ mot, \end{cases} \tag{3.4}$$

where the last three inequalities represent limitations on the instantaneous engine and electric motor torque ($T_{(\cdot)}$), power ($P_{(\cdot)}$) and speed ($\omega_{(\cdot)}$) respectively; $(\cdot)_{min}, (\cdot)_{max}$ are the minimum and maximum values of power, SOC, torque and speed at each instant.

45

Moreover, the instantaneous constraints are also enforced at each instant to ensure that the total power demanded at the wheels is satisfied. In a pre-transmission parallel HEV, like the one shown in Fig. 2.1, the engine is connected in parallel with the electric motor and battery pack and can be engaged or disengaged from the wheels using a clutch. The vehicle can operate in three different modes depending on the status of clutch and gear position, namely:

1. Electric mode: The constraints that must be satisfied in this mode (Fig. 2.2) are listed here for convenience;

$$
\begin{cases}
T_{mot}(t) = T_{gb}(t), \\
P_{batt}(t) = P_{mot,e}(t) + P_{accelec}(t), \\
\omega_{mot}(t) = \omega_{gb}(t).
\end{cases}
\tag{3.5}
$$

2. Parallel mode with neutral gear: The constraints that must be satisfied in this mode (Fig. 2.3) are listed here for convenience;

$$
\begin{cases}
T_{mot}(t) + T_{ice}(t) = T_{accmech}(t), \\
P_{batt}(t) = P_{mot,e}(t) + P_{accelec}(t), \\
\omega_{mot}(t) = \omega_{ice}(t) = \omega_{ice,opt}(t).
\end{cases}
\tag{3.6}
$$

3. Parallel mode: The constraints that must be satisfied in this mode (Fig. 2.4 are

$$
\begin{cases}
T_{mot}(t) + T_{ice}(t) = T_{gb}(t) + T_{accmech}(t), \\
P_{batt}(t) = P_{mot,e}(t) + P_{accelec}(t), \\
\omega_{mot}(t) = \omega_{ice}(t) = \omega_{gb}(t).
\end{cases}
\tag{3.7}
$$

## 3.2  Dynamic Programming

This section describes an open-source [3] MATLAB based DP function used to solve the energy management problem in a charge-sustaining HEV, the method of implementation and the simulation results for a variety of driving cycles.

[3]a code that has been published in the literature and available for free redistribution and usage

### 3.2.1 Overview

Dynamic programming (DP), the brainchild of an American mathematician, Richard Bellman, is a method for solving complex optimization problems by breaking them down into simpler subproblems [62]. In general, to solve a given problem, different parts of the problem (subproblems) are to be solved and then combined to reach an overall solution. This approach is especially useful when the number of repeating subproblems grows exponentially as a function of the size of the input. In terms of mathematical optimization, DP [63] usually refers to simplifying a decision by breaking it down into a sequence of decision steps over time. The discrete formulation of DP is given here, because it is the most useful for solving complex problems, especially those that are not easily described analytically (for example, when maps need to be used).

Consider a dynamic system described by the discrete-time dynamic equation

$$x(k+1) = f(x(k), u(k)), \quad k = 0, 1, \cdots, N-1 \tag{3.8}$$

where $k$ is the index used to indicate the value of a variable at time step $t(k)$, $x(k) \in \mathbb{R}^n$ is the state vector, $u(k) \in \mathbb{R}^p$ is the control input, $N$ is the length of the optimization interval, i.e. the number of times control is applied, and $f(\cdot, \cdot)$ is a nonlinear, time-varying, discrete-time mapping of the state variable and control input. At each step $k$, the state of the system must remain in an admissible range: $x(k) \in \mathcal{S}(k) \subset \mathbb{R}^n$ . Similarly, the control variable is constrained to belong to a set $U$ of admissible values, which depends on the current state: $u(x(k)) \in \mathcal{U}(k) \subset \mathbb{R}^p$.

An admissible control policy is a sequence of state feedback control actions in the admissible set:

$$\psi = u(0), u(1), \cdots, u(N-1), \quad u(k) \in U(x(k)). \tag{3.9}$$

Given an initial state $x(0)$ and a sequence of functions $L(x(k), u(k))$ that represent the cost of each step, the optimal policy $\psi^*$ is the one that minimizes the functional cost $J$ expressed as

$$J_\psi = \phi(x(N)) + \sum_{k=0}^{N-1} L(x(k), u(k)), \tag{3.10}$$

where $\phi(x(N))$ represents the terminal cost function and the optimal cost is $J^* = J_{\psi^*} = \min_\psi J_\psi$.

The dynamic programming algorithm based on Bellman's principle of optimality [62] can be stated as follows:

**Theorem 3.2.2.** *An optimal policy has the property that, whatever the initial state and initial decision are, the remaining decisions must constitute an optimal policy with regard to the state resulting from the initial decision.*

In terms of mathematical optimization [63] this can be stated as follows:

**Definition 1.** *Let $\psi^* = u^*(0), u^*(1), \cdots, u^*(N-1)$ be an optimal control policy over the interval $[0, N-1]$, and assume that, while using $\psi^*$, a given state $x(i)$ occurs at time $i$. Consider now the sub-problem defined in the interval $[i, N-1]$ and starting at $x(i)$. Then the truncated policy $\psi_i^* = u^*(i), u^*(i+1), \cdots, u^*(N-1)$ is optimal for this sub-problem.*

The principle of optimality can be justified very intuitively: if the truncated policy $\psi_i^*$ were not optimal for the subproblem, there would be another policy that would generate a lower cost in the interval $[i, N-1]$. The total cost of the original problem could then be reduced by switching to this other policy, once $x(i)$ is reached. This, however, is in contrast with the hypothesis that $\psi^*$ is optimal for the full problem. Therefore, $\psi_i^*$ is optimal for the subproblem defined over $[i, N-1]$.

Because of this principle, it is possible to determine the optimal sequence of control actions starting from the final state and proceeding backwards, choosing at each step $i$ the path that minimizes the *cost-to-go* function

$$J(x(i)) = \phi(x(N)) + \sum_{k=i}^{N-1} L(x(k), u(k)). \tag{3.11}$$

The dynamic programming algorithm can be implemented proceeding backward in time from step $N-1$ to step $0$. The optimal cost-to-go is the cost to go from the current state to the final state when the optimal control policy $\psi^*$ is applied, calculated recursively as,

$$\begin{cases} J^*(x(N)) = \phi(x(N)), \\ J^*(x(k)) = \min_{u \in \mathcal{U}(\|)} \left[ L(x(k), u(k)) + J^*(x(k+1)) \right], \ k = N-1, N-2, \cdots, 0. \end{cases} \tag{3.12}$$

The proof of optimality of dynamic programming is fundamentally derived from the sufficient conditions of optimality given by the Hamilton-Jacobi-Bellman equation [62].

### 3.2.3   DP as Energy Management Strategy for HEVs

Based on the overview of DP presented in the previous section, DP is used to solve the energy management problem in the pre-transmission parallel HEV. The state variable, control input, instantaneous and integral constraints and the performance objective of the energy management problem in a charge sustaining HEV were stated in Section 3.1. The battery SOC dynamics in the discrete-time version are expressed as

$$SOC(k+1) = F_{SOC}(SOC(k), P_{batt}(k)), \quad k = 0, 1, \cdots, N-1, \tag{3.13}$$

where $SOC(k), P_{batt}(k)$ represent the battery SOC and battery power in discrete time, $F_{SOC}$ denotes the nonlinear mapping $f_{SOC}$ expressed in discrete time and $N$ is the number of intervals considered over the length of the driving cycle $t_0 - t_f$.
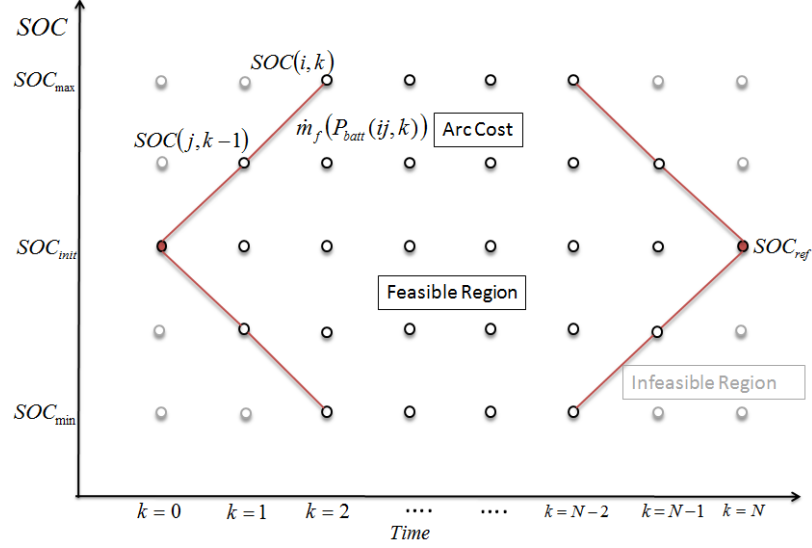
Figure 3.1: DP algorithm applied to HEV

In order to apply DP, the entire range of operation of SOC $(SOC_{min} - SOC_{max})$ is discretized into several levels as shown in Fig. 3.1. The number of discretization levels $(N_{SOC})$ in SOC is an important parameter of the DP algorithm and it determines the accuracy and computational requirement of the DP solution. In the grid, the battery SOC value at each discretization level $j$ and time step $k$ is denoted by $SOC(j, k)$. Each arc in the Fig. 3.1 corresponds to the change in battery SOC $(\Delta SOC(j, k))$ which is expressed as

$$\Delta SOC(j, i) = SOC(j, k-1) - SOC(i, k), \quad i, j = 1, \cdots N_{SOC}, \ k = 1, 2, \cdots N. \quad (3.14)$$

The cost function of the energy management problem shown in (3.1) is used to find the cost of all the arcs shown in Fig. 3.1. For example, the arc cost for $\Delta SOC(j, i)$ is calculated as $\dot{m}_f(P_{batt}(ij, k))$, where, $P_{batt}(ij, k)$ represents the battery power necessary to change the battery SOC from $SOC(j, k-1)$ to $SOC(i, k)$ at time step $k-1$. Once the arc costs for the entire grid are generated, the optimal control sequence of battery power $\psi = P_{batt}(0), P_{batt}(1), \cdots, P_{batt}(k), \cdots, P_{batt}(N-1), \ k = 1, \cdots, N$ is calculated backwards

50
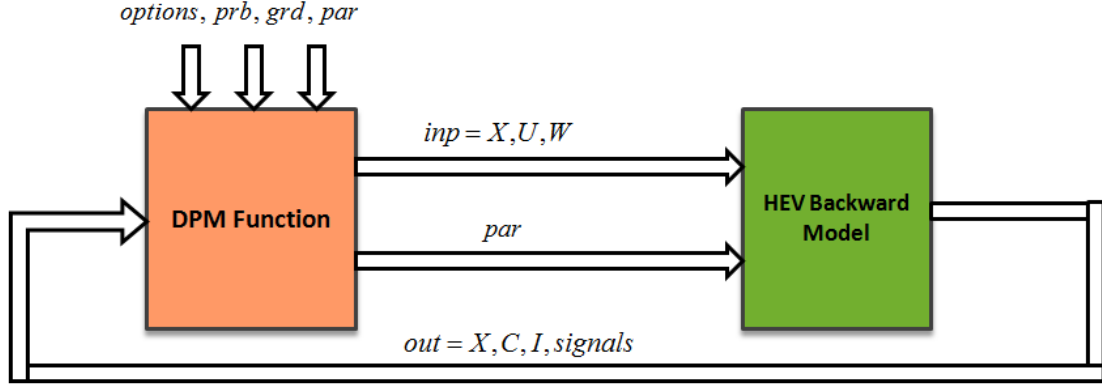
Figure 3.2: Implementation of DP Algorithm

using the following recursive formulation of DP,

$$
\begin{cases}
J_{N-1}^{*}(SOC(N-1)) = \displaystyle\min_{P_{batt}(N-1)} \left[ \dot{m}_f(P_{batt}(ij, N-1)) \right], \\
J_{k}^{*}(SOC(k)) = \displaystyle\min_{P_{batt}(k)} \left[ \dot{m}_f(P_{batt}(ij, k)) + J_{k+1}^{*}(SOC(k+1)) \right], \ k = N-1, N-2, \cdots, 0.
\end{cases}
$$
$$(3.15)$$

where $J_{k}^{*}(SOC(k))$ is the *optimal cost-to-go* function at state $SOC(k)$ to reach the final state $SOC_{ref}$ from time $k$ to $N-1$.

## 3.2.4 Implementation of DP Algorithm

In order to implement DP algorithm to solve the energy management problem for charge-sustaining HEVs (Section 3.1), an open-source generic DP code in MATLAB environment [60] is used. This function solves the discrete-time optimal control problem using Bellman's principle of optimality. The DPM MATLAB function is used in conjunction with a backward vehicle dynamics and powertrain model as shown in Fig. 3.2. In the implementation, the DPM function has parameters such as $options, prb, grd, par$ listed in

Table 3.1: Parameters of DPM function

| Parameters | Description |
| --- | --- |
| $dpm$ | DP algorithm function handle |
| $model$ | HEV backward model function handle |
| $options$ | Options structure for DPM function<br>(e.g., Maximum number of iterations, Tolerance allowed) |
| $prb$ | Problem structure: External inputs to DPM function<br>(e.g., Time step, Number of time steps in the problem, Vehicle velocity) |
| $grd$ | Grid Structure<br>(e.g., Number of state grid points, control input grid points, limits) |
| $par$ | User defined parameter structure<br>(e.g., Vehicle characteristics, component maps) |
| $res$ | Results using optimal control sequence |
| $dyn$ | Dynamic structure used by the DPM function<br>(e.g., Optimal cost-to-go function, optimal control input map) |

Table 3.1 and is implemented as

$$[res, dyn] = dpm\,(model, options, prb, grd, par)\,. \qquad (3.16)$$

The DPM function accepts the variables $prb, grd, par$ as inputs which has information about the vehicle velocity, length of the optimization interval, number of state and control

Table 3.2: Parameters of HEV backward model

| Parameters | Description |
|---|---|
| $inp$ | $X$: State variables at the current time step<br>$U$: Control input variables at the current time step<br>$W$: External input variables (from $prb$) |
| $X$ | Resulting state variables after applying control input $U$ |
| $C$ | Resulting cost after applying control input $U$ |
| $I$ | Infeasibility combinations |
| $signals$ | User defined output variables |

input grids, vehicle characteristics, etc., as shown in Table 3.1. The function calls the backward vehicle model for each combination of the state variable and control input variable in order to solve the problem backwards. The arc cost for each state transition is calculated and used by DP. The HEV backward vehicle model is implemented using the input and output variables in the manner

$$Function\,[X, C, I, signals] = model\,(inp, par)\,,\qquad(3.17)$$

where $X, C, I, signals$ are listed in Table 3.2.

In summary, the DP algorithm calculates the *optimal* sequence of engine torque, electric machine torque, engine status and clutch status such that the constraints on battery SOC are satisfied and minimum amount of fuel is consumed over the driving cycle. Because the DP algorithm is given the complete choice to select the different modes of vehicle operation and the torque/split between the devices, it produces the *global optimal* solution to the

energy management problem. The control input and state variables used by DP are shown in Table 3.1 and the variables used in the model function are shown in Table 3.2.

## 3.2.5   Simulation Results

Table 3.3: Performance of DP for different driving cycles

| Driving Cycle | $FC_{eqv}$ [kg] |
|---|---|
| Manhattan | 1.3191 |
| WVU-Interstate | 7.5353 |
| WVU-Suburban | 3.4391 |
| UDDS Truck | 2.8885 |
| HTUF | 6.2261 |
| APTA | 4.6715 |

The DP algorithm is applied to the pre-transmission parallel HEV using the backward vehicle simulator (Fig. 2.22) and the simulation results for several heavy-duty driving cycles are reported. In order to evaluate the performance of the energy management strategy, the equivalent fuel consumed ($FC_{eqv}$) are used. They are defined as

$$\left\{ FC_{eqv} = \int_{t_0}^{t_f} \dot{m}_f + \frac{\Delta\, SOCE_{max}}{\eta_{path}\, Q_{LHV}}, \right. \tag{3.18}$$

where $SOC(t_f)$ is the battery SOC at the end of the driving cycle and $\eta_{path}$ is the approximate efficiency of the drivetrain used in regenerating/discharging the battery. Because in a charge-sustaining HEV, the energy management strategy should ensure that the net change in battery SOC at the end of the driving cycle is close to zero, an equivalent fuel consumed ($FC_{eqv}$) is used as a performance metric. The equivalent fuel consumed is defined as the sum of the amount of fuel consumed along with a correction for the net
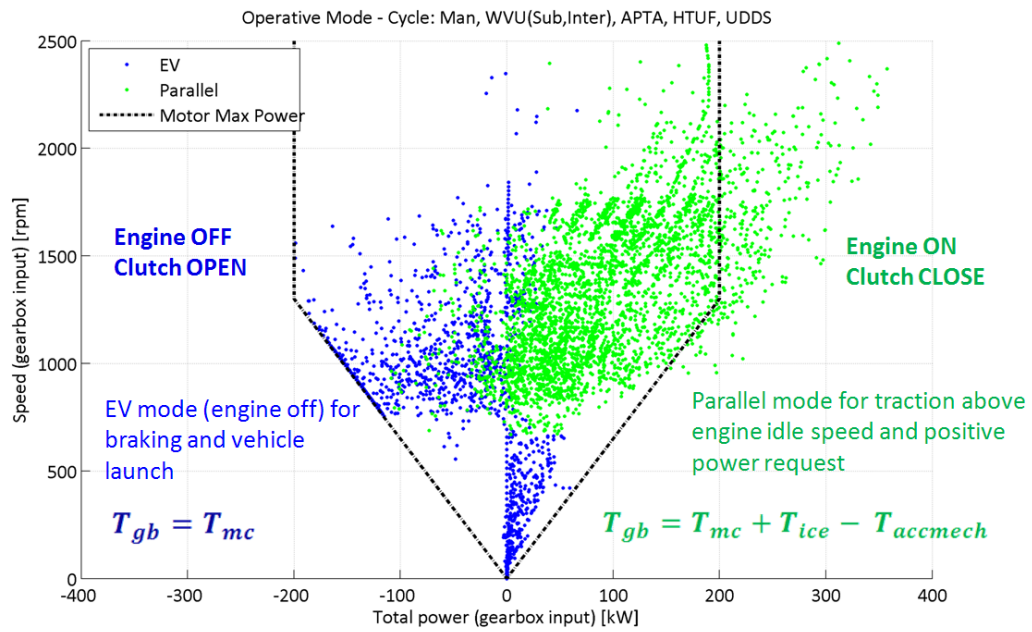
Figure 3.3: Mode selection strategy of DP
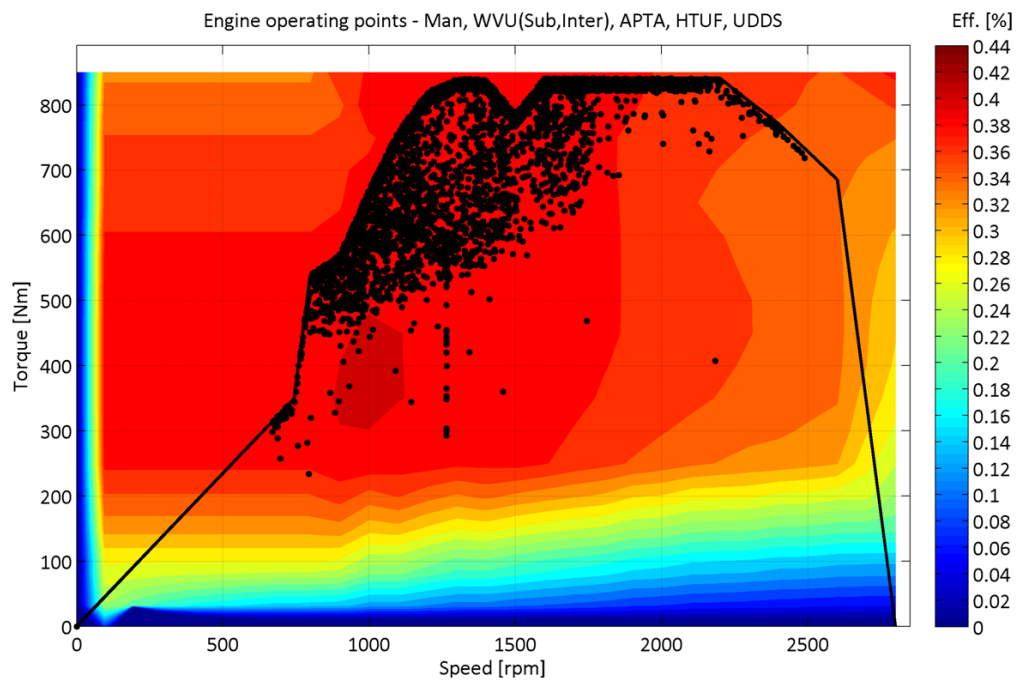


Figure 3.4: Engine operating points selected by DP
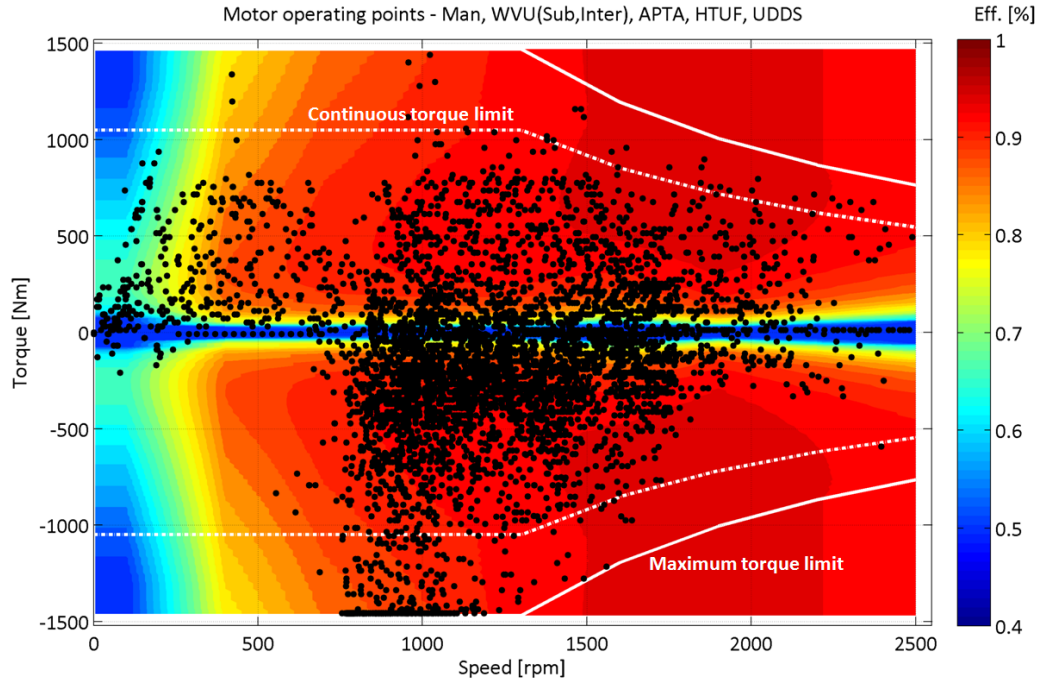
Figure 3.5: Electric motor operating points selected by DP

change in battery SOC, assuming that charging/discharging of the battery can be associated with an approximate efficiency $\eta_{path}$.

The performance metrics of the global optimal solution from DP for urban driving cycles (Manhattan, WVU-suburban, Heavy truck urban cycle (HTUF)), highway driving cycles (WVU-interstate) and a combination of highway and urban driving conditions (Urban duty driving scheme (UDDS)) are shown in Table 3.3. The DP was given complete freedom in selecting the vehicle mode of operation (electric or parallel) by selecting the engine and clutch status (see Fig. 2.1). For both the operating modes, the algorithm then decides optimal torque/power split between the engine and electric machine.

The mode selection choices made by DP shown in Fig. 3.3 indicate that there are well-defined regions of operation for the different vehicle modes. The electric mode (EV)
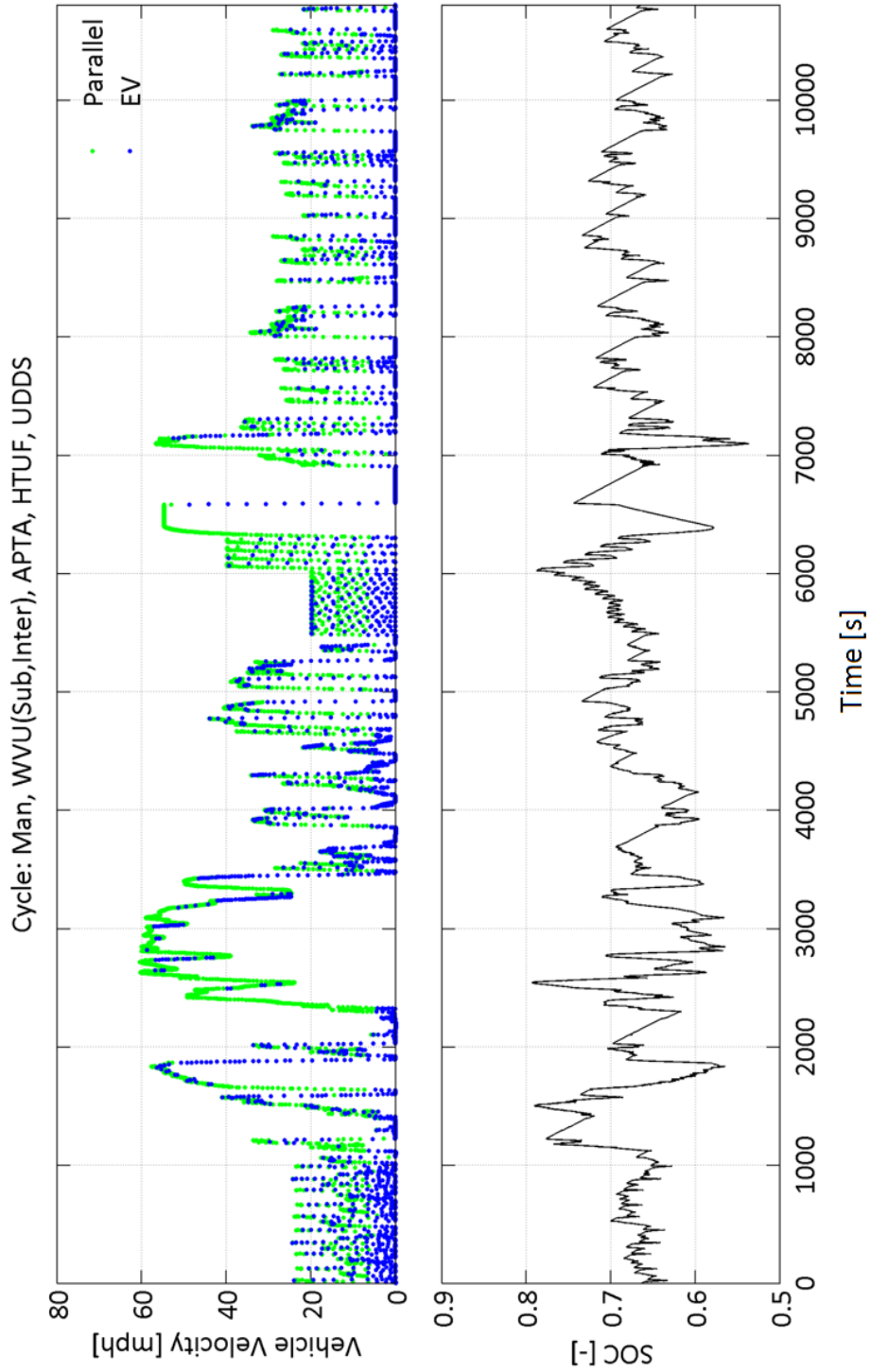
Figure 3.6: Battery SOC profile selected by DP

shown in Fig. 2.2 is chosen by DP by opening the clutch and switching off the engine predominantly during the following driving conditions:

1. **Braking/Coasting event**: If the requested gearbox power ($P_{gb}$ is negative, indicating that the vehicle is either coasting or braking, the clutch is open and engine is off. The electric machine is used as a generator to recharge the battery. This mode of operation ensures that maximum energy can be regenerated from the event.

2. **Vehicle launch**: If the gearbox speed ($\omega_{gb}$) is less than the idle speed of the engine ($\omega_{ice,idle}$), it is not efficient to operate the engine at these speeds. The DP decides to operate the vehicle in the electric mode of operation.

The parallel mode of operation (Fig. 2.4) is chosen by DP whenever the gearbox speed is greater than the engine idle speed and the gearbox torque is positive. The parallel mode of operation uses both the engine and electric motor and the points which are beyond the maximum power of the electric machine indicate that electric machine is used at its maximum limit. The engine and electric motor operating points selected by DP during all the driving cycles are shown in Fig. 3.4 and Fig. 3.5. It is evident that both the devices are operated very close to their maximum efficiency operating points.

The battery SOC profile resulting from DP for all the driving cycles is shown in Fig. 3.6. For all the driving cycles, DP clearly produces a charge sustaining solution which can also be seen from the Table 3.3. The equivalent fuel consumed ($FC_{eqv}$) for the different driving cycles is also shown in Table 3.3. Because DP results in the global optimal solution to the energy management problem, the other energy management strategies developed in the dissertation are compared against these values. Moreover, the DP based energy management strategy cannot be implemented in a real vehicle because it requires *a-priori*

knowledge of the entire driving cycle. This is the primary reason for implementing the DP algorithm using a backward vehicle simulator and the DP solution is used as a benchmark solution in HEV literature.

## 3.3 Equivalent Consumption Minimization Strategy

This section involves the design and development of equivalent consumption minimization strategy (ECMS) derived from the necessary conditions of optimality given by Pontryagin's minimum principle (PMP). Section 3.3.1 involves an overview of PMP in general and its application as an energy management strategy in HEVs. Then Section 3.3.2 derives ECMS from PMP and the simulation results for such a strategy in comparison with the global optimal solution from DP are shown in Section 3.3.3.

### 3.3.1 Overview of Pontryagin's Minimum Principle

Consider a nonlinear and possibly time varying dynamical system described by

$$\dot{x}(t) = f(x, u, t), \tag{3.19}$$

where $x(t) \in \mathbb{R}^n$ is the state variable, $u \in \mathbb{R}^p$ is the control input and $f(\cdot, \cdot, \cdot)$ is a continuously differentiable function with respect to $x$ and continuous in $u$. A certain set $U \subset \mathbb{R}^p$ of admissible values of the control input, the initial and final state is fixed $(x(t_0), x(t_f))$, the initial time $t_0$ and the final time $t_f$ is fixed. Any piecewise-continuous function $u(t) \in U, t_0 \leq t \leq t_f$ is called an admissible control if it can transfer the state trajectory from $x(t_0)$ to $x(t_f)$ where $x(t)$ is the solution of the system (3.19). The solution satisfies the initial condition $x(t_0) = x_0$ and is defined for all $t \in [t_0, t_f]$ and $x(t_f) = x_f$.

The state and control input of the system must remain, at all times, in the admissible range:

$$\begin{cases} x_{min}(t) \le x(t) \le x_{max}(t), \\ u \in \mathcal{U} : u_{min}(t) \le u(t) \le u_{max}(t). \end{cases} \tag{3.20}$$

Among all admissible controls transferring the state from the position $x_0$ to $x_f$ it is required to find an optimal control, i.e. a function $u^*(t) : [t_0, t_f] \to \mathbb{R}$ for which the functional

$$J(x, u, t) = \phi(x(t_f), t_f) + \int_{t_0}^{t_f} L(x(\tau), u(\tau), \tau)d\tau \tag{3.21}$$

is minimum with respect to $u(\cdot)$ such that the dynamics (3.19) and state constraint (3.20) are satisfied. $L(x(t), u(t), t)$ is the functional cost, $\phi(x(t_f), t_f)$ is the terminal cost. The constraints at the final time $t_f$ are given by

$$\phi(x(t_f), t_f) = 0. \tag{3.22}$$

The *cost-to-go* function is defined as the minimum cost to go from any state $x(t)$ to the final state $x(t_f)$, defined as

$$J(u) = \min_{u(\cdot)} \left( \phi(x(t_f), t_f) + \int_{t_0}^{t_f} L(x(\tau), u(\tau), \tau)d\tau \right). \tag{3.23}$$

The Hamiltonian function is introduced as

$$\mathcal{H}(x, u, t) = L(x(t), u(t), t) + \lambda^T f(x, u, t), \tag{3.24}$$

where $L(x, u, t)$ is the instantaneous cost function and $\lambda(t)$ is the Lagrange multiplier used to include the constraints on the system dynamics. $\lambda(t)$ is also called the *co-state* of the system. In order to solve the optimal control problem while minimizing the cost function $J(u(\cdot))$ while satisfying the state and control input constraints, Pontryagin's Minimum Principle is used [64]. The necessary conditions that must be satisfied by any optimal control law are explained in detail.

Let $u^*(t) : [t_0, t_f] \to \mathbb{R}$ be an optimal control trajectory and let $x^*(t) : [t_0, t_f] \to \mathbb{R}$ be the corresponding state trajectory, i.e.,

$$\dot{x}^*(t) = f(x^*(t), u^*(t)), \quad x^*(t_0) = x(0). \tag{3.25}$$

Let $\lambda(t)$ be the solution of the co-state equation

$$\dot{\lambda}(t) = -\frac{\partial H(x^*(t), u^*(t), \lambda(t))}{\partial x}, \tag{3.26}$$

with the boundary condition

$$\lambda(t_f) = \frac{\partial \phi(x^*(t_f), t_f)}{\partial x}, \ t = t_f, \tag{3.27}$$

where $\phi(\cdot)$ is the terminal cost function. Then, $\forall t \in [t_0, t_f]$,

$$u^*(t) = \min_{u \in \mathcal{U}} \mathcal{H}(x^*(t), u, \lambda(t)). \tag{3.28}$$

Furthermore, if the Hamiltonian function $H(\cdot, \cdot, \cdot)$ is not an explicit function of time, there exists a constant $c$ such that

$$\mathcal{H}(x^*(t), u^*(t), \lambda(t)) = c, \quad \forall t \in [t_0, t_f]. \tag{3.29}$$

In other words, Pontryagin's Minimum Principle states that the optimal state trajectory $x^*$, optimal control $u^*$ and the corresponding Lagrange multiplier $\lambda^*$ must minimize the Hamiltonian $\mathcal{H}$ so that

$$\mathcal{H}(x^*(t), \lambda^*(t), u^*(t)) < \mathcal{H}(x^*(t), \lambda^*(t), u(t)) \tag{3.30}$$

is satisfied $\forall t \in [t_0, t_f]$ and $\forall u \in \mathcal{U}$ in the admissible control set.

These are only the necessary conditions (not sufficient) for any optimal control law. The set of control laws that satisfy these conditions are known as the *extremal* solutions to

the control problem. If the optimal solution exists, then it is also extremal. The opposite, however, is not true: a solution may be extremal without being optimal. If the optimal control law is unique, these conditions provide an explicit way of finding the optimal control law. Thus finding the optimal control input $u^*$ using these necessary conditions, involves solving two nonlinear differential equations ((3.25, 3.26)) with boundary conditions on $x^*(t_0), \lambda(t_f)$.

The HEV energy management problem shown in Section 3.1 minimizes the fuel consumed over the driving cycle, satisfying the constraints on engine, electric motor and battery. The corresponding Hamiltonian function is [4]:

$$\mathcal{H}(SOC, P_{batt}, \lambda) = \dot{m}_f(P_{batt}) + \lambda f_{SOC}(SOC, P_{batt}), \qquad (3.31)$$

where $\dot{m}_f(P_{batt})$ is the engine fuel consumption rate expressed as a function of battery power and $f_{SOC}(SOC, P_{batt})$ is the nonlinear mapping of $SOC$ and $P_{batt}$ used to calculate battery SOC dynamics ($\dot{SOC}$). The engine fuel consumption rate, $\dot{m}_f$, which is typically a function of engine speed and torque (2.9), is expressed as a function of the control input $P_{batt}$ (2.12).

The optimal battery SOC ($SOC^*$) and control input $P_{batt}^*$ satisfy the constraints on the state and control input as seen in equations (3.2) - (3.7). Consider the *optimal* co-state $\lambda^*$ which satisfies the dynamic equation

$$\begin{cases} \dot{\lambda}^* = -\frac{\partial \mathcal{H}(SOC^*, P_{batt}^*, \lambda^*)}{\partial SOC}, \\ = -\lambda^* \frac{\partial f_{SOC}(SOC^*, P_{batt}^*)}{\partial SOC}. \end{cases} \qquad (3.32)$$

Then $P_{batt}^*(t)$ minimizes the Hamiltonian function and hence the fuel consumed over the driving cycle, i.e.,

$$\mathcal{H}(SOC^*, \lambda^*, P_{batt}^*) < \mathcal{H}(SOC^*, \lambda^*, P_{batt})), \qquad (3.33)$$

[4]For ease of representation, we suppress time dependence for the variables.

is satisfied $\forall t \in [t_0, t_f]$ and $\forall P_{batt} \in \mathcal{U}$ in the admissible control set. In order to find the optimal control input $P_{batt}^*(t)$ that minimizes the fuel consumed over the driving cycle, the SOC dynamics and the co-state variable dynamics must be solved. The boundary condition for SOC dynamics is the initial value of SOC ($SOC_{init}$), while the co-state variable can take any initial value. This gives a set of extremal control laws that might satisfy the necessary conditions. The optimal initial value $\lambda_0^*$ (depends on the driving cycle) is the one that satisfies the terminal constraint on SOC for charge-sustainability. Because the optimal initial value of $\lambda$ ($\lambda_0^*$) depends on the complete knowledge of the driving cycle, the energy management strategy based on PMP cannot be implemented in a real-vehicle. In order to leverage the extensive amount of work in the HEV literature on equivalent consumption minimization strategy, a version of ECMS that has been formulated based on PMP [16, 17] is used in this dissertation.

### 3.3.2 ECMS based on PMP

The equivalent consumption minimization strategy (ECMS) is based on the engineering intuition that in a charge sustaining HEV, the energy that is used to propel the vehicle, even if it is supplied by the battery, must eventually come from the fuel [15, 20, 19]. Hence the amount of fuel consumed during a driving cycle also includes an *electrical* fuel consumption which is equivalent to the amount of energy used from the battery. The sum of actual fuel consumption rate and electrical fuel consumption rate is known as the equivalent fuel consumption rate expressed as,

$$\dot{m}_{f,eqv} = \dot{m}_f + \dot{m}_{f,elec} = \dot{m}_f + s\frac{P_{batt}}{Q_{LHV}}, \tag{3.34}$$

where $\dot{m}_{f,eqv}$ is the equivalent fuel rate, $s(t)$ is the *equivalence factor* between the electric energy and the fuel, and $Q_{lhv}$ is the lower heating value of the fuel. The amount of

equivalent fuel consumed ($m_{f,eqv}$) over the driving cycle is minimized to solve the energy management problem. The global optimization problem over an entire driving cycle is reduced to a local minimization problem where the equivalent fuel consumed is minimized at each instant. In this formulation of ECMS, the equivalent fuel consumption rate is expressed as a function of the equivalence factor $s(t)$, battery power at the terminals $P_{batt}$ and lower heating calorific value of the fuel $Q_{LHV}$. Because this formulation does not account for the inefficiency in transforming the battery energy into fuel and vice versa, the losses involved are lumped into the equivalence factor $s(t)$. This is the primary reason for having two different equivalence factors ($s_{chg}, s_{dis}$), one for charging and one for discharging the battery [20]. In order to reduce the number of calibration parameters, an equivalent but alternative formulation for ECMS is shown in [58, 17]. According to this formulation the equivalent fuel consumption rate can be expressed as

$$\dot{m}_{f,eqv} = \dot{m}_f + \dot{m}_{f,elec} = \dot{m}_f + s\frac{P_{batt,chem}}{Q_{LHV}}, \tag{3.35}$$

where $P_{batt,chem}$ is the available chemical battery power (includes the efficiency of the battery). Using the expression for $P_{batt,chem}$ as a function of $V_{oc,max}$ and battery current $I$, the equivalent fuel consumption rate can be re-formulated as

$$\begin{cases} P_{batt,chem} = V_{oc,max}I, \\ \dot{m}_{f,eqv} = \dot{m}_f + s\frac{V_{oc,max}I(t)}{Q_{LHV}}, \end{cases} \tag{3.36}$$

where $\eta_{batt}$ is the approximate efficiency of the battery, $V_{oc,max}$ is the constant open-circuit voltage of the battery and $I(t)$ is the battery current flowing in and out of the battery.

The Hamiltonian function developed using PMP can be expressed as a function of the battery current ($I(t)$) using (2.18) as

$$\begin{aligned} \mathcal{H}(SOC, P_{batt}, \lambda) &= \dot{m}_f(P_{batt}) + \lambda \dot{SOC}, \\ &= \dot{m}_f - \lambda\frac{\alpha I(t)}{Q_{max}}. \end{aligned} \tag{3.37}$$

64

Now, using the relation between the maximum capacity of the battery ($Q_{max}$) and the maximum energy capacity ($E_{max}$), $Q_{max} = \frac{E_{max}}{V_{oc,max}}$, the Hamiltonian function can be expressed in the manner

$$\mathcal{H}(SOC, P_{batt}, \lambda) = \dot{m}_f - \lambda \frac{\alpha I(t) V_{oc,max}}{E_{max}}. \tag{3.38}$$

Comparing the equations (3.36) and (3.38), the equivalence factor $s(t)$ can be expressed as a function of the co-state variable $\lambda(t)$ in the manner

$$s(t) = -\lambda(t) \frac{Q_{lhv}}{E_{max}}. \tag{3.39}$$

The Hamiltonian function (equation (3.31)) physically represents the equivalent fuel consumption and the co-state variable represents the equivalence between the battery and fuel use. This can be shown in the ECMS formulation as:

$$\begin{aligned} \mathcal{H}(SOC, P_{batt}, s) &= \dot{m}_{eqv}(SOC, P_{batt}, s) \\ &= \dot{m}_f(P_{batt}) - s(t) \frac{E_{max}}{Q_{lhv}} f_{SOC}(SOC, P_{batt}). \end{aligned} \tag{3.40}$$

This Hamiltonian function is to be minimized at every instant during the entire driving cycle and the optimal battery power is calculated. Depending on the mode of operation in a pre-transmission parallel HEV (electric, parallel with neutral gear and parallel), the local optimization is performed at each instant to find the optimal torque/power split. The difference between the original formulation of ECMS [19] as shown in equation (3.34) and the Hamiltonian function as seen in equation (3.40) is that in the former formulation, the equivalence factor represents the chain of inefficiencies involved in the transformation of the fuel to electric power and vice-versa, and it changes for each operating condition of the powertrain. In equation (3.40), instead, the inefficiencies involved in the conversion are included in the nonlinear mapping of the battery dynamics and the equivalence factor acts as a single tunable parameter of the system. The dynamics of the equivalence factor $s(t)$ is

obtained by substituting equation (3.39) into equation (3.32):

$$\dot{s}(t) = -s(t) \frac{Q_{lhv}}{E_{max}} \frac{\partial f_{SOC}(SOC, P_{batt})}{\partial SOC}. \tag{3.41}$$

In general, based on PMP formulation, the equivalence factor $s(t)$ is a dynamic variable which satisfies (3.41) whose initial value ($s_0$) is free to be chosen. If the battery model used is a zero-*th* model as shown in Fig. 2.19 and the circuit model parameters ($R_{eq}, V_{oc}$) are assumed independent of SOC, then $s$ is time-invariant during the driving cycle. In the implementation, $s(t)$ is considered time varying because the computational load introduced by the differential equation is negligible. Thus the single tuning parameter is the initial value of equivalence factor $s_0$.

In order to ensure charge sustainability over any driving cycle, a penalty function $p(SOC)$ [19, 20, 58, 17, 32] is included the Hamiltonian function that is minimized at each time step. The new Hamiltonian function which represents the equivalent fuel consumption rate is expressed as

$$\mathcal{H}(SOC, P_{batt}, s) = \dot{m}_f(P_{batt}) - s(t) \frac{E_{max}}{Q_{lhv}} p(SOC) f_{SOC}(SOC, P_{batt}). \tag{3.42}$$

The penalty function $p(SOC)$ a nonlinear function of $SOC$ which corrects the Hamiltonian function whenever the $SOC$ deviates from $SOC_{ref}$. As seen from Fig. 3.7, the penalty is negligible whenever $SOC$ is close to the reference value and increases nonlinearly as the SOC deviates from its reference. This function is crucial in ensuring a charge-sustainable solution from ECMS derived from PMP; that is,

$$\begin{aligned}
p(SOC) &= 1 + \left( \frac{SOC_{ref} - SOC}{SOC_{ref} - SOC_{min}} \right)^{n_{SOC}} &\forall\, SOC < SOC_{ref}, \\
p(SOC) &= 1 &\forall\, SOC = SOC_{ref}, \\
p(SOC) &= 1 + \left( \frac{SOC_{ref} - SOC}{SOC_{max} - SOC_{ref}} \right)^{n_{SOC}} &\forall\, SOC > SOC_{ref},
\end{aligned} \tag{3.43}$$

where $SOC_{min}, SOC_{max}$ represent the minimum and maximum SOC, typically 50% and 80%, respectively, and $n_{SOC}$ is the exponential coefficient governing the shape of the
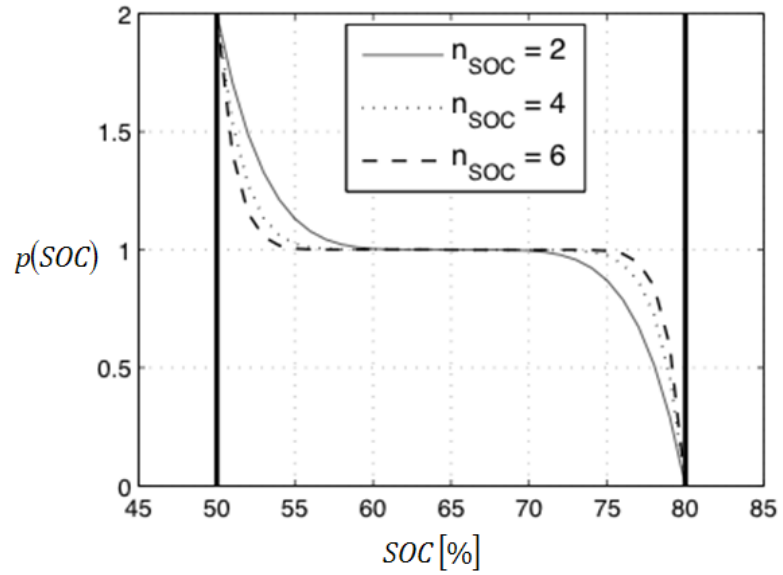
Figure 3.7: Penalty function used in ECMS based on PMP

penalty function. The ECMS derived from PMP consists of minimizing the Hamiltonian function at each time step respecting the constraints on the battery SOC, battery power, equivalence factor and other instantaneous constraints. The global optimization problem is transformed into a local problem and the single calibration parameter is $s_0$. Since the evolution of the battery $SOC$ depends on the value of $s(t)$, it is possible to find an appropriate initial value $s_0$ such that the terminal constraint ((3.3)) is satisfied. In other words, there is a value of $s_0$ for which the solution is perfectly charge-sustaining and is defined as the *optimal* equivalence factor for that particular driving cycle.

### 3.3.3 Simulation Results

This subsection describes the simulation environment used to implement the ECMS developed using Pontryagin's Minimum Principle (Section 3.3.2) and its performance compared to the global optimal solution obtained from DP (Section 3.2). The pre-transmission parallel HEV (Fig. 2.1) is modeled in the MATLAB/Simulink environment. The characteristics of the vehicle used here are shown in Table 2.1. In order to compare the performance of ECMS with the optimal global solution obtained from dynamic programming, backward vehicle simulator (Section 2.2.2) is used. Based on the assumption that the vehicle follows the desired velocity trajectory, the torque required at the wheels and subsequently the torque/speed required from the components are calculated (Fig. 2.22). The simulator primarily uses simplified quasi-static map based models for all the components as shown in Table 2.2.

**Calibration of parameter-$s_0$**

The ECMS derived from PMP has one tuning parameter $s_0$ which is directly related to the co-state $\lambda$ of the PMP solution as shown in (3.39). The equivalence factor $s$ has to satisfy the dynamic equation (3.41), whose initial value $s_0$ can be independently selected. As shown in the numerous papers on ECMS [19, 20, 13, 17], there is a direct correlation between $s_0$ and the battery SOC usage during any driving cycle. The effect of the calibration parameter $s_0$ is shown in Fig. 3.8. As seen from these plots, the value of $s_0$ impacts the convergence of $SOC$ to $SOC_{ref}$ at the end of the driving cycle. The optimal value of $s_0$ is selected based on the equivalent fuel consumed ($FC_{eqv}$) defined in (3.18). The effects of using different values of $s_0$ are summarized in Table 3.4. The *optimal* value of $s_0$ ensures
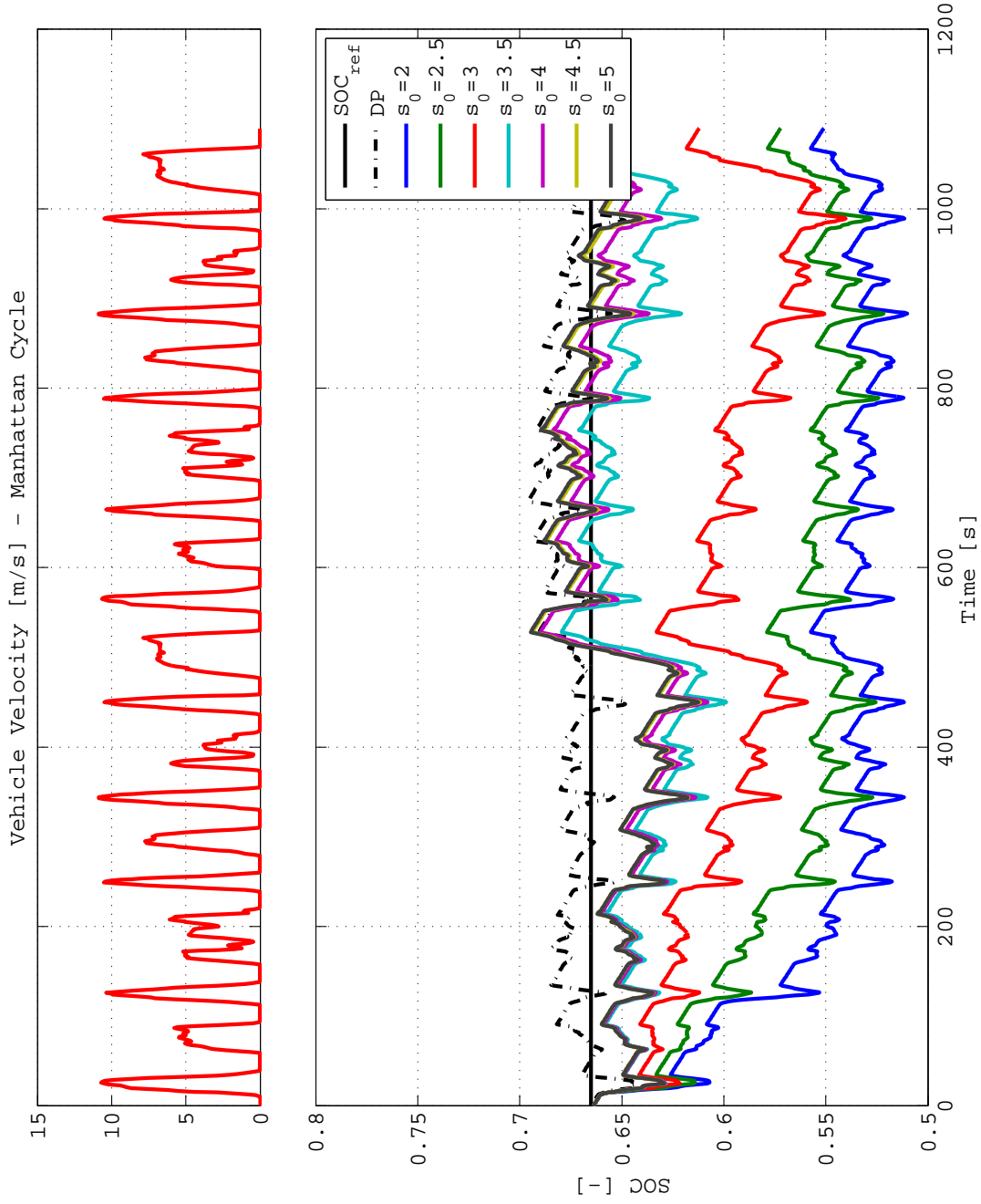
Figure 3.8: Effect of $s_0$ on $SOC$

69

convergence of SOC to the reference value $SOC_{ref}$ while consuming the least amount of fuel over the driving cycle.

Table 3.4: Effect of $s_0$ for Manhattan driving cycle

| Strategy | $s_0$ [-] | Normalized $FC_{eqv}$ [%] |
|---|---|---|
| ECMS based on PMP | 2 | 108.3 |
| | 2.5 | 107.1 |
| | 3 | 106.5 |
| | 3.5 | 104.1 |
| | 4 | 105.8 |
| | 4.5 | 106.3 |
| | 5 | 106.8 |
| DP | - | 100 |

**Performance for Manhattan driving cycle**

Table 3.5: Performance comparison with DP for Manhattan driving cycle

| Strategy | Normalized $FC_{eqv}$ [%] |
|---|---|
| ECMS based on PMP($s_0^* = 3.3$) | 102.6 |
| DP | 100 |

The calibration parameter $s_0$ of the control law is optimized for the Manhattan driving cycle by selecting the value of $s_0$ that corresponds to the minimum value of $FC_{eqv}$. In order to find the optimal $s_0$ ($s_0^*$) for each driving cycle, an iterative shooting method is used [17]. The results of such a shooting method are shown in Table 3.5. The performance of
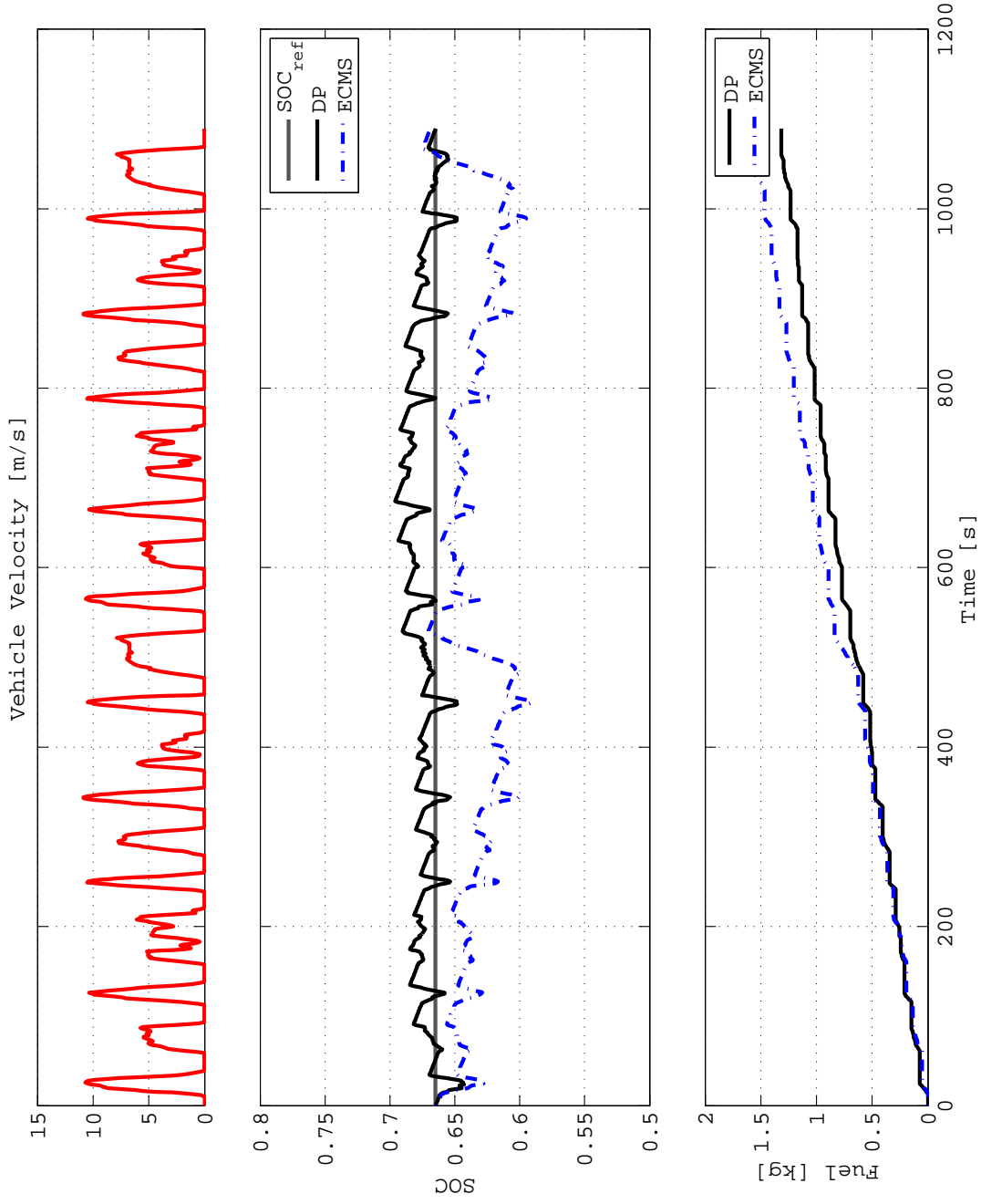
Figure 3.9: Velocity, SOC and equivalent fuel consumed (Manhattan)
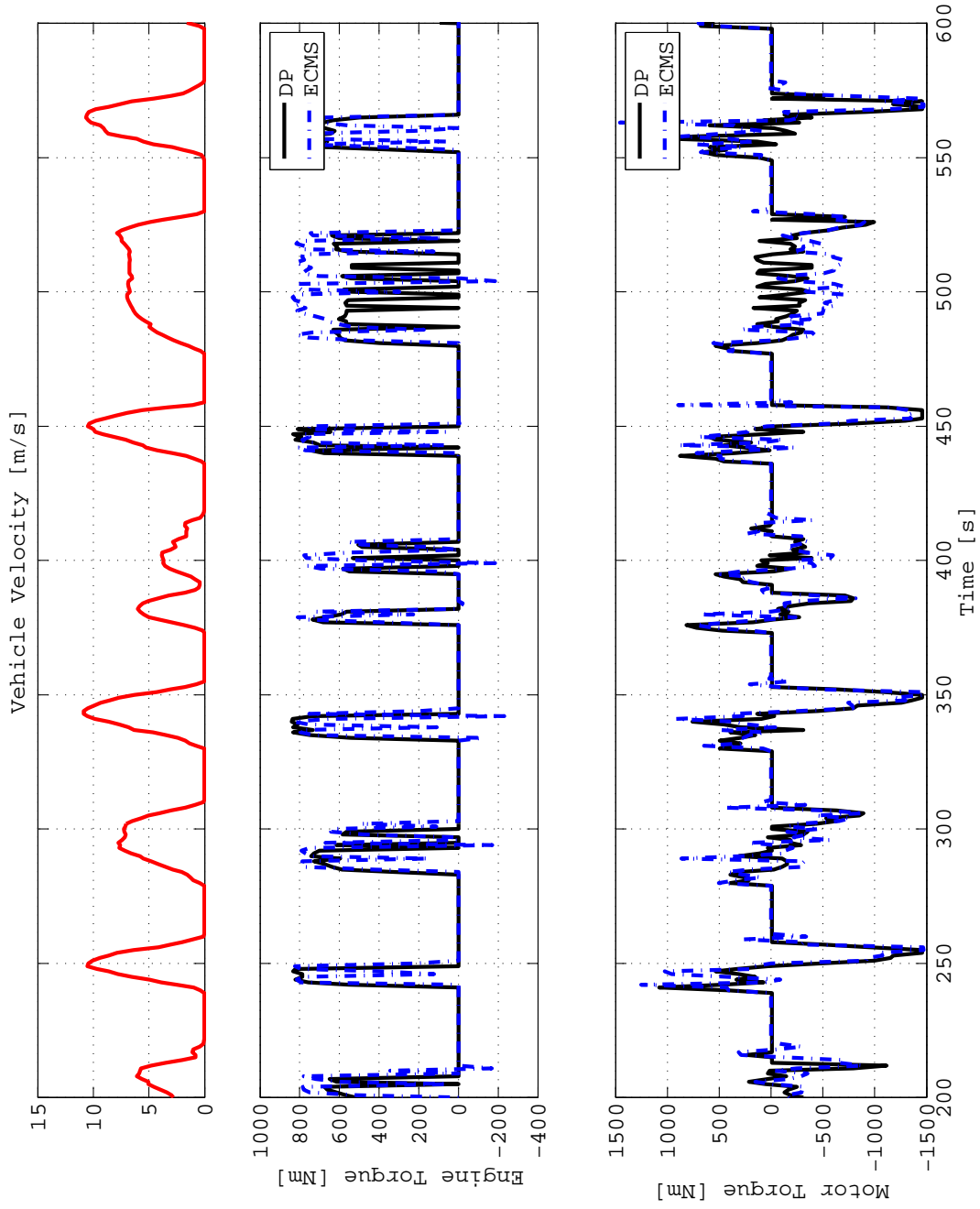
Figure 3.10: Velocity, engine and electric motor torques - detail (Manhattan)
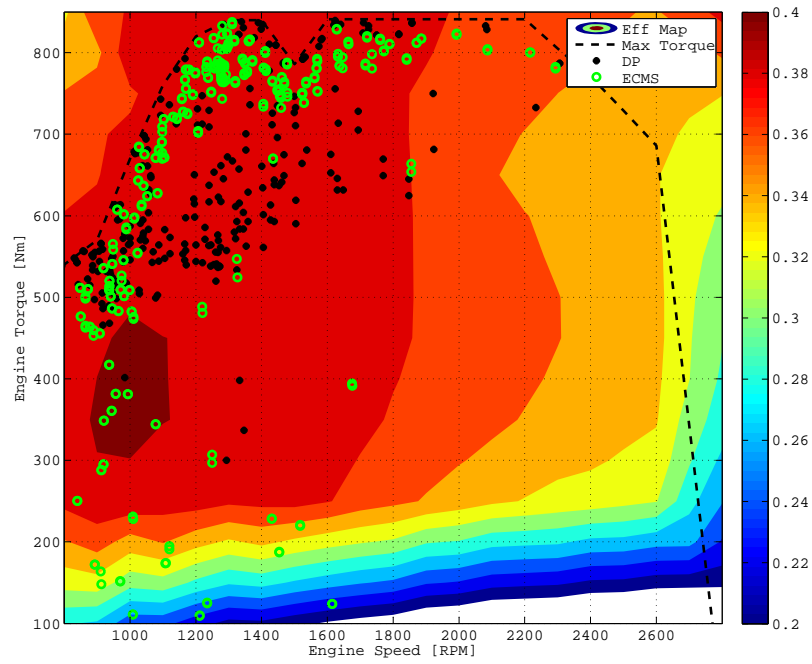
Figure 3.11: Engine operating points (Manhattan)
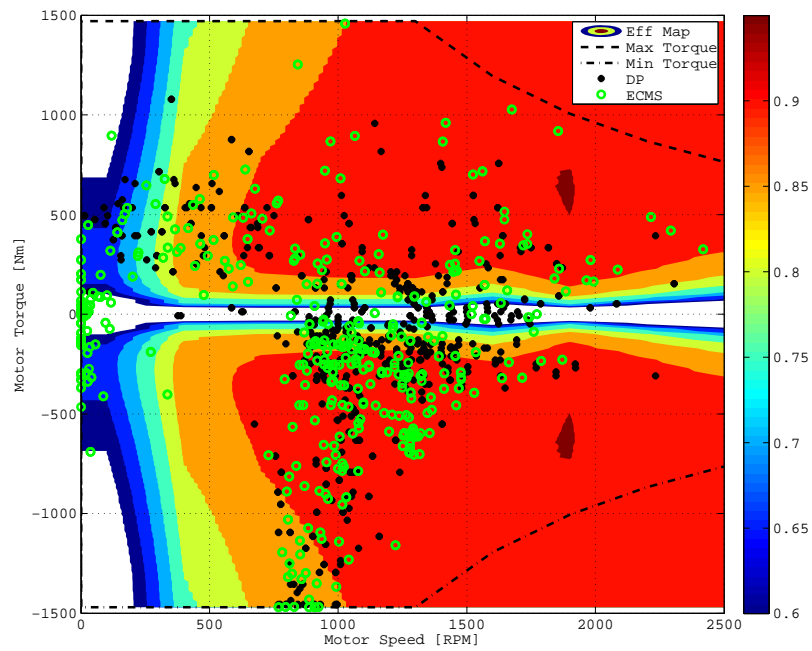


Figure 3.12: Electric motor operating points (Manhattan)

ECMS based on PMP with the optimum value of $s_0$ is evaluated against the global optimal solution obtained from DP and is shown in Figures 3.9 - 3.12.

The ECMS strategy (with $s_0^*$) consumes 3% more fuel than the global optimal solution and uses the battery SOC similar to the DP solution throughout the driving cycle. Because DP has the knowledge of the entire driving cycle, it charges the battery above the $SOC_{ref}$ and uses the battery whenever needed. ECMS, on the other hand, minimizes the Hamiltonian function at each instant and results first in battery discharge, and then recharge to the reference value. The engine and electric motor torque resulting from the ECMS based on PMP and DP are compared in Fig. 3.10 which shows that the torque split choices of ECMS are very close to DP. The excessive change in engine torque is a characteristic of the instantaneous minimization performed by ECMS. The engine and electric motor are operated mainly in their most efficient regions similar to the DP solution as shown in Fig. 3.11 and Fig. 3.12. In general, ECMS operates the engine closer to its maximum torque curve which indicates the use of the engine to recharge the battery in addition to propelling the vehicle.

In order to evaluate the performance of the ECMS for different driving conditions, the simulation results for WVU-Interstate, WVU-Suburban, UDDS truck and APTA driving cycles are shown in the following subsections.

**Performance for WVU-Interstate driving cycle**

This section describes the performance of the ECMS based on PMP applied to the WVU-Interstate driving cycle, which is representative of the highway driving conditions experienced by heavy-duty HEVs. The performance of the ECMS based on PMP in comparison with the global optimal solution from DP is shown in Figures 3.13 - 3.16 and Table 3.6. The ECMS strategy consumes approximately 4% more than DP, evident from the huge
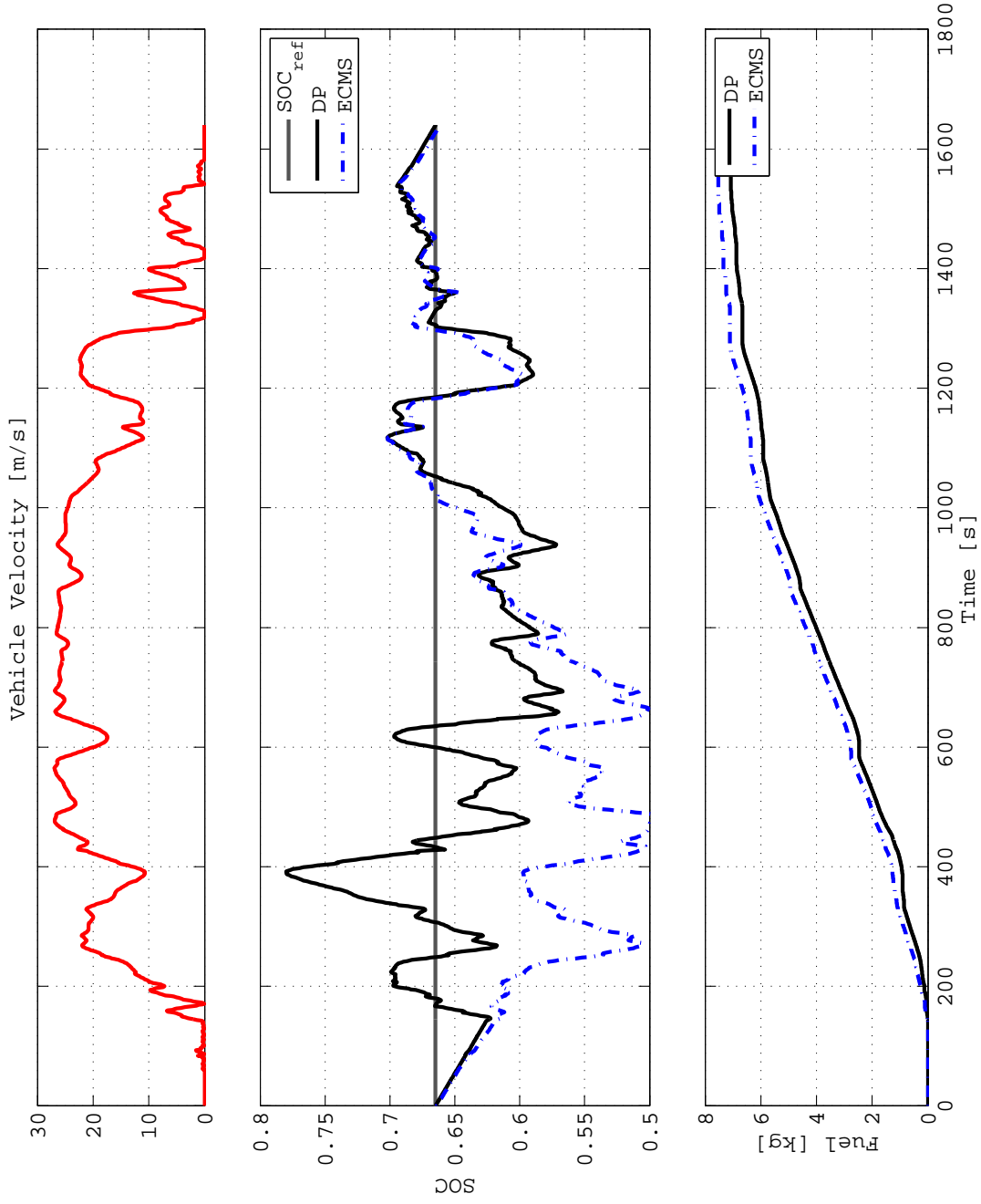
Figure 3.13: Velocity, SOC and equivalent fuel consumed (WVU-Interstate)
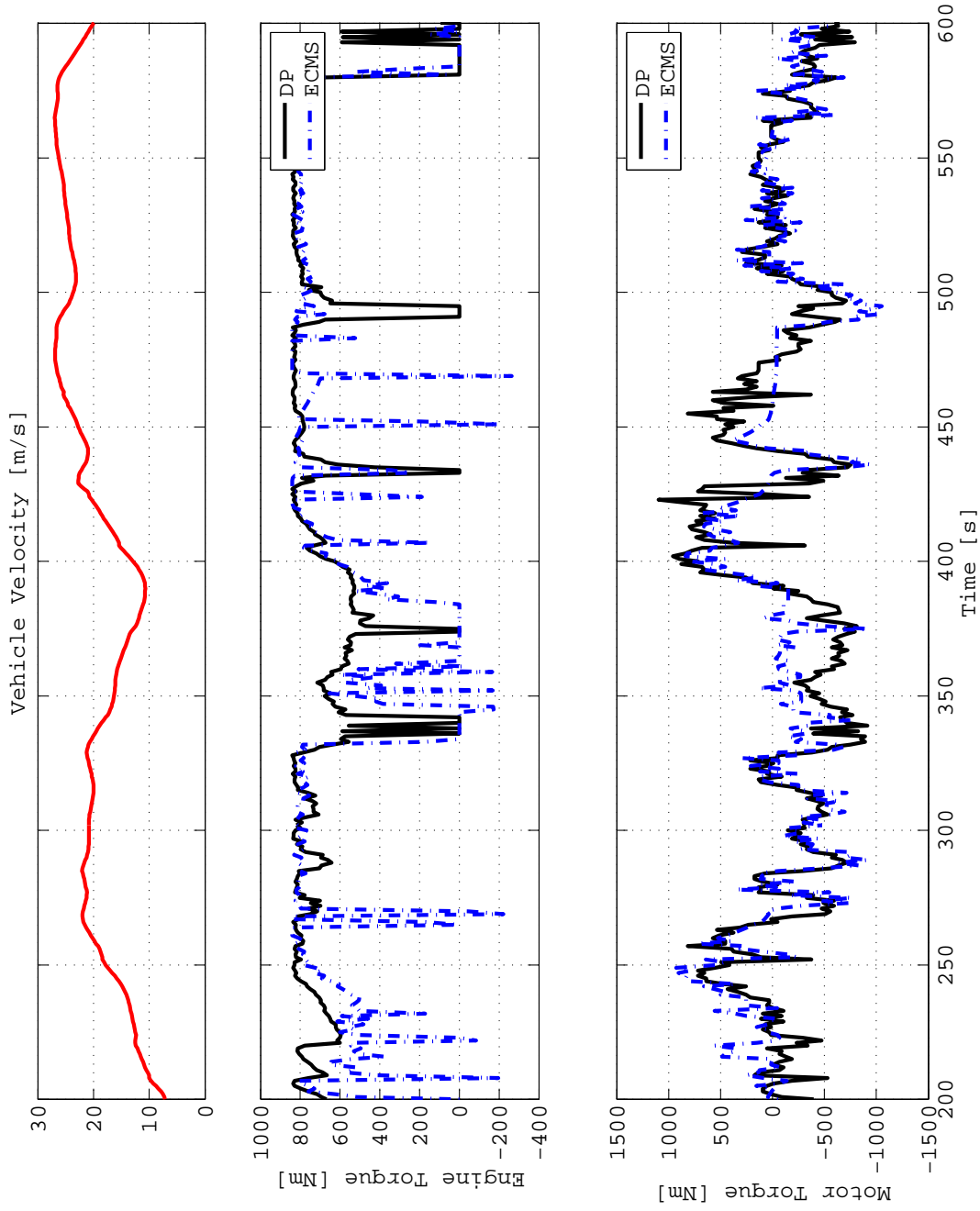
Figure 3.14: Velocity, engine and electric motor torques - detail (WVU-Interstate)
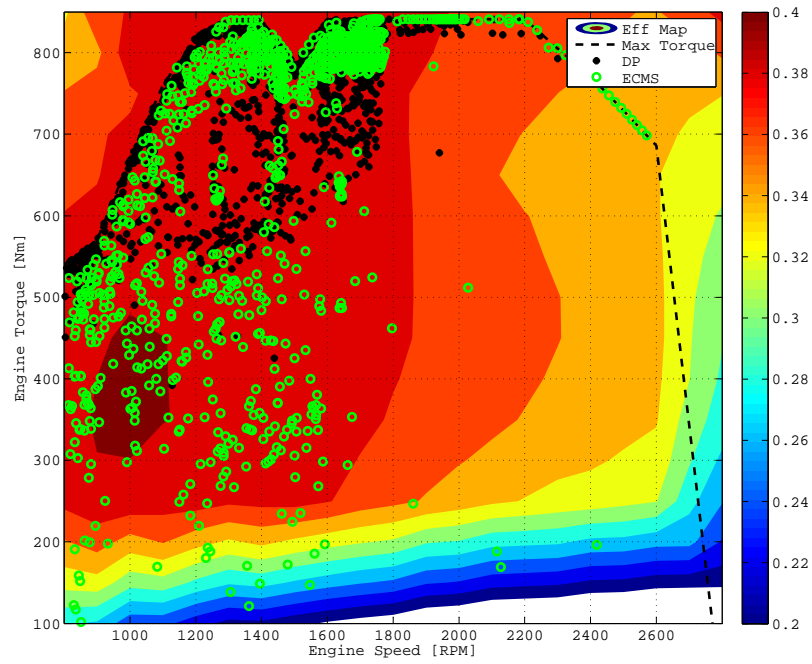
Figure 3.15: Engine operating points (WVU-Interstate)
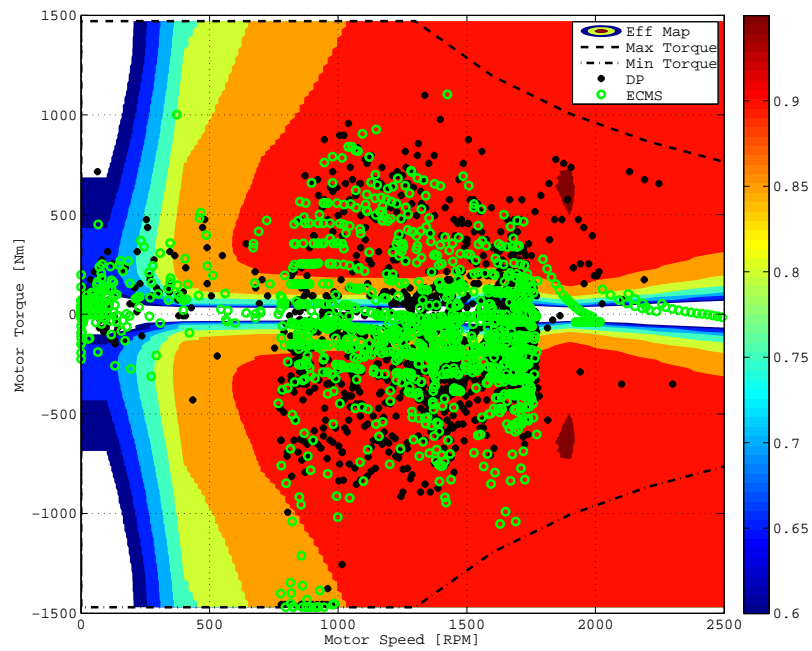


Figure 3.16: Electric motor operating points (WVU-Interstate)

Table 3.6: Performance comparison with DP for WVU-Interstate driving cycle

| Strategy | Normalized $FC_{eqv}$ [%] |
|---|---|
| ECMS based on PMP ($s_0^* = 2.82$) | 103.9 |
| DP | 100 |

difference in battery SOC usage. The strategy initially uses the battery more and because of the penalty function and the equivalent fuel, the battery is recharged to the reference value. The sudden change in engine torque during the higway portion of the driving cycle as seen in Fig. 3.14 is the cause for several operating points in the lesser efficient regions (Fig. 3.15). The electric machine operating points resulting from ECMS are close to DP.

**Performance for WVU-Suburban driving cycle**

Table 3.7: Performance comparison with DP for WVU-Suburban driving cycle

| Strategy | Normalized $FC_{eqv}$ [%] |
|---|---|
| ECMS based on PMP ($s_0^* = 4.56$) | 102.8 |
| DP | 100 |

The ECMS strategy is compared with DP in Figures 3.17 - 3.20 and Table 3.7 for the WVU-suburban driving cycle, which represents suburban driving conditions experienced by heavy-duty HEVs. ECMS uses the battery within a band very close to DP, but the SOC profiles of the two strategies are significantly different in the first half of the driving cycle. During the driving cycle, the engine switches on/off more frequently than DP which
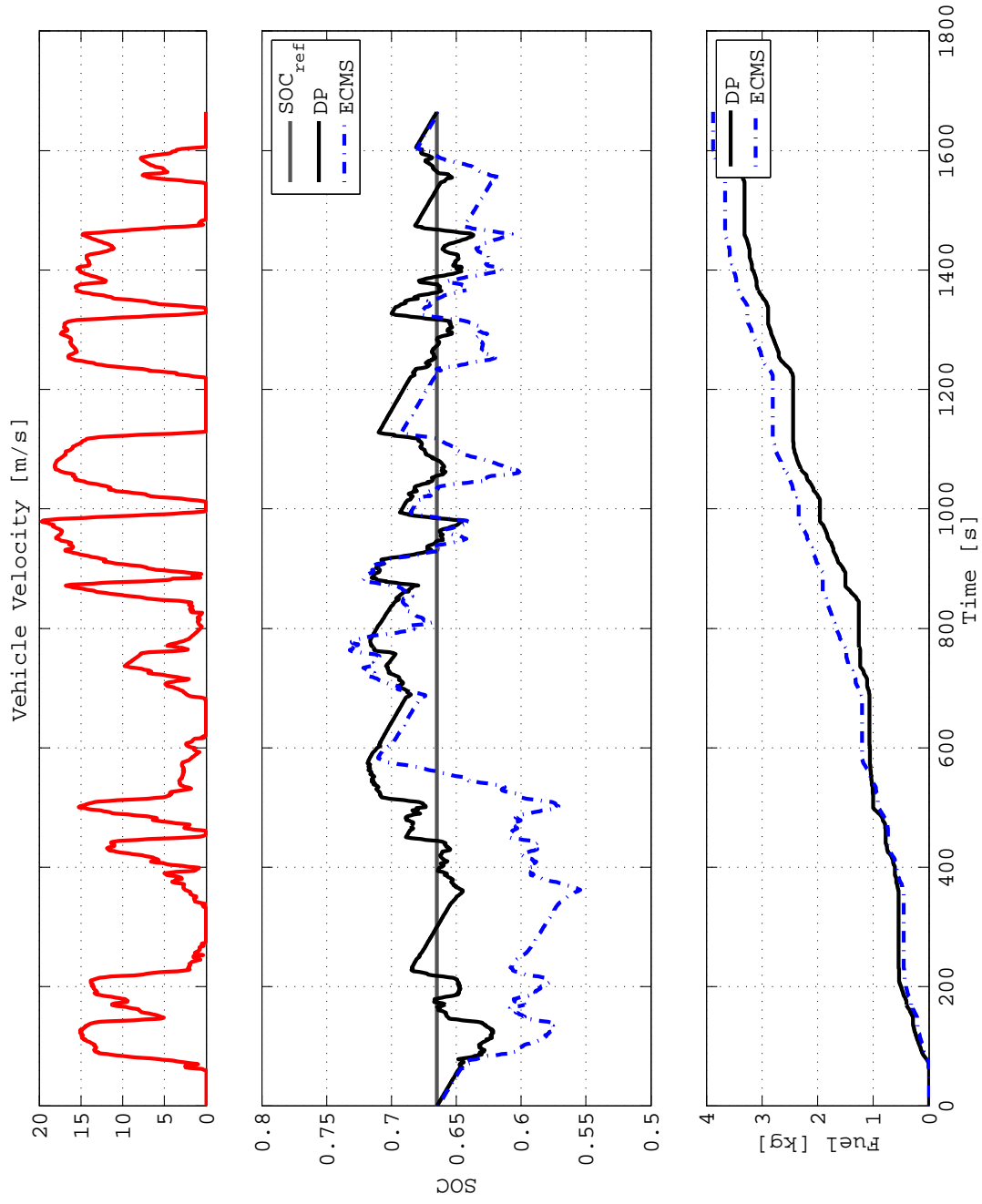
Figure 3.17: Velocity, SOC and equivalent fuel consumed (WVU-Suburban)
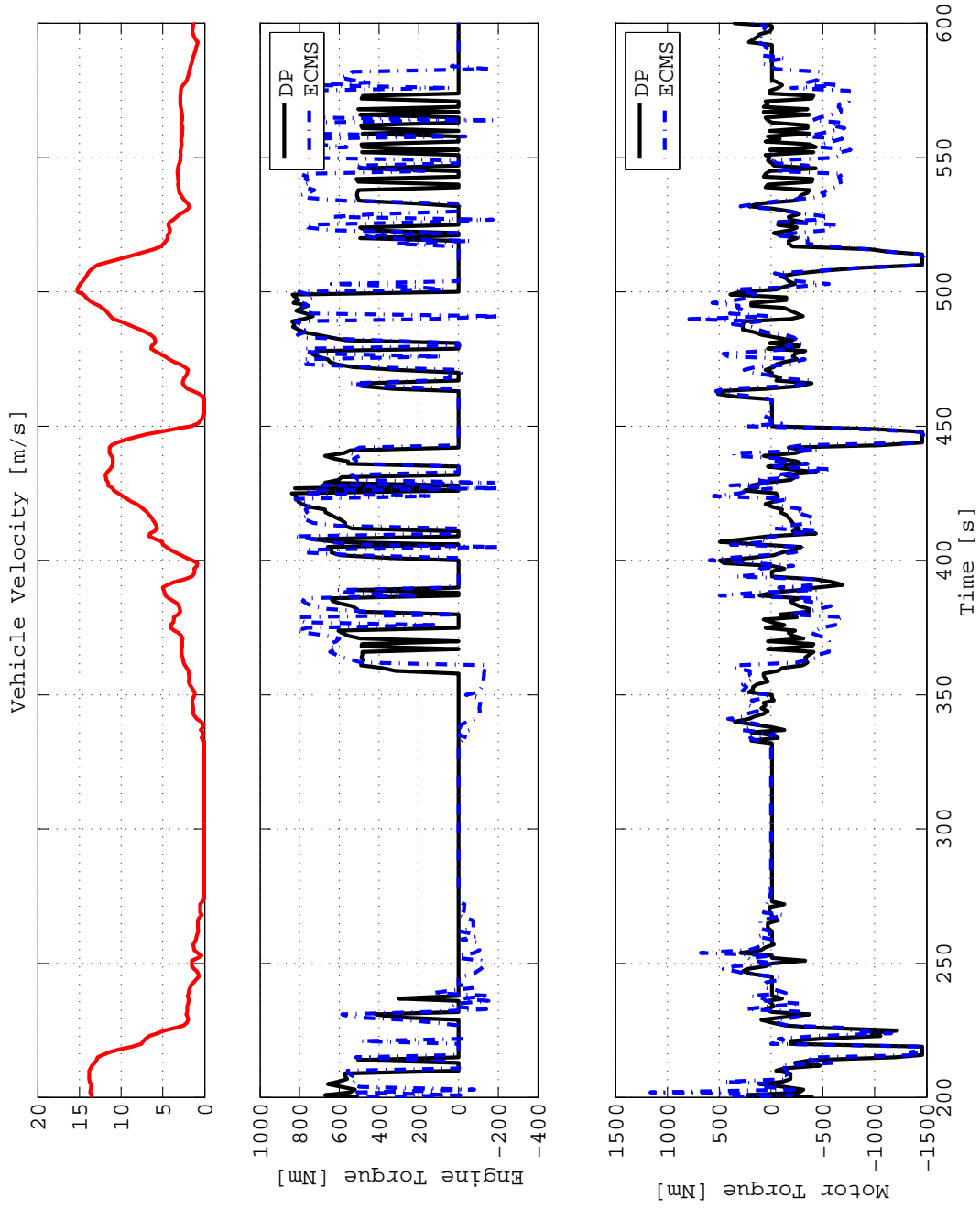
Figure 3.18: Velocity, engine and electric motor torques - detail (WVU-Suburban)
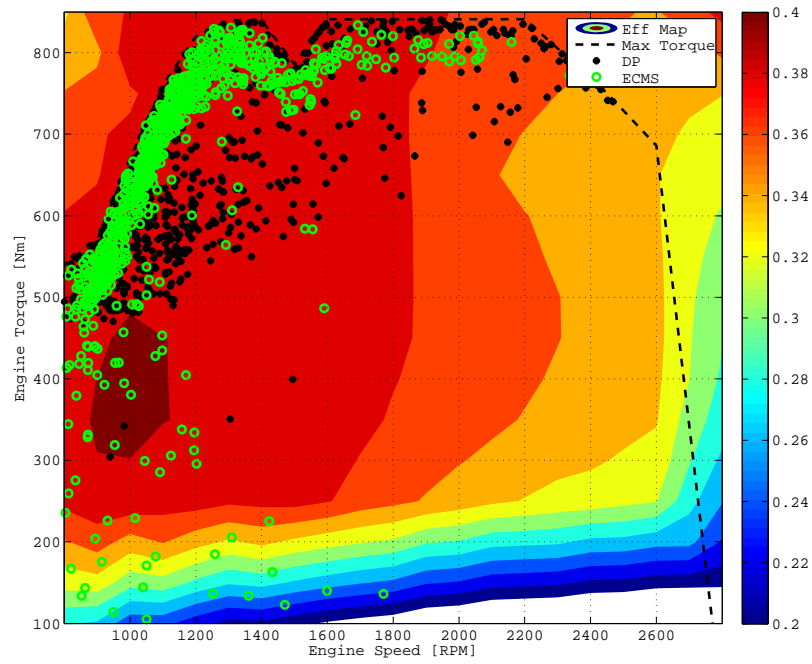
Figure 3.19: Engine operating points (WVU-Suburban)
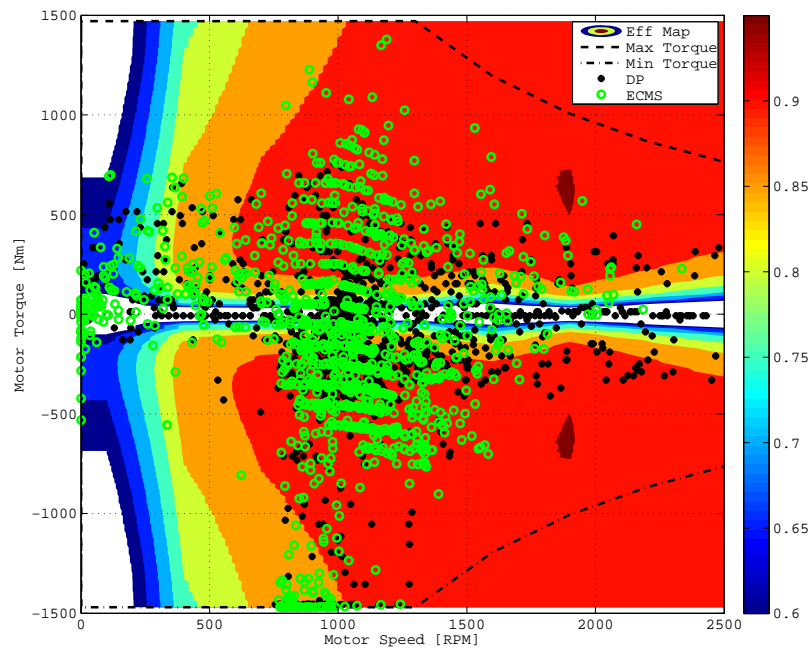


Figure 3.20: Electric motor operating points (WVU-Suburban)

81

results in less efficient operation of the engine and the electric motor. This accounts for the

increased amount of fuel consumed (4.4%) for this particular driving cycle.

**Performance for UDDS driving cycle**

Table 3.8: Performance comparison with DP for UDDS driving cycle

| Strategy | Normalized $FC_{eqv}$ [%] |
|---|---|
| ECMS based on PMP ($s_0^* = 12.65$) | 106.5 |
| DP | 100 |

This driving cycle is representative of the urban driving conditions experienced by

heavy-duty HEVs, which is generally a combination of city and highway driving. For

example, a school bus would undergo similar driving patterns throughout its life time. The

performance of the ECMS in comparison with DP is shown in Figures 3.21 - 3.24 and Ta-

ble 3.8. The battery SOC used by ECMS is significantly different from the DP solution,

which is also evident from the engine and electric motor torques shown in Fig. 3.22. This

accounts for the difference in the amount of fuel consumed (6.5%) betweeen ECMS and

DP for this driving cycle.

**Sensitivity of ECMS based on PMP with $s_0$**

Because the optimality properties of ECMS based on PMP depends on the *optimal*

value of $s_0$, it is important to study the sensitivity of the results to $s_0$.The effect of different

values of $s_0$ is shown in Fig. 3.25. For all the driving cycles, there is a single value

of $s_0$ that assures charge sustainability and consumes the least amount of fuel. As seen

from the plot, the ECMS based on PMP developed is sensitive to the variation of $s_0$. This
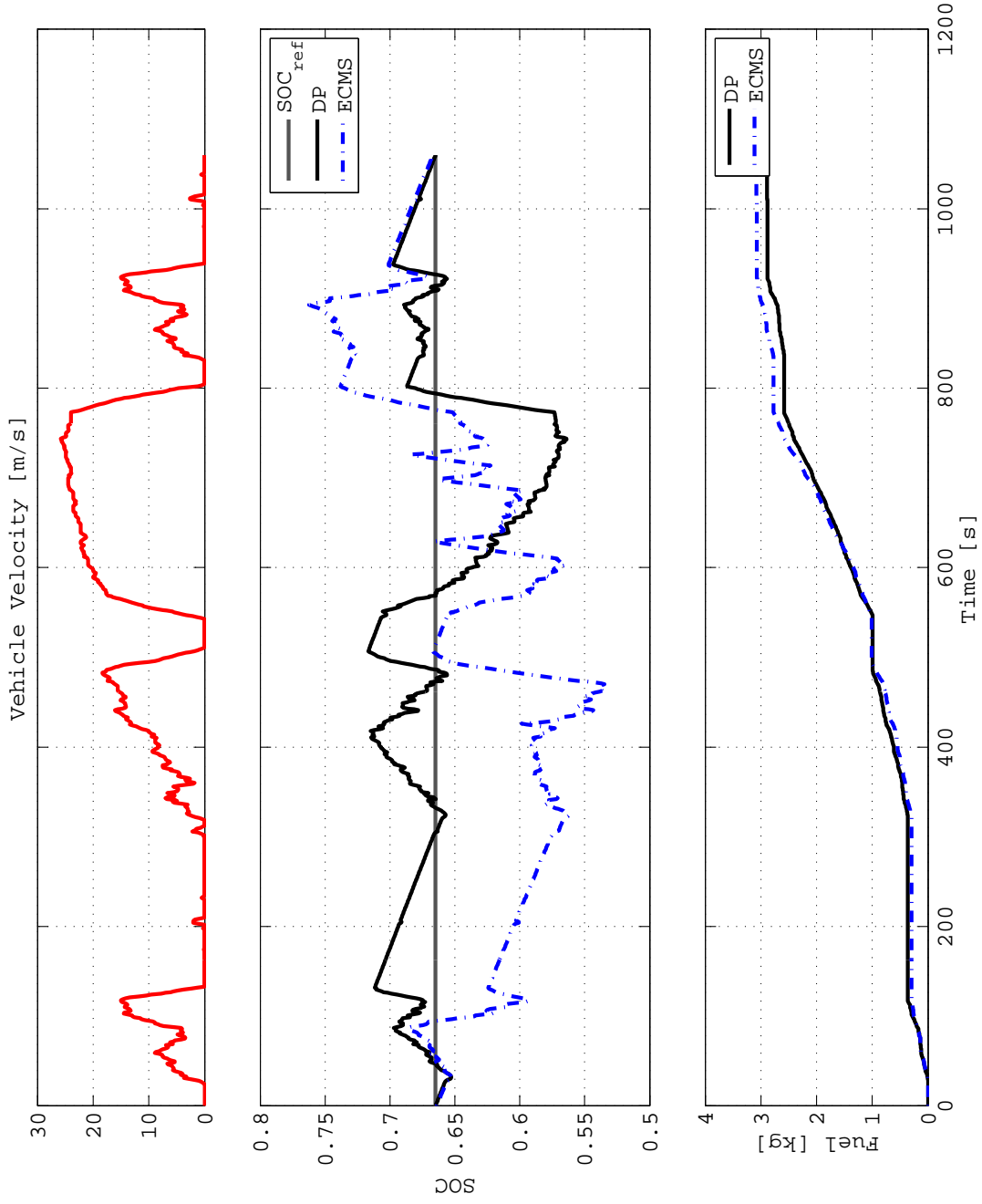
Figure 3.21: Velocity, SOC and equivalent fuel consumed (UDDS)
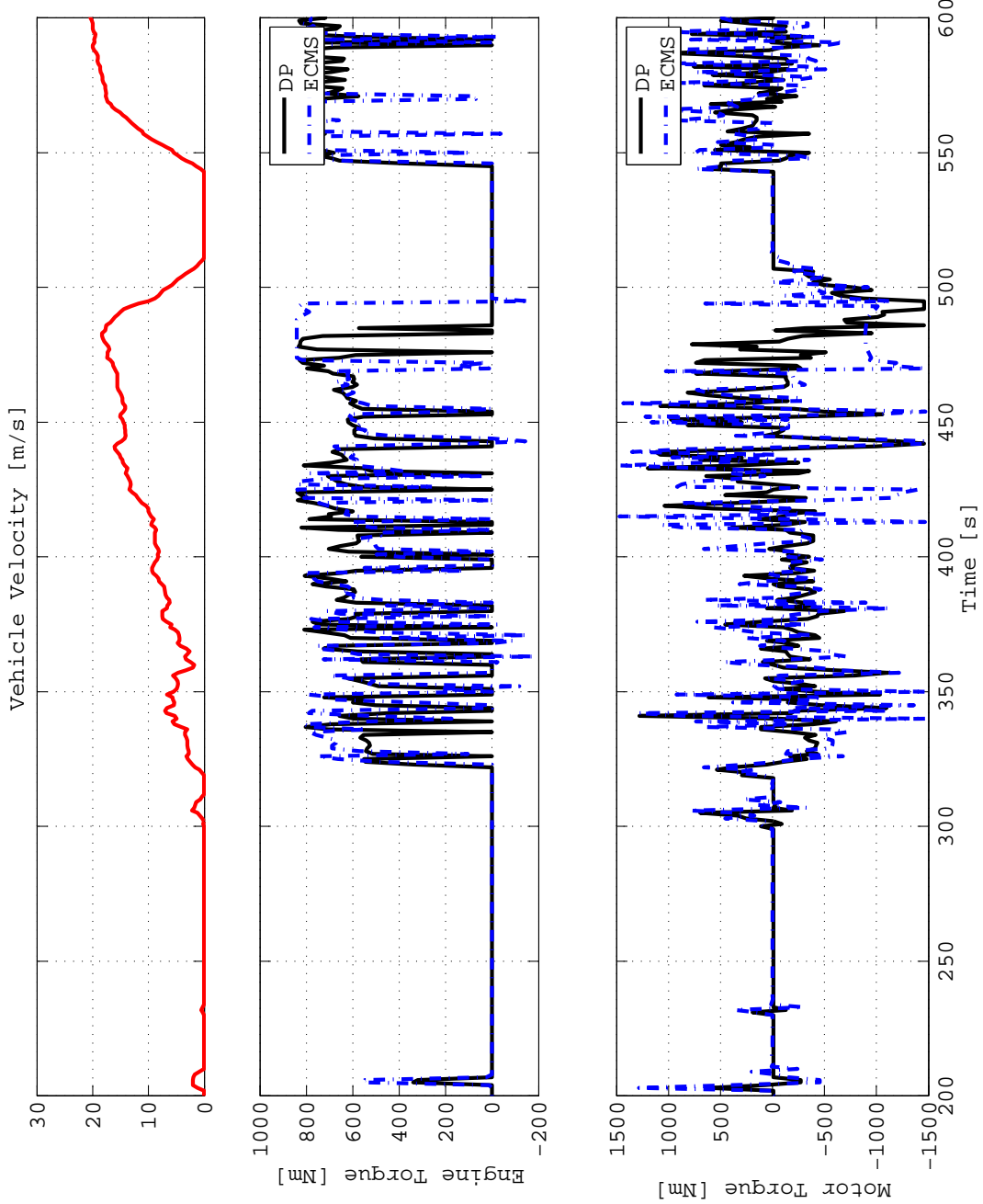
Figure 3.22: Velocity, engine and electric motor torques - Detail (UDDS)
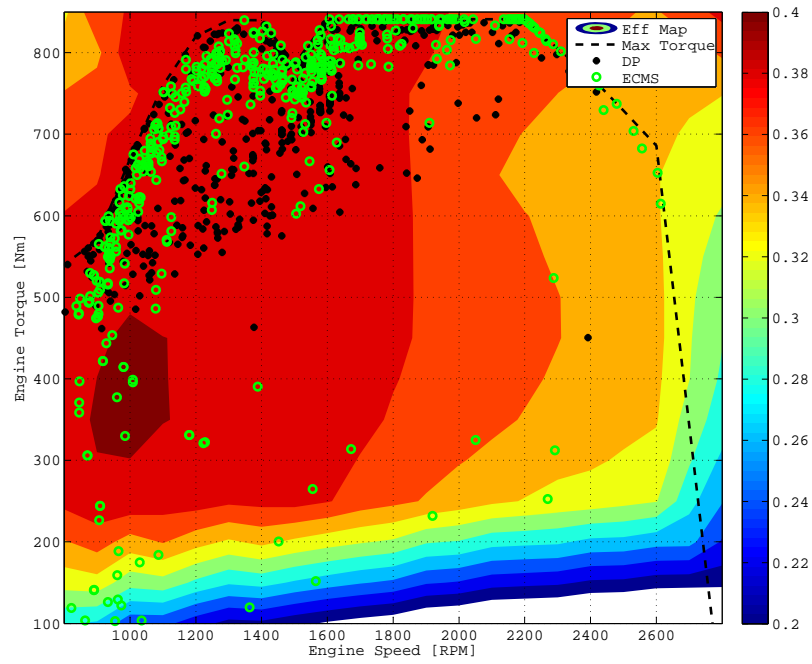
Figure 3.23: Engine operating points (UDDS)
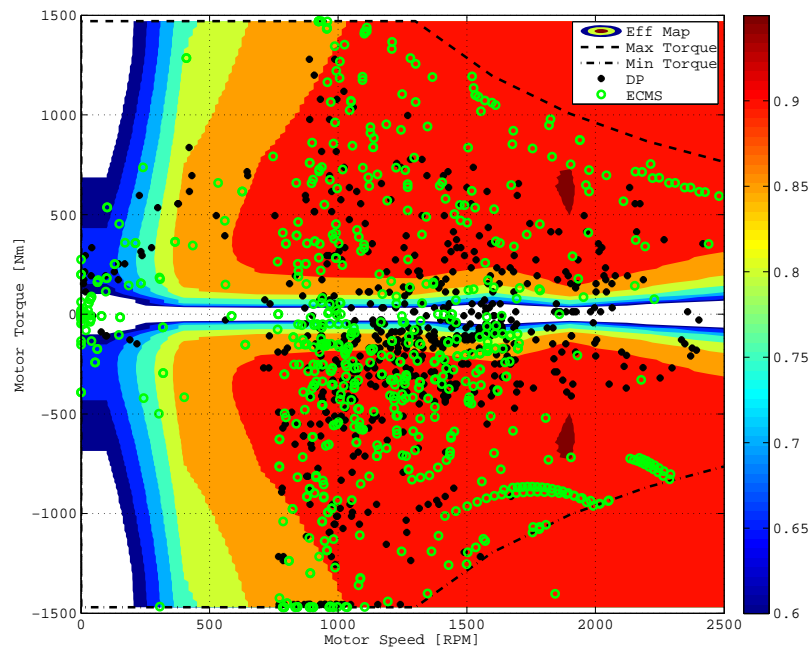


Figure 3.24: Electric motor operating points (UDDS)
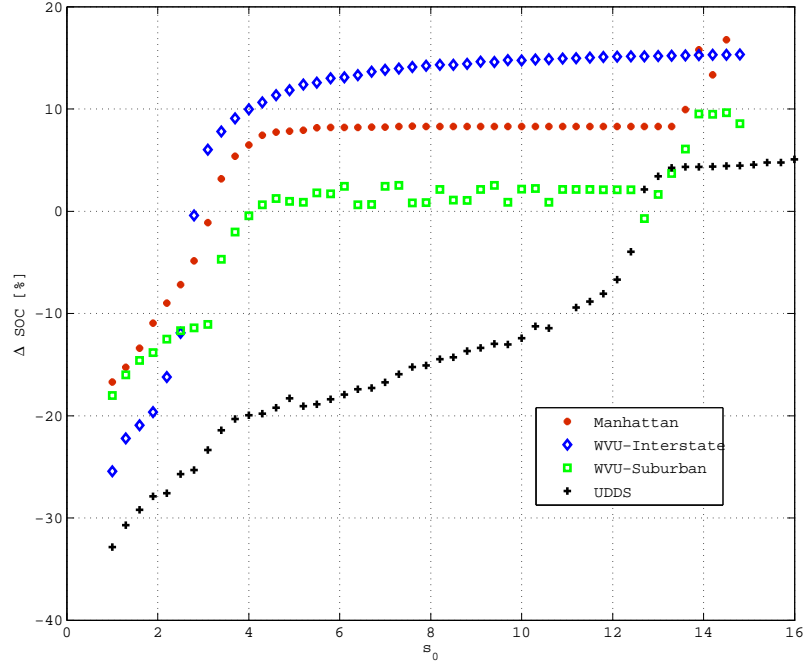
Figure 3.25: Effect of $s_0$ on deviation of SOC

is significant because the optimality and stability properties for a wrong guess of $s_0$ are affects the performance of ECMS based on PMP.

## 3.4 Adaptive Equivalent Consumption Minimization Strategy

The optimality of ECMS (as derived from PMP) depends on the *optimal* value of $s(t)$ whose dynamics are shown in equation (3.41). The initial value $(s_0))$, which depends on the driving cycle, must be guessed to find the *optimal* from the extremal solutions obtained from PMP. This is also true from the definition of the equivalence factor as the fuel-equivalent cost of the battery usage, which can clearly change with driving conditions. For example, if there is a long downhill driving segment, then the equivalence factor should

be as low as possible to allow for maximum regenerative capability. Clearly the same value of $s_0$ would not be optimal during a highway driving segment.

The results of ECMS implementation corresponding to different values of $s_0$ are shown in Fig. 3.8 and Table 3.4. The optimality of ECMS derived from PMP depends on the *optimal* value of $s_0^*$ for the particular driving cycle. Because the vehicle is always subjected to a multitude of conditions different from the calibrated driving cycles, the sensitivity of the ECMS solution to the wrong guess of $s_0$ is crucial. The sensitivity of ECMS to $s_0$ as shown in Fig. 3.25 is an important concern for a real-time implementation of ECMS because the optimal value of $s_0$ can be found only if the entire driving cycle is known *a-priori*. Hence a real-time implementation of ECMS with a given single equivalence factor is clearly sub-optimal. In order to have an ECMS that is at least close to the optimal solution, adaptation of the equivalence factor is crucial.

The version of adaptive ECMS (referred to as AECMS) proposed in [26] and used in this research is based on the following facts:

- The optimal value of equivalence factor is the one that generates a charge-sustaining solution;

- If the equivalence factor is smaller than the optimal value, the battery SOC tends to decrease and tends to increase if the equivalence factor is too high;

- The interval over which charge-sustainability is required should ideally be the entire trip, but this is impossible because its duration is not known *a-priori*; thus, it is assumed that the SOC should return to a reference value at regular intervals, of duration $T$;

87

- The charge-sustainability interval $T$ should be long enough to allow battery charging and discharging in the entire operating range.

Based on these facts, the adaptive strategy updates the value of the equivalence factor at the end of each of these intervals (defined as adaptation intervals). The adaptation is based on the measured SOC variation from the reference value at the end of the interval: if the SOC has decreased, it means that that the value of $s_0$ previously used was too low; if the SOC has increased, $s_0$ was too high. The adaptation law used is:

$$s_{0,k+1} = \frac{(s_{0,k-1} + s_{0,k})}{2} + K_p \Delta SOC(kT)$$

$$\Delta SOC(kT) = SOC_{ref} - SOC(kT); \; k = 1, 2, ... \qquad (3.44)$$

$$s_{0,1} = s_{0,0} = any\; initial\; guess \quad \in [1, 5],$$

where $K_p$ is the adaptation gain, $T$ is the adaptation period, $SOC_{ref}$ is the reference value of SOC and $s_{0,i}$ is the initial value of equivalence factor at the $i^{th}$ interval, i.e., $s_{0,i} = s_0(iT)$. Though there have been strategies [27, 28] in the literature that have used adaptation laws based on SOC feedback, the strategy proposed here is conceptually different because the adaptation is not done for each time step (Fig. 3.26). In fact, in a HEV, it is normal that the SOC deviates from its reference value during the operation of the vehicle, but the charge sustainability constraint requires that only the SOC at the end of driving cycle is equal to the reference value. Since in real-world conditions, the duration of the driving cycle is not known *a-priori*, the charge-sustainability condition is enforced on shorter time frames (more specifically for every $T$ seconds). In the basic formulation of the algorithm the SOC difference between two generic operating points separated by T seconds is calculated. For example, the SOC should be higher after a regenerative braking phase and will be lower after a high acceleration transient. Hence the adaptation should be done only when the
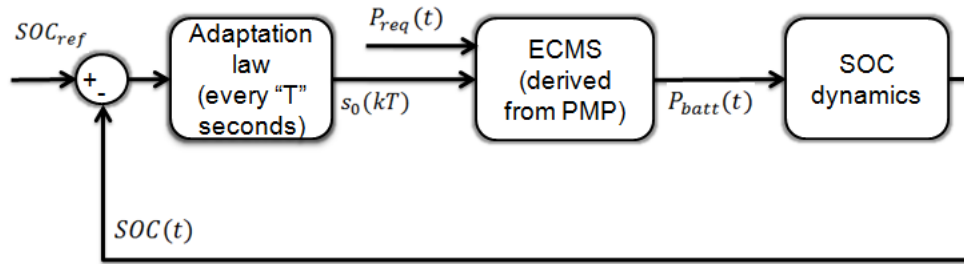
Figure 3.26: Adaptive ECMS system

vehicle is in a similar operating condition (for e.g. vehicle stop). The adaptation interval is not strictly $T$ seconds, but rather a stretchable time to allow for the vehicle to come to a stop. This is a very reasonable assumption to make in the transit bus application for which the strategy has been developed.

### 3.4.1 Simulation Results

This subsection describes the simulation environment used to implement the AECMS proposed in the previous section and its performance is compared to the global optimal solution obtained from DP (Section 3.2). The pre-transmission parallel HEV is modeled using a backward vehicle simulator (Section 2.2.2) in the MATLAB/Simulink environment. Based on the assumption that the vehicle follows the desired velocity trajectory, the torque required at the wheels and subsequently the torque/speed required from the components are calculated (Fig. 2.22). The simulator primarily uses simplified quasi-static map based models for all the components as shown in Table 2.2. Because AECMS is developed for real-time implementation, the performance of the strategy is evaluated over several repetitions of driving cycles.

**Performance for Manhattan driving cycle**

Table 3.9: Performance comparison with DP for Manhattan driving cycle

| **Strategy** | Normalized $FC_{eqv}$ [%] |
|---|---|
| AECMS | 109.6 |
| DP | 100 |

AECMS is tested for eight repetitions of the Manhattan driving cycle and its perfor-
mance is evaluated against the global optimal solution from DP. The Manhattan driving cy-
cle is representative of the city/urban driving cycle with many start stop events. Similar to
the results shown in the previous sections, the deviation of battery SOC from its reference
and the equivalent fuel consumed ($FC_{eqv}$) as defined in (3.18), are used as performance
metrics. Adaptive ECMS consumes 10% more fuel than DP over the eight repetitions of
the driving cycle. The performance of AECMS is compared with DP in Fig. 3.27, Fig.
3.28 and Table 3.9. Though the initial guess of equivalence factor ($s_0$) is different from the
*optimal* value, the adaptation ensures the convergence of $s_0$ and the battery SOC. As seen
from Fig. 3.28, the convergence of $s_0$ to $s_0^* = 3.3$ guarantees the convergence of battery
SOC to its reference.

**Performance for WVU-Interstate driving cycle**

The performance of AECMS is compared with DP in Fig. 3.29, Fig. 3.30 and Table
3.10. The WVU-Interstate driving cycle is representative of the highway driving conditions
experience by heavy-duty HEVs. In order to evaluate the performance of adaptation, eight
repetitions of the driving cycle are considered. Teh strategy consumes 5% more fuel than
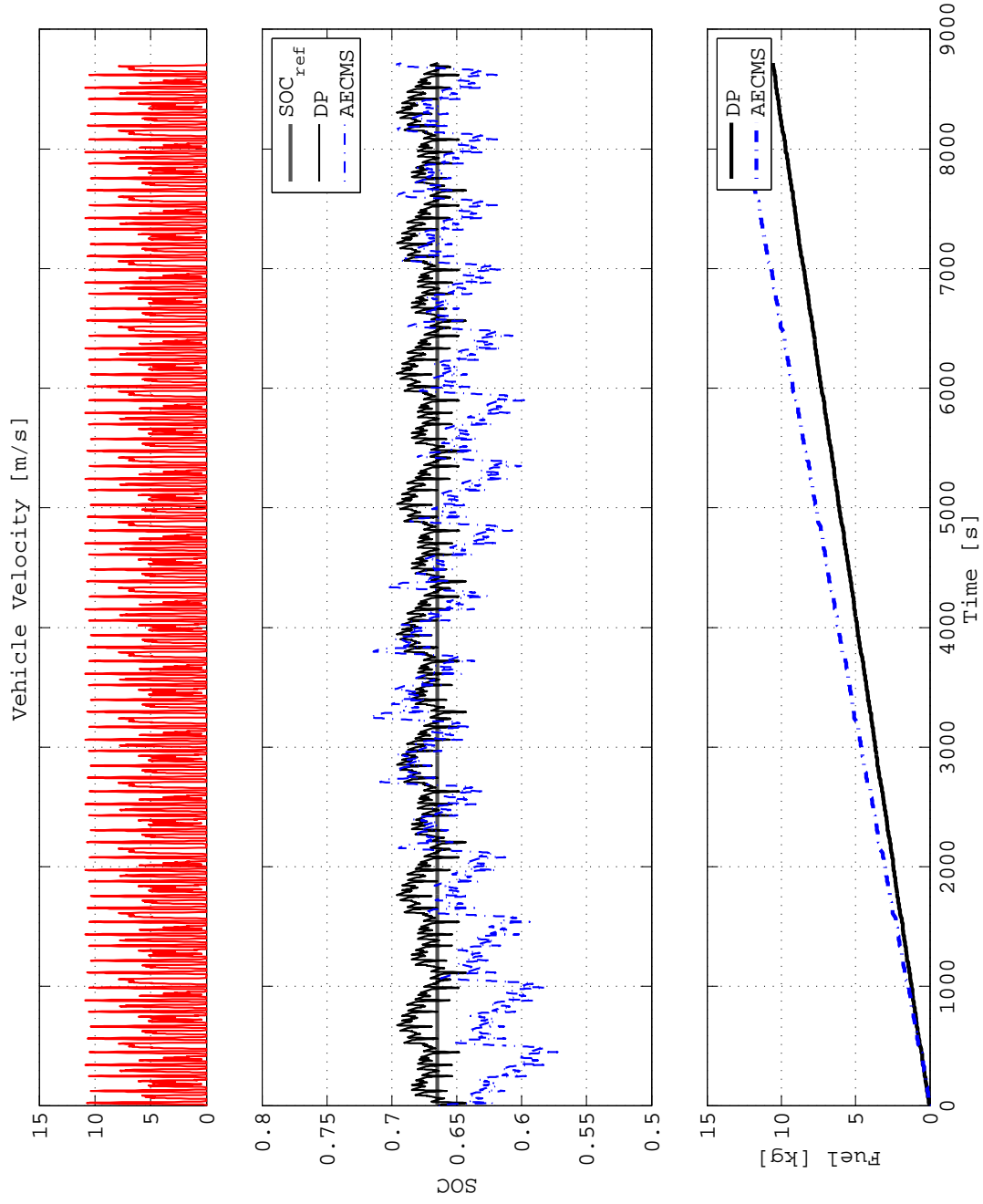
Figure 3.27: Velocity, SOC and equivalent fuel consumed (8 X Manhattan)
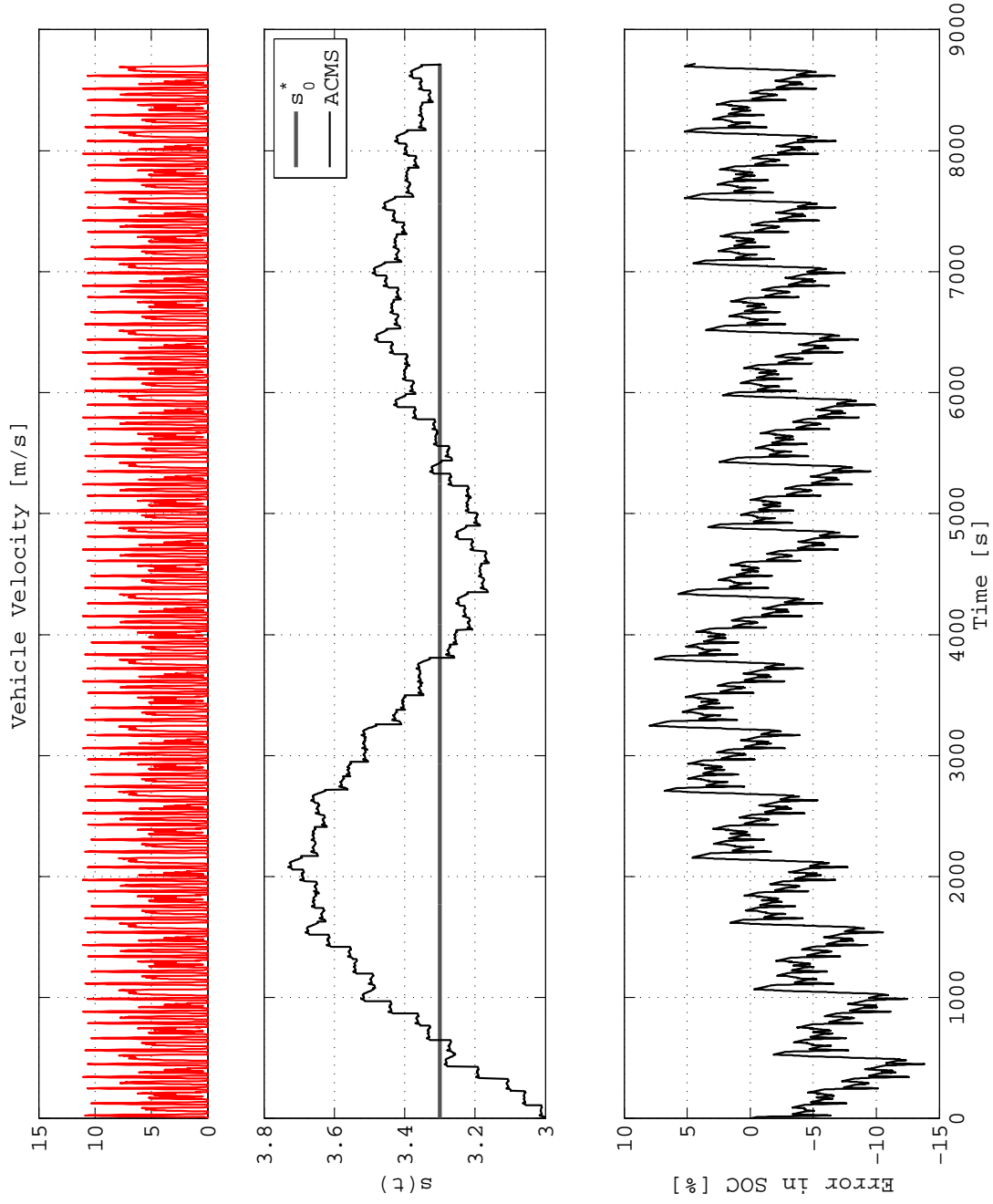
Figure 3.28: Velocity, equivalence factor and error in SOC (8 X Manhattan)
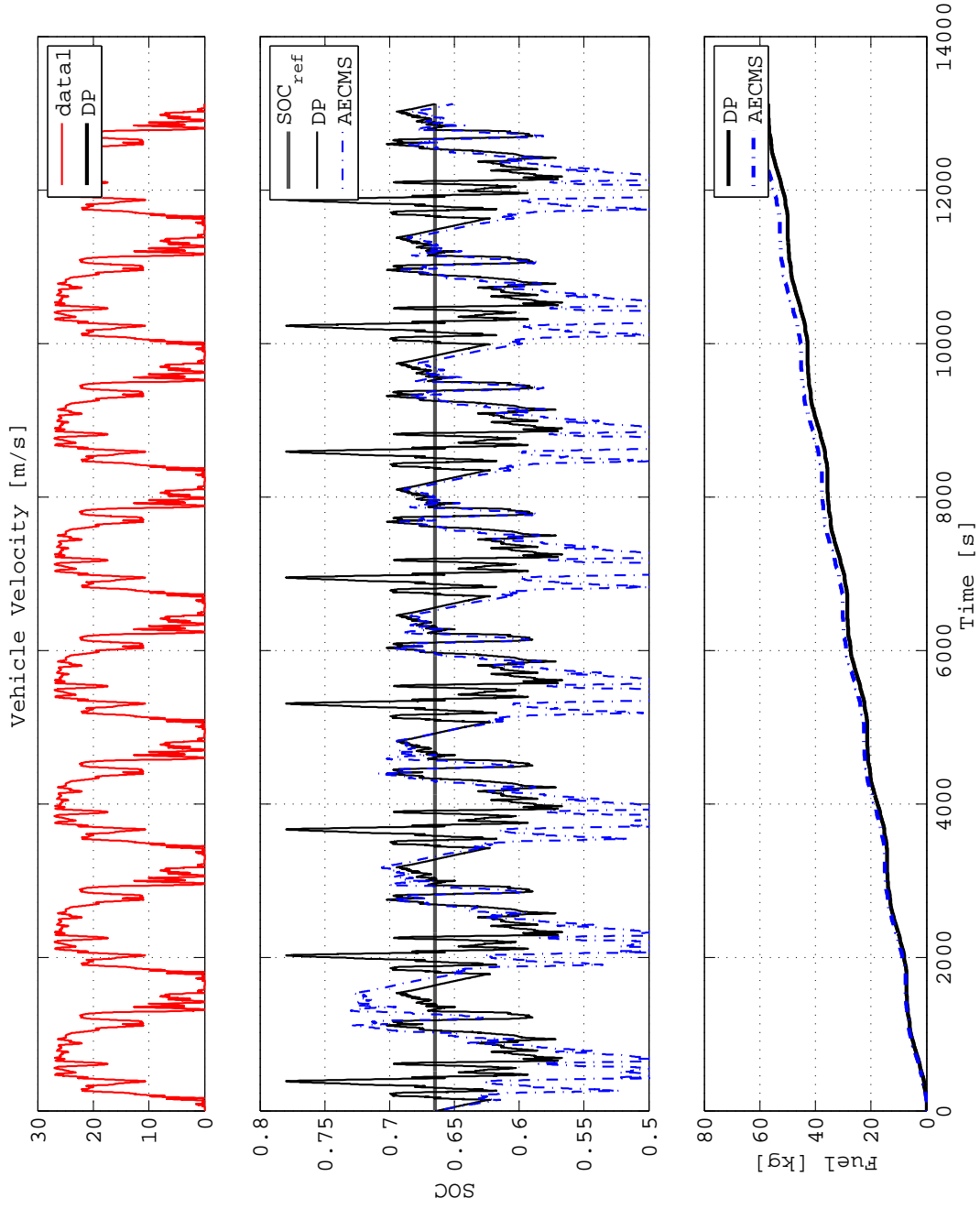
Figure 3.29: Velocity, SOC and equivalent fuel consumed (8 X WVU-Interstate)
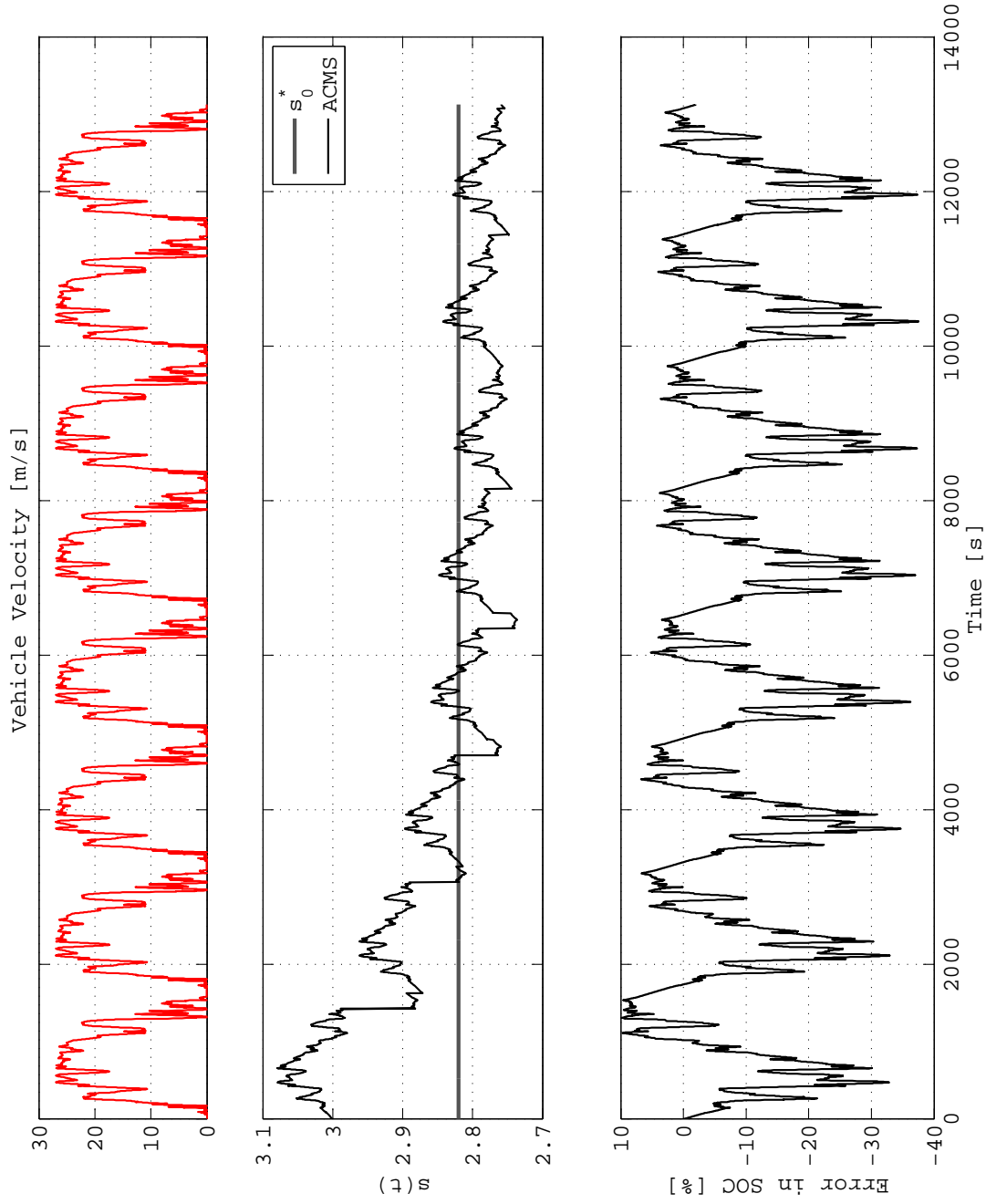
Figure 3.30: Velocity, equivalence factor and error in SOC (8 X WVU-Interstate)

Table 3.10: Performance comparison with DP for WVU-Interstate driving cycle

| Strategy | Normalized $FC_{eqv}$ [%] |
|----------|---------------------------|
| AECMS    | 105.3                     |
| DP       | 100                       |

DP over the eight repetitions of the driving cycle while $\Delta SOC = 2\%$ at the end of eight repetitions. The adaptation ensures the convergence of $s_0$ to its *optimal* value $s_0^* = 2.82$. This convergence guarantees that the battery SOC is close to $SOC_{ref}$ at the end of the driving cycle.

**Performance for WVU-Suburban driving cycle**

Table 3.11: Performance comparison with DP for WVU-Suburban driving cycle

| Strategy | Normalized $FC_{eqv}$ [%] |
|----------|---------------------------|
| AECMS    | 108.9                     |
| DP       | 100                       |

The WVU-Suburban is a suburban driving cycle which is representative of the suburban driving conditions experience by heavy-duty HEVs like school buses, pick up trucks etc.,. The $\Delta SOC$ and $FC_{eqv}$ for eight repetitions of WVU-suburban driving cycle are shown in Fig. 3.31, Fig. 3.32 and Table 3.11. The adaptive strategy consumes 9% more fuel than DP which is clearly due to less efficient operation of the engine. As seen from Fig. 3.32, the adaptation ensures the convergence of $s_0$ to its *optimal* value $s_0^* = 4.56$. This convergence
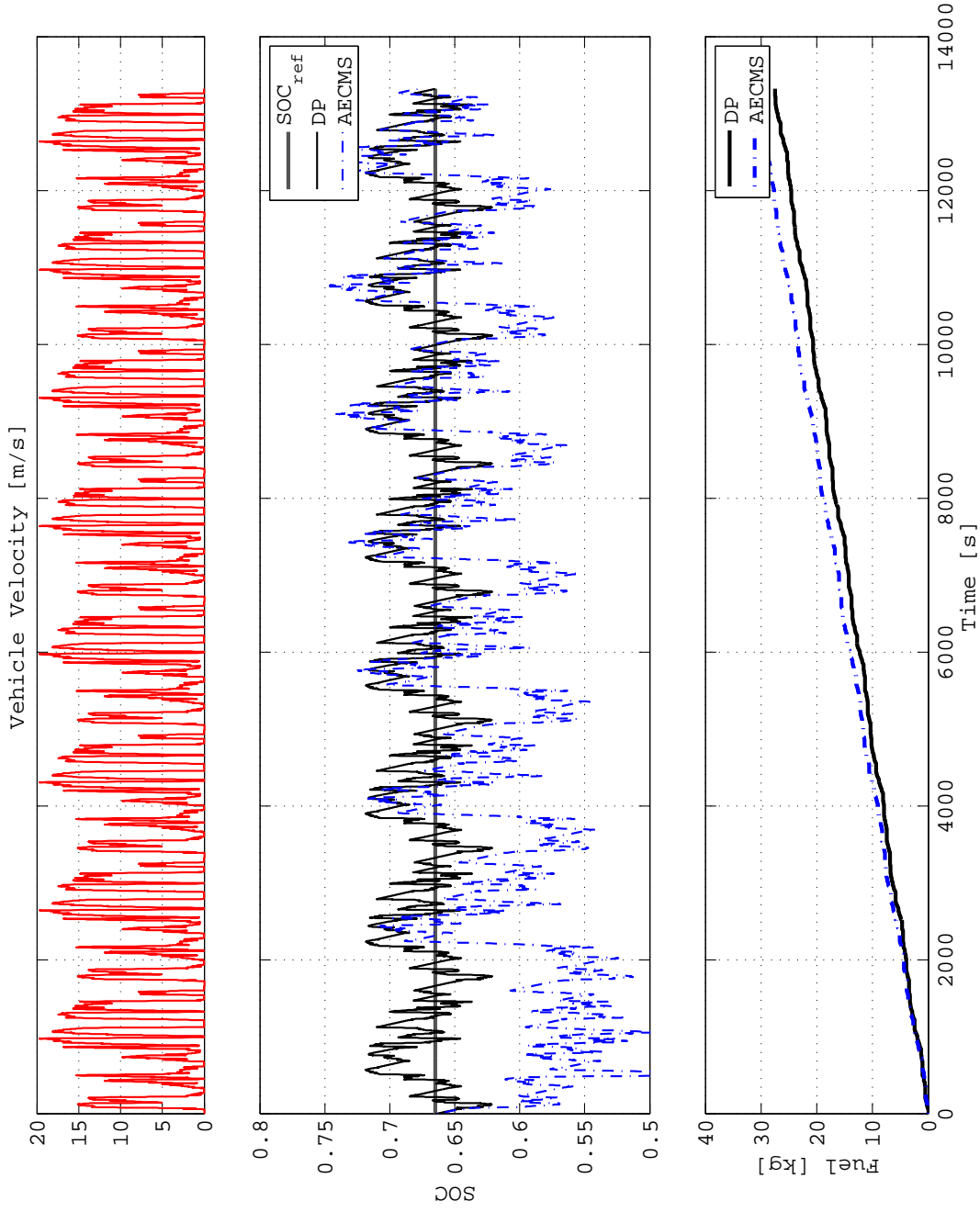
Figure 3.31: Velocity, SOC and equivalent fuel consumed (8 X WVU-Suburban)
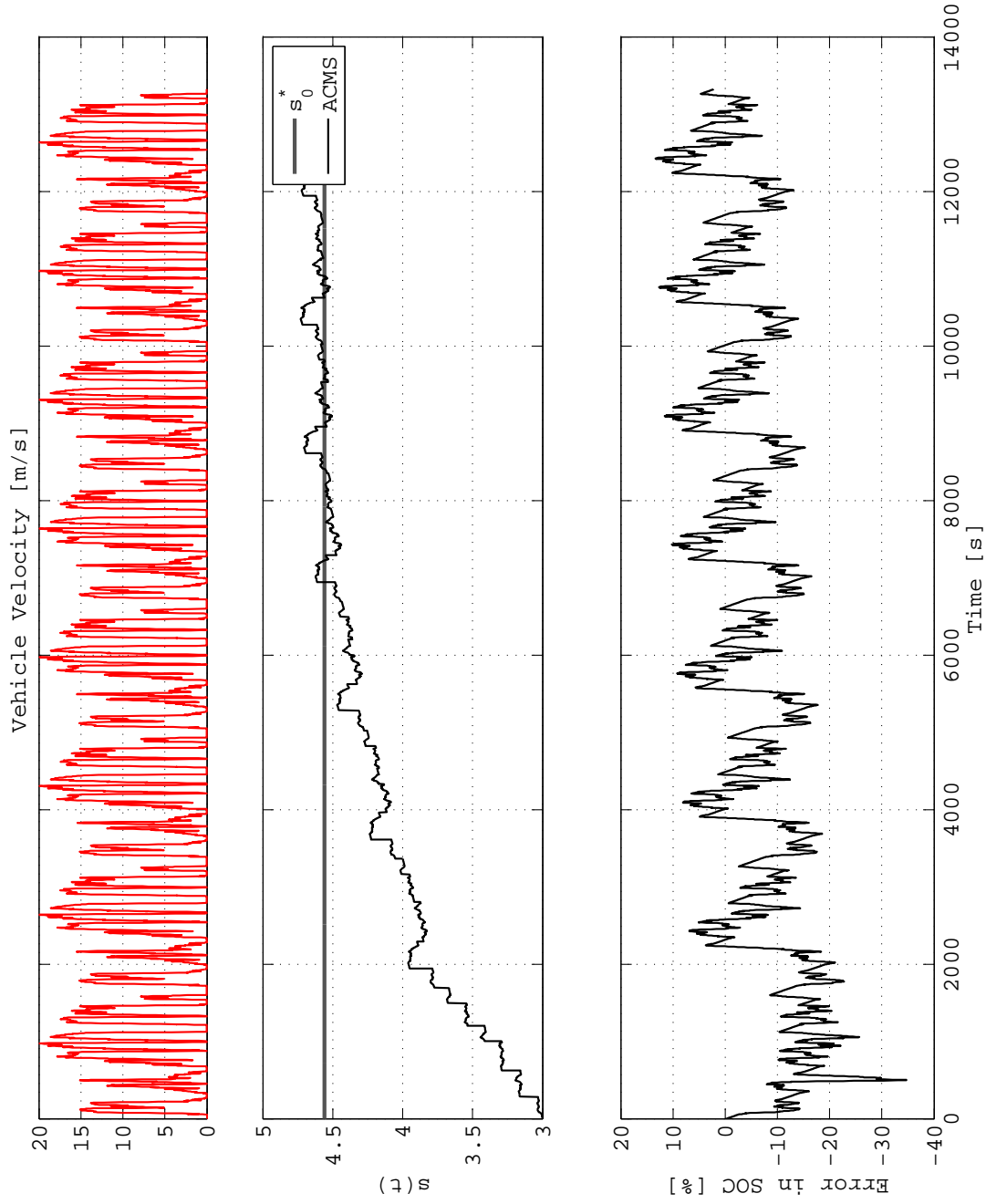
Figure 3.32: Velocity, equivalence factor and error in SOC (8 X WVU-Suburban)

guarantees that the battery SOC is as close to $SOC_{ref}$ with $\Delta SOC = 2.2\%$ at the end of eight repetitions of the driving cycle.

**Performance for UDDS driving cycle**

Table 3.12: Performance comparison with DP for UDDS driving cycle

| Strategy | Normalized $FC_{eqv}$ [%] |
|----------|---------------------------|
| AECMS | 108.8 |
| DP | 100 |

The performance of the adaptive strategy over eight repetitions of UDDS driving cycle is compared with the global optimal solution from DP. Table 3.12 shows that the strategy consumes 9% more fuel than DP with $\Delta SOC = 4\%$. This driving cycle represents realistic driving conditions undergone by many semi-urban heavy-duty vehicles likes UPS pick up trucks. The battery SOC profile, equivalent fuel consumed, variation of equivalence factor and error in SOC is shown in Figures 3.33 - 3.34. Though the initial guess for equivalence factor is not optimal, the adaptation ensures the convergence of $s_0$ to its *optimal* value $s_0^* = 12.65$.

## 3.5   Conclusion

The main contributions from the chapter are the design and development of different energy management strategies such as DP, ECMS and AECMS for pre-transmission parallel HEV. The energy management problem in a charge-sustaining HEV is formulated and several optimal control techniques are used to solve the problem. Because DP solves the
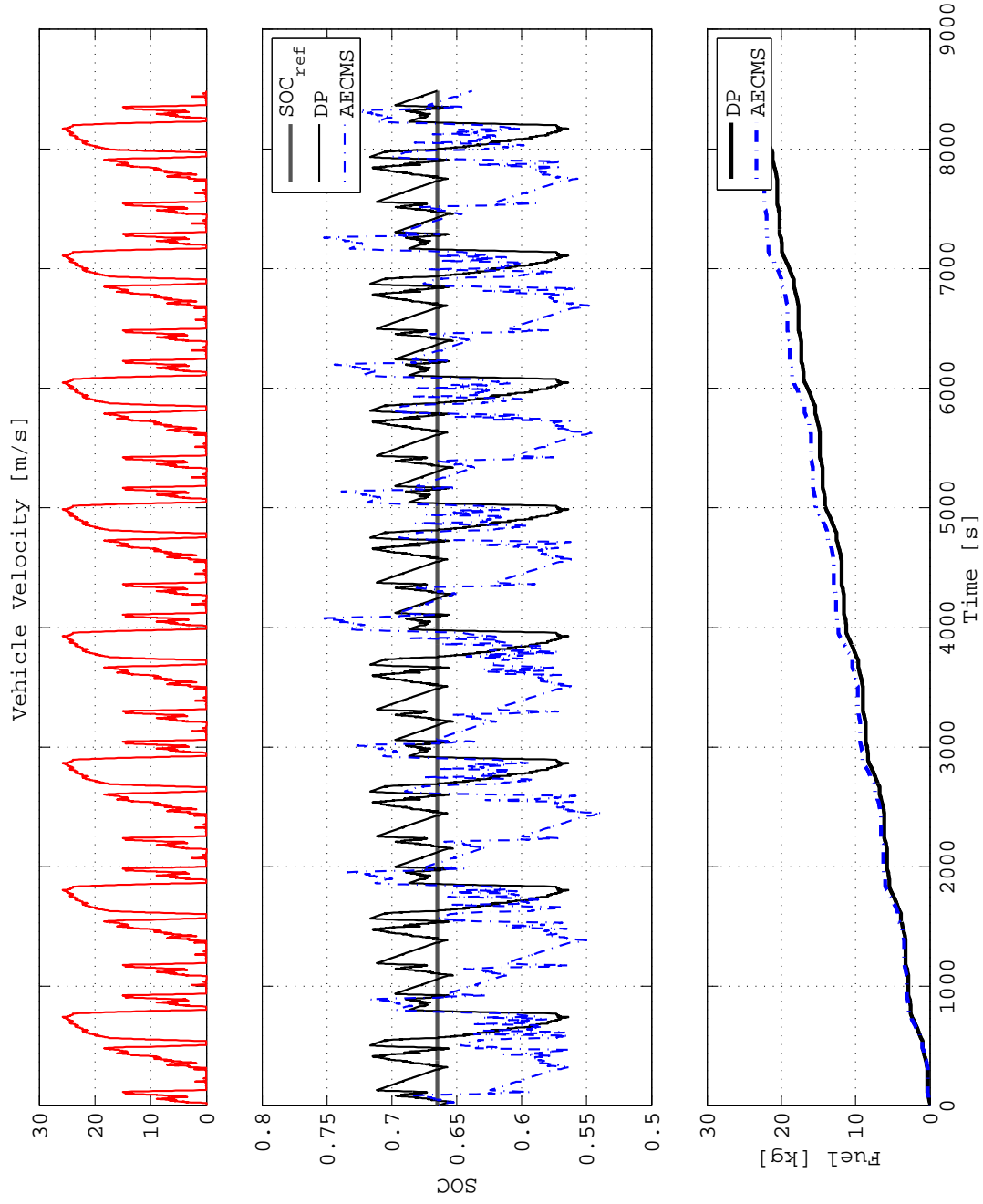
Figure 3.33: Velocity, SOC and equivalent fuel consumed (8 X UDDS)
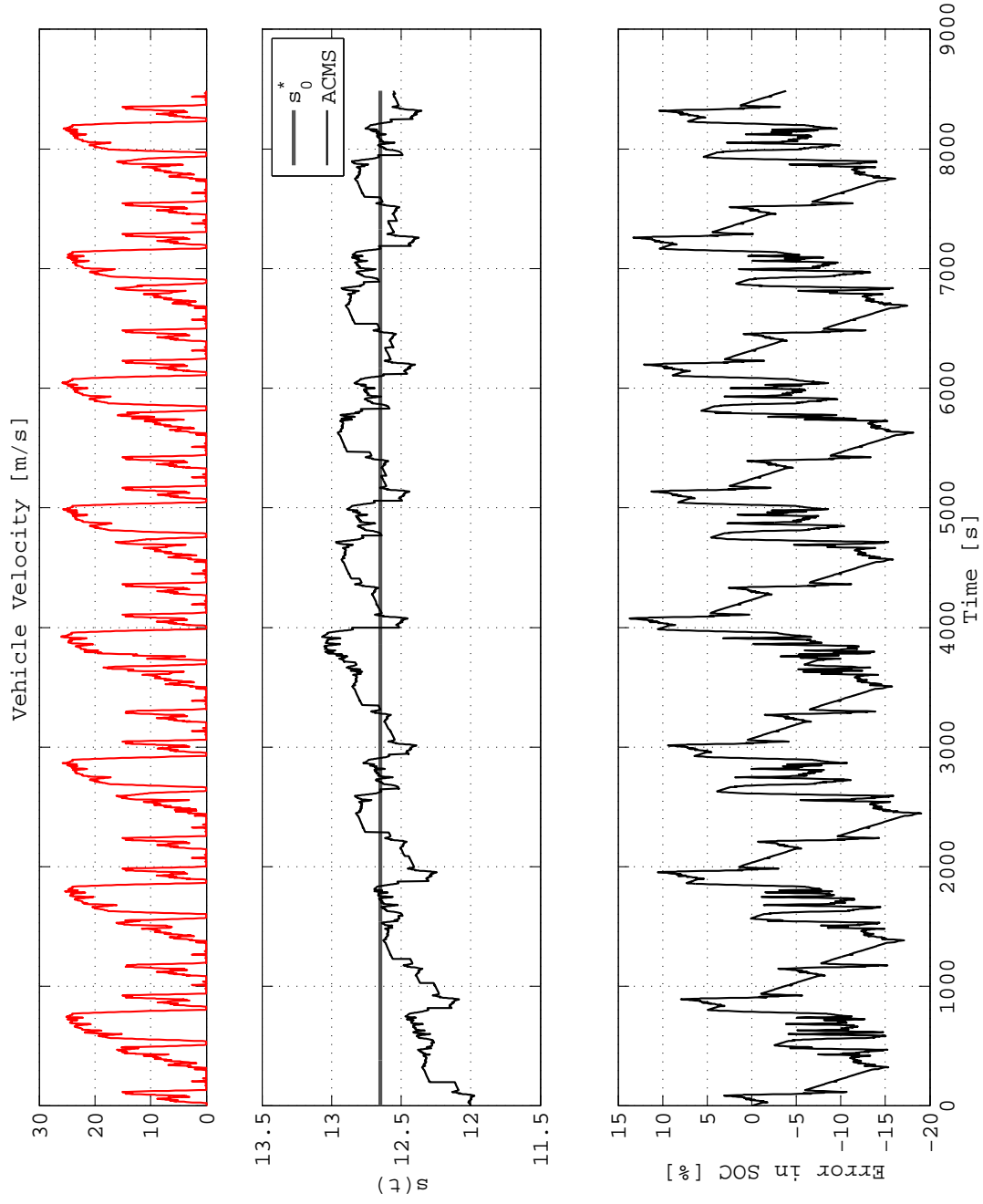
Figure 3.34: Velocity, equivalence factor and error in SOC (8 X UDDS)

problem backwards and provides the global optimal solution based on the sufficient conditions of optimality, it is a benchmark solution for the rest of the dissertation. The DP algorithm is given the complete freedom of selecting the vehicle mode of operation and the torque/power split between engine and electric machine. The mode selecting strategy used by DP is analyzed and simple rules to select the most appropriate mode of operation is formulated. Though ECMS has been studied in the literature for a long time, the equivalence between ECMS and PMP is a relatively new result. The dissertation utilizes this equivalence between ECMS and PMP to design an ECMS based on the necessary conditions of optimality provided by PMP. The equivalence factor is written as a function of the co-state variable and the strategy has been implemented with a single calibration parameter. The reduction of the number of calibration parameters is significant because the amount of calibration effort necessary to implement the strategy in a real-vehicle is decreased considerably. The relationship between the equivalence factor and the battery SOC deviation from the reference at the end of the driving cycle is utilized to develop an adaptive strategy. Both the ECMS and AECMS proposed in this dissertation have been derived from results found in the literature, while the application of the strategies in a backward vehicle simulator for a pre-transmission parallel HEV is a contribution to the literature. The implementation of DP algorithm available in the literature for a pre-transmission parallel HEV is an important contribution. The extraction of mode selection strategy from DP results for this particular vehicle architecture and the comparative analysis of the strategies are some of the other contributions of the chapter. The energy management strategies developed in this chapter will be implemented and compared in Chapter 5 using a forward vehicle simulator.

# Chapter 4: Stability and Optimality Framework

Though there have been several energy management strategies in the literature (Section 1.1), there has not been a stability framework within which stable and optimal energy management strategies can be designed. Such a framework is considered in this chapter which facilitates the definition of stability in charge sustaining HEVs and utilizes the theoretical results in nonlinear optimal regulation theory to analyze and design energy management strategies. The main contribution here is in developing a useful mathematically rigorous framework, and the goal is in developing an energy management strategy that can be easily implemented in a real-vehicle while assuring stability and optimality. It is shown that by suitably casting the energy management problem into a nonlinear optimal regulation problem and using an appropriate Lyapunov function candidate, it can be proved that the state-feedback based optimal control law (with respect to minimum fuel consumption) produces a charge-sustaining behavior. The control Lyapunov function[5] is also used in deriving an analytical closed-form expression for the optimal control law.
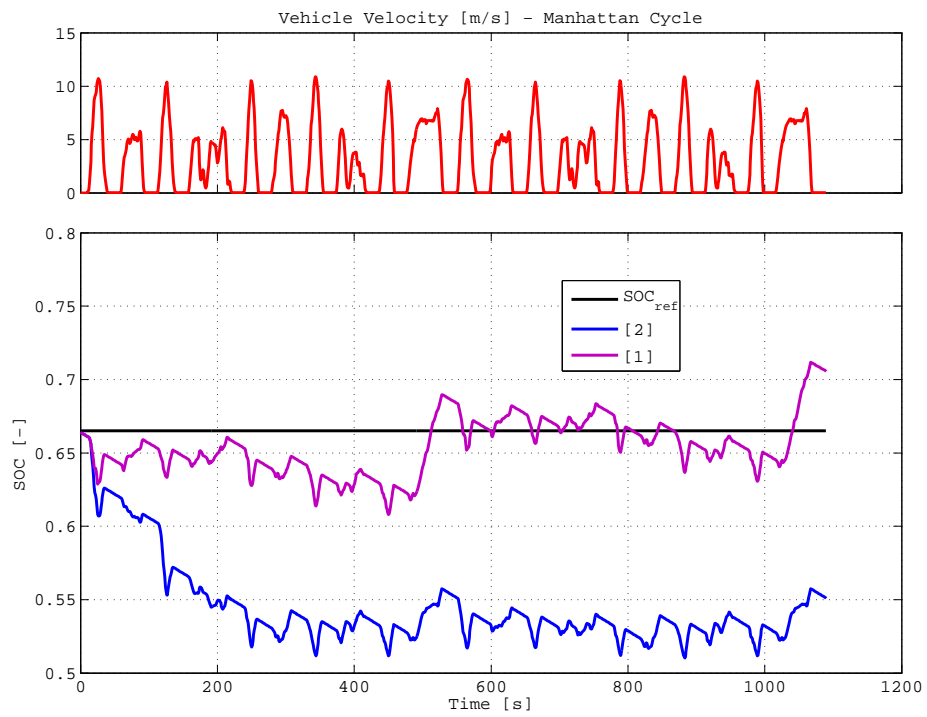
Figure 4.1: Motivation for stability analysis: [1] Charge sustaining solution; [2] Charge depleting solution.

## 4.1 Stable and Optimal Energy Management Strategies

In order to develop the framework, *stable* and *optimal* energy management strategies for charge-sustaining HEVs must be defined. For example, if the battery SOC at the end of a driving cycle is either too high or too low from the reference SOC, the capability of the strategy to either recharge the battery (say, using a regenerative braking event) or to discharge the battery (say, to assist the engine during a high acceleration event) is severely compromised. The most important and pertinent variable of interest in energy management strategies is the deviation of battery SOC from the reference SOC. Two different battery SOC error profiles ($e = SOC_{ref} - SOC$) are shown in Fig. 4.1. Because in a charge-sustaining HEV all the energy used for propulsion effectively comes from the fuel, it is crucial to have zero net change in battery SOC over the driving cycle. This is essential to utilize the vehicle's hybrid potential and to extend the life of the battery. In Figure 4.1, the battery SOC error profile 1 shows a charge sustaining solution, in which the average SOC over the driving cycle close to the reference value. The SOC error profile 2 shows a charge depleting solution at the end of the driving cycle. Ideally in a charge sustaining HEV, the average value of SOC throughout a given driving cycle is desired to be close to the reference value.

The primary objective of the energy management strategy is to *optimally* split the torque/power between the energy conversion devices minimizing the amount of fuel consumed over the driving cycle, while respecting the constraints on the devices and on battery SOC. An energy management strategy is *optimal* if it consumes the least amount of fuel

---

[5]A control-Lyapunov function [64] is a function $V(x, u)$ that is continuous, positive-definite ($V(x, u) > 0 \; \forall x \neq 0$), proper ($V(x) \to \infty \; as \; |x| \to \infty$), and such that

$$\forall x \neq 0, \; \exists u \;\; \dot{V}(x, u) < 0.$$
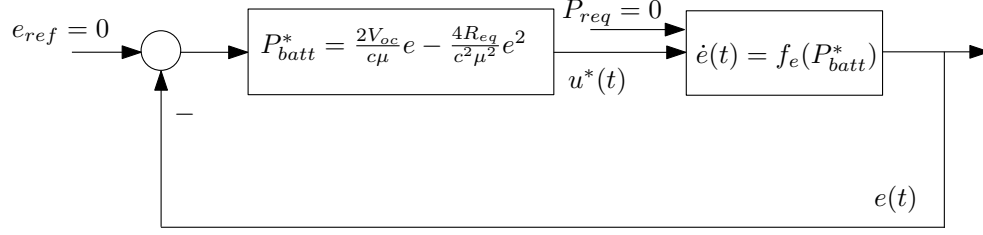
Figure 4.2: Energy management strategy as a nonlinear optimal regulation problem

over a driving cycle in addition to satisfying the constraints. For what follows, the different SOC error profiles (profiles [1] and [2]) are categorized as:

**Definition 1**: *An energy management strategy for a charge-sustaining HEV is called charge-sustaining if the system origin ($e = 0$) is asymptotically stable, while minimizing the fuel consumed over the driving cycle*

The asymptotic stability of the origin guarantees that the battery SOC is sufficiently close to the reference SOC at the end of the driving cycle ($t_0 - t_f$) and thus ensures the non-drifting property of the battery SOC. In order to evaluate energy management strategies, the battery SOC is the primary state variable. Considering the error in battery SOC from the reference value ($e = SOC_{ref} - SOC$) as the state variable, the state dynamics (4.1) is defined. With origin ($e = 0$) being the only equilibrium point of the system, asymptotic stability of the origin over an infinite interval guarantees that the average value of SOC over the driving cycle is close to the reference value.

$$
\begin{cases}
e = SOC_{ref} - SOC, \\
\dot{e} = \alpha \frac{V_{oc} - \sqrt{(V_{oc})^2 - 4R_{eq}P_{batt}}}{2R_{eq}Q_{max}} = f_e(P_{batt}), \\
P_{batt} = 0 \Rightarrow \dot{e} = 0.
\end{cases}
\tag{4.1}
$$

## 4.2 Nonlinear Optimal Regulation for Pre-transmission Parallel HEV

This section deals with formulating a theorem that uses a control Lyapunov function to develop a state-feedback based control law that minimizes the fuel consumption over an infinite horizon and stabilizes the battery SOC in the absence of external disturbances. We formulate the energy management problem with the vehicle operating in parallel mode with neutral gear (Fig. 2.3) as a nonlinear optimal regulation problem as shown in Fig. 4.2 (see List of Symbols for symbol definitions). The error in battery SOC ($e = SOC_{ref} - SOC$) and battery power are considered as the state and control variables of the system. The battery $SOC$ error dynamics are defined as

$$
\begin{cases}
e = SOC_{ref} - SOC, \\
\dot{e} = \alpha \frac{V_{oc} - \sqrt{(V_{oc})^2 - 4R_{eq}P_{batt}}}{2R_{eq}Q_{max}} = f_e(P_{batt}),
\end{cases}
\tag{4.2}
$$

where $P_{batt}$ is the control input of the system and $\dot{SOC}(t)$ describes the battery SOC dynamics (see (2.22)).

### 4.2.1 Mathematical Preliminaries

The mathematical preliminaries for the scalar system (4.2) with single control input, which are instrumental to the discussion, are presented in this sub section.

Consider an open set $\mathcal{D} \subset \mathbb{R}$ such that $e \in \mathcal{D}$, an arbitrary set $\mathcal{U}_1 \subset \mathbb{R}$ such that $P_{batt} \in \mathcal{U}_1$ and $0 \in \mathcal{D}, 0 \in \mathcal{U}_1$. In the HEV problem, the state domain and control domain can be defined as

$$
\begin{cases}
e \in \mathcal{D} = [SOC_{ref} - SOC_{max}, SOC_{ref} - SOC_{min}], \\
P_{batt} \in \mathcal{U}_1 = [P_{batt,min}, P_{batt,max}].
\end{cases}
\tag{4.3}
$$

Furthermore, let $f_e : \mathcal{U}_1 \rightarrow \mathbb{R}$ satisfy $f_e(0) = 0$. Now consider the controlled system

$$
\dot{e} = f_e(P_{batt}), \quad e(0) = e_0, \quad t \geq 0,
\tag{4.4}
$$

where the control input $P_{batt}(\cdot)$ is restricted to the class of functions such that

$$P_{batt} \in \Omega_1, \quad t \geq 0, \tag{4.5}$$

where the control constraint set $\Omega_1 \subset \mathcal{U}_1$ is compact and $0 \in \Omega_1$. The control input constraint set $\Omega_1$ is defined by the maximum and minimum battery power depending on the battery parameters at each instant. Let the *optimal control law* $P_{batt}^*$ be a measurable mapping $P_{batt}^* : \mathcal{D} \to \Omega_1$ satisfying $P_{batt}^*(0) = 0$. Now the system (4.2) with feedback control $P_{batt} = P_{batt}^*(e)$, has the form

$$\dot{e} = f_e(P_{batt}^*(e)), \quad e(0) = e_0, \quad t \geq 0. \tag{4.6}$$

In order to address the problem of characterizing feedback controllers that minimize a performance functional, let $\mathcal{H}_1 : \mathbb{R} \times \mathbb{R} \times \mathbb{R} \to \mathbb{R}$, $\dot{m}_f : \mathbb{R} \to \mathbb{R}$ and $\lambda \in \mathbb{R}$ such that,

$$\mathcal{H}_1(e, P_{batt}, \lambda) \triangleq \dot{m}_f(P_{batt}) + \lambda \cdot f_e(P_{batt}), \tag{4.7}$$

where $\mathcal{H}_1(\cdot, \cdot, \cdot)$ is the Hamiltonian function, $\lambda$ is the co-state variable and $\dot{m}_f(\cdot)$ is the instantaneous fuel consumption rate of the engine. Because the vehicle is operating in parallel mode in neutral gear, the engine can be disconnected from the wheels and operated along the maximum efficiency line. In this mode of operation, the engine fuel consumption rate can be expressed as an affine function of the engine power ($P_{ice}$) as in (2.14). Moreover, because $P_{ice}$ is a function of the control input $P_{batt}$ as given by (2.3), ultimately the fuel consumption rate $\dot{m}_f(t)$ can be expressed as a direct function of the control input, $P_{batt}$, i.e.,

$$\dot{m}_f(t) = p_0 + p_1 P_{batt}(t), \tag{4.8}$$

through coefficients $p_0, p_1$ expressed as follows:

$$\begin{cases} p_0 = m_0 + m_1 \left( P_{accmech} + \frac{1}{\eta_{mot}} P_{accelec} \right), \\ p_1 = -m_1 \eta_{mot}. \end{cases} \tag{4.9}$$

where $\eta_{mot}$ represents the efficiency of the electric machine and $P_{accmech}$, $P_{accelec}$ represent the mechanical and electrical accessory power. Finally, without loss of generality, a new Hamiltonian function $\bar{\mathcal{H}}_1$ is defined to take on zero-value when evaluated at the optimal control, as

$$
\begin{cases}
\mathcal{H}_1(e, P_{batt}, \lambda) = \dot{m}_f(P_{batt}) + \lambda f_e(P_{batt}), \\
\bar{\mathcal{H}}_1(e, P_{batt}, \lambda) \triangleq \mathcal{H}_1(e, P_{batt}, \lambda) - p_0,
\end{cases}
\tag{4.10}
$$

where $p_0$ is a parameter of the engine fuel consumption rate model defined in (4.9).

The result that follows gives sufficient conditions under which the origin $e = 0$ can be locally asymptotically stabilized under nonlinear state feedback control, while also assuring optimality of the fuel consumption over an infinite time horizon. Sufficient conditions for stability and optimality are given in the case where no external inputs or disturbances enter the system (4.4), which corresponds to $P_{gb} = 0 \, \forall \, t \geq 0$, with the system initial condition different from zero, i.e. $e_0 \neq 0$. In the context of charge-sustaining HEVs, the considered scenario (Fig. 4.2) corresponds to having the vehicle switched on without any tractive force at the wheels (vehicle velocity = 0) and the battery $SOC$ is not at the reference value, i.e. $SOC_{ref} \neq SOC(0)$. What follows is the first of a series of original results on stability and optimality in the context of the energy management problem in HEVs, that builds upon the main results appearing in [48]

**Theorem 1.** *Consider the system (4.4) with performance functional*

$$
J(e_0, P_{batt}(\cdot)) \triangleq \int_0^\infty \dot{m}_f(P_{batt}) dt.
\tag{4.11}
$$

*Then with the feedback control $P_{batt} = P_{batt}^*(e)$, where $P_{batt}^*(e)$ satisfies*

$$
\begin{cases}
P_{batt}^*(e) = \frac{2V_{oc}}{c\mu} e - \frac{4R_{eq}}{c^2\mu^2} e^2, \\
c = \frac{2R_{eq}Q_{max}p_1}{\alpha},
\end{cases}
\tag{4.12}
$$

*the solution $e(t) = 0$, $t \geq 0$ of the closed-loop system (4.6) is locally asymptotically stable and the optimal feedback control law $P_{batt}^*(e(\cdot))$ minimizes $J(e_0, P_{batt}(\cdot))$*

**Proof**: Considering the candidate Lyapunov function $V(e) = \frac{1}{2}\mu e^2$; $\mu > 0$, local asymptotic stability of the origin $e(t) = 0$ and optimality of $P^*_{batt}$ with respect to $J(e_0, P_{batt}(\cdot))$ are proved using the following conditions given in Theorem 4.7.4 in the Appendix:

1. The Lyapunov function $V(e)$ has a minimum value of $0$ at the origin

$$V(0) = 0. \tag{4.13}$$

2. The candidate Lyapunov function $V(e)$ is a positive definite function of $e$

$$V(e) > 0 \; \forall \, e \in \mathcal{D}, e \neq 0. \tag{4.14}$$

3. The optimal feedback control law is zero at the origin:

$$P^*_{batt}(0) = 0. \tag{4.15}$$

4. Asymptotic stability of the origin is achieved when the optimal control law is applied, i.e. $\dot{V}(P^*_{batt}) < 0$:

$$\begin{cases} \frac{\partial V}{\partial e} f_e(P^*_{batt}(e)) < 0 \; \forall e \in \mathcal{D}, e \neq 0, \\ = \mu e f_e(P^*_{batt}(e)) < 0, \\ \Rightarrow \begin{cases} f_e(P^*_{batt}(e) < 0 \Rightarrow P^*_{batt}(e) < 0 \; \forall e > 0, \\ f_e(P^*_{batt}(e) > 0 \Rightarrow P^*_{batt}(e) > 0 \; \forall e < 0. \end{cases} \end{cases} \tag{4.16}$$

5. The Hamiltonian function $\bar{\mathcal{H}}_1$ takes on the minimum value of zero when the optimal control law $(P_{batt} = P^*_{batt}(e))$ is applied:

$$\begin{cases} \bar{\mathcal{H}}_1(e, P^*_{batt}(e), \left(\frac{\partial V}{\partial e}\right)^T) = 0, \\ \Rightarrow \dot{m}_f(P^*_{batt}(e)) = -\frac{\partial V}{\partial e} f_e(P^*_{batt}(e)) \; \forall e \in \mathcal{D}. \end{cases} \tag{4.17}$$

From (4.17), substituting the expression of fuel consumption (4.8), the optimal control law $P^*_{batt}(e)$ from nonlinear state feedback is:

$$\begin{cases} P^*_{batt} = \frac{2V_{oc}}{c\mu} e - \frac{4R_{eq}}{c^2 \mu^2} e^2, \\ c = \frac{2R_{eq} Q_{max} p_1}{\alpha}. \end{cases} \tag{4.18}$$

109
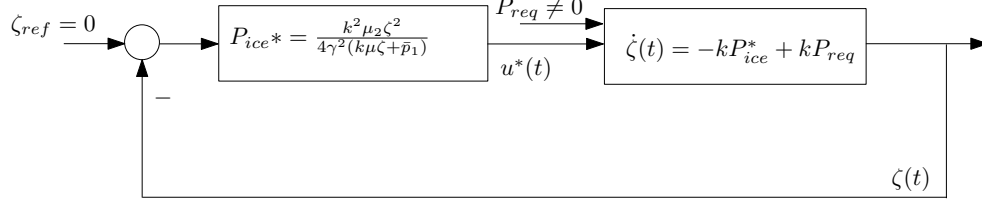
Figure 4.3: Energy management strategy as a nonlinear optimal regulation problem with disturbance rejection

6. The Hamiltonian function $\bar{\mathcal{H}}_1$ takes on a value greater than zero when a control law $(P_{batt})$ other than the optimal control law $(P_{batt}^*)$ is applied:

$$\begin{cases} \bar{\mathcal{H}}_1(e, P_{batt}, \left(\frac{\partial V}{\partial e}\right)^T) \geq 0, \\ \Rightarrow \dot{m}_f(e, P_{batt}) \geq \frac{\partial V}{\partial e} f_e(P_{batt}) \ \ \forall e \in \mathcal{D}, \ u \in \Omega_1. \end{cases} \tag{4.19}$$

All the sufficient conditions are satisfied and the optimal control law $(P_{batt}^*(e))$ as a function of the state variable is obtained.

## 4.3    Extension to Disturbance Rejection Case

This section deals with extending the theorem proved in Section 4.2 to include the case of external disturbances. The theorem formulated in the last section assumes that the vehicle is stopped and the requested power at the wheels is zero. The situation considered now corresponds to the vehicle moving and the energy management strategy must find the optimal torque/power split between the engine and electric motor. Thus we formulate the energy management problem with the vehicle operating in parallel mode (Fig. 2.4) as a nonlinear optimal regulation problem with disturbance rejection as shown in Fig. 4.3. The battery SOE is used instead of battery SOC because it is more convenient in formulating the theorem and its proof from a control design stand point. The battery SOE is defined as the amount of battery energy stored, relative to the maximum energy capacity of the

battery, which can be expressed as

$$
\begin{cases}
\dot{SOE} = -\eta_{batt}\frac{P_{batt}}{E_{max}}, \\
E_{max} = Q_{max}V_{oc,max},
\end{cases}
\tag{4.20}
$$

where $\eta_{batt}$ is the constant efficiency of the battery, $V_{oc,max}$ is the constant maximum open-circuit voltage of the battery and $E_{max}$ is the constant maximum battery energy capacity. The battery SOE can be calculated from SOC using a simple relationship,

$$
SOE = SOC\frac{V_L}{V_{oc,max}},
\tag{4.21}
$$

where $V_L$ is the terminal voltage of the battery and $SOC$ is the battery state of charge as defined in (2.22). The power requested at the wheels ($P_{req}$) is considered as disturbance to the system. The error in battery state of energy, SOE, ($\zeta = SOE_{ref} - SOE$) and engine power ($P_{ice}$) are considered as the state and control variables of the system. Define the battery $SOE$ error ($\zeta$) dynamics as a function of the control input ($P_{ice}$) in the manner

$$
\begin{cases}
\zeta = SOE_{ref} - SOE, \\
\dot{\zeta} = -kP_{ice} + kP_{req}, \\
k = \frac{\eta_{batt}}{E_{max}\eta_{mot}},
\end{cases}
\tag{4.22}
$$

where $k$ is a constant dependent on the battery and electric motor parameters, $\eta_{mot}$ is the electric motor efficiency and $P_{req}$ is the requested power at the gearbox (external disturbance to the system).

### 4.3.1 Mathematical Preliminaries

Consider an open set $\mathcal{Z} \subset \mathbb{R}$ such that $\zeta \in \mathcal{Z}$, an arbitrary set $\mathcal{U}_2 \subset \mathbb{R}$ such that $P_{ice} \in \mathcal{U}_2$ and $0 \in \mathcal{Z}, 0 \in \mathcal{U}_2$. In this case, the state domain and control domain can be defined as

$$
\begin{cases}
\zeta \in \mathcal{Z} = [SOE_{ref} - SOE_{max}, SOE_{ref} - SOE_{min}], \\
P_{ice} \in \mathcal{U}_2 = [0, P_{ice,max}].
\end{cases}
$$

Also consider the disturbance input to the system as $w \in \mathcal{W}$ such that $\mathcal{W} \subset \mathbb{R}$. In the parallel mode of operation, the power requested at the gearbox ($P_{req}$) as defined in (2.5) is the disturbance input $w = P_{req}$. Now consider the controlled system

$$\begin{cases} \dot{\zeta} = -kP_{ice} + kP_{req}, & \zeta(0) = \zeta_0, \quad t \geq 0, \\ z = \zeta, \end{cases} \tag{4.23}$$

where $z$ is the performance variable. The control input $P_{ice}(\cdot)$ is restricted to the class of *admissible* controls consisting of measurable functions $P_{ice}(\cdot)$ such that

$$P_{ice} \in \Omega_2, \quad t \geq 0, \tag{4.24}$$

where the control constraint set $\Omega_2 \subset \mathcal{U}_2$ is compact and $0 \in \Omega_2$. Let the *optimal control law* $P_{ice}^*$ be a measurable mapping $P_{ice}^* : \mathcal{Z} \to \Omega_2$ satisfying $P_{ice}^*(0) = 0$. Now the system (4.23) with feedback control $P_{ice} = P_{ice}^*(\zeta)$, has the form

$$\dot{\zeta} = -kP_{ice}^* + kP_{req}, \quad \zeta(0) = \zeta_0, \quad t \geq 0. \tag{4.25}$$

In order to address the problem of characterizing feedback controllers that minimize a performance functional, let $\Gamma(\zeta) : \mathcal{Z} \to \mathbb{R}, \mathcal{H}_2 : \mathbb{R} \times \mathbb{R} \times \mathbb{R} \to \mathbb{R}, \dot{m}_f : \mathbb{R} \to \mathbb{R}$ and $\lambda \in \mathbb{R}$ such that,

$$\mathcal{H}_2(\zeta, P_{ice}, \lambda) \triangleq \dot{m}_f(P_{ice}) + \Gamma(\zeta) + \lambda \cdot (-kP_{ice}), \tag{4.26}$$

where $\mathcal{H}_2(\cdot, \cdot, \cdot)$ is the Hamiltonian function, $\Gamma(\zeta)$ is a positive definite function of $\zeta$, $\lambda$ is the co-state variable and $\dot{m}_f(\cdot)$ is the instantaneous fuel consumption rate of the engine. Because the vehicle is operating in parallel mode, the engine speed ($\omega_{ice}$) is directly determined from the gearbox speed ($\omega_{gb}$). The fuel consumption rate model (2.9) can be written as

$$\dot{m}_f(t) = \frac{1}{Q_{LHV}} [e_0(\omega_{gb}(t)) + e_1(\omega_{gb}(t)) P_{ice}(t)]. \tag{4.27}$$

112

Under the assumption that the slope and intercept of the Willans line model are independent of the engine speed, the fuel consumption rate can be expressed as an affine function of the control input, i.e., engine power $P_{ice}$ in the manner

$$\dot{m}_f(t) = p_2 + p_3 P_{ice}(t), \tag{4.28}$$

where $p_2, p_3$ are known constants obtained from fitting the fuel consumption rate map with the engine power $P_{ice}$. Finally, without loss of generality, a new Hamiltonian function $\bar{\mathcal{H}}_2$ is defined to take on zero-value when evaluated at the optimal control, as

$$\begin{cases} \mathcal{H}_2(\zeta, P_{ice}, \lambda) = \dot{m}_f(P_{ice}) + \Gamma(\zeta) + \lambda \cdot (-kP_{ice}), \\ \bar{\mathcal{H}}_2(\zeta, P_{ice}, \lambda) \triangleq \mathcal{H}_2(\zeta, P_{ice}, \lambda) - p_2, \end{cases} \tag{4.29}$$

where $p_2$ is a parameter of the engine fuel consumption rate model as given in (4.28).

The result that follows gives sufficient conditions under which the origin $\zeta = 0$ can be locally asymptotically stabilized under nonlinear state feedback control, while assuring optimality with respect to the fuel consumed over an infinite time horizon in the presence of external disturbances. The feedback controller guarantees stability, minimizes an auxiliary performance functional, and guarantees that the input-output map of the closed-loop system is dissipative, nonexpansive, and passive [49] for bounded input disturbances. In the context of charge-sustaining HEVs, the considered scenario corresponds to the vehicle driven for a driving cycle considering the power request at the wheels as an external disturbance to the system (Fig. 4.3). What follows is an extension of the theorem proposed in Section 4.2 in the presence of external disturbances based on the results given in [49].

**Theorem 2.** *Consider the system (4.23) with performance functional*

$$J(\zeta_0, P_{ice}(\cdot)) \triangleq \int_0^\infty \dot{m}_f(P_{ice})dt. \tag{4.30}$$

*Then with the feedback control $P_{ice} = P_{ice}^*(\zeta)$, where $P_{ice}^*$ satisfies*

$$P_{ice}^* = \frac{k^2\mu^2\zeta^2}{4\gamma^2\left(k\mu\zeta + p_3\right)}, \tag{4.31}$$

*the solution $\zeta(t) = 0$, $t \geq 0$ of the closed-loop system (4.25) is locally asymptotically stable and the optimal feedback control law $P_{ice}^*(\zeta(\cdot))$ minimizes $J(\zeta_0, P_{ice}(\cdot))$.*

**Proof**: Considering the candidate Lyapunov function $V(\zeta) = \frac{1}{2}\mu\zeta^2$, $\mu > 0$ and functions $\Gamma(\zeta) = \frac{1}{4\gamma^2}\left(\frac{\partial V}{\partial \zeta}\right)^2 k^2$, and $r(\zeta, P_{req}) = \gamma^2 P_{req}^2 - \zeta^2, \gamma, k > 0$, the local asymptotic stability of the origin $\zeta(t) = 0$ and optimality of $P_{ice}^*$ with respect to $J(\zeta_0, P_{ice}(\cdot))$ are proved using the following conditions taken from Theorem 4.7.4 and from the book [49]:

1. The Lyapunov function $V(\zeta)$ has a minimum value of $0$ at the origin

$$V(0) = 0. \tag{4.32}$$

2. The candidate Lyapunov function $V(\zeta)$ is a positive definite function. In fact, $V(\zeta)$ is a quadratic function of $\zeta$, and

$$V(\zeta) > 0 \ \forall \zeta \in \mathcal{Z}, \zeta \neq 0. \tag{4.33}$$

3. The optimal feedback control law is zero at the origin:

$$P_{ice}^*(0) = 0. \tag{4.34}$$

4. Asymptotic stability of the origin is achieved when the optimal control law is applied, i.e. $\dot{V}(P_{ice}^*) < 0$:

$$\begin{cases} \frac{\partial V}{\partial \zeta}(-kP_{ice}^*(\zeta)) < 0 \ \forall \zeta \in \mathcal{Z}, \zeta \neq 0, \\ \Rightarrow \begin{cases} P_{ice}^*(e) < 0 \ \forall e < 0, \\ P_{ice}^*(e) > 0 \ \forall e > 0. \end{cases} \end{cases} \tag{4.35}$$

114

This analysis provides conditions on the sign of state feedback control law $P_{ice}^*(\zeta)$ and because the engine power cannot be negative, the signs of the optimal feedback law can be expressed as:

$$\begin{cases} P_{ice}^*(\zeta) = 0, & \forall \, e \leq 0, \\ P_{ice}^*(\zeta) > 0, & \forall \, e > 0. \end{cases} \tag{4.36}$$

5. The Hamiltonian function $\bar{\mathcal{H}}_2$ takes on the minimum value of zero when the optimal control law $(P_{ice} = P_{ice}^*(\zeta))$ is applied:

$$\begin{cases} \bar{\mathcal{H}}_2\left(\zeta, P_{ice}^*, \left(\frac{\partial V}{\partial \zeta}\right)\right) = 0, \\ p_3 P_{ice}^* + \frac{1}{4\gamma^2} k^2 \mu^2 \zeta^2 - k\mu\zeta P_{ice}^* = 0 \ \forall \zeta \in \mathcal{Z}. \end{cases} \tag{4.37}$$

The optimal nonlinear state feedback control law $(P_{ice}^*)$ can now be expressed as

$$\begin{cases} P_{ice}^* = \frac{k^2 \mu^2 \zeta^2}{4\gamma^2 (k\mu\zeta + p_3)}, \\ k = \frac{\eta_{batt}}{E_{max}\eta_{mot}} > 0, \gamma > 0, \mu > 0. \end{cases} \tag{4.38}$$

6. The Hamiltonian function $\bar{\mathcal{H}}_2$ takes on a value greater than zero when a control law $(P_{ice})$ other than the optimal control law $(P_{ice}^*)$ is applied:

$$\bar{\mathcal{H}}\left(\zeta, P_{ice}, \left(\frac{\partial V}{\partial e}\right)\right) \geq 0. \tag{4.39}$$

7. In order to prove passivity with respect to the disturbance input $P_{req}(t)$, the following condition must be satisfied:

$$\begin{cases} \frac{\partial V}{\partial \zeta} k P_{req} \leq r(\zeta, Preq) + \dot{m}_f(P_{ice}^*(\zeta)) + \Gamma(\zeta), \\ \Rightarrow k\mu\zeta P_{req} \leq \gamma^2 P_{req}^2 + \zeta^2 \left[\frac{k^2 \mu^2}{4\gamma^2} - 1\right] + p_3. \end{cases} \tag{4.40}$$

If there exists a constant $\gamma$ such that $\gamma \geq 3k$, then a minimum bound for $\mu$ can be calculated as

$$\frac{\zeta^2}{36}\mu^2 - (k\zeta P_{req})\mu + 9k^2 P_{req}^2 - \zeta^2 + p_3 \geq 0. \tag{4.41}$$

The passivity condition (4.40) is satisfied only if we can find a suitable $\gamma$ and $\mu$.

All the conditions are satisfied and the optimal control law $(P_{ice}^*(\zeta))$ as a function of the state variable is obtained.

## 4.4 Optimal and Stabilizing Control law

The control law $(P_{ice} = P_{ice}^*(\zeta))$ developed using the previous results can be expressed as

$$P_{ice}^* = \frac{k^2 \mu^2 \zeta^2}{4\gamma^2 (k\mu\zeta + p_3)}, \tag{4.42}$$

where $\zeta(t)$ is the error in battery SOE, $k, \gamma, p_3 > 0$ are known constants, and $\mu$ is the only calibration parameter of the control law. These parameters and constants depend on the powertrain architecture and the components; for example,

1. $k = \frac{\eta_{batt}}{E_{max}\eta_{mot}}$ is a constant depending on the battery capacity, efficiency and electric motor efficiency and the size/type of battery and electric machine;

2. $\gamma = 3k$ is a constant expressed as a function of $k$ obtained from the passivity condition in (4.40);

3. $p_3$ is a Willans line coefficient of the engine as in (4.28) which depends on the size and type of the engine used; and,

4. $\mu$ is the calibration parameter that must be tuned to achieve the best performance.

According to the previous results, the control law $P_{ice}^*$ locally asymptotically stabilizes the origin $e = 0$. This implies that the battery SOE asymptotically converges to the SOE reference value. Because the battery SOC is linearly related to the battery SOE (4.21), the control law results in asymptotic convergence of the battery SOC to its reference value. In a charge-sustaining HEV, the battery SOC reference value is ideally the initial value with which the trip began. In addition to stabilizing the battery SOC, the control law minimizes the amount of fuel consumed over the infinite time horizon. That is, it is also optimal with

respect to the performance functional $J(\zeta_0, P_{ice}(\cdot))$,

$$J(\zeta_0, P_{ice}^*(\zeta)) = \min_{P_{ice}} J(\zeta_0, P_{ice}(\zeta)). \tag{4.43}$$

Though the theorem guarantees that the control law minimizes the fuel consumed over an infinite time horizon, the energy management problem in a HEV minimizes the amount of fuel consumed over a finite length (see (3.1) in Section 3.1). The presence of calibration parameter $\mu$ in the control law (4.42) signifies the application of a theoretically developed control law in a real-world application. Thus, for a given driving cycle, the sufficient conditions of asymptotic stability of battery SOE and optimality with respect to fuel consumed are assured only with the *optimal* $\mu$ ($\mu^*$). The *optimal* value of $\mu$ for a given driving cycle is obtained by studying the behavior of battery SOC and the fuel consumed over the driving cycle. The calibration of $\mu$ and its performance in comparison with the global optimal solution are described in Section 4.5.

### 4.4.1  Analysis over a simple driving cycle

In order to understand the effect of calibration parameter $\mu$, a simple synthetic driving cycle as shown in Fig. 4.4 is used. The driving cycle consists of three events namely acceleration, cruise and deceleration. The acceleration event lasts for 2 minutes, the deceleration event for 4 minutes and the vehicle is at a constant speed of 20 m/s for about 9 minutes. The optimizing and stabilizing control law (4.42) is used to find the optimal power split between the engine and the battery using different values of $\mu$. As $\mu$ is increased from very low to very high values, the optimal engine power $P_{ice}^*$ increases and the power requested is supplied primarily by the engine as seen in figures 4.5 and 4.6. The effect of increasing $\mu$ on battery $SOC$ and current is clearly seen in figures 4.9 and 4.10. As seen in Fig. 4.10, the battery is used more as the value of $\mu$ decreases.
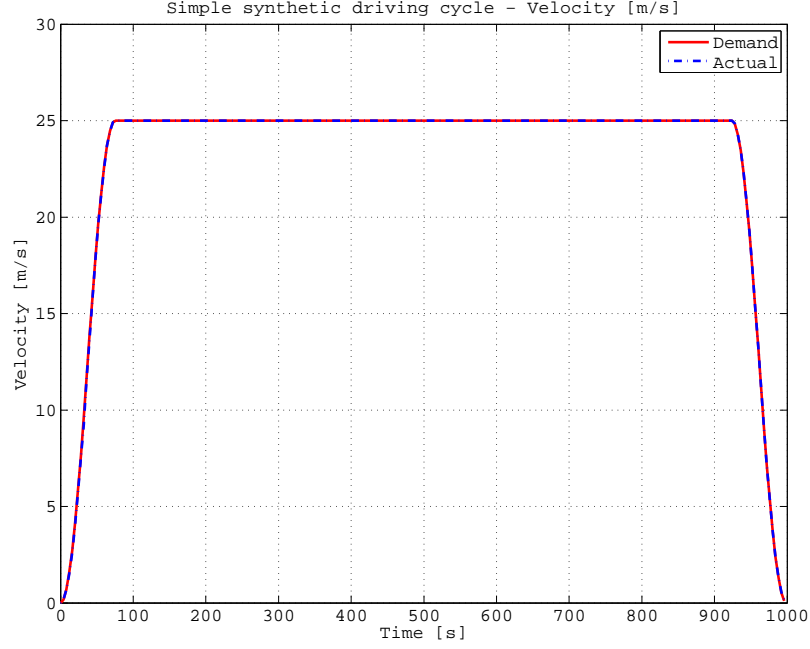
Figure 4.4: Synthetic driving cycle

The performance of the control law for different values of $\mu$ is evaluated using the metrics defined as,

- Deviation in $SOC$: Because in a charge-sustaining HEV, the net energy used from the battery is zero, the average battery $SOC(\bar{SOC})$ over a driving cycle is desired to be close to the reference value ($SOC_{ref}$). The amount of deviation in the average battery SOC from the reference value over a driving cycle of length $T$ is defined as,

$$
\begin{cases}
\bar{SOC} = \frac{1}{T} \int_{t_0}^{t_f} SOC(t)dt, \\
DEV = \frac{\bar{SOC} - SOC_{ref}}{SOC_{ref}} * 100\%.
\end{cases}
\tag{4.44}
$$

118
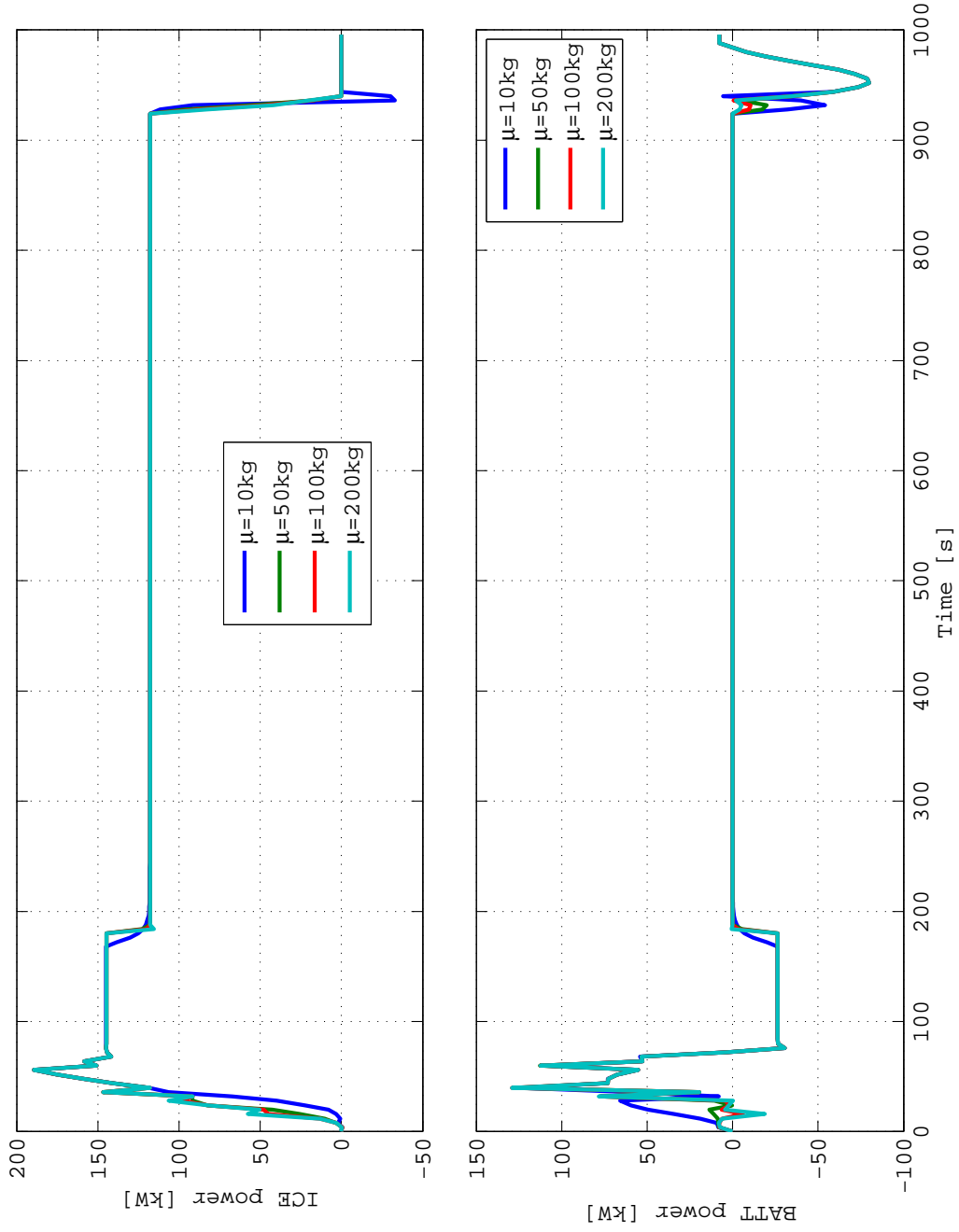
Figure 4.5: Effect of $\mu$ on engine and battery power

119
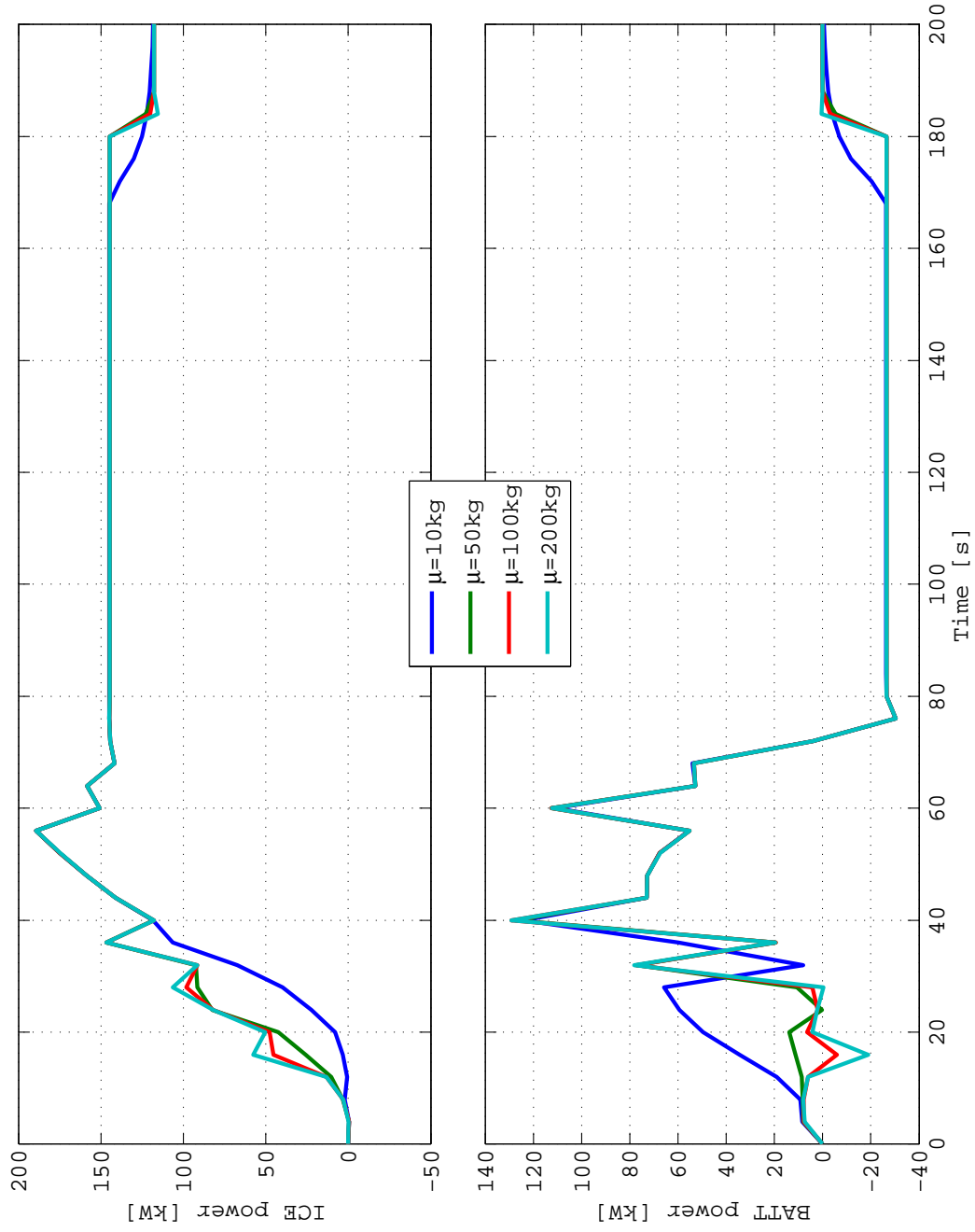
Figure 4.6: Effect of $\mu$ on engine and battery power-detailed

120
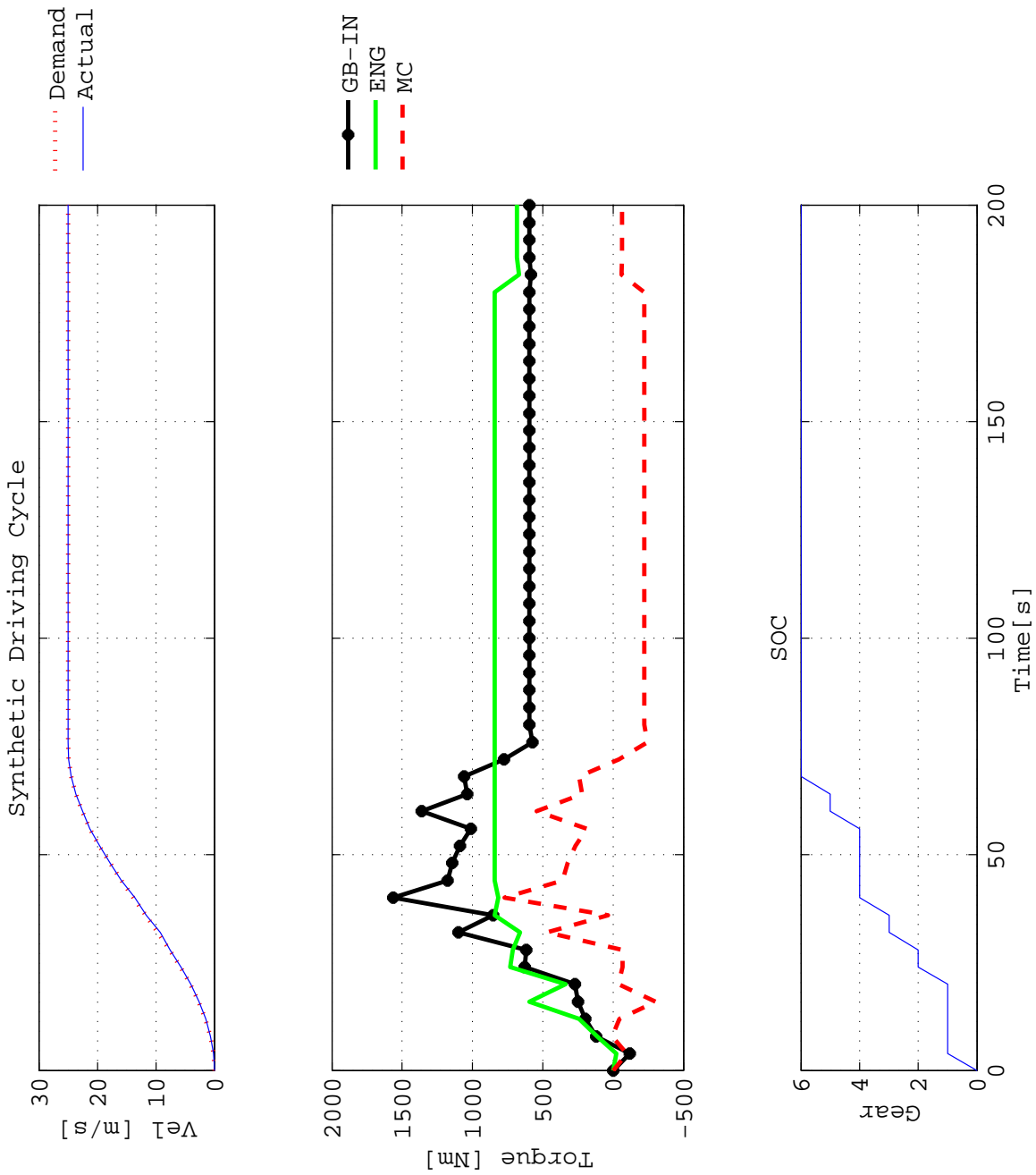
Figure 4.7: Velocity, Torque and Gear Number-detailed for $\mu = 200$
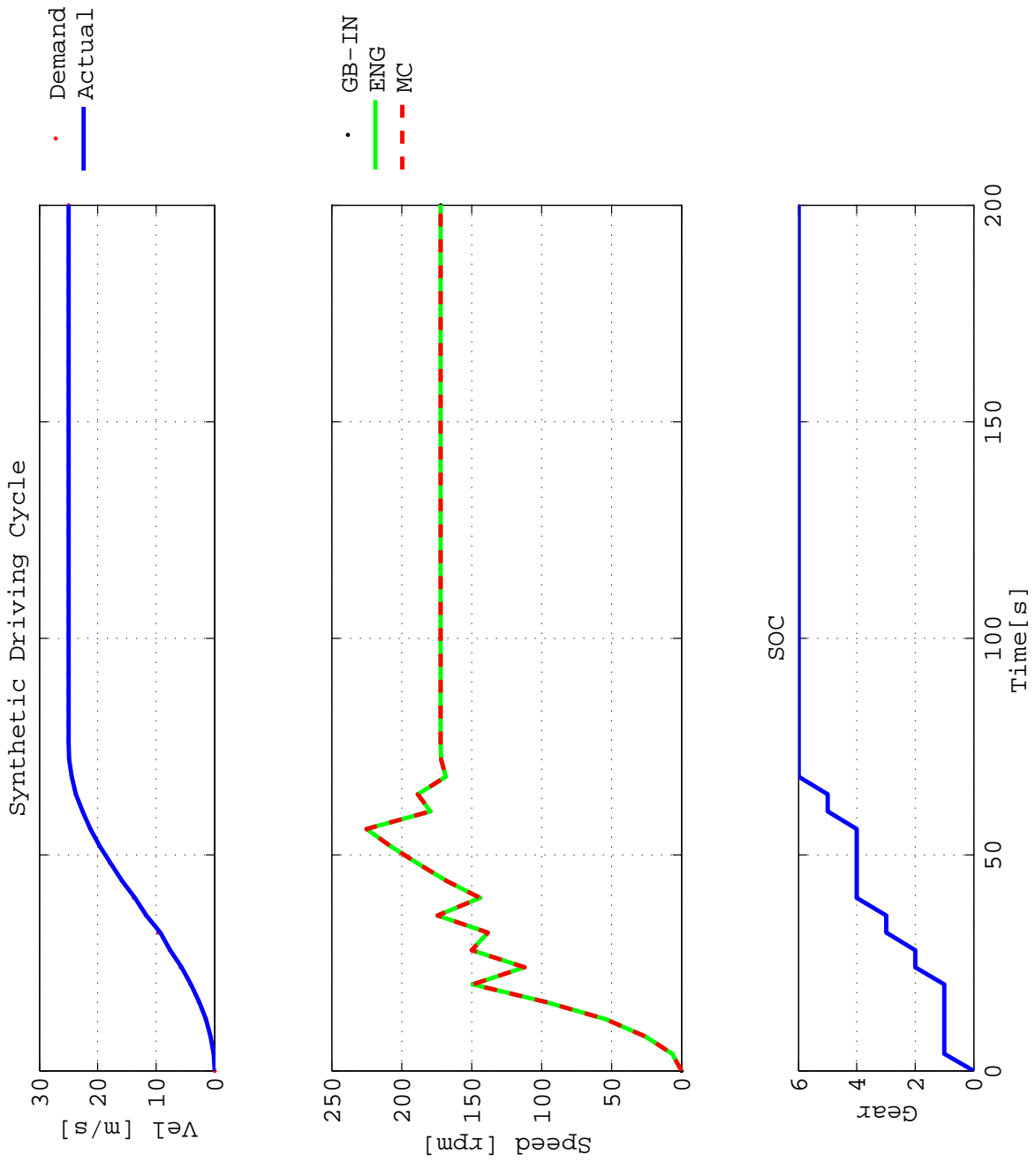
Figure 4.8: Velocity, Speed and Gear Number-detailed for $\mu = 200$
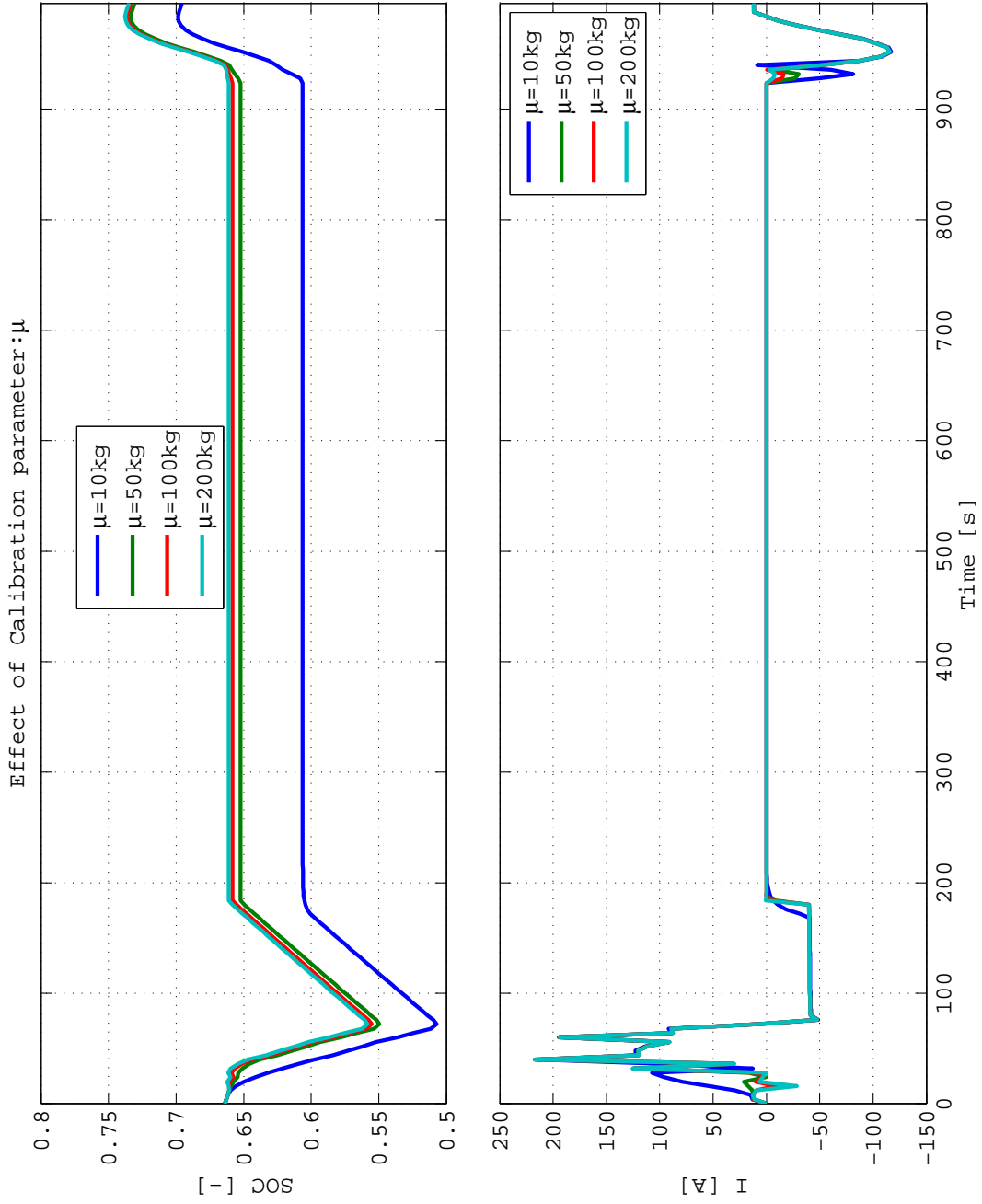
Figure 4.9: Effect of $\mu$ on $SOC$ and battery current
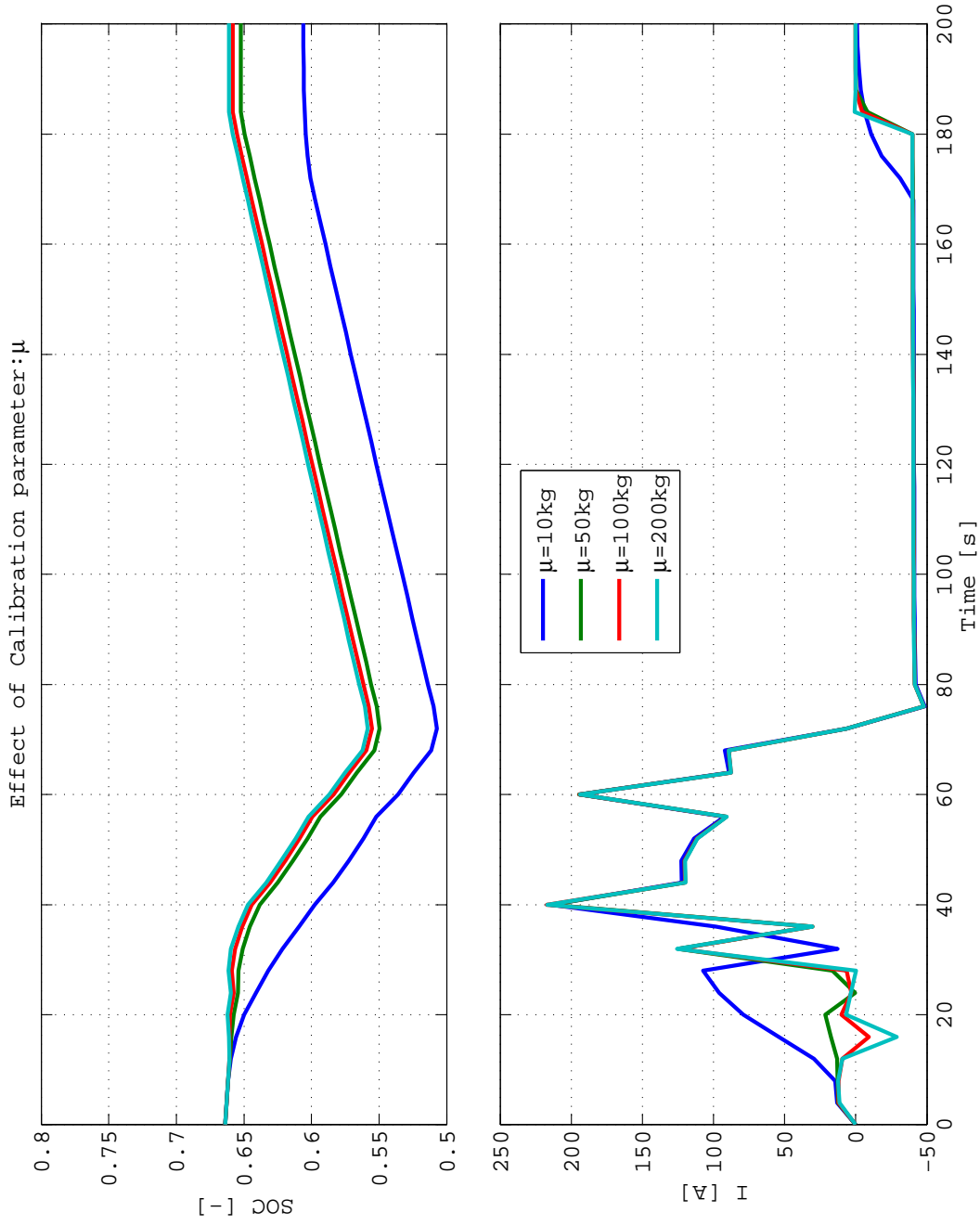
Figure 4.10: Effect of $\mu$ on *SOC* and battery current-detailed

124
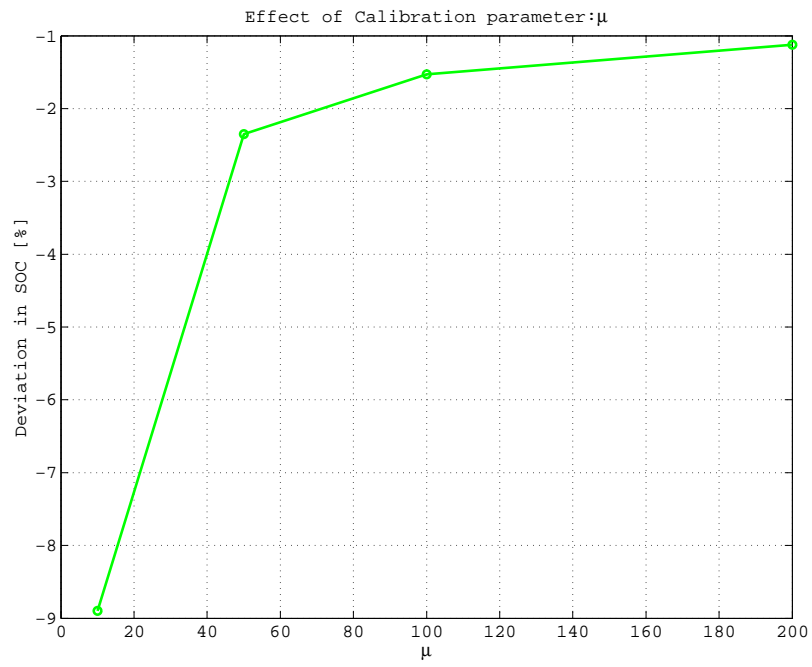
Figure 4.11: Effect of $\mu$ on deviation of SOC
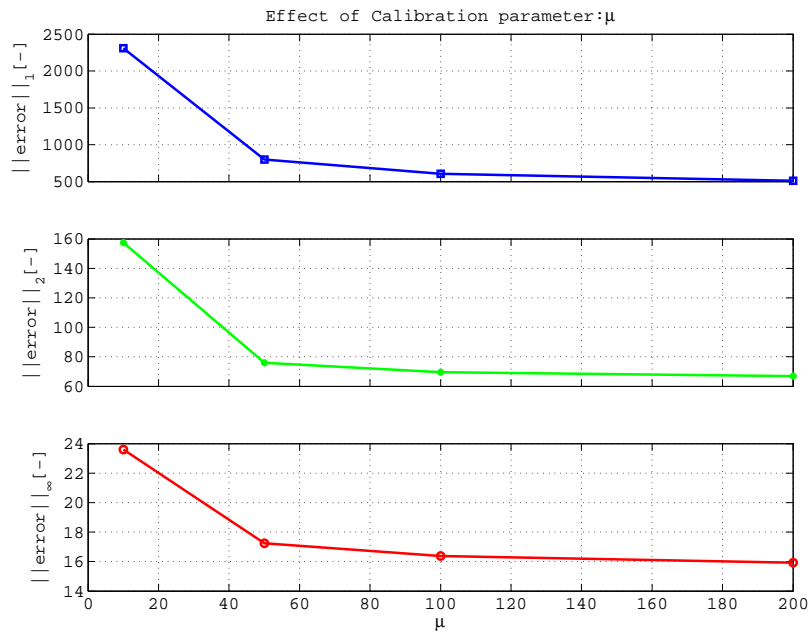


Figure 4.12: Effect of $\mu$ on norm of SOC error

- Norm in $SOC$ error: The deviation of the battery SOC at each instant over the driving cycle is characterized as $\mathcal{L}_1, \mathcal{L}_2, \mathcal{L}_\infty$ norm in battery $SOC$ error.

$$\begin{cases} error = \frac{SOC - SOC_{ref}}{SOC_{ref}} * 100\%, \\ \|error\|_1 = |error(1)| + |error(2)| + \cdots + |error(T)|, \\ \|error\|_2 = \sqrt{|error(1)|^2 + |error(2)|^2 + \cdots + |error(T)|^2}, \\ \|error\|_\infty = \max_i |error(i)|, \quad i = 1, 2, 3, \cdots, T. \end{cases} \quad (4.45)$$

The deviation in battery $SOC$ quantifies the performance of the control law in achieving charge sustainability and the norm in $SOC$ error quantifies the usage of the battery $SOC$ over the entire operating range. The effect of the calibration parameter $\mu$ on these performance metrics is shown in figures 4.11 and 4.12. It can be seen that the deviation in battery $SOC$ and the norm in $SOC$ error decreases and reaches a steady state value as $\mu$ increases.

## 4.5    Simulation Results

This section describes the simulation environment used to implement the optimal control law (abbreviated as OCL) developed using Theorem 2 from Section 4.3. The performance of the control law is compared with the global optimal solution obtained from DP (Section 3.2). The pre-transmission parallel HEV (Fig. 2.1) is modeled in the MATLAB/Simulink environment. The characteristics of the vehicle used here are shown in Table 2.1. In order to compare the performance of the proposed OCL with DP, a backward vehicle simulator (Section 2.2.2) is used. Based on the assumption that the vehicle follows the desired velocity trajectory, the torque required at the wheels and the components are calculated (Fig. 2.22). The simulator primarily uses simplified quasi-static map based models for all the components as shown given in Table 2.2. Although Theorem 2 proved in Section 4.3 assumes an infinite time horizon, the developed OCL has been implemented over a driving cycle of finite length. The implementation of OCL as a solution

of the energy management problem involves calibrating the parameter $\mu$, and comparing the performance of OCL with DP for several driving cycles. The driving cycles (Manhattan, WVU-interstate, WVU-suburban, UDDS) used here are representative of the the city, urban and highway driving conditions experienced by heavy-duty HEVs.

## 4.5.1  Calibration of parameter-$\mu$

Table 4.1: Effect of $\mu$ for Manhattan driving cycle

| Strategy | $\mu$ [kg] | Normalized $FC_{eqv}$ [%] |
|---|---|---|
| Optimal Control Law (OCL) | 10 | 106.3 |
| | 50 | 104.2 |
| | 100 | 103.6 |
| | 200 | 103.5 |
| DP | - | 100 |

The optimal control law $P_{ice}^*(\zeta)$ shown in (4.42) has a tuning parameter $\mu$ that must be calibrated to ensure convergence of battery SOC to $SOC_{ref}$ at the end of the driving cycle. Thus the *optimal and stable* energy management strategy is assured only with the *optimal* $\mu$ i.e., $\mu = \mu^*$, for each driving cycle. The effect of the calibration parameter $\mu$ on the battery SOC profile for Manhattan driving cycle is shown in Fig. 4.13. It is evident that $\mu$ affects the convergence of $SOC$ to $SOC_{ref}$ at the end of the driving cycle. The control law depletes the battery with a smaller value for $\mu$. As $\mu$ is increased, the battery SOC profile becomes increasingly similar to the DP solution. The optimal value of $\mu$ is selected based on the equivalent fuel consumed ($FC_{eqv}$) (see (3.18 for definition). The effect of using different values of $\mu$ on $FC_{eqv}$ is summarized in Table 4.1. In order to find the optimal $\mu$ ($\mu^*$) for each driving cycle, an iterative shooting method is used [17].
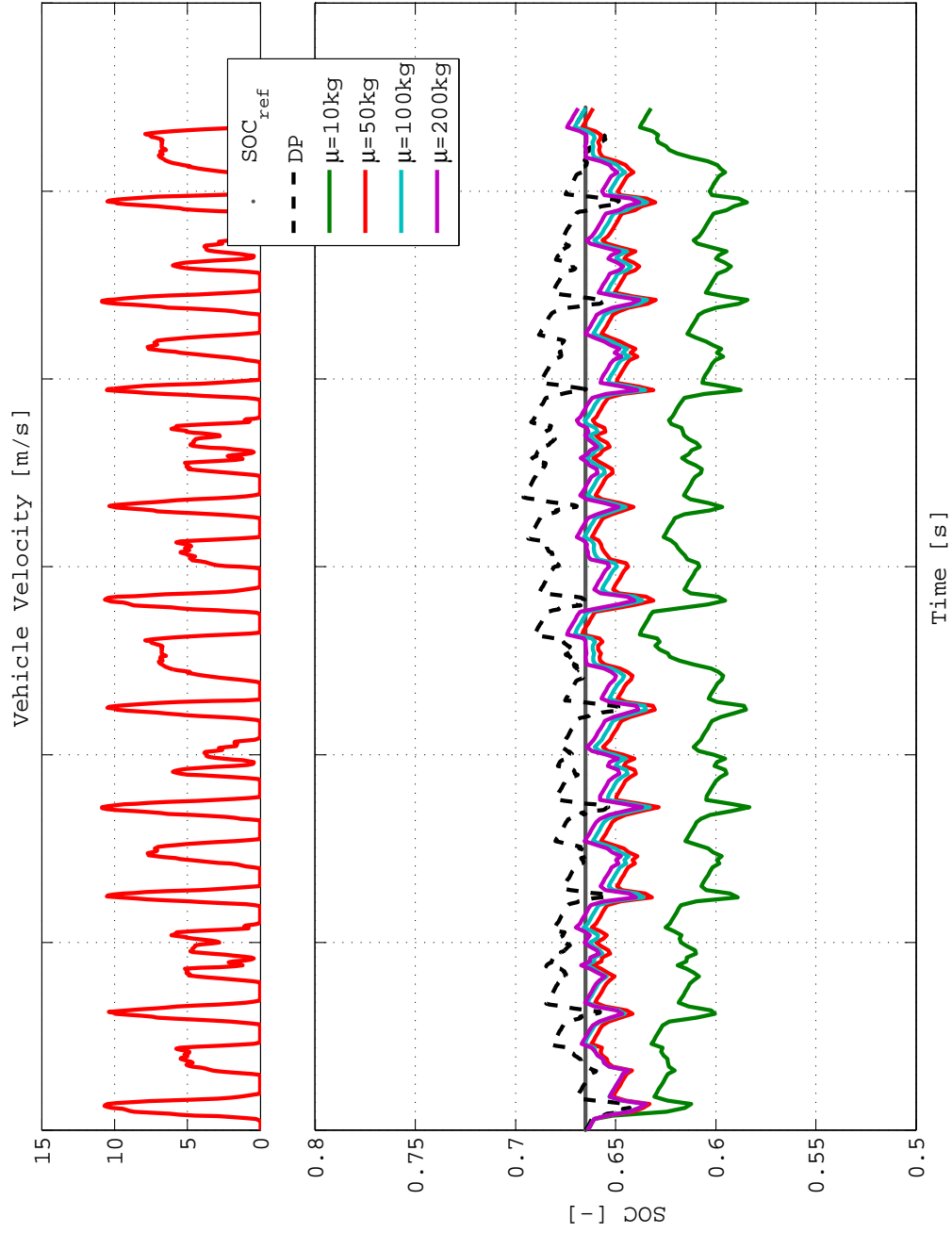
Figure 4.13: Effect of $\mu$ on *SOC*
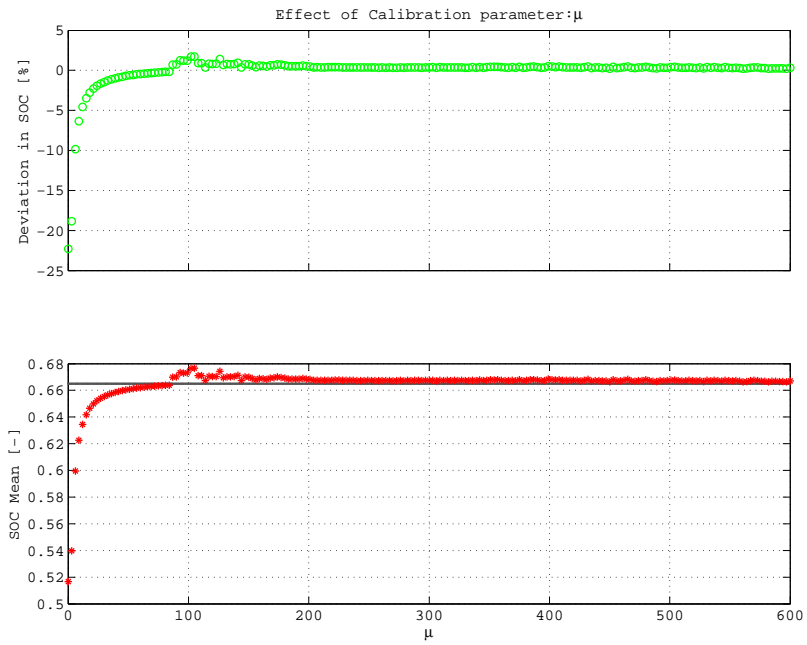
Figure 4.14: Effect of $\mu$ on deviation of SOC-Manhattan
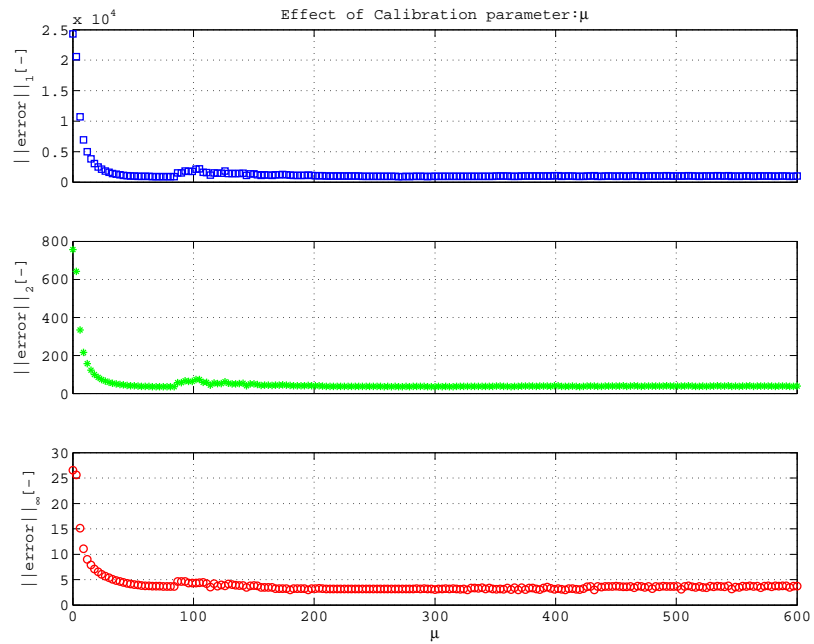


Figure 4.15: Effect of $\mu$ on norm of SOC error-Manhattan

This off-line optimization method must be performed for each driving cycle to obtain its corresponding $\mu^*$. The effect of increasing the value of $\mu$ on the deviation in battery $SOC$ can be seen in Fig. 4.14. After a particular value of $\mu$, the deviation in battery $SOC$ from the reference value saturates to a value close to zero. The variability in the battery $SOC$ over the driving cycle is characterized by $\mathcal{L}_1, \mathcal{L}_2, \mathcal{L}_\infty$ norm in battery $SOC$ error. All the three norms in battery SOC error settle to a steady state value as $\mu$ is increased.

## 4.5.2 Performance for Manhattan driving cycle

Table 4.2: Performance comparison with DP for Manhattan driving cycle

| Strategy | Normalized $FC_{eqv}$ [%] |
|---|---|
| OCL ($\mu^* = 200 \ kg$) | 103.5 |
| DP | 100 |

The performance of OCL with $\mu^* = 200 \ kg$ is compared with DP in Figures 4.16 - 4.19 and Table 4.2. As shown in Fig. 4.16, the battery SOC profile resulting from OCL is close to that of DP. Throughout the driving cycle, DP decides to use the engine at the most efficient region of operation and recharges the battery whenever possible. On the other hand, OCL calculates the engine power according to the nonlinear function of the error in SOC (4.42) which results in wider range of operating points as shown in Fig. 4.18. The electric motor operating points decided by both DP and OCL as shown in Fig. 4.19.

## 4.5.3 Performance for WVU-Interstate driving cycle

The WVU-Interstate driving cycle is representative of the highway driving conditions experienced by heavy-duty HEVs. The OCL developed in Section 4.3 is compared with the
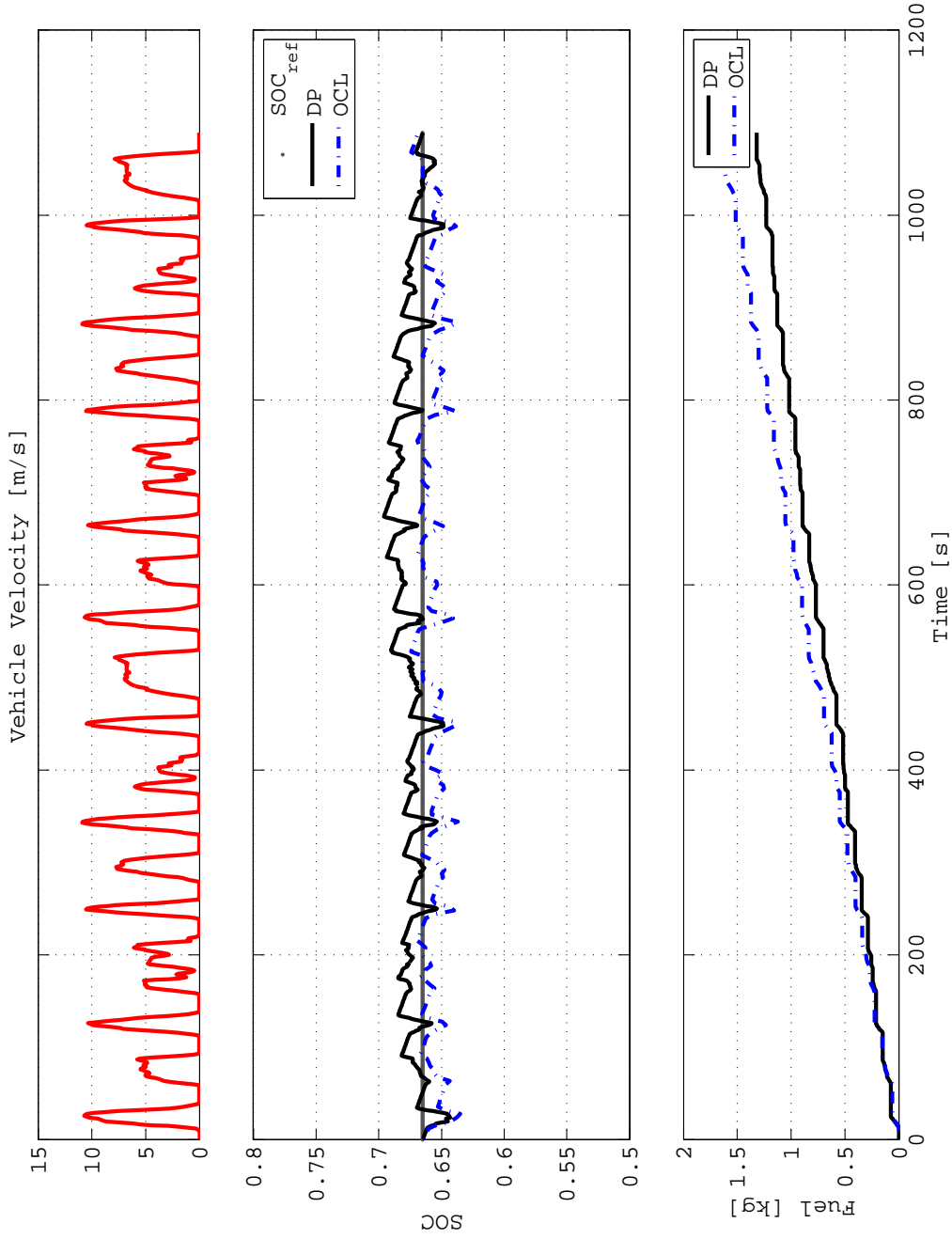
Figure 4.16: Velocity, SOC and equivalent fuel consumed (Manhattan)
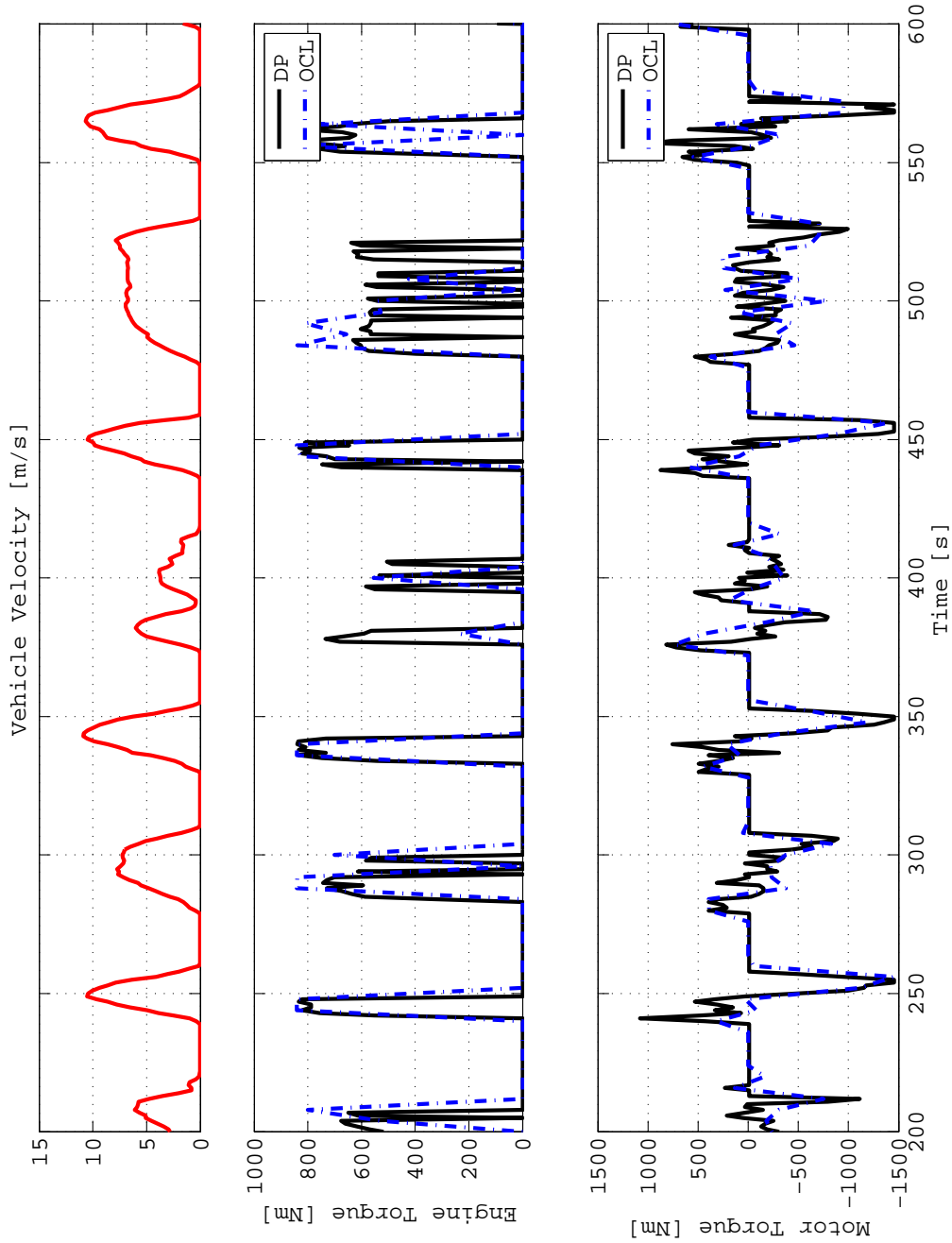
Figure 4.17: Velocity, engine and electric motor torques - detail (Manhattan)
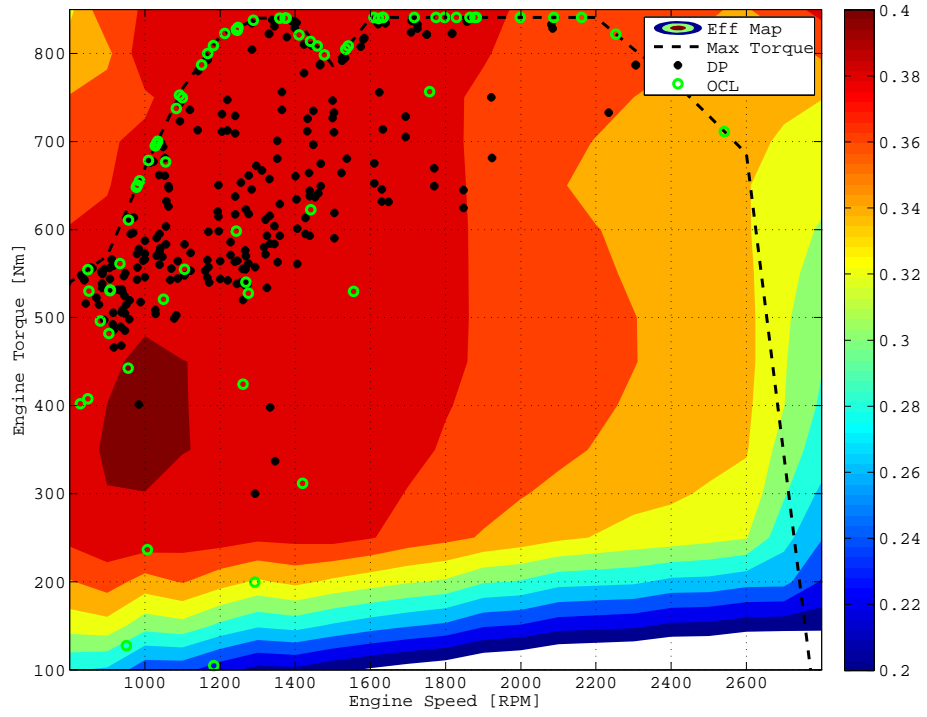
Figure 4.18: Engine operating points (Manhattan)
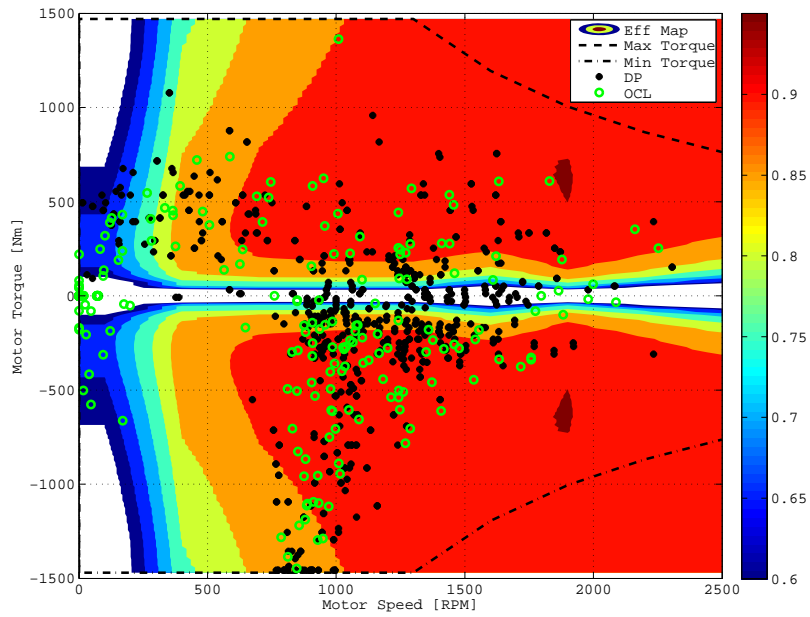


Figure 4.19: Electric motor operating points (Manhattan)

133
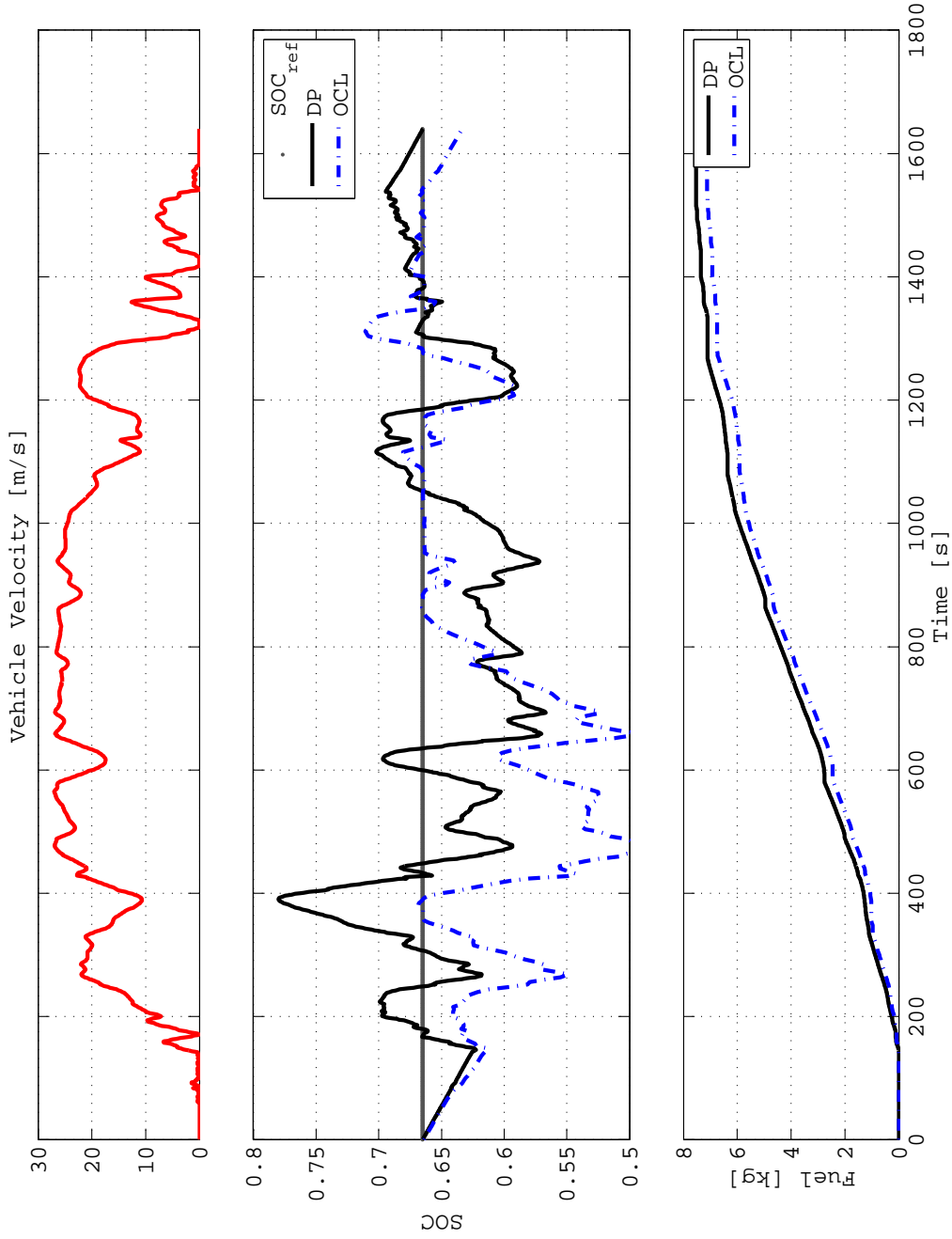
Figure 4.20: Velocity, SOC and equivalent fuel consumed (WVU-Interstate)
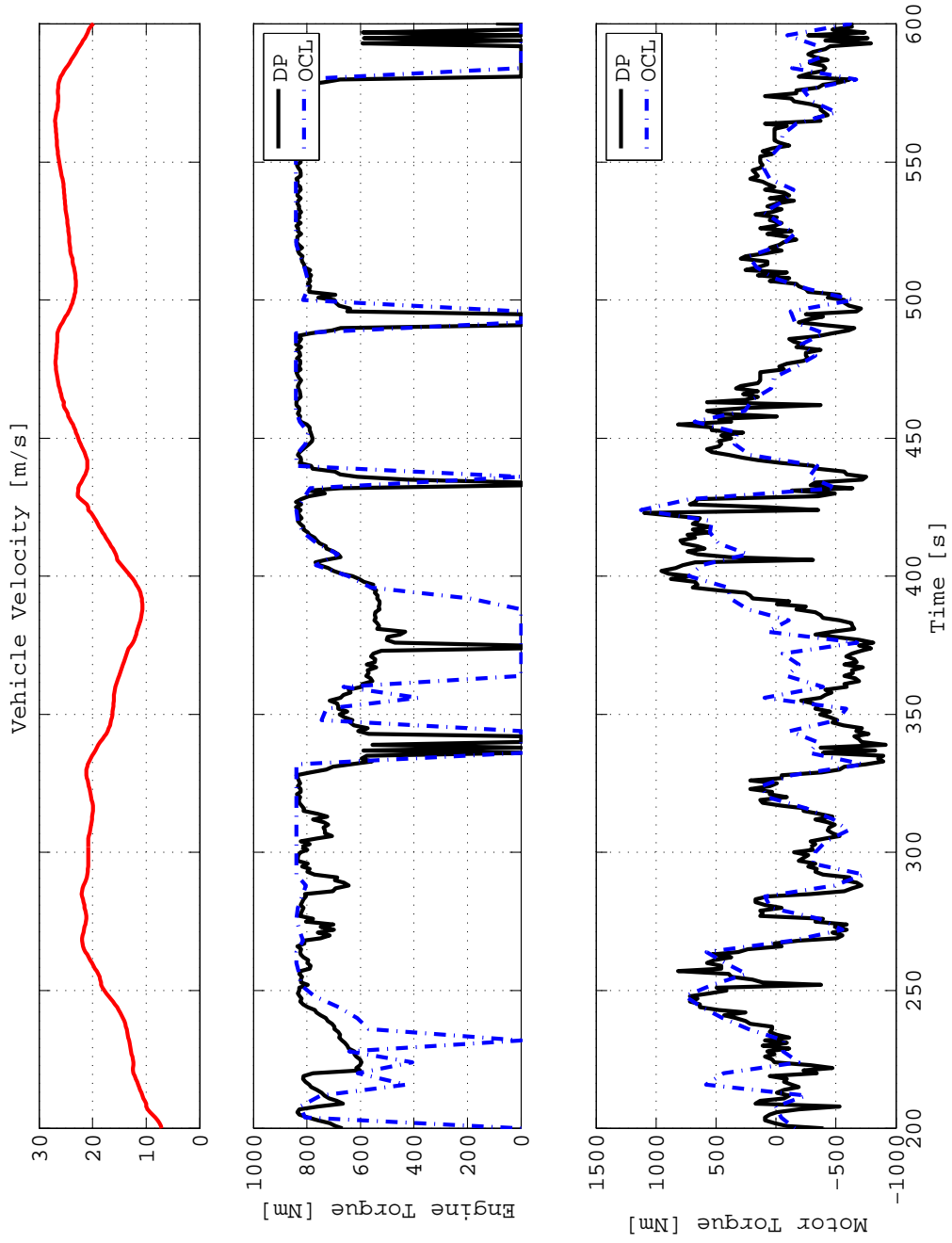
Figure 4.21: Velocity, engine and electric motor torques - detail (WVU-Interstate)
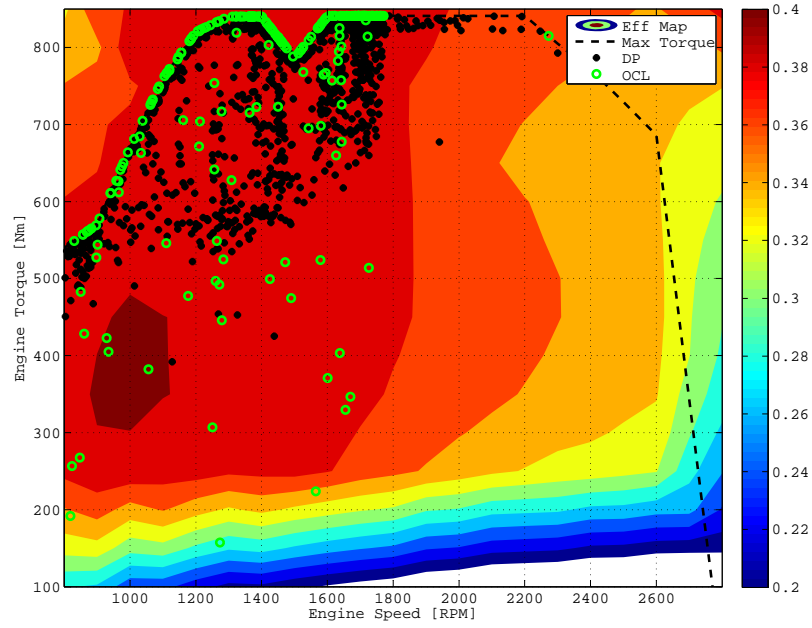
Figure 4.22: Engine operating points (WVU-Interstate)
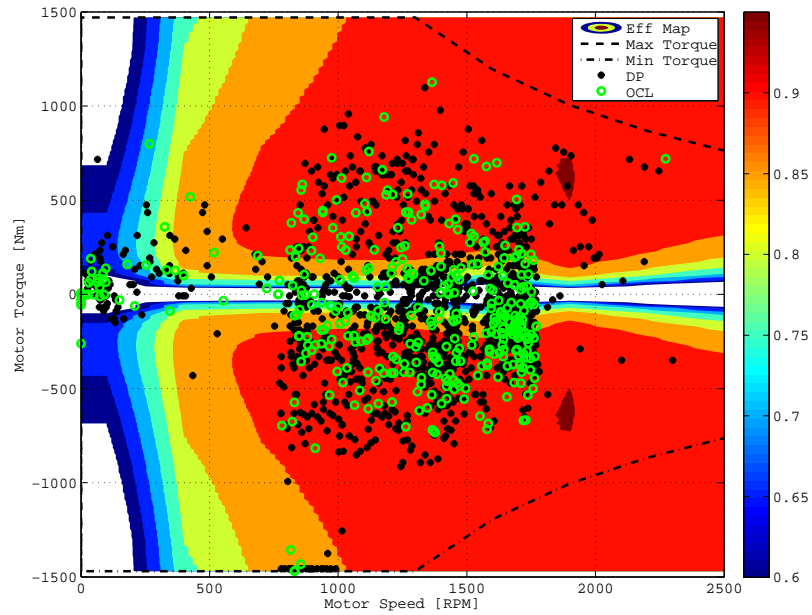


Figure 4.23: Electric motor operating points (WVU-Interstate)

136

Table 4.3: Performance comparison with DP for WVU-Interstate driving cycle

| Strategy | Normalized $FC_{eqv}$ [%] |
|---|---|
| OCL ($\mu^* = 200\ kg$) | 103.7 |
| DP | 100 |

DP solution in Figures 4.20 - 4.23 and Table 4.3. Although the battery SOC profile resulting from OCL and DP are similar in shape, the amount of charging and discharging is different. Because of the complete *a-priori* knowledge of the driving cycle, DP uses the battery by operating the engine at its most efficient regions (Fig. 4.22). On the other hand, the OCL depletes the battery more during the initial phase of the driving cycle and then recharges the battery to ensure convergence with $SOC_{ref}$ (Fig. 4.20). The engine operating points resulting from OCL are not always the most efficient because of the sudden mode change from parallel to electric, evident from Fig. 4.21. The battery SOC profile and engine and electric motor operating points resulting from OCL account for the excess amount of fuel consumed (3% more than DP).

## 4.5.4   Performance for WVU-Suburban driving cycle

Table 4.4: Performance comparison with DP for WVU-Suburban driving cycle

| Strategy | Normalized $FC_{eqv}$ [%] |
|---|---|
| OCL ($\mu^* = 200\ kg$) | 104.4 |
| DP | 100 |
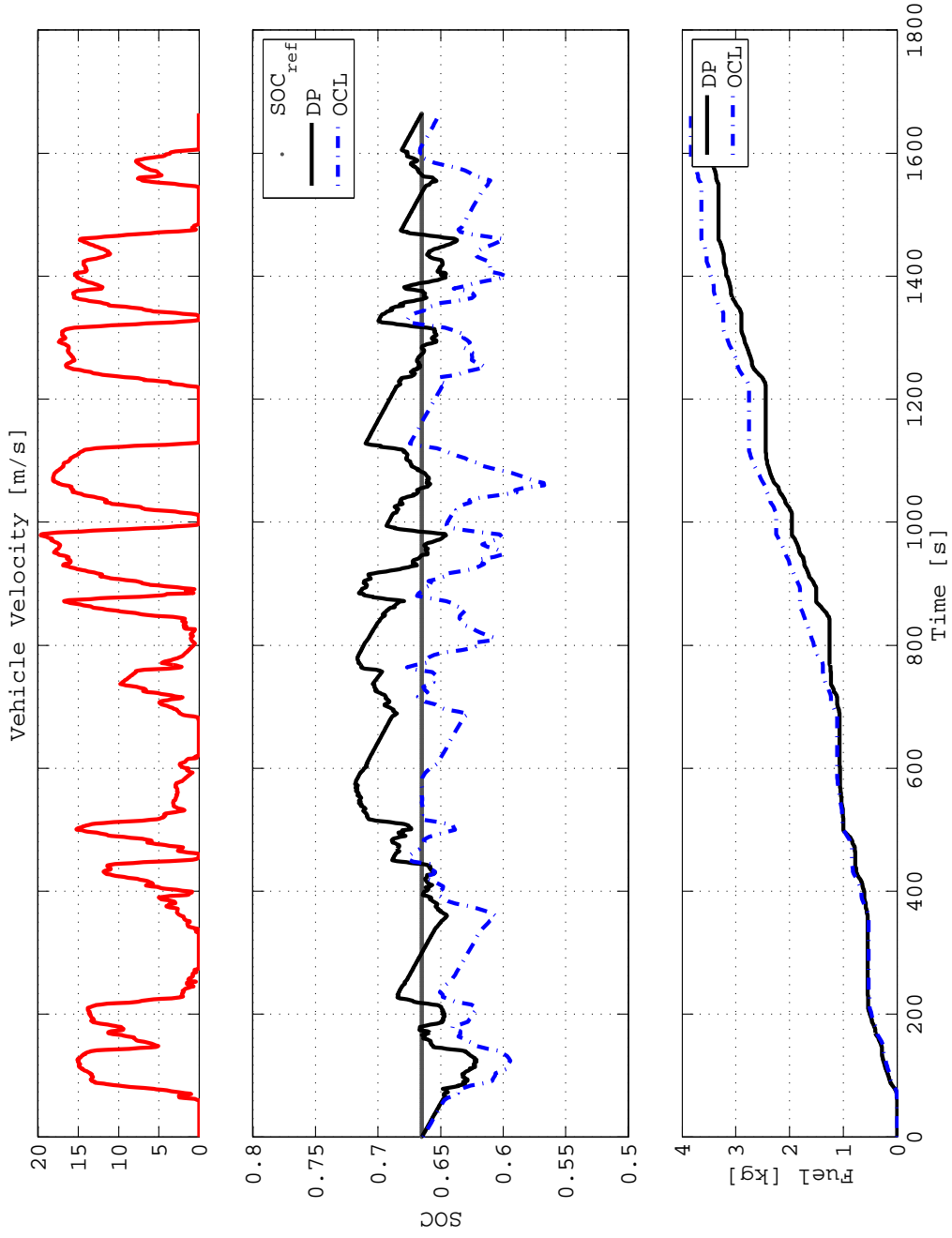
Figure 4.24: Velocity, SOC and equivalent fuel consumed (WVU-Suburban)
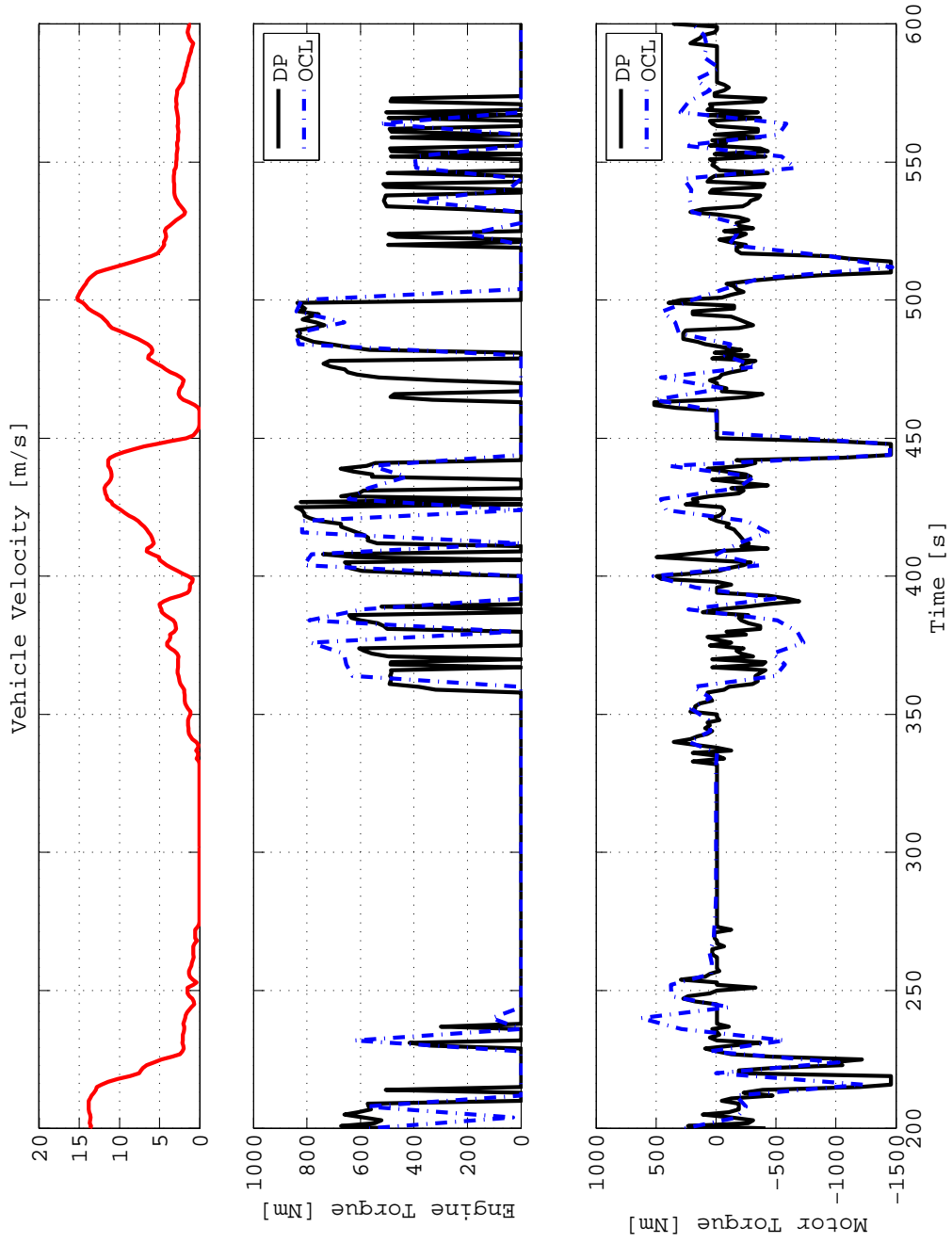
Figure 4.25: Velocity, engine and electric motor torques - detail (WVU-Suburban)
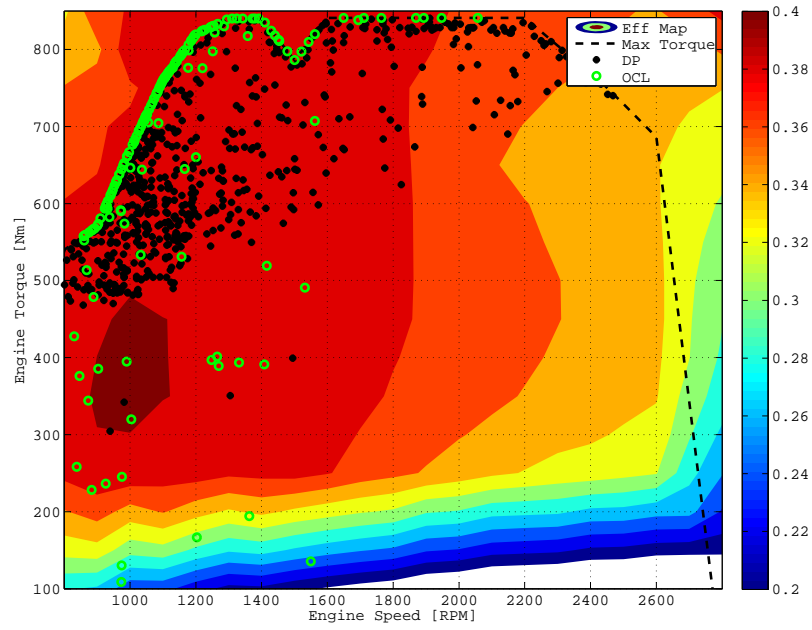
Figure 4.26: Engine operating points (WVU-Suburban)
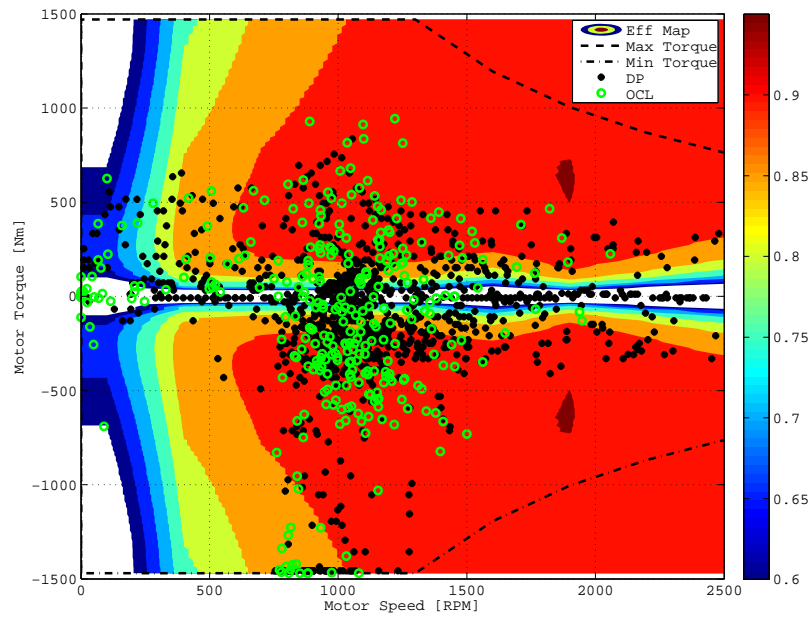


Figure 4.27: Electric motor operating points (WVU-Suburban)

Similar to the Manhattan driving cycle, the WVU-Suburban driving cycle is an urban heavy-duty driving cycle. The performance of OCL is compared with DP in Figures 4.24 - 4.27 and Table 4.4. The torque split decision taken by OCL coincides with the optimal solution from DP during selected sections of the driving cycle as seen in Fig. 4.24. Moreover, the OCL switches off the engine whenever there is small braking event, evident from the engine and electric motor torque plots shown in Fig. 4.25. This kind of engine and electric motor operation can be also seen from the operating points shown in Figures 4.26 and 4.27. The difference in the amount of fuel consumed between OCL and DP (4.4%) is a direct result of the issues mentioned here.

### 4.5.5 Performance of Optimal Control Law for Combined Driving Cycle

In order to check the effectiveness of the optimal control law, the strategy is implemented in the pre-transmission parallel HEV over a driving cycle that is a combination of urban and highway driving cycles. The driving cycle consists of the manhattan driving cycle, wvu-interstate and wvu-suburban driving cycle. As seen from Fig. 4.28, the optimal control law maintains the battery SOC close to the reference throughout the driving cycle. The torque split between the engine and electric motor is shown in Fig. 4.29 and the operating points are shown in figures 4.30 and 4.31.

### 4.5.6 Sensitivity of optimal control law with respect to $\mu$

Because the optimality and stability properties of the control law developed in Section 4.3 depends on the *optimal* value of $\mu$, it is important to study the sensitivity of the results with respect to $\mu$. In order to generalize the effects of $\mu$, the deviation in $SOC$ (4.44) is calculated for a wide range of $\mu$ for different representative driving cycles. The effect of

141
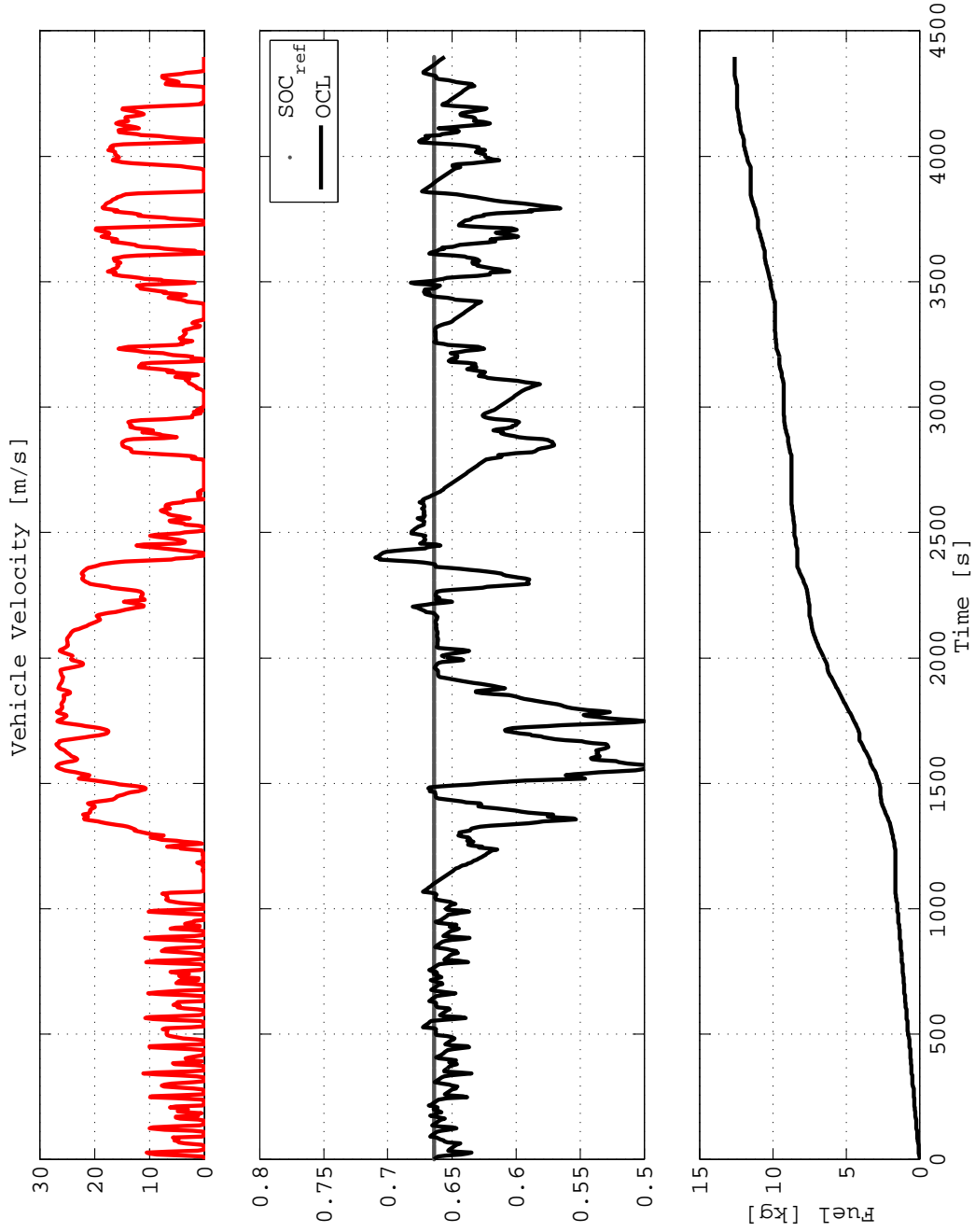
Figure 4.28: Velocity, SOC and equivalent fuel consumed (Manh-WVUinter-WVUsub)
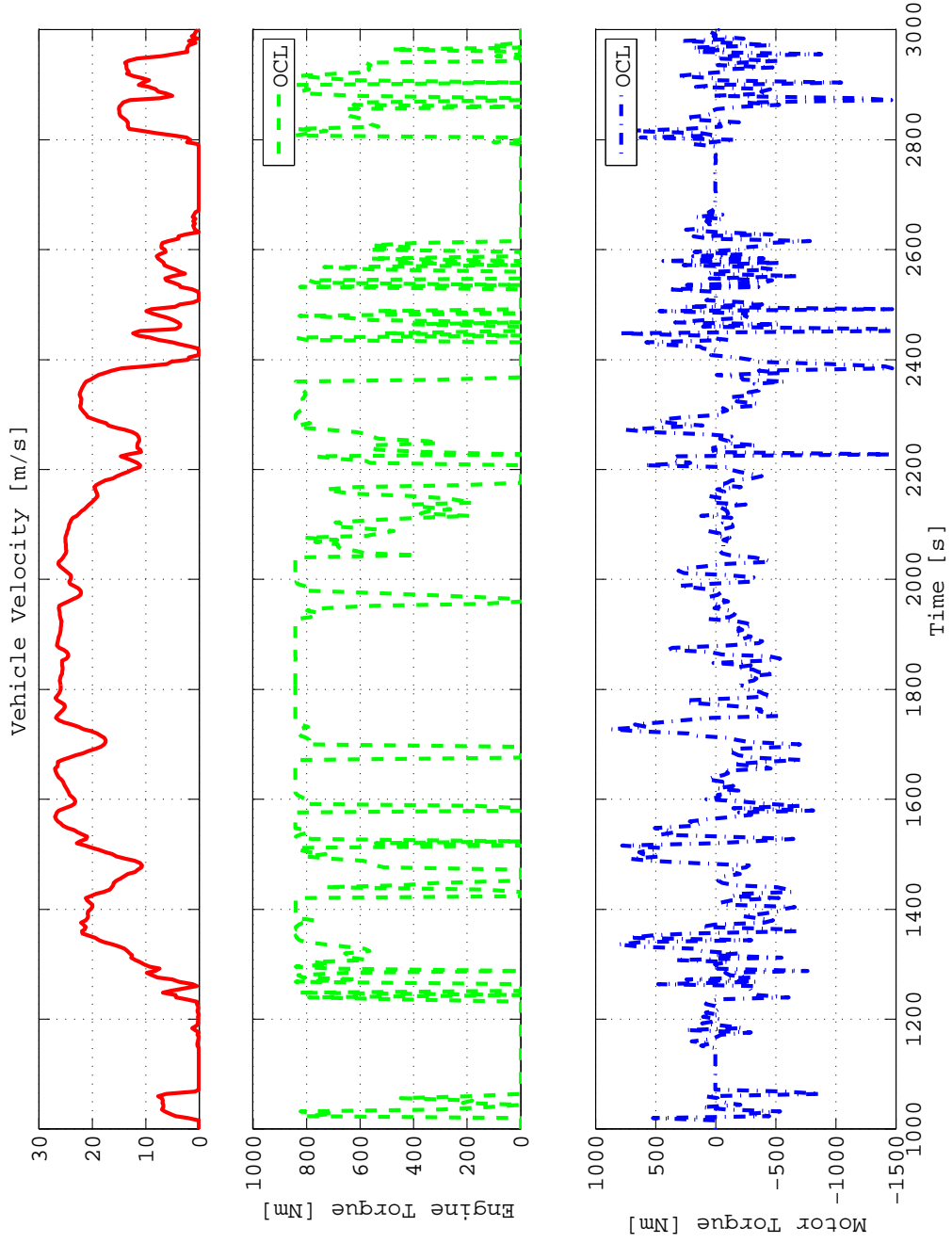
Figure 4.29: Velocity, engine and electric motor torques - detail (Manh-WVUinter-WVUsub)
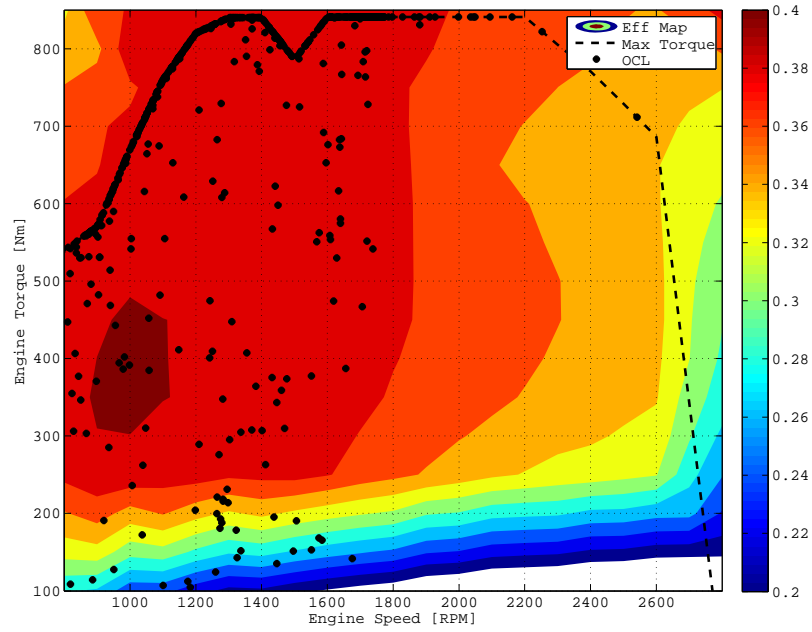
Figure 4.30: Engine operating points (Manh-WVUinter-WVUsub)
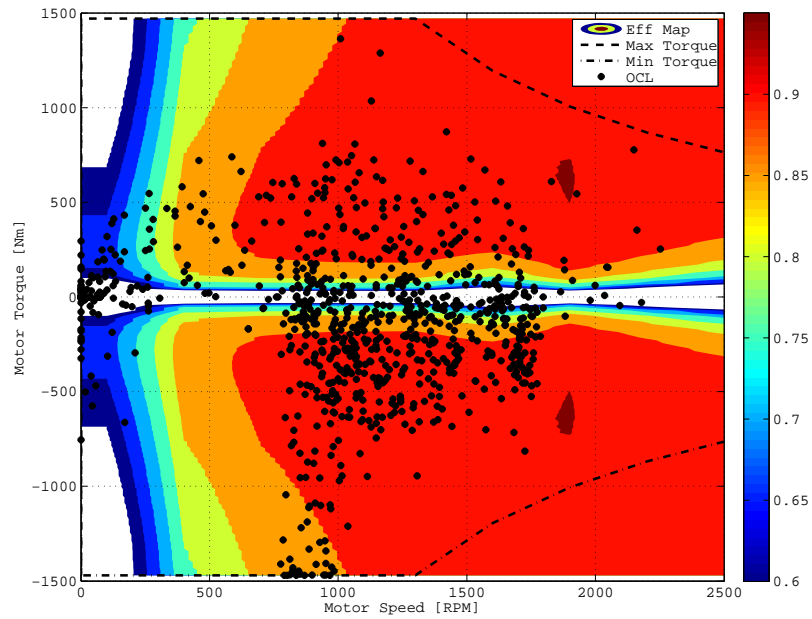


Figure 4.31: Electric motor operating points (Manh-WVUinter-WVUsub)

144
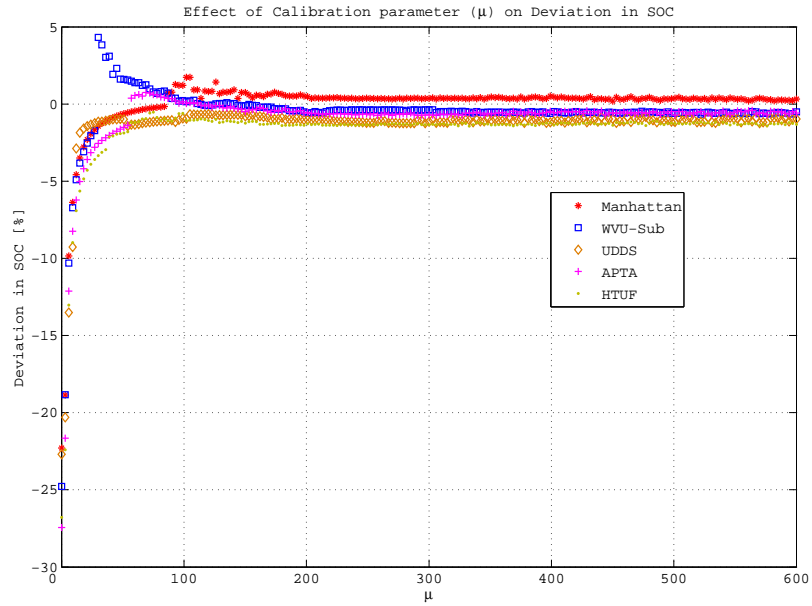
Figure 4.32: Effect of $\mu$ on deviation in SOC for several driving cycles
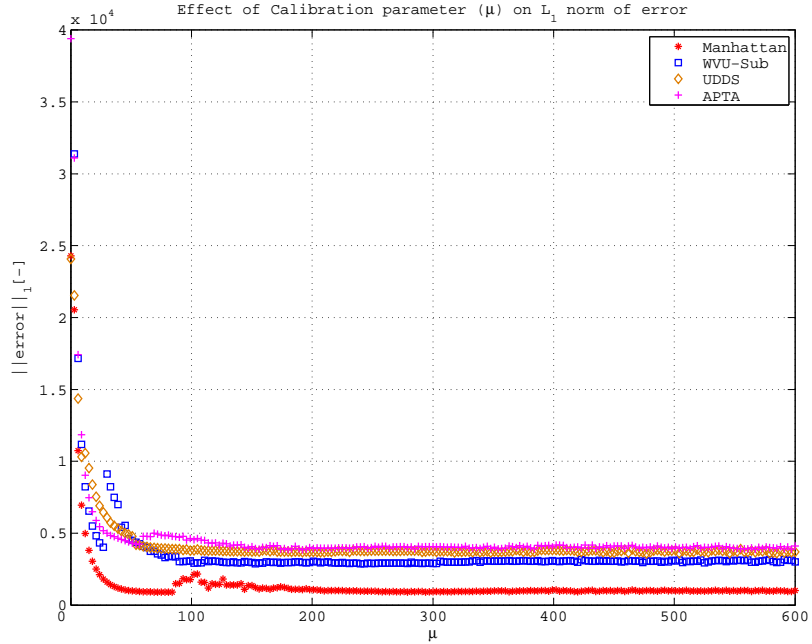


Figure 4.33: Effect of $\mu$ on $\mathcal{L}_1$ norm of error for several driving cycles

145
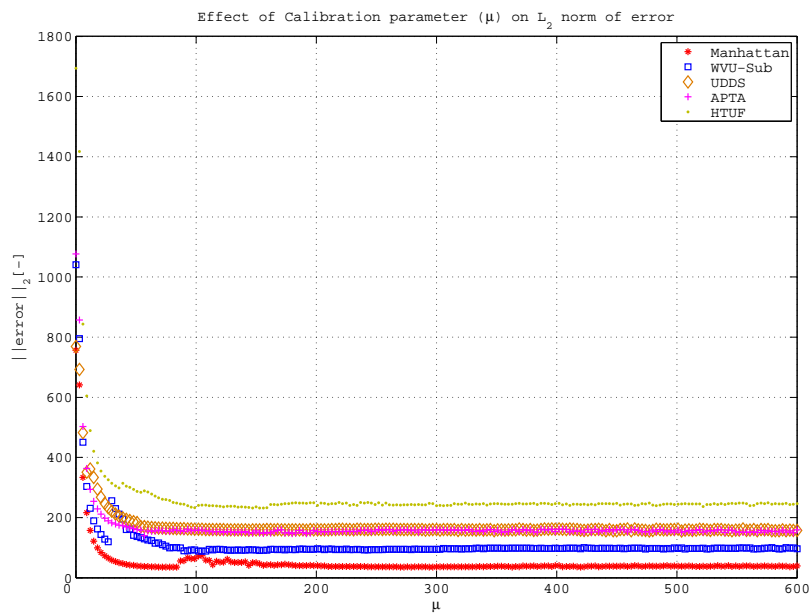
Figure 4.34: Effect of $\mu$ on $\mathcal{L}_2$ norm of error for several driving cycles
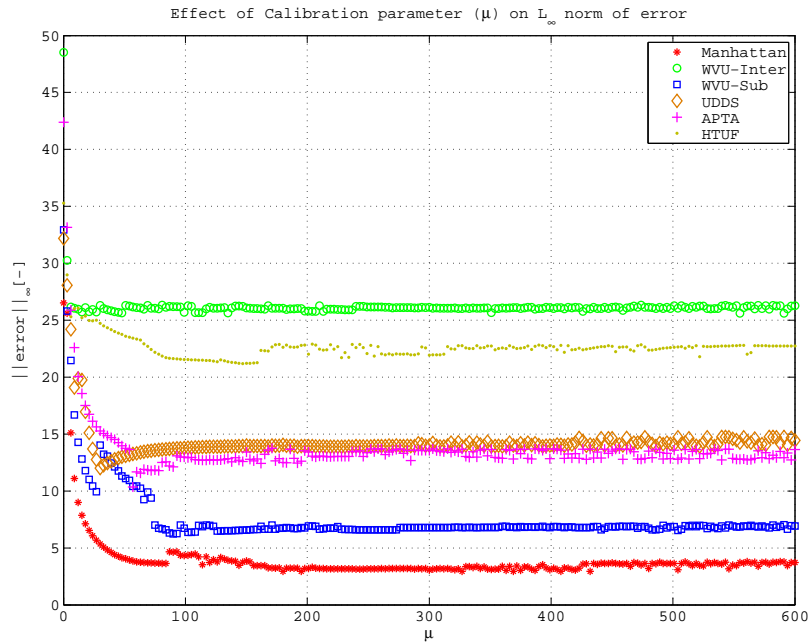


Figure 4.35: Effect of $\mu$ on $\mathcal{L}_\infty$ norm of error for several driving cycles

different values of $\mu$ is shown in figures 4.32,4.33,4.34 and 4.35. For all the driving cycles, there is a single value of $\mu$ that assures charge sustainability ($\Delta SOC = 0$) and consumes the least amount of fuel. As seen from the plot, the optimal control law developed is relatively insensitive to the variation of $\mu$. This is significant because the optimality and stability properties for a wrong guess of $\mu$ are still close to the performance of $\mu^*$.

## 4.6 Conclusion

The main contribution of this chapter is a new stability and optimality framework for designing analytical energy management strategy. The proposed strategy is designed and developed for a charge sustaining pre-transmission parallel HEV, but the methodology is scalable to different vehicle architectures and component sizes. The chapter proves a series of theorems on solving the problem as a nonlinear optimal regulation problem with and without disturbance rejection. The theorems are instrumental in developing a closed-form expression for the nonlinear state feedback based optimal control law. The resulting novel control law is proved optimal with respect to the fuel consumed over an infinite time horizon and guarantees local asymptotic stability of the origin. Although the optimality of the control law and asymptotic stability property of the origin are proved for an infinite time horizon, the results show the performance of the optimal control law when applied to a finite time driving cycle. The optimality ensures that minimum fuel is consumed and stability guarantees that battery SOC at the end of the driving cycle converges to $SOC_{ref}$. The optimal control law is implemented in a simplified backward simulator and its performance is compared with the global optimal solution from DP for several representative driving cycles such as Manhattan, WVU-Interstate, WVU-suburban and UDDS. The control law developed is a nonlinear state feedback based control law which depends on the

vehicle architecture and parameters of the components (engine, electric machine and battery). The calibration parameter ($\mu$) must be tuned for each driving cycle using iterative shooting methods to guarantee optimality and stability. The strategy with the optimal $\mu^*$ for each driving cycle consumes within $4.5\%$ of the fuel consumed by DP and ensures that the SOC variation at the end of the driving cycle is less than $0.06\%$. Although the optimality and stability properties of the control law depend on the optimal value of the calibration parameter, because the strategy is reatively insensitive to the parameter, the closed-form control law developed is a signifcant contribution to the HEV energy management literature. The optimal control law shown here can also be easily implemented in a real vehicle because of its simplicity, and this is emphasized by implementing the strategy in a forward vehicle simulator (see Chapter 5).

## 4.7 Appendix

This section of the chapter describes the theoretical results available in the nonlinear optimal regulation theory that have been used in Sections 4.2 and 4.3. The theorems shown here are taken from the book [49].

### 4.7.1 Nonlinear Optimal Regulation

Let $D \subset \mathbb{R}^n$ be an open set and let $U \subset \mathbb{R}^m$ be an arbitrary set, where $0 \in D$ and $0 \in U$. Furthermore, let $f : D \times U \to \mathbb{R}^n$ satisfy $f(0,0) = 0$. Now consider the controlled system

$$\dot{x}(t) = f(x(t), u(t)), \quad x(0) = x_0, \quad t \geq 0. \tag{4.46}$$

The control $u(\cdot)$ in (4.46) is restricted to the class of *admissible* controls consisting of measurable functions $u(\cdot)$ such that

$$u(t) \in \Omega, \quad t \geq 0, \tag{4.47}$$

where the control constraint set $\Omega \subset U$ is compact and $0 \in \Omega$. A measurable mapping $\phi : D \to \Omega$ satisfying $\phi(0) = 0$ is called a *control law*. Given a control law $\phi(\cdot)$ and a feedback control $u(t) = \phi(x(t))$, the *closed-loop system* has the form

$$\dot{x}(t) = f(x(t), \phi(x(t))), \quad x(0) = x_0, \quad t \geq 0. \tag{4.48}$$

In order to address the problem of characterizing feedback controllers that minimize a performance functional, let $L : \mathbb{R}^n \times \mathbb{R}^m \times \mathbb{R}^n \to \mathbb{R}$, $L : \mathbb{R}^n \times \mathbb{R}^m \to \mathbb{R}$ and $p \in \mathbb{R}^n$ such that,

$$H(x(t), u(t), p) \triangleq L(x(t), u(t)) + p^T f(x(t), u(t)). \tag{4.49}$$

Furthermore, define the set of asymptotically stabilizing controllers $S(x_0)$ for each initial condition $x_0 \in D$, that is, $S(x_0) \triangleq u(\cdot) : u(\cdot)$ is admissible and $x(\cdot)$ given by (4.46) satisfies $x(t) \to 0$ as $t \to \infty$.

**Theorem 4.7.2.** *[48] Consider the controlled system (4.46) with performance functional*

$$J(x_0, u(\cdot)) \triangleq \int_0^{\infty} L(x(t), u(t)) dt. \tag{4.50}$$

*Assume that there exists a $C^1$ function $V : D \to \mathbb{R}$ and a control law $\phi : D \to \Omega$ such that*

*1.*

$$V(0) = 0, \tag{4.51}$$

*2.*

$$V(x(t)) > 0, \quad x(t) \in D, \quad x(t) \neq 0, \tag{4.52}$$

*3.*

$$\phi(0) = 0, \tag{4.53}$$

149

4.

$$\frac{\partial V}{\partial x} f(x(t), \phi(x(t))) < 0, \quad x(t) \in D, \quad x(t) \neq 0, \tag{4.54}$$

5.

$$H(x(t), \phi(x(t)), \left(\frac{\partial V}{\partial x}\right)^T) = 0, \quad x(t) \in D, \tag{4.55}$$

6.

$$H(x(t), u(t), \left(\frac{\partial V}{\partial x}\right)^T) \geq 0, \quad x \in D, \quad u \in \Omega. \tag{4.56}$$

*Then with the feedback control $u(\cdot) = \phi(x(\cdot))$, the solution $x(t) = 0$, $t \geq 0$, of the closed-loop system (4.48) is locally asymptotically stable, and*

$$J(x_0, \phi(x(\cdot))) = V(x_0). \tag{4.57}$$

*Furthermore, the feedback control $u(\cdot) = \phi(x(\cdot))$ minimizes $J(x_0, u(\cdot))$ in the sense that*

$$J(x_0, \phi(x(\cdot))) = \min_{u(\cdot) \in S(x_0)} J(x_0, u(\cdot)). \tag{4.58}$$

### 4.7.3   Nonlinear Optimal Regulation with Disturbance Rejection

Let $D \subset \mathbb{R}^n$ be an open set and let $U \subset \mathbb{R}^m$ be an arbitrary set, where $0 \in D$ and $0 \in U$. Let $W \subset \mathbb{R}^d$ be a subset of measurable functions. Furthermore, let $f : D \times U \to \mathbb{R}^n$ satisfy $f(0,0) = 0$. Now consider the controlled system

$$\dot{x}(t) = f(x(t), u(t)) + J_1(x(t)) \cdot w(t), \quad x(0) = x_0, \quad t \geq 0. \tag{4.59}$$

The control $u(\cdot)$ in (4.59) is restricted to the class of *admissible* controls consisting of measurable functions $u(\cdot)$ such that

$$u(t) \in \Omega, \quad t \geq 0, \tag{4.60}$$

where the control constraint set $\Omega \subset U$ is compact and $0 \in \Omega$. A measurable mapping $\phi : D \rightarrow \Omega$ satisfying $\phi(0) = 0$ is called a *control law*. Given a control law $\phi(\cdot)$ and a feedback control $u(t) = \phi(x(t))$, the *closed-loop system* has the form

$$\dot{x}(t) = f(x(t), \phi(x(t))) + J_1(x(t)) \cdot w(t), \quad x(0) = x_0, \quad t \geq 0. \tag{4.61}$$

In order to address the problem of characterizing feedback controllers that minimize a performance functional, let $L : \mathbb{R}^n \times \mathbb{R}^m \times \mathbb{R}^n \rightarrow \mathbb{R}$, $L : \mathbb{R}^n \times \mathbb{R}^m \rightarrow \mathbb{R}$ and $p \in \mathbb{R}^n$ such that,

$$H(x(t), u(t), p) \triangleq L(x(t), u(t)) + p^T f(x(t), u(t)) + \Gamma(x(t), u(t)). \tag{4.62}$$

Furthermore, define the set of asymptotically stabilizing controllers $S(x_0)$ for each initial condition $x_0 \in D$, that is, $S(x_0) \triangleq u(\cdot) : u(\cdot)$ is admissible and $x(\cdot)$ given by (4.59) satisfies $x(t) \rightarrow 0$ as $t \rightarrow \infty$.

**Theorem 4.7.4.** *[48] Consider the controlled system (4.59) with performance functional*

$$J(x_0, u(\cdot)) \triangleq \int_0^\infty L(x(t), u(t)) dt. \tag{4.63}$$

*Assume that there exists a $C^1$ function $V : D \rightarrow \mathbb{R}$ and a control law $\phi : D \rightarrow \Omega$ such that*

*1.*

$$V(0) = 0, \tag{4.64}$$

*2.*

$$V(x(t)) > 0, \quad x(t) \in D, \quad x(t) \neq 0, \tag{4.65}$$

*3.*

$$\phi(0) = 0, \tag{4.66}$$

4.

$$\frac{\partial V}{\partial x} f(x(t), \phi(x(t))) < 0, \quad x(t) \in D, \quad x(t) \neq 0, \tag{4.67}$$

5.

$$\frac{\partial V}{\partial x} \cdot J_1(x(t)) \cdot w(t) \leq r(x, w) + L(x, \phi(x)) + \Gamma(x, \phi(x)), \quad x(t) \in D, \quad w(t) \in W, \tag{4.68}$$

6.

$$H(x(t), \phi(x(t)), \left(\frac{\partial V}{\partial x}\right)^T) = 0, \quad x(t) \in D, \tag{4.69}$$

7.

$$H(x(t), u(t), \left(\frac{\partial V}{\partial x}\right)^T) \geq 0, \quad x \in D, \quad u \in \Omega. \tag{4.70}$$

*Then with the feedback control* $u(\cdot) = \phi(x(\cdot))$, *the solution* $x(t) = 0$, $t \geq 0$, *of the closed-loop system (4.61) is locally asymptotically stable, and*

$$J(x_0, \phi(x(\cdot))) = V(x_0). \tag{4.71}$$

*Furthermore, the feedback control* $u(\cdot) = \phi(x(\cdot))$ *minimizes* $J(x_0, u(\cdot))$ *in the sense that*

$$J(x_0, \phi(x(\cdot))) = \min_{u(\cdot) \in S(x_0)} J(x_0, u(\cdot)). \tag{4.72}$$

*Furthermore, the solution* $x(t)$, $t \geq 0$ *satisfies the dissipativity constraint*

$$\int_0^T r(x(t), w(t)) dt + V(x_0), \ T \geq 0, \ w(\cdot) \in W. \tag{4.73}$$

152

## Chapter 5: Comparative Analysis of Energy Management Strategies

This chapter is devoted to the comparison and evaluation of the different energy management strategies developed in the previous chapters. The energy management strategies developed in the dissertation can be categorized based on the feasibility of implementation in a real vehicle. Thus they can be classified into realizable and non-realizable strategies.

- **Non-realizable Strategy:** A non-realizable strategy requires complete *a-priori* knowledge of the driving cycle in order to solve the energy management problem and therefore cannot be implemented in a real vehicle. DP, ECMS (with optimal $s_0$) and OCL (with optimal $\mu$) are in this category.

  DP developed in Section 3.2 solves the energy management problem backwards assuming complete knowledge of the driving cycle and cannot be implemented in a real vehicle.

  ECMS strategy developed in Section 3.3 has a calibration parameter $s_0^*$ that must be tuned for every driving cycle in order to ensure a charge sustainable solution. Clearly this strategy cannot be implemented in a real vehicle, because for each driving cycle, the optimal $s_0^*$ must be calculated.

The OCL strategy developed in Section 4.3 has a single calibration parameter $\mu$ that must be tuned for every driving cycle in order to assure optimality and stability properties. Such a strategy cannot be realized in a real vehicle because calibration requires the complete knowledge of the driving cycle.

- **Realizable Strategy:** A realizable strategy does not require knowledge of the driving cycle to solve the energy management problem and can be implemented in a real vehicle. Adaptive ECMS (referred to as AECMS) and an implementable version of OCL referred to as real-time OCL are in this category.

  The adaptive ECMS (AECMS) developed in Section 3.4 is a version of ECMS where the equivalence factor $s_0$ is adapted based on the deviation of battery SOC from its reference. The adaptation law ensures convergence of battery SOC to its reference as the driving cycle is repeated for a long duration. This strategy does not require *a-priori* knowledge of the driving cycle and therefore can be implemented in a real vehicle.

  Because the OCL strategy developed in Section 4.3 is relatively insensitive to $\mu^*$ and a single value of $\mu$ can be used for any driving cycle, the strategy (referred to here as real-time OCL) can be implemented in a real vehicle. The real-time OCL strategy does not require knowledge of the driving cycle and therefore belongs to the category of realizable strategies.

The realizability of the different strategies proposed and developed in the dissertation are summarized in Table 5.1. Unlike the simulation results shown in Chapters 3 and 4, where the strategies were implemented using a backward vehicle simulator, this chapter deals

Table 5.1: Realizability of energy management strategies

| Strategy | Realizable |
|---|---|
| DP | NO |
| ECMS (with $s_0^*$) | NO |
| OCL (with $\mu^*$) | NO |
| AECMS | YES |
| Real-time OCL | YES |

with the implementation using a forward vehicle simulator. Because DP cannot be implemented in a forward vehicle simulator, the results shown in Section 3.2 are used here as the benchmark solution. In order to compare and evaluate the performance of the strategies, several performance metrics such as calibration effort, SOC variation and equivalent fuel consumed are defined as follows:

1. Calibration effort: The amount of calibration necessary in assuring that the energy management strategy produces a charge sustaining solution while minimizing the amount of fuel over the length of the driving cycle;

2. SOC variation and equivalent fuel consumed: The deviation of battery SOC from its reference throughout the driving cycle and the amount of fuel consumed corrected for the net battery SOC change at the end of the driving cycle.

The comparative study is performed over different driving cycles such as Manhattan, WVU-interstate, WVU-suburban and UDDS. The real world driving conditions experienced by vehicles are simulated by evaluating the realizable strategies over combined driving cycles, also used to evaluate realizable strategies.

## 5.1 Non-realizable Energy Management Strategies

This section of the chapter describes the calibration effort, battery SOC variation and equivalent fuel consumed for the non-realizable energy management strategies such as DP, ECMS and OCL.

### 5.1.1 Calibration Effort for ECMS

Table 5.2: Effect of $s_0$ for Manhattan driving cycle

| Strategy | $s_0$ [-] | Normalized $FC_{eqv}$ [%] |
|----------|-----------|---------------------------|
| ECMS     | 2         | 108.3                     |
|          | 2.5       | 107.1                     |
|          | 3         | 106.5                     |
|          | 3.5       | 104.1                     |
|          | 4         | 105.8                     |
|          | 4.5       | 106.3                     |
|          | 5         | 106.8                     |
| DP       | -         | 100                       |

The ECMS derived from PMP has one tuning parameter $s_0$ which is directly related to the co-state $\lambda$ of the PMP solution as discussed in Chapter 3 (see (3.39)). The equivalence factor $s$ has to satisfy the dynamic equation (3.41), whose initial value $s_0$ can be independently selected. As shown in the numerous papers on ECMS [19, 20, 13, 17], there is a direct correlation between $s_0$ and the battery SOC usage during any driving cycle. The effect of the calibration parameter $s_0$ is shown in Fig. 5.1.

As seen from these plots, the value of $s_0$ impacts the convergence of $SOC$ to $SOC_{ref}$ at the end of the driving cycle. The optimal value of $s_0$ is selected based on the equivalent fuel consumed ($FC_{eqv}$) defined in (3.18). The effects of using different values of $s_0$ are
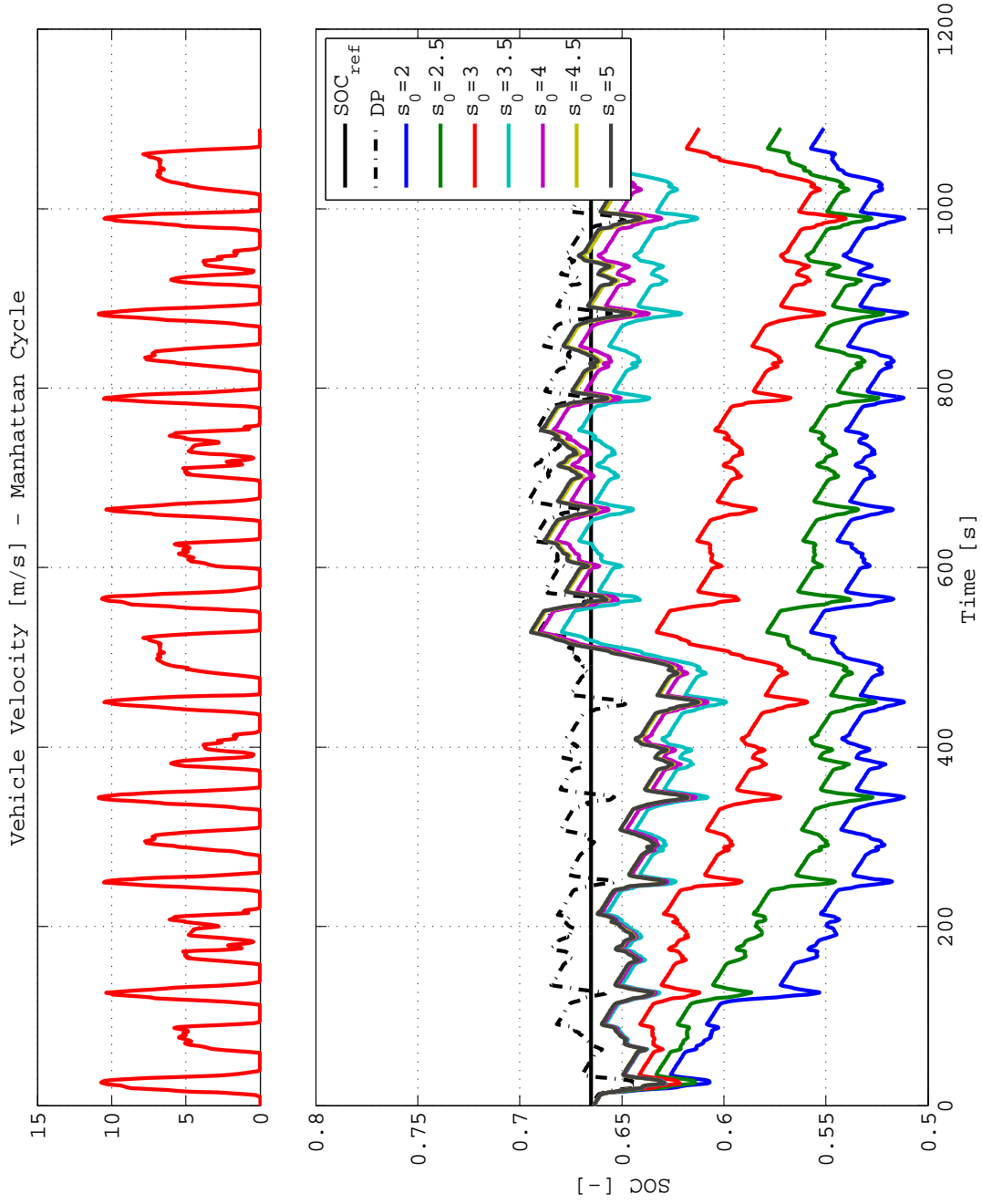
Figure 5.1: Effect of $s_0$ on $SOC$

157

summarized in Table 5.2 for the Manhattan driving cycle. The *optimal* value of $s_0$ ensures convergence of SOC to the reference value $SOC_{ref}$ while consuming the least amount of fuel over the driving cycle. Because the optimality properties of ECMS based on PMP depends on the *optimal* value of $s_0$, it is important to study the sensitivity of the results to $s_0$. For all the driving cycles, there is a single value of $s_0$ that assures charge sustainability and consumes the least amount of fuel [14]. As seen from the Figures 5.1 and Table 5.2, ECMS is highly sensitive to the variation of $s_0$ and the value of $s_0$ directly determines the optimality and charge sustainability of the ECMS solution.

## 5.1.2 Calibration Effort for OCL

Table 5.3: Effect of $\mu$ for Manhattan driving cycle

| Strategy | $\mu$ [kg] | Normalized $FC_{eqv}$ [%] |
|----------|------------|---------------------------|
| OCL | 10 | 106.3 |
| | 50 | 104.2 |
| | 100 | 103.6 |
| | 200 | 103.5 |
| DP | - | 100 |

The optimal control law $P_{ice}^*(\zeta)$ developed in Chapter 4 (see (4.42)) has a tuning parameter $\mu$ that must be calibrated to ensure convergence of battery SOC to $SOC_{ref}$. Thus the *optimal and stable* energy management strategy is assured only with the *optimal* $\mu$ i.e., $\mu = \mu^*$, for each driving cycle. The effect of the calibration parameter $\mu$ on the battery SOC profile for Manhattan driving cycle is shown in Fig. 5.2. It is evident that $\mu$ affects the convergence of $SOC$ to $SOC_{ref}$ throughout the driving cycle. The control law depletes the battery with a smaller value for $\mu$. As $\mu$ is increased, the battery SOC profile
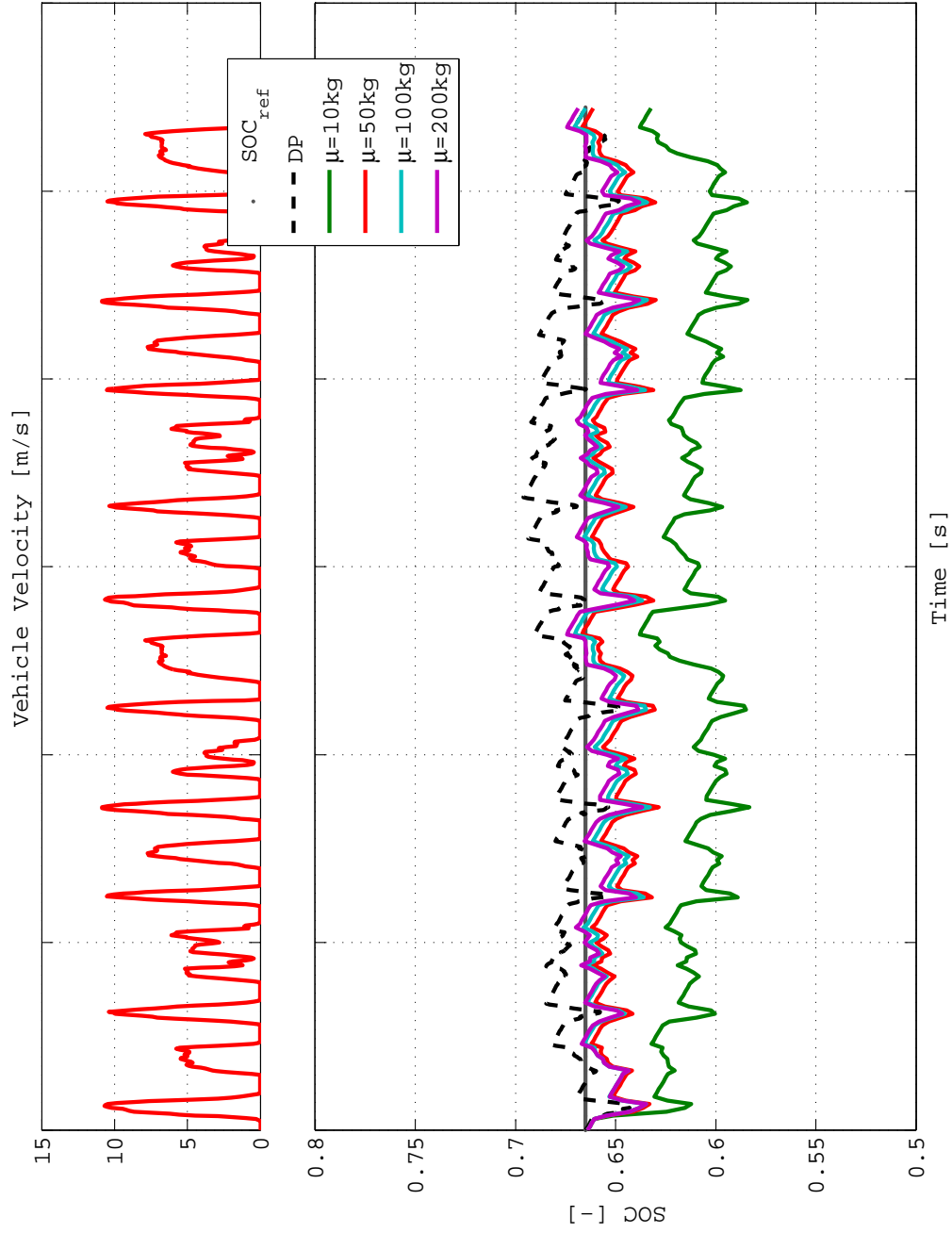
Figure 5.2: Effect of $\mu$ on *SOC* for Manhattan driving cycle

159
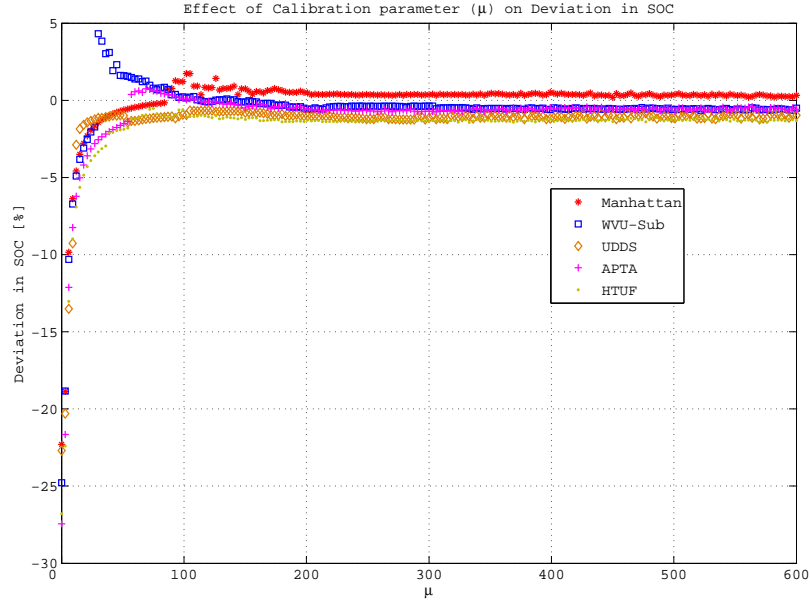
Figure 5.3: Effect of $\mu$ on deviation in SOC for different driving cycles

becomes increasingly similar to the DP solution. The optimal value of $\mu$ is selected based on the equivalent fuel consumed ($FC_{eqv}$) (see (3.18 for definition). The effect of using different values of $\mu$ on $FC_{eqv}$ is summarized in Table 5.3 for the Manhattan driving cycle.

Because the optimality and stability properties of the control law developed in Section 4.3 depend on the *optimal* value of $\mu$, it is important to study the sensitivity of the results with respect to $\mu$. In order to generalize the effects of $\mu$, deviation in battery $SOC$ (4.44) and $\mathcal{L}_1, \mathcal{L}_2, \mathcal{L}_\infty$ (4.45) norm in battery $SOC$ error are calculated for a wide range of $\mu$ for different representative driving cycles. For example, the Manhattan, WVU-suburban and UDDS truck driving cycles represent the urban driving conditions of heavy-duty vehicles. The WVU-interstate and HTUF driving cycles represent a combination of urban and highway driving cycles. The effect of different values of $\mu$ is shown in figures 5.3,5.4,5.5 and
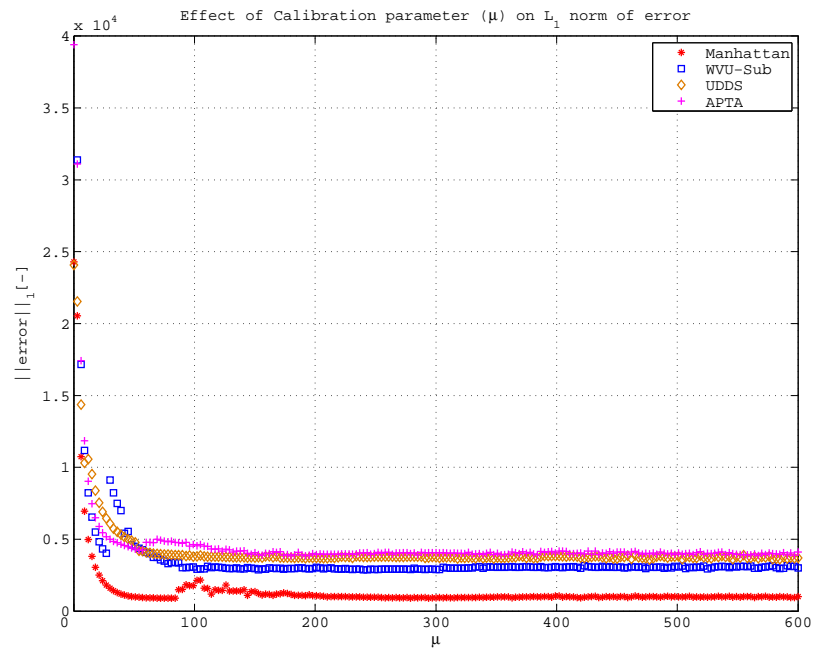
Figure 5.4: Effect of $\mu$ on $L_1$ norm on error for different driving cycles
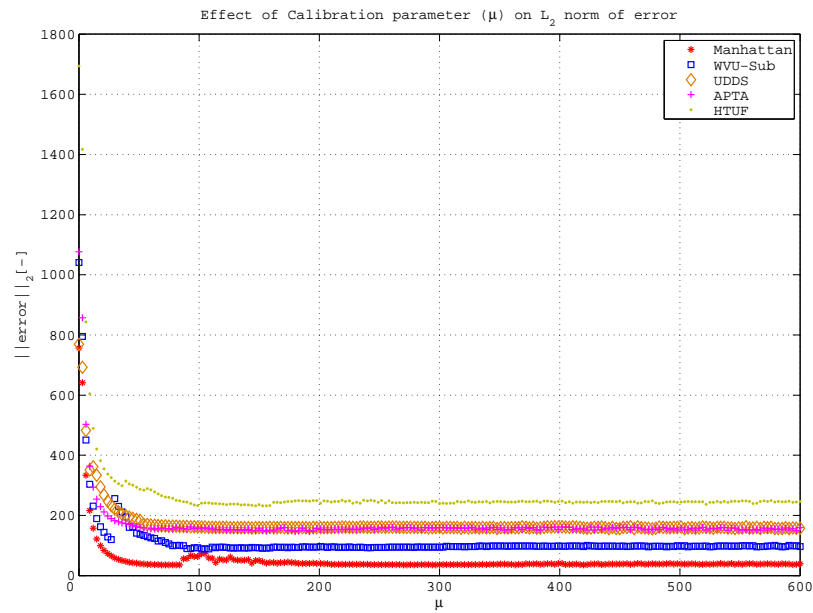


Figure 5.5: Effect of $\mu$ on $L_2$ norm on error for different driving cycles

161
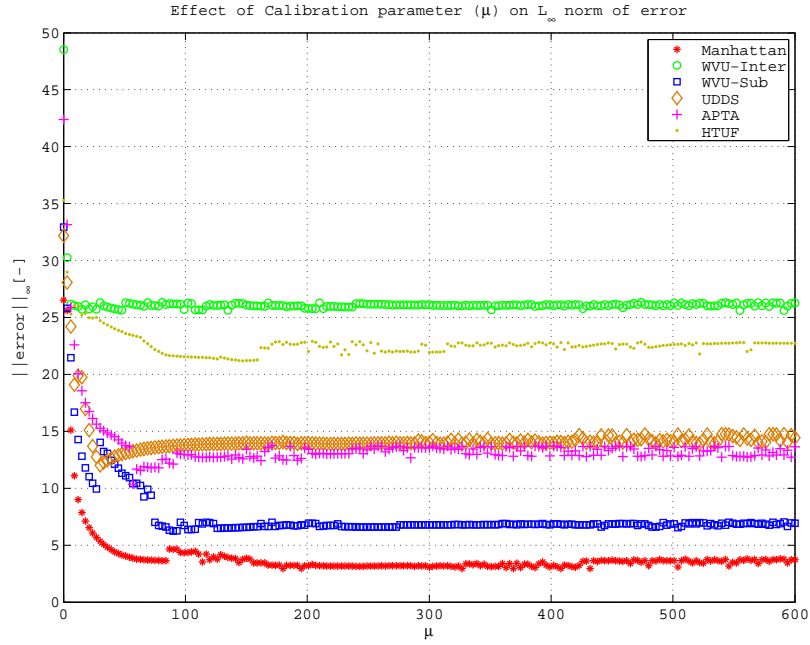
Figure 5.6: Effect of $\mu$ on $L_\infty$ norm on error for different driving cycles

5.6. For all the driving cycles, an optimal value of $\mu$ assures charge sustainability and consumes the least amount of fuel. As seen from the plot, the optimal control law developed is relatively insensitive to the variation of $\mu$. This is significant because the optimality and stability properties for a wrong guess of $\mu$ are still close to those for $\mu^*$.

### 5.1.3 Comparison of Calibration Effort

Table 5.4: Calibration effort for non-realizable energy management strategies

| Strategy | Calibration effort |
|---|---|
| DP | None |
| ECMS (with $s_0^*$) | Medium |
| OCL (with $\mu^*$) | Medium |

The calibration effort required for the non-realizable energy management strategies proposed and developed in this dissertation is listed in Table 5.4. The DP algorithm which has been used to find the global optimal solution has no calibration parameters that must be tuned for different driving cycles. Because the strategy cannot be implemented in a real vehicle and there are no calibration parameters involved, no calibration effort involved in its implementation. The ECMS and OCL have their corresponding calibration parameters $s_0$ and $\mu$ that must be calibrated to ensure the strategy produces a charge sustaining solution while minimizing the fuel consumed over any driving cycle. The effect of using sub-optimal calibration for both the strategies can be seen in Figures 5.1 and 5.2. Though the variation of battery SOC with different values of $s_0$ is wider than the effect of $\mu$, both strategies require a similar amount of calibration effort in tuning the parameters. Thus, for both the strategies the amount of calibration effort involved is characterized as *medium* compared to DP and the other realizable strategies described in Section 5.2.

## 5.1.4    SOC Variation and Equivalent Fuel Consumption

In a charge-sustaining HEV, the primary assumption is that all the energy used to propel the vehicle is derived from the primary energy source (fuel). The net change in the battery energy at the end of the driving cycle should ideally be zero. The equivalent fuel consumed ($FC_{eqv}$) are used as performance metrics to characterize any energy management strategy. They are defined as

$$\begin{cases} \Delta SOC = \frac{SOC(t_f) - SOC_{ref}}{SOC_{ref}} \cdot 100, \\ FC_{eqv} = \int_{t_0}^{t_f} \dot{m}_f + \frac{\Delta SOC E_{max}}{\eta_{path} Q_{LHV}}, \end{cases} \tag{5.1}$$

where $SOC(t_f)$ is the battery SOC at the end of the driving cycle and $\eta_{path}$ is the approximate efficiency of the drivetrain used in regenerating/discharging the battery. The equivalent fuel consumed is defined as the sum of the amount of fuel consumed along with

163

Table 5.5: Performance comparison of strategies

| Driving cycle | Strategy | Normalized $FC_{eqv}$ [%] |
|---|---|---|
| Manhattan | DP | 100 |
| | ECMS ($s_0^* = 3.3$) | 106.1 |
| | OCL ($\mu^* = 200kg$) | 103.5 |
| WVU-Interstate | DP | 100 |
| | ECMS ($s_0^* = 2.82$) | 102.9 |
| | OCL ($\mu^* = 200kg$) | 103.7 |
| WVU-Suburban | DP | 100 |
| | ECMS ($s_0^* = 4.56$) | 102.8 |
| | OCL ($\mu^* = 200kg$) | 104.4 |
| UDDS | DP | 100 |
| | ECMS ($s_0^* = 12.65$) | 104.5 |
| | OCL ($\mu^* = 200kg$) | 104.2 |

a correction for the net change in battery SOC, assuming that the charging/discharging of the battery can be associated with an approximate efficiency $\eta_{path}$. For example, if an energy management strategy depletes the battery at the end of a driving cycle, evidently the amount of fuel consumed (by the engine) will be less. The fuel consumed does not account for the fact that the depleted battery energy must be replenished. Thus, the equivalent fuel consumed will add an equivalent amount of fuel proportional to the battery energy used as shown in (5.1). If $\Delta SOC$ is positive, this implies that $SOC(t_f) > SOC_{ref}$ and the excess battery SOC can be used later to save fuel. If $\Delta SOC$ is negative, it implies that more fuel is required to recharge the battery SOC to the reference value. The best strategy is clearly the one with the minimum $\Delta SOC$ and minimum $FC_{eqv}$.

The equivalent fuel consumed $FC_{eqv}$ for several driving cycles are shown in Table 5.5. Both ECMS and OCL developed in Sections 3.3 and 4.3 are implemented using a forward vehicle simulator and compared with the benchmark solution from DP (Section 3.2). It

can be seen that the ECMS and OCL perform very close (within 3%) to each other over all the driving cycles. Because the DP provides the global optimal solution to the problem, no energy management strategy can match its performance. The detailed discussion of the results shown in the Table 5.5 is given in the following subsections.

**Performance for Manhattan driving cycle**

Both ECMS and OCL are implemented with their respective optimal calibration parameters and compared with DP in Figures 5.7 - 5.10 and Table 5.5. Even with the optimal value for the calibration parameters, the battery SOC profile resulting from both ECMS and OCL are different from the benchmark DP solution (Fig. 5.7). Because DP has entire *a-priori* knowledge of the driving cycle, it uses the battery and engine at the most efficient operating regions. This is also seen from the engine and electric machine operating points shown in Figures 5.9 and 5.10.

**Performance for WVU-Interstate driving cycle**

The performance of ECMS and OCL strategies are compared with DP in Figures 5.11 - 5.14. The WVU-Interstate is a highway driving cycle with very few start-stop events. The DP algorithm is able to use the knowledge that the driving cycle does not contain any significant braking events, and therefore uses the engine at its most efficient region, recharging the battery whenever possible. This can be seen in operating points chosen (Fig. 5.13). Both ECMS and OCL operate the engine over its entire range, resulting in more fuel consumption (Table 5.5). Moreover, as seen from Fig. 5.12, ECMS and OCL switches off the engine whenever there is a small braking event, which is also evident from the engine and electric machine operating points in Figures 5.13 and 5.14. The sudden

165
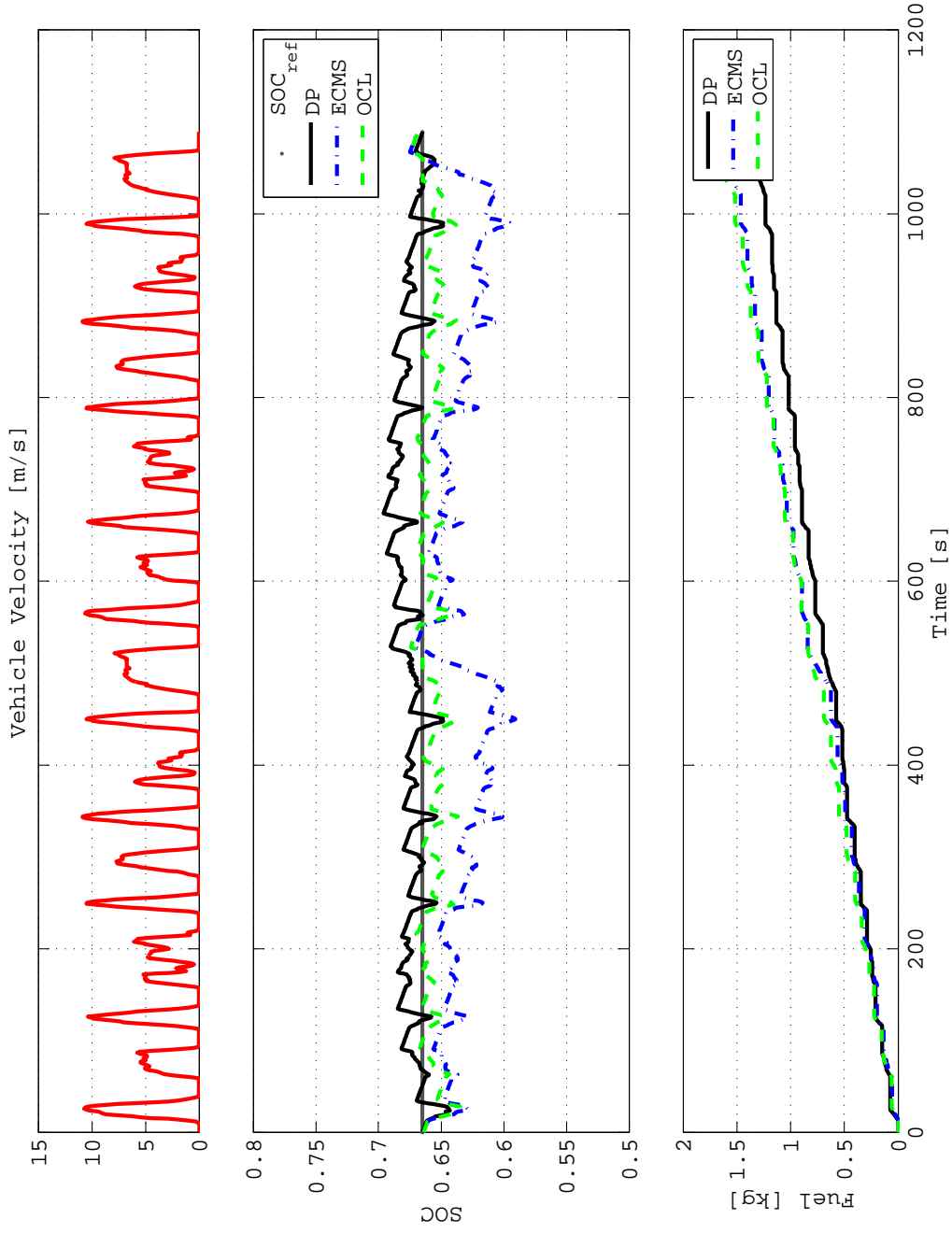
Figure 5.7: Velocity, SOC and equivalent fuel consumed (Manhattan)
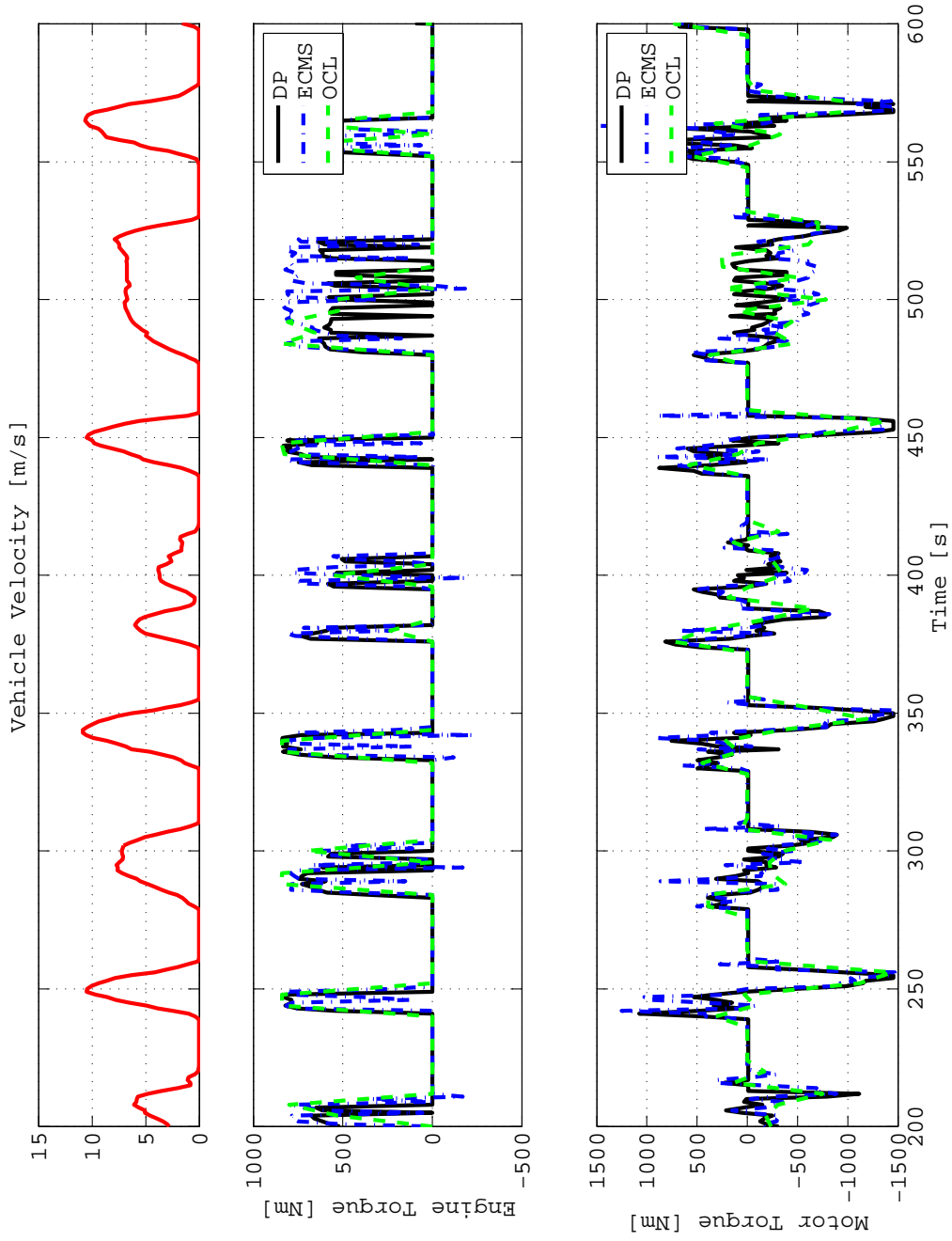
Figure 5.8: Velocity, engine and electric motor torques - detail (Manhattan)

167
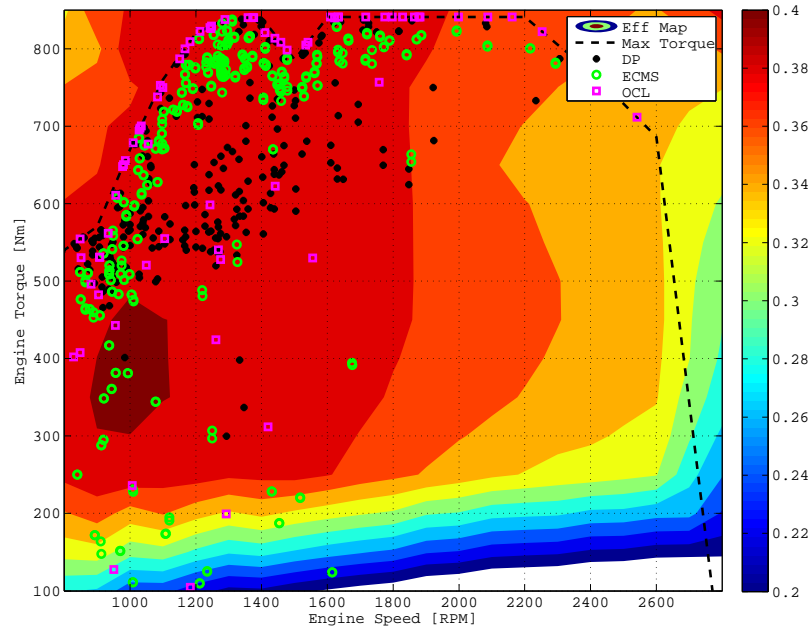
Figure 5.9: Engine operating points (Manhattan)
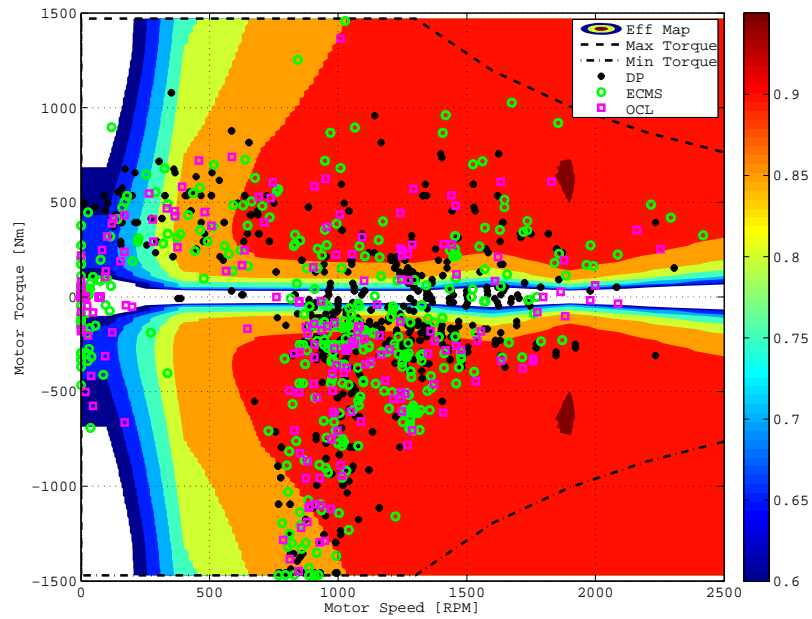


Figure 5.10: Electric motor operating points (Manhattan)
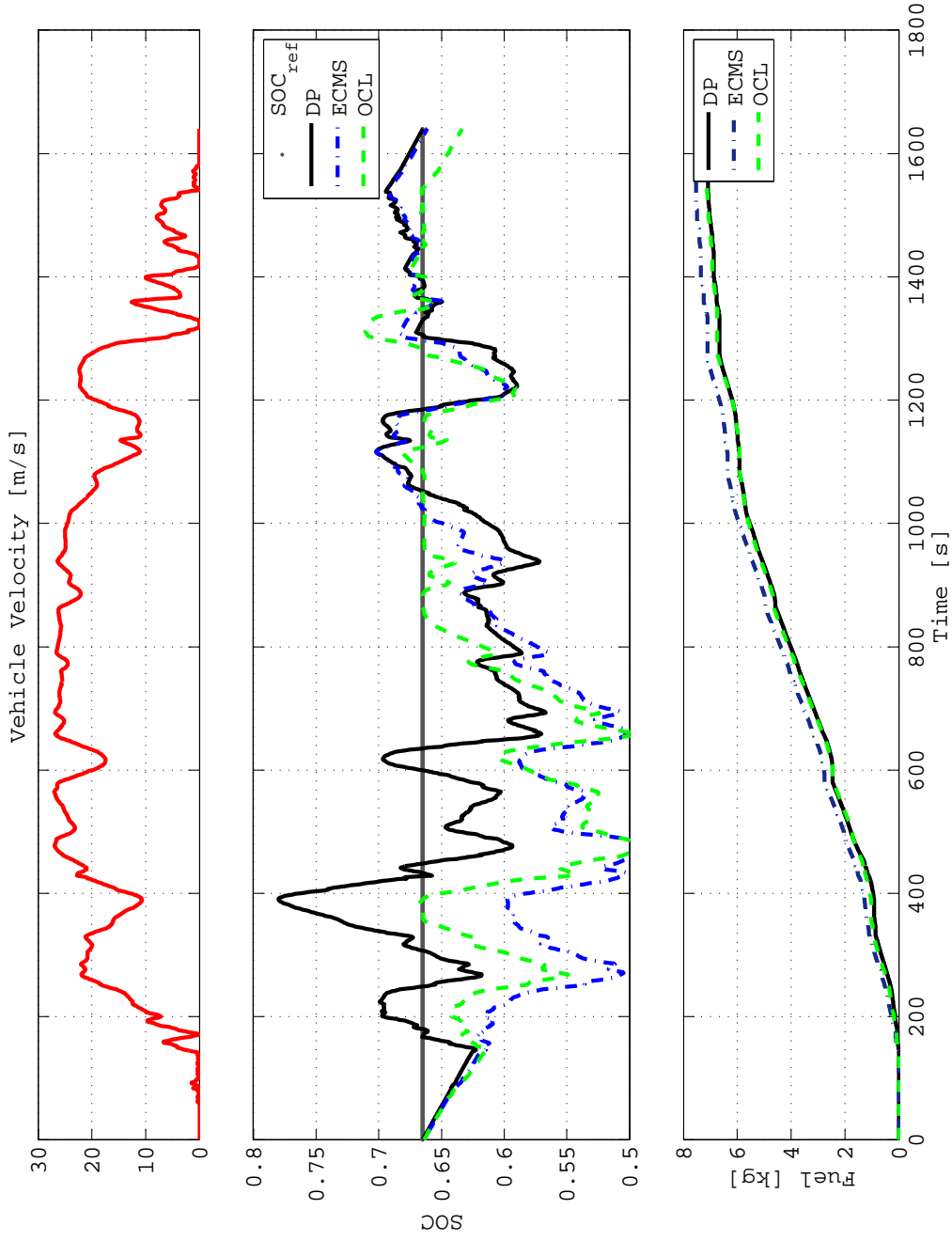
Figure 5.11: Velocity, SOC and equivalent fuel consumed (WVU-Interstate)
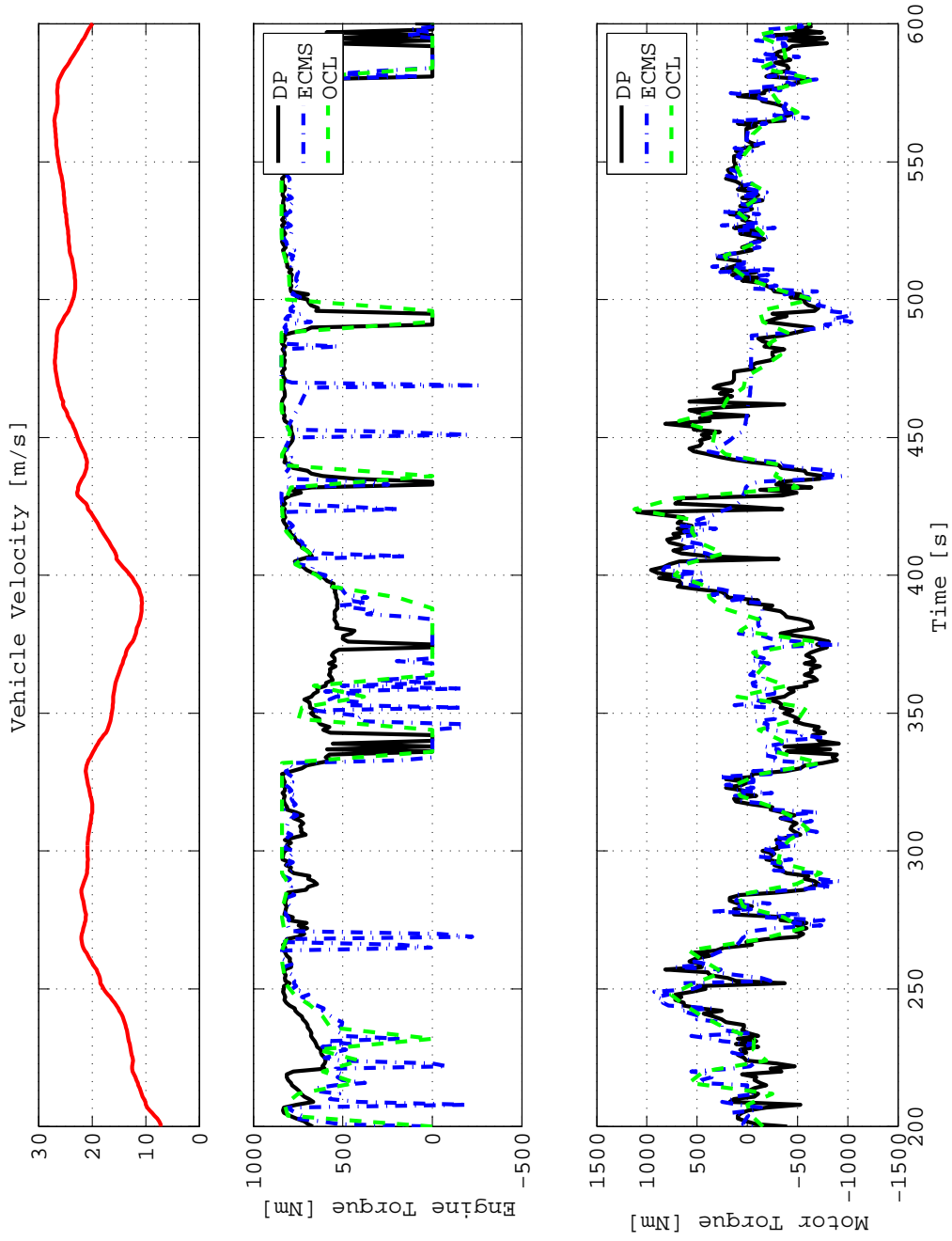
Figure 5.12: Velocity, engine and electric motor torques - detail (WVU-Interstate)
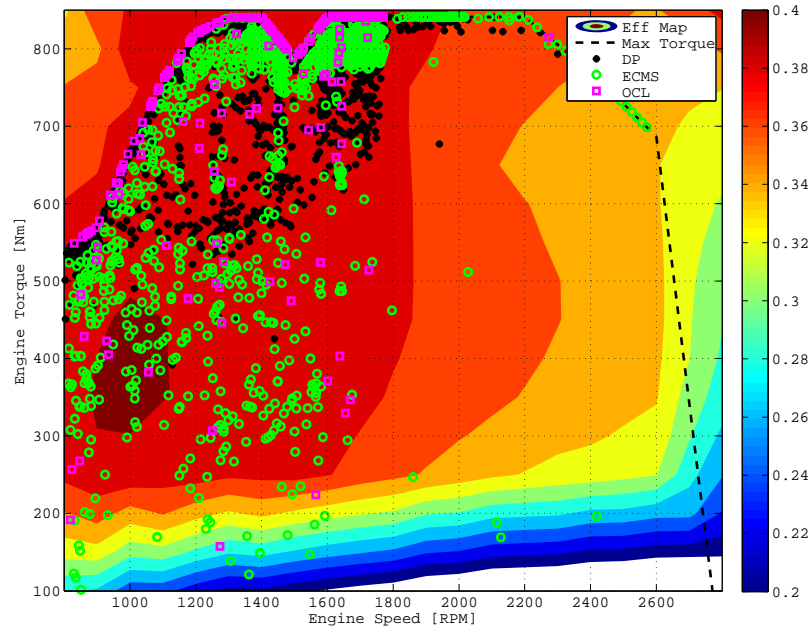
Figure 5.13: Engine operating points (WVU-Interstate)
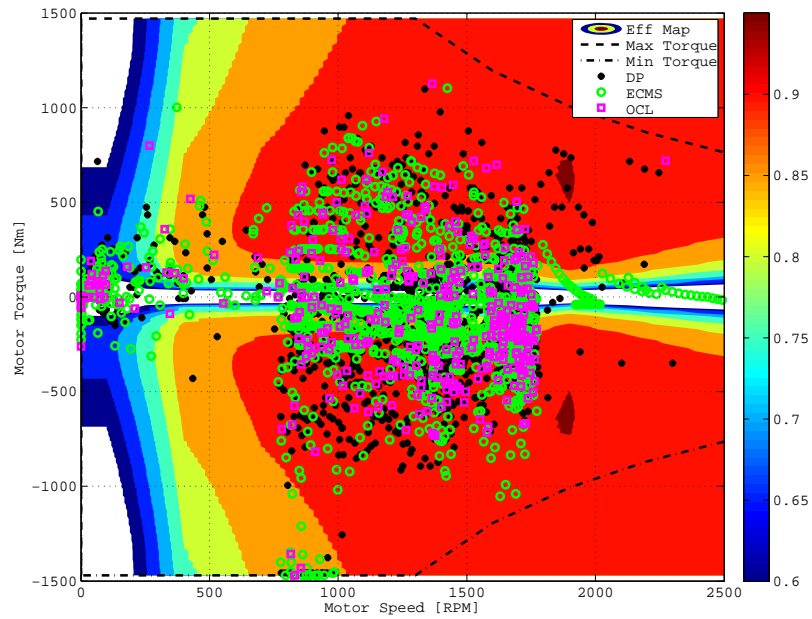


Figure 5.14: Electric motor operating points (WVU-Interstate)

switching of the engine state might be undesirable from the vehicle driveability stand-point and it can be rectified by including a timer to monitor engine on/off events.

**Performance for WVU-Suburban driving cycle**

Unlike the interstate driving cycle, the suburban driving cycle consists of many start-stop events as shown in Fig. 5.15, which facilitates regenerative braking. During the first 600 seconds of the driving cycle, the battery SOC profile resulting from OCL coincides with the choice made by DP, while ECMS decides to deplete the battery to propel the vehicle during this phase. After this phase, the choice made by both ECMS and OCL is very different from DP. This is also seen from the engine operating points shown in Fig. 5.17. Both ECMS and OCL use the engine at its limits, which is not necessarily the most efficient region of operation. The electric motor is also operated in several inefficient regions by OCL as shown in Fig. 5.18. The effect of this is the amount of fuel consumed by OCL over the WVU-suburban driving cycle (Table 5.5).

**Performance for UDDS driving cycle**

The performance of ECMS and OCL strategies are compared with the optimal solution from DP in Figures 5.19 - 5.22 for the UDDS driving cycle. The battery SOC profile resulting from OCL is very similar to DP while the battery SOC profile resulting from ECMS is different from DP (Fig. 5.19). The engine and electric motor operating points are widespread over the entire region of operation of engine and electric machine. This operation leads to the increase in fuel consumption for ECMS and OCL, compared with DP. As seen from the plots, the performances of ECMS and OCL are very close to each other (see also Table 5.5).
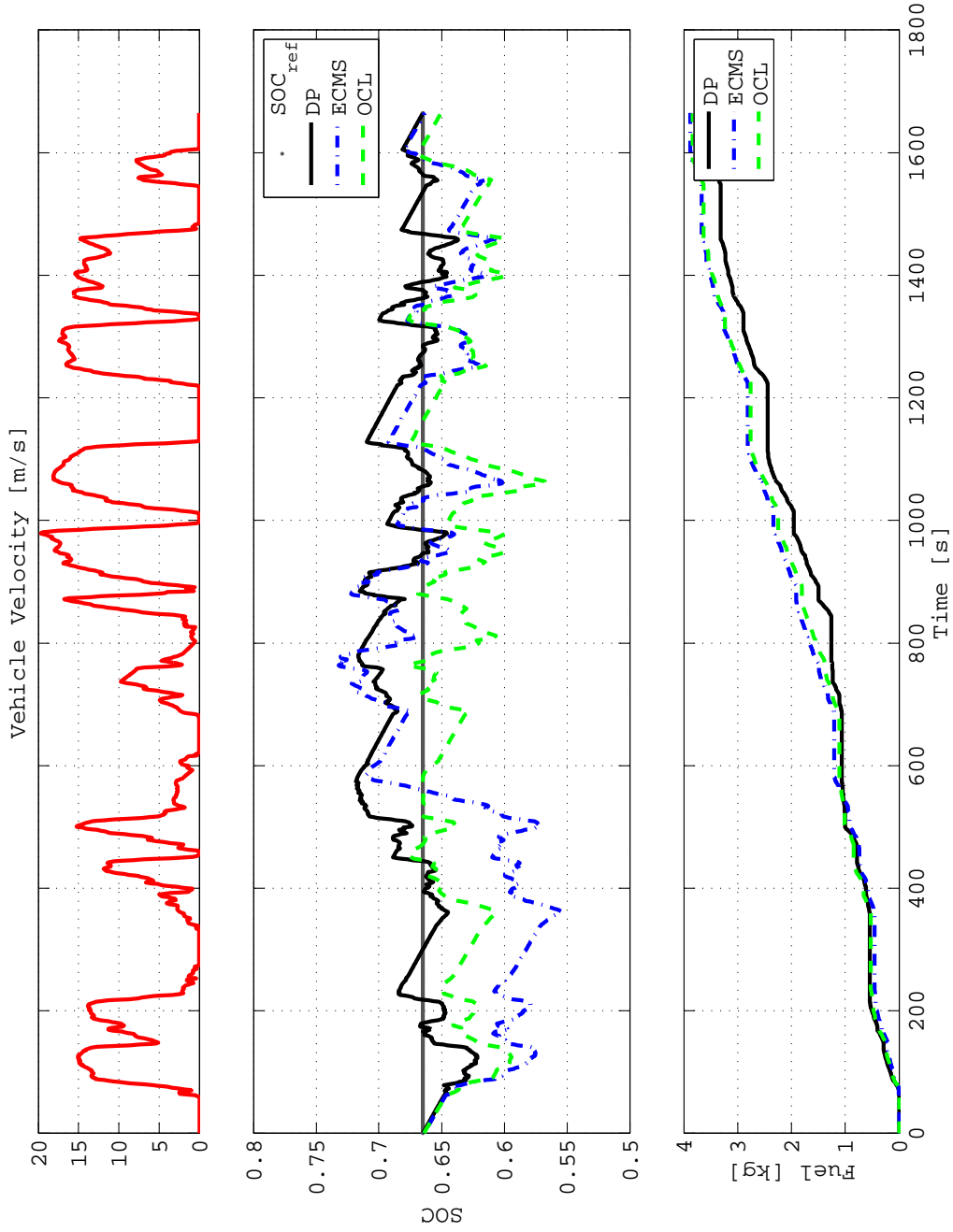
Figure 5.15: Velocity, SOC and equivalent fuel consumed (WVU-Suburban)
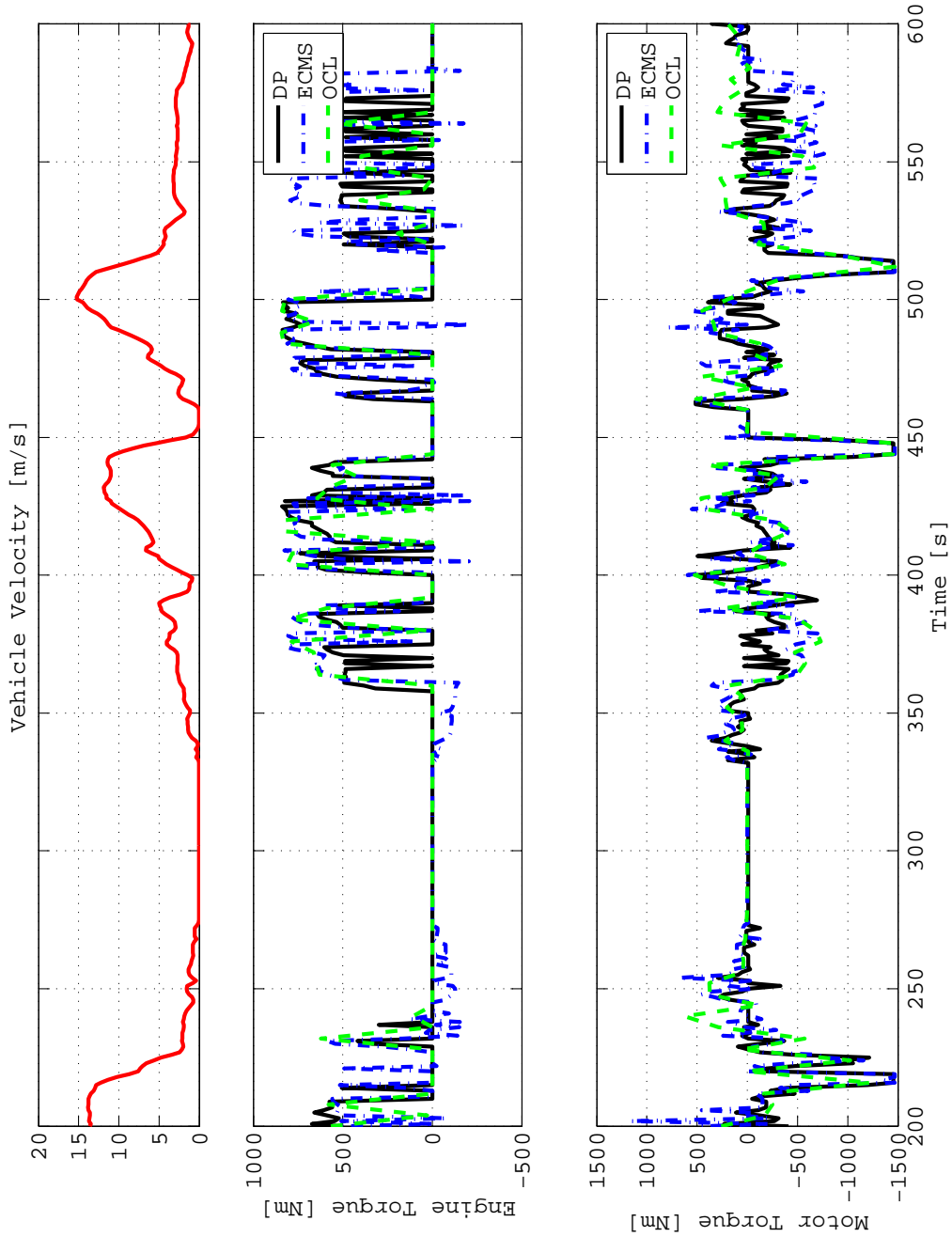
Figure 5.16: Velocity, engine and electric motor torques - detail (WVU-Suburban)
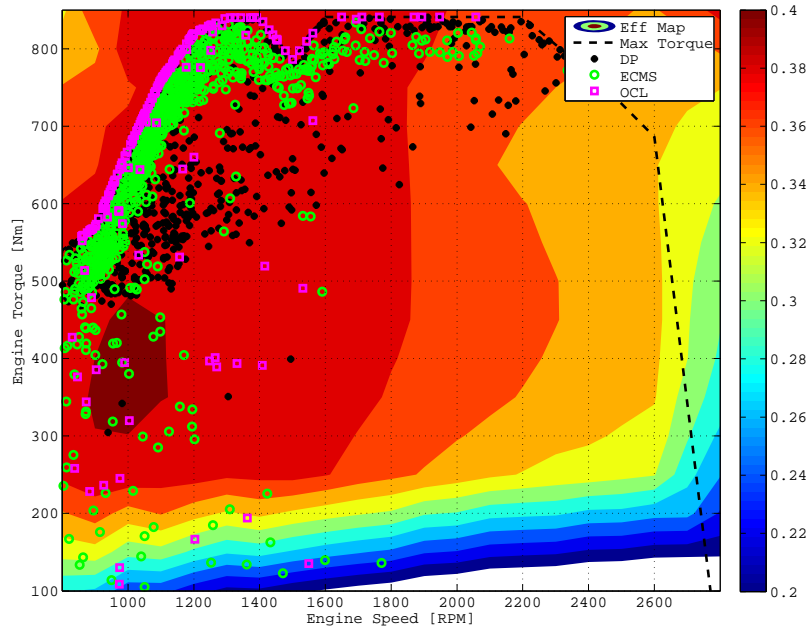
Figure 5.17: Engine operating points (WVU-Suburban)
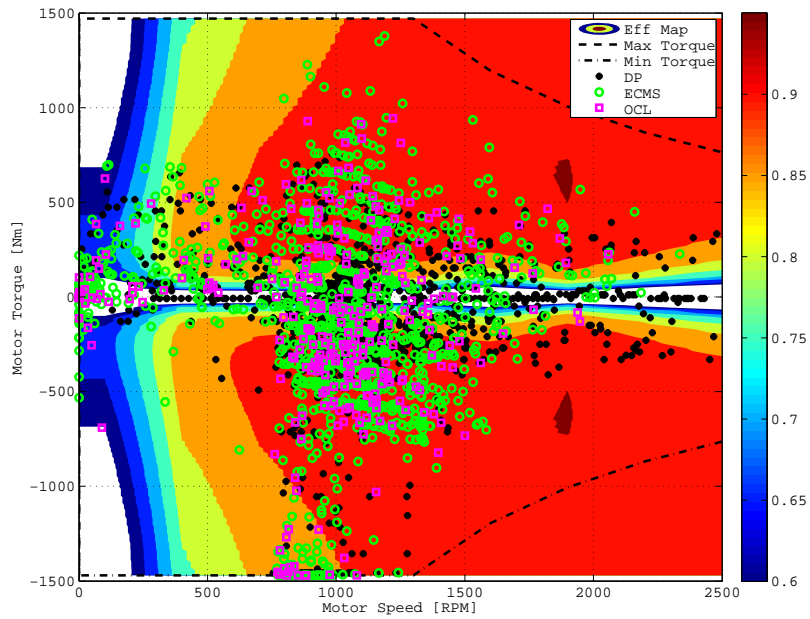


Figure 5.18: Electric motor operating points (WVU-Suburban)

175
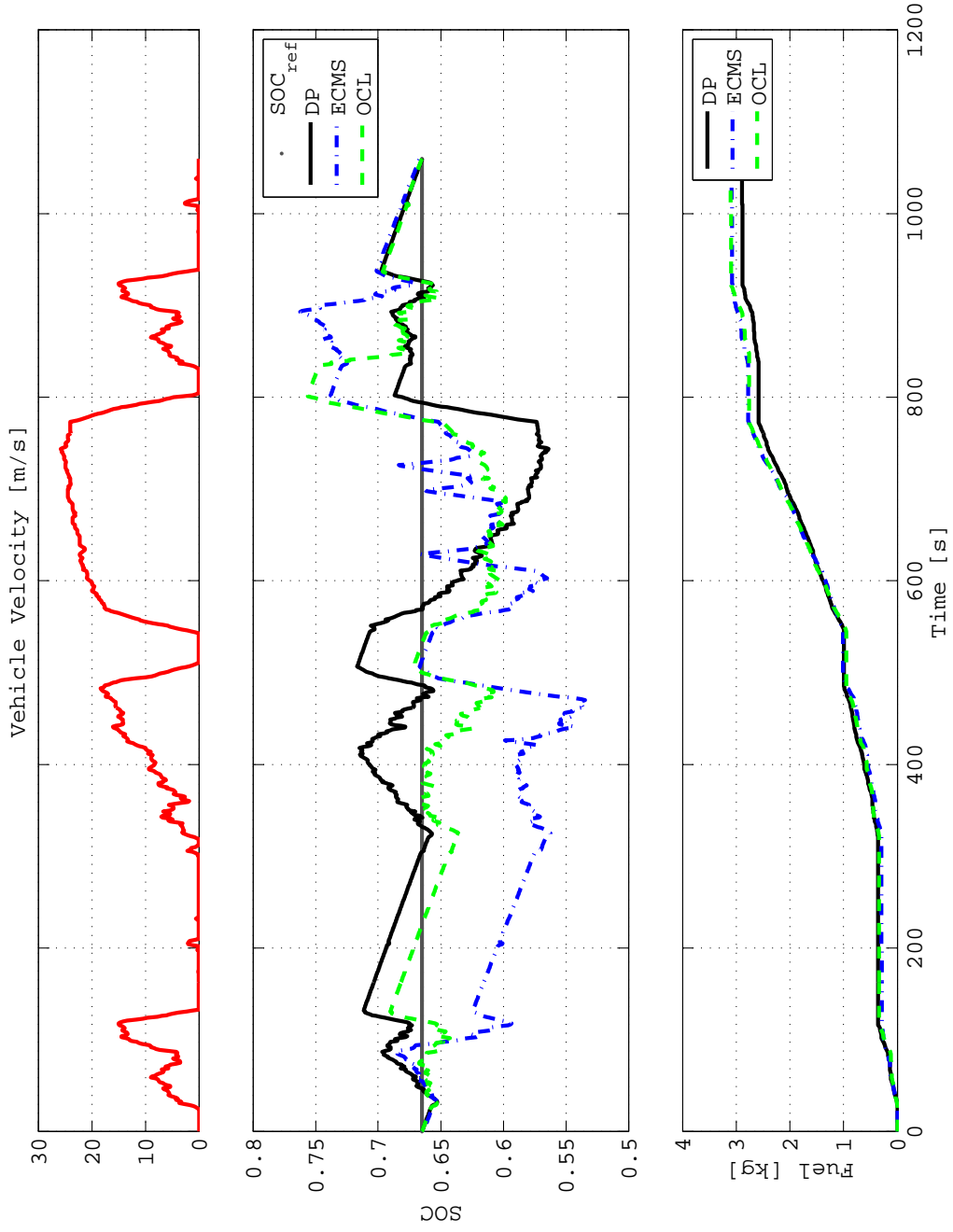
Figure 5.19: Velocity, SOC and equivalent fuel consumed (UDDS)

176
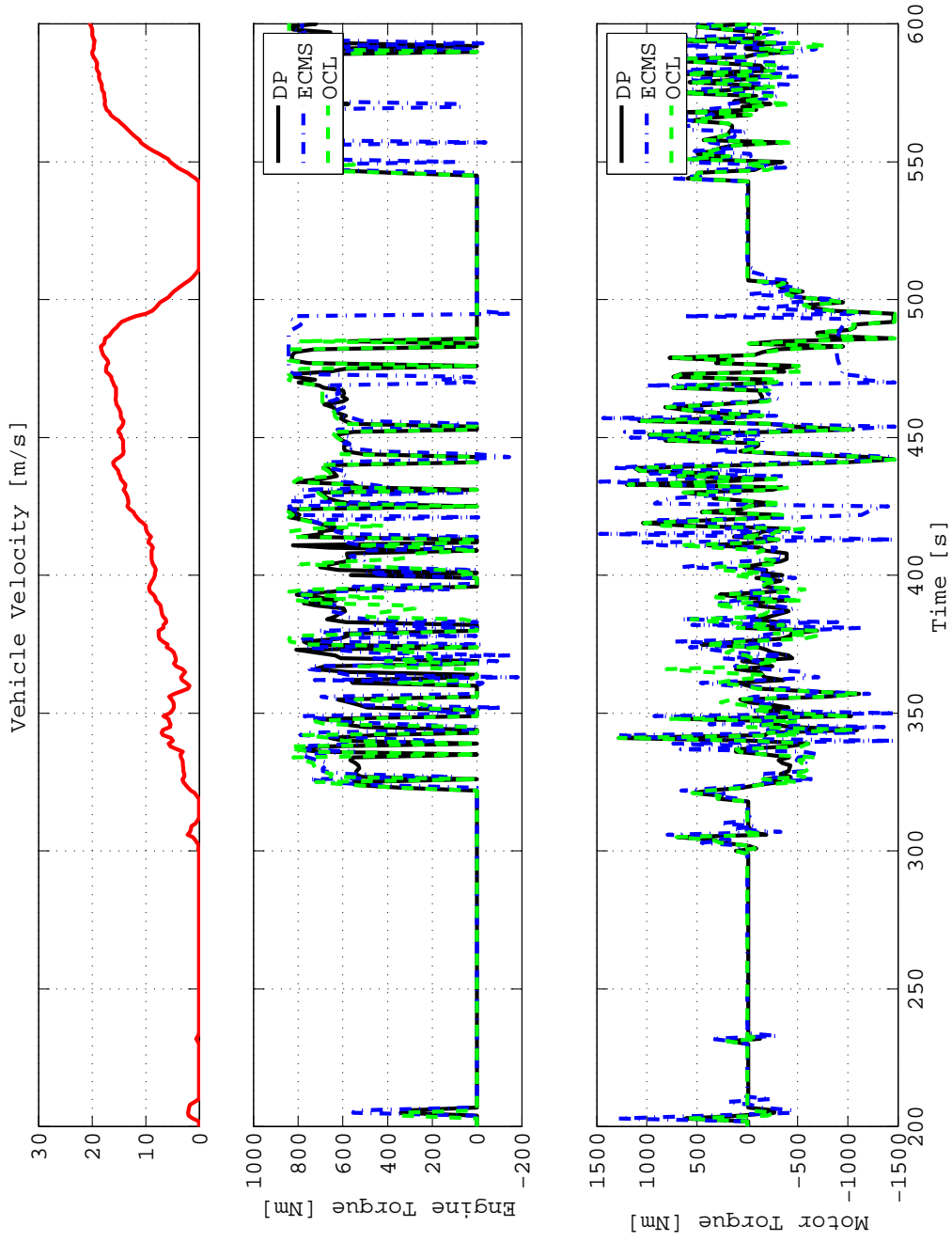
Figure 5.20: Velocity, engine and electric motor torques - Detail (UDDS)
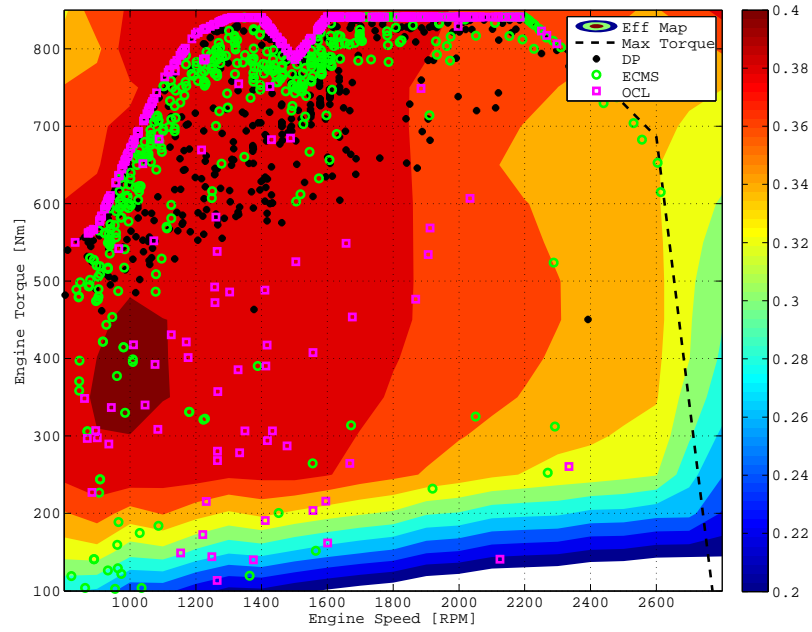
Figure 5.21: Engine operating points (UDDS)
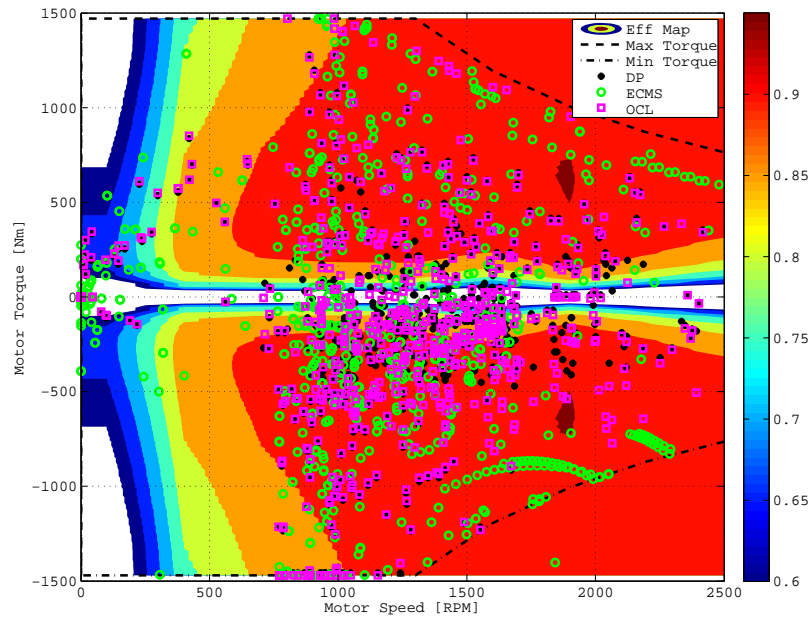


Figure 5.22: Electric motor operating points (UDDS)

## 5.2 Realizable Energy Management Strategies

This section of the chapter describes the calibration effort, battery SOC variation and the equivalent fuel consumed for the realizable energy management strategies such as AECMS and real-time OCL.

### 5.2.1 Comparison of Calibration Effort

The AECMS developed in Section 3.4 has low calibration effort because the initial value of the equivalence factor $s_0$ is adapted using the feedback from battery SOC. The adaptation law ensures convergence of battery SOC with $SOC_{ref}$ at the end of the driving cycle. Though the adaptation gain $K_p$ and adaptation period $T$ must be calibrated in order to guarantee an optimal and charge sustainable solution from AECMS, a single value of $K_p$ and $T$ can be used for all driving cycles. Thus the calibration effort for AECMS to be implemented in a real vehicle is reasonable. The real-time OCL is a version of OCL developed in Section 4.3, that uses a single value for the calibration parameter $\mu$ for any driving cycle. Because the OCL strategy developed is relatively insensitive to the value of $\mu$, a real-time version of OCL can be developed and implemented in a real vehicle. Therefore such a strategy has a low calibration effort.

### 5.2.2 SOC Variation and Equivalent Fuel Consumption

In this chapter, several non-realizable energy management strategies (DP, ECMS, OCL) have been compared over different types of driving cycles. Although these strategies have been implemented using a forward vehicle simulator and compared with the global optimal solution from DP, they cannot guarantee a similar performance when implemented in a real vehicle. This is because the real vehicle undergoes a multitude of driving conditions

Table 5.6: Combination of driving cycles

| Letter | Driving cycle |
|---|---|
| A | Manhattan |
| B | WVU-Interstate |
| C | WVU-Suburban |
| ABC-CBA-BAC | Combination-1 |
| BCA-ACB-CAB | Combination-2 |

which might be a random combination of different driving conditions. Thus, in order to evaluate the realizable energy management strategies developed in the dissertation over varied driving conditions, a combination of driving cycles must be used. The driving cycles can be arranged in many ways and two such combinations of Manhattan, WVU-Interstate, WVU-Suburban and UDDS driving cycle are selected here. For brevity, the driving cycles have been denoted using letters (A,B,C,D) as shown in Table 5.6 and two combinations of the driving cycles (combination-1 and combination-2) are used to evaluate the performance of the adaptive ECMS and real-time OCL strategies.

**Performance for combined driving cycles**

The AECMS developed in Section 3.4 is an adaptive version of ECMS, where the initial value of equivalence factor $s_0$ is adapted using battery SOC feedback. This strategy can be implemented in a real vehicle because it does not require any *a-priori* knowledge of the driving cycle. The simulation results for Manhattan, WVU-interstate, WVU-suburban and UDDS driving cycles shown in Section 3.4.1 suggest that the strategy produces charge-sustaining results over several repetitions of driving cycles. The initial guess of equivalence factor $s_0$ is taken as the average of the optimal values of $s_0$ for the driving cycles. The adaptation law adapts $s_0$ such that $SOC$ does not deviate from $SOC_{ref}$ at the end of $T$

seconds. Extensive simulation results with different values for the adaptation period $T$ and gain $K_p$ suggest that the sensitivity of the strategy with respect to these parameters is small. These values have been chosen as $T = 100\ s$ and $K_P = 5$ for all the simulations shown in the dissertation.

The OCL developed in Section 4.3 and shown in (4.42) has a single calibration parameter $\mu$ which must be tuned for each driving cycle in order to assure the optimality and stability properties. Because the strategy is less sensitive to the optimal $\mu = \mu^*$ as shown in figures 5.3 to 5.6, a single value of $\mu$ can be used for any combination of driving cycles. This variation of OCL strategy is called the real-time OCL strategy. The single value of $\mu$ used in this part of the section is an average of the optimal values for Manhattan, WVU-interstate, WVU-suburban and UDDS driving cycle. This property of the optimal control law facilitate the real-time implementation of the strategy without requiring *a-priori* knowledge of the driving cycle. Because the strategy uses a nonlinear state feedback based control law

$$P^*_{ice} = \frac{k^2\mu^2\zeta^2}{4\gamma^2\left(k\mu\zeta + p_3\right)},$$ (5.2)

where $\zeta(t)$ is the error in battery SOE, $k, \gamma, p_3 > 0$ are known constants, and $\mu$ is the only calibration parameter of the control law, the strategy aims at reducing the deviation of battery SOC from its reference during the entire length of the driving cycle. This feature eliminates the need for an adaptation of the calibration parameter similar to adaptive ECMS.

The results of the comparison between two real-time implementable strategies (adaptive ECMS, real-time OCL) over a combined driving cycle is shown in Figures 5.23 - 5.27 and Table 5.7. The battery SOC profile resulting from AECMS (Fig. 5.23) is spread across the entire region of operation $(0.5 - 0.8)$, while the real-time OCL uses the battery mostly

181
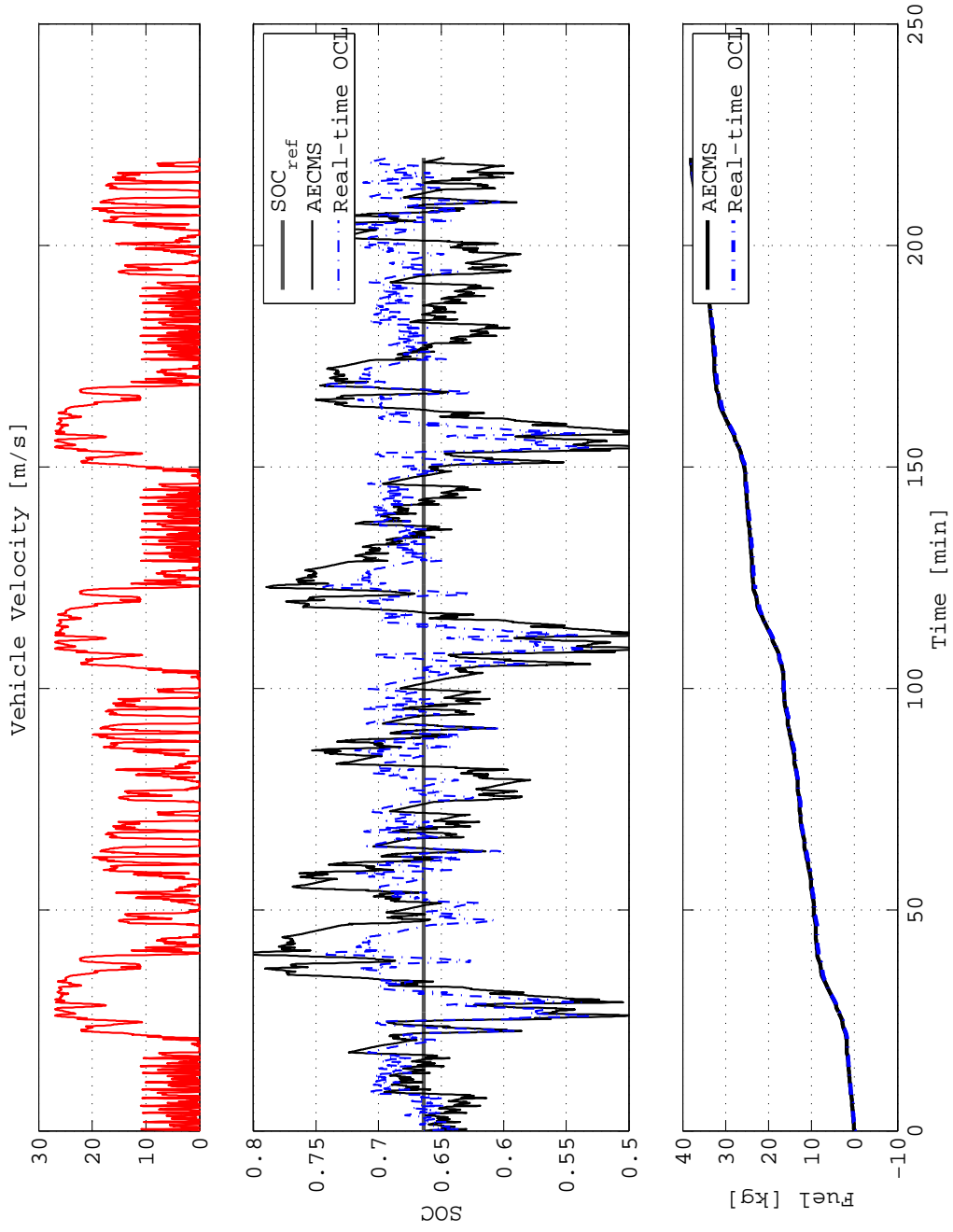
Figure 5.23: Velocity, SOC and equivalent fuel consumed (Combination-1)
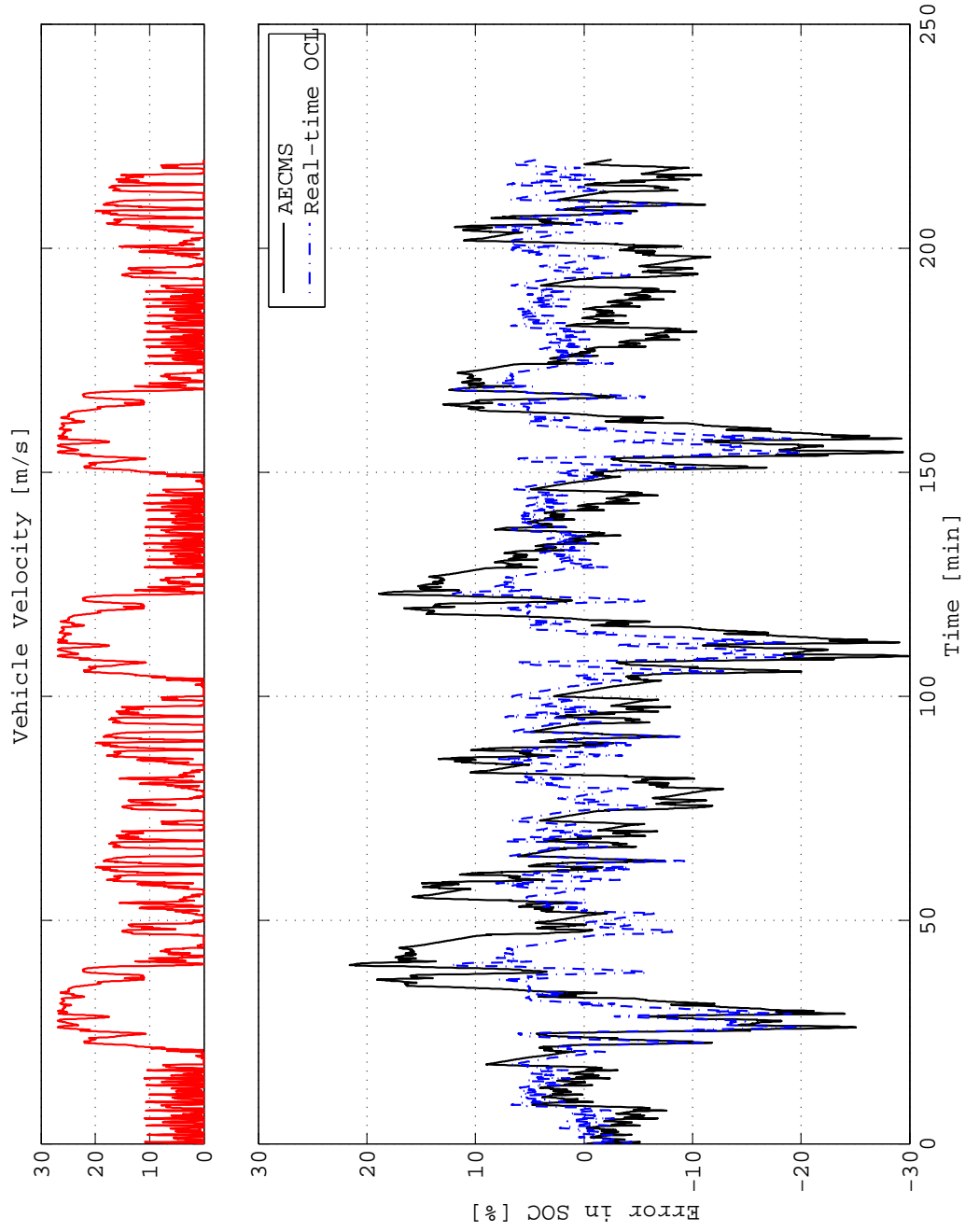
Figure 5.24: Velocity and error in SOC (Combination-1)
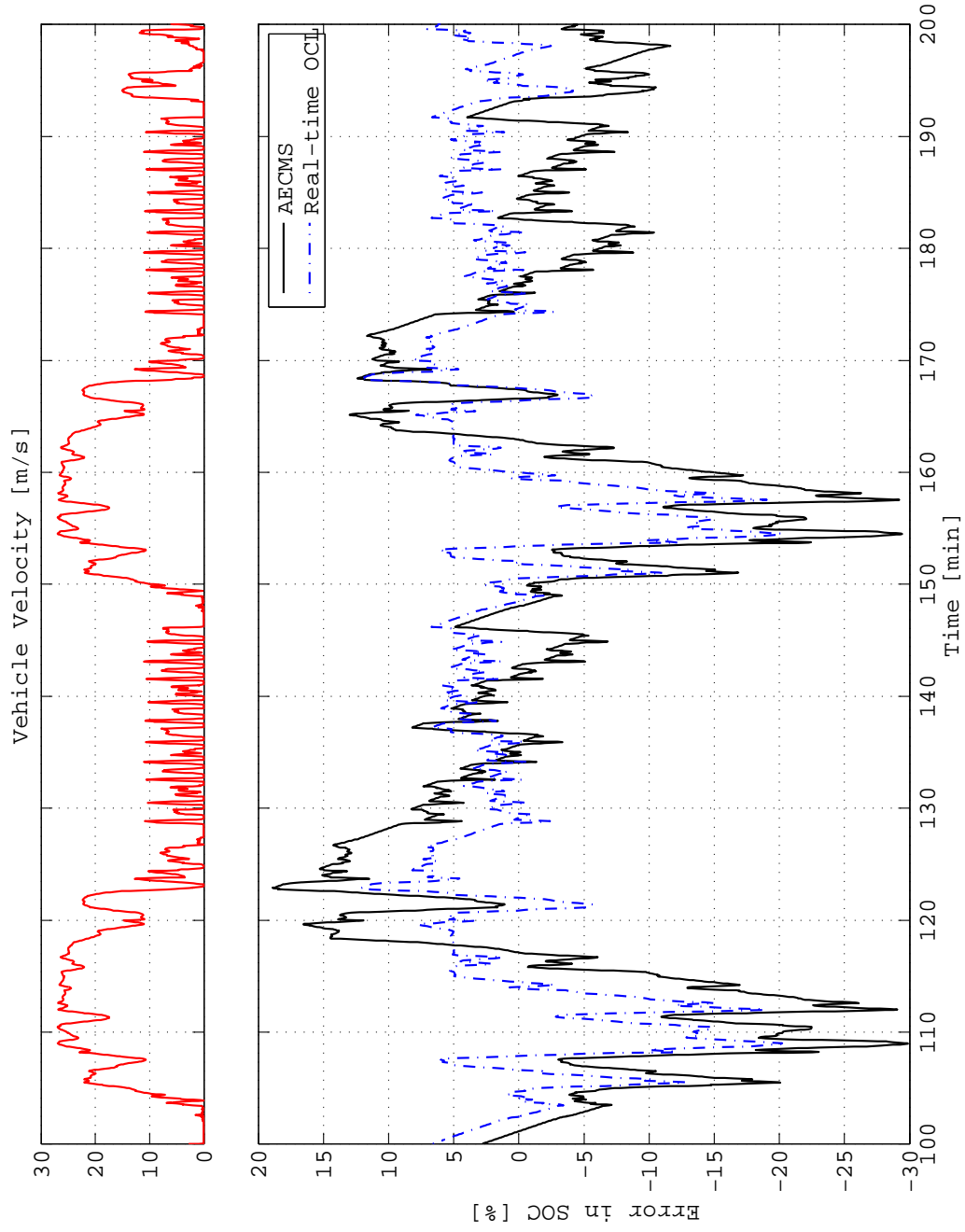
Figure 5.25: Velocity and error in SOC - detail (Combination-1)
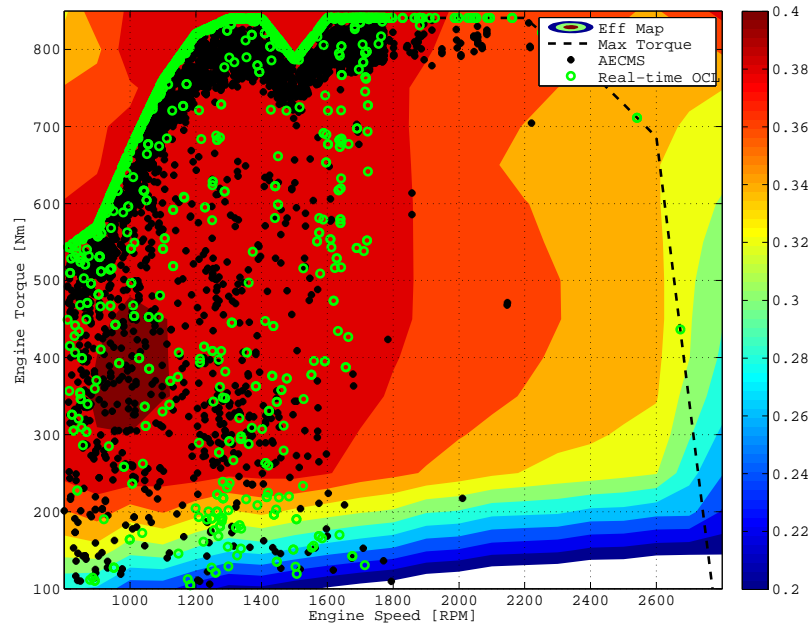
Figure 5.26: Engine operating points (Combination-1)
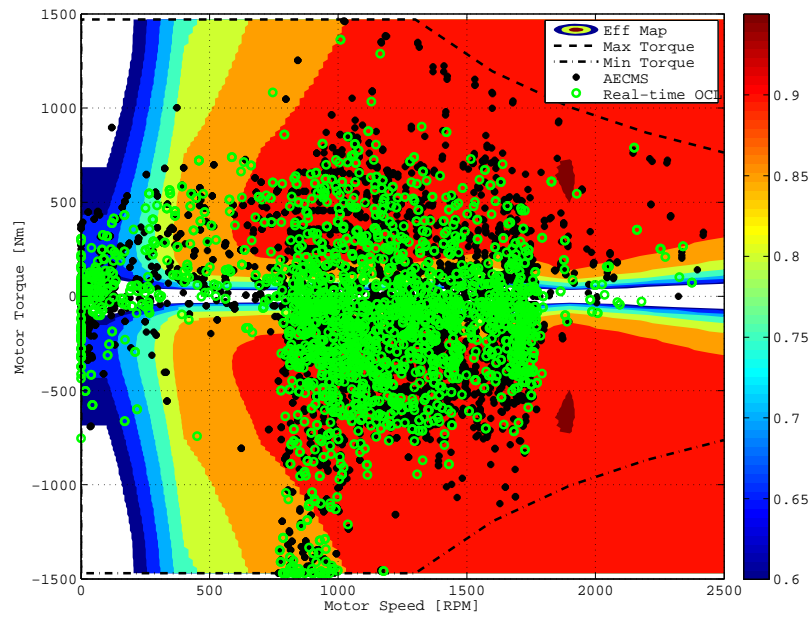


Figure 5.27: Electric motor operating points (Combination-1)

Table 5.7: Performance comparison of AECMS and Real-time OCL for combined driving cycles

| Driving cycle | Strategy | Normalized $FC_{eqv}$ [%] |
|---|---|---|
| Combination-1 | AECMS ($s_0^* = 5.83$) | 100 |
|  | Real-time OCL ($\mu = 200\ kg$) | 99.31 |
| Combination-2 | AECMS ($s_0^* = 5.83$) | 100 |
|  | Real-time OCL ($\mu = 200\ kg$) | 99.14 |

below the reference SOC. Whenever the battery SOC deviates from $SOC_{ref}$, the nonlinear state feedback based control law aims at reducing the error in battery SOC as seen from Fig. 5.24. The real-time OCL strategy consumed around $2\%$ less fuel than AECMS during the long driving cycle. The engine and electric motor operating points decided by AECMS and real-time OCL are shown in Figures 5.26 and 5.27. The AECMS operates the engine over a band close to the maximum torque curve at all speeds, while real-time OCL operates the engine over a wider range.

The AECMS and real-time OCL strategies are compared over another combined driving cycle and the results are shown in Figures 5.28 - 5.32 and Table 5.7. Similar to the first combination of driving cycles, the real-time OCL strategy performs better than the AECMS in terms of both the equivalent fuel consumed and battery SOC variation. Even though the battery SOC profile produced by the real-time OCL strategy is different from that of AECMS, as seen in Fig. 5.28, the fuel consumed is very similar. The engine and electric motor operating points shown in Figures 5.31 and 5.32 suggest that AECMS uses the engine over a band close to the maximum torque while the real-time OCL uses the engine over a
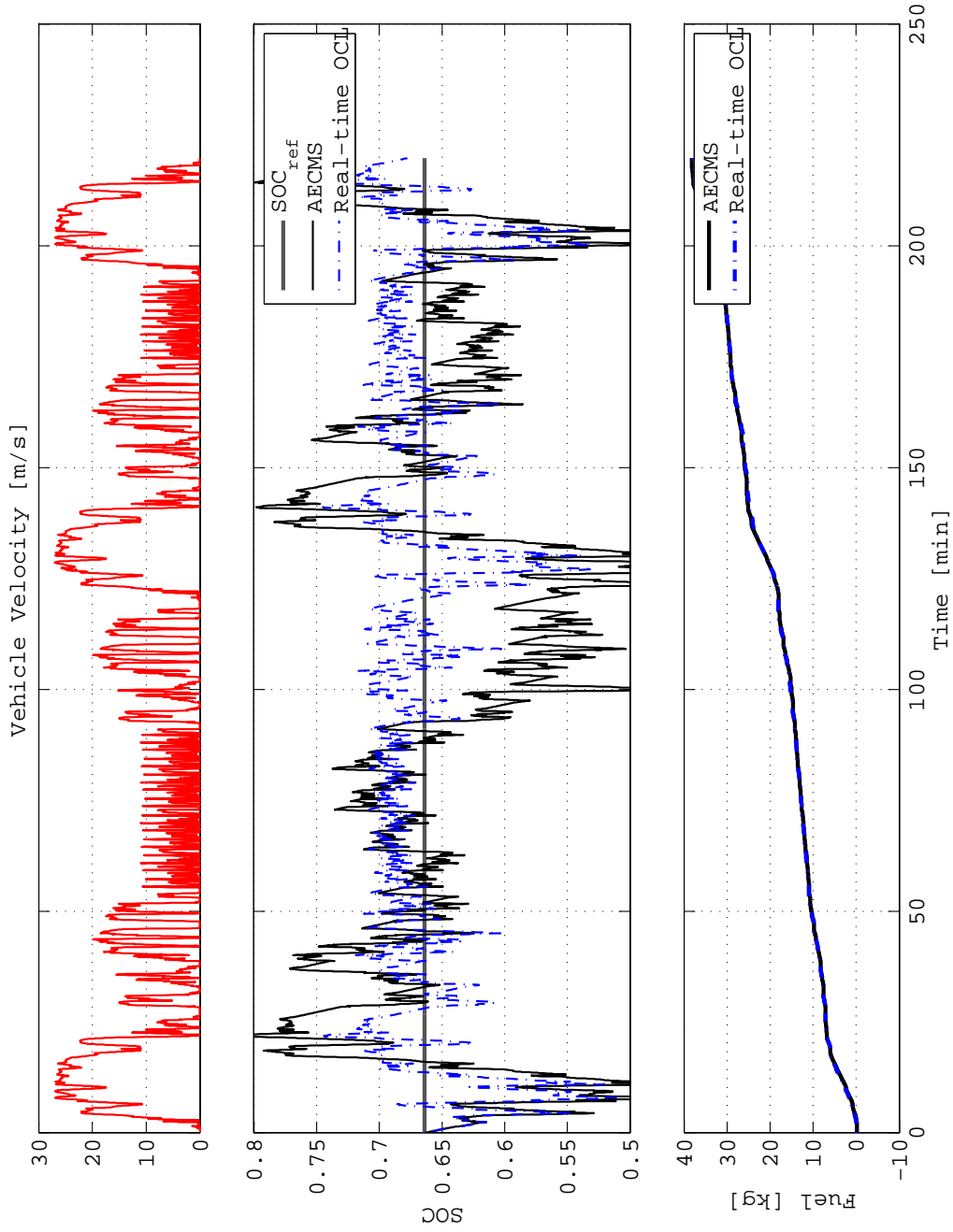
Figure 5.28: Velocity, SOC and equivalent fuel consumed (Combination-2)
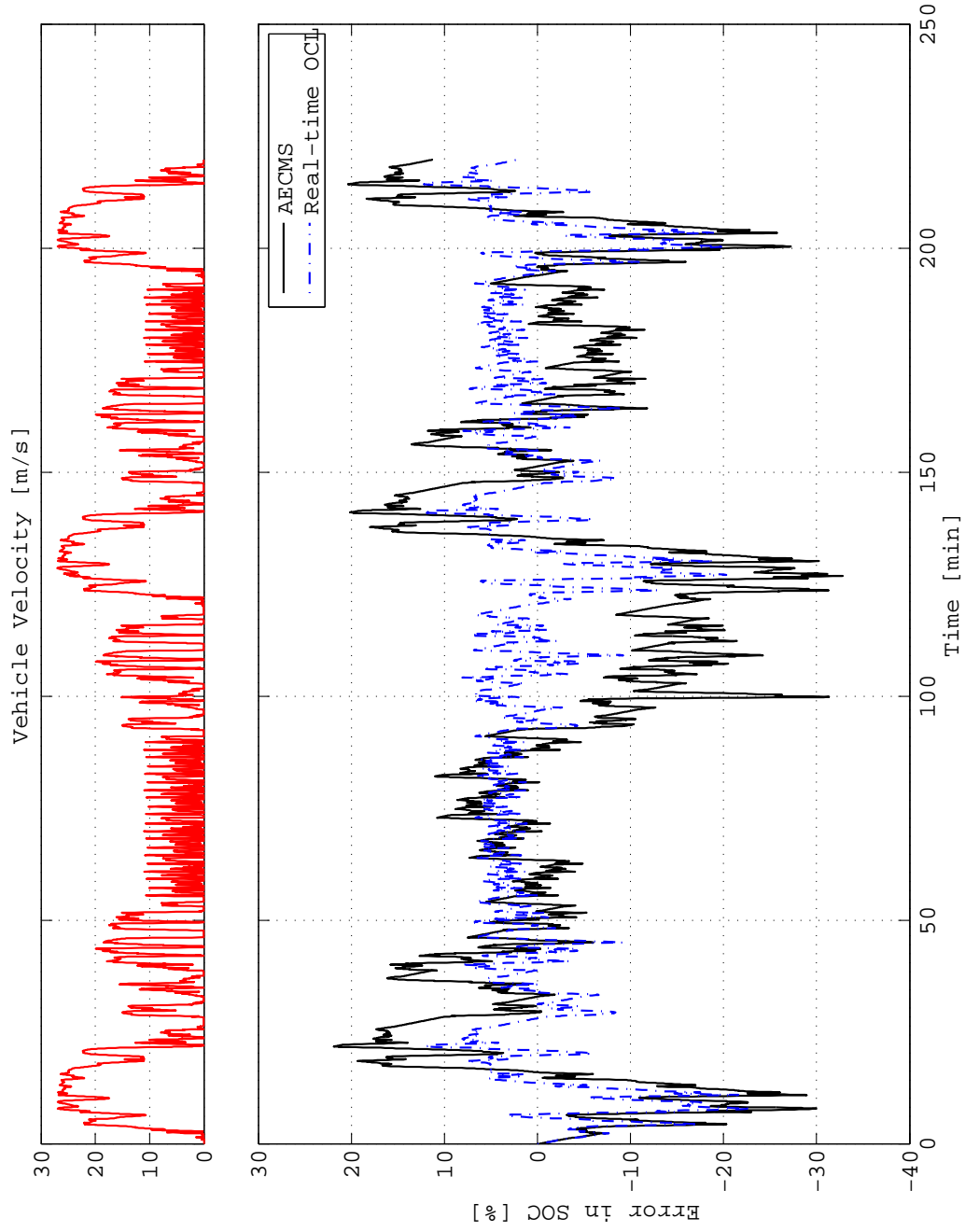
Figure 5.29: Velocity and error in SOC (Combination-2)
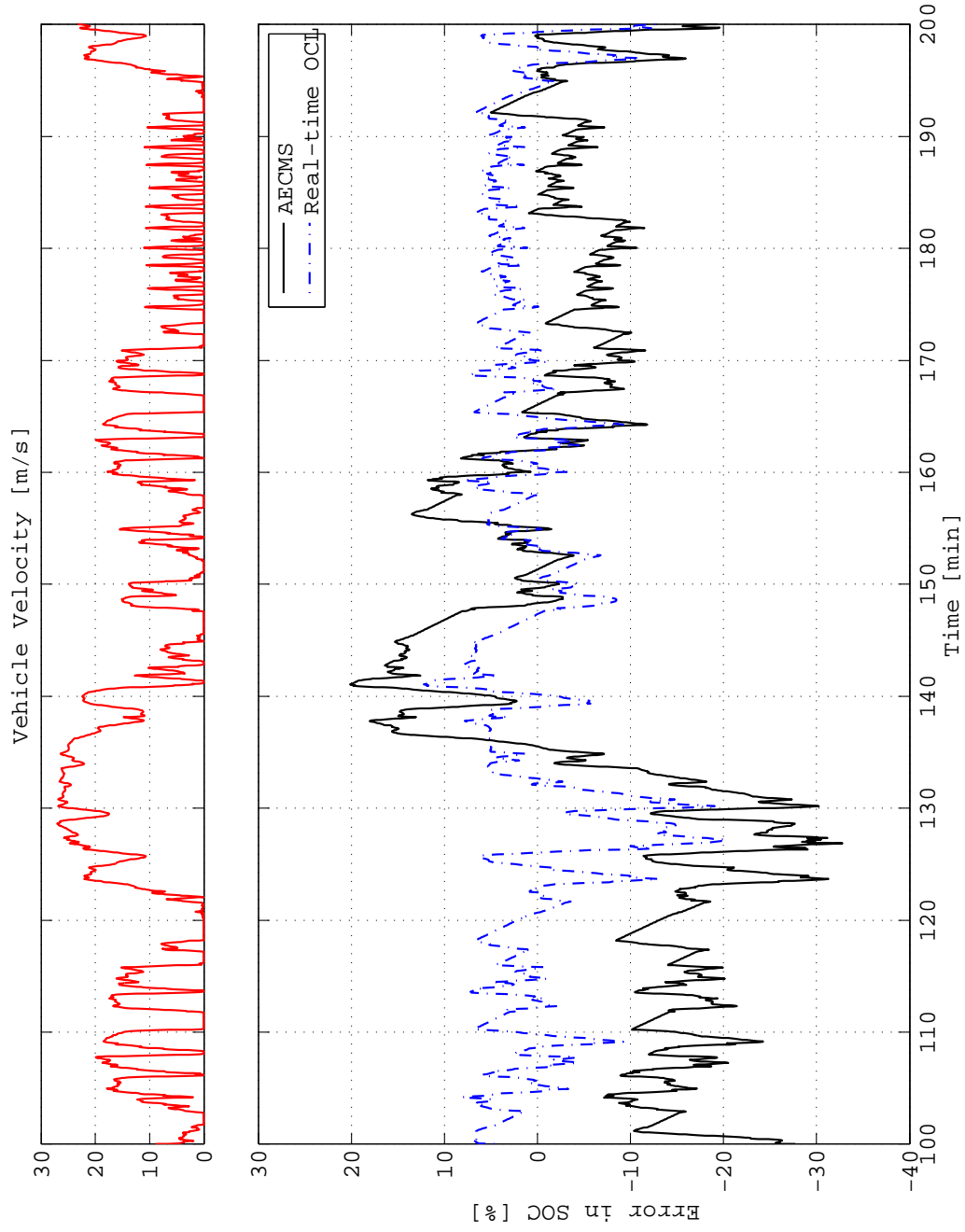
Figure 5.30: Velocity and error in SOC - detail (Combination-2)
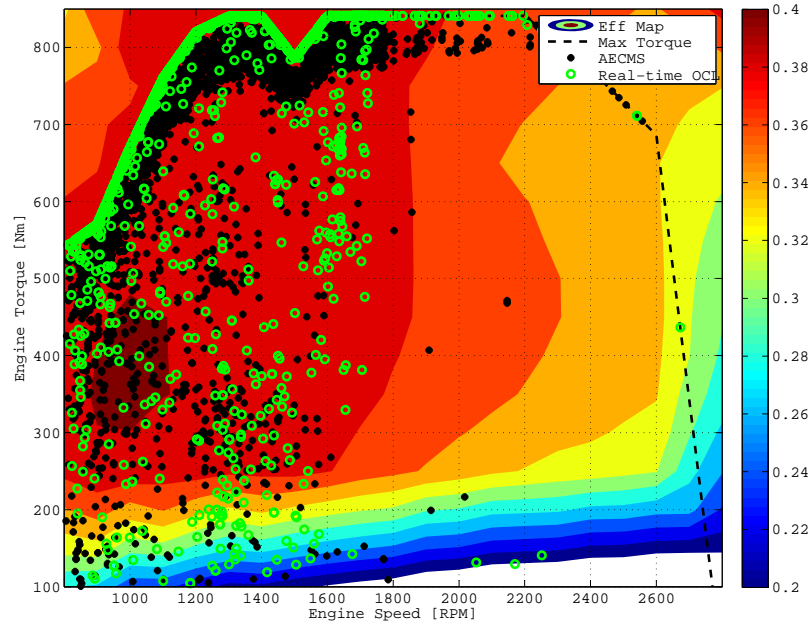
Figure 5.31: Engine operating points (Combination-2)
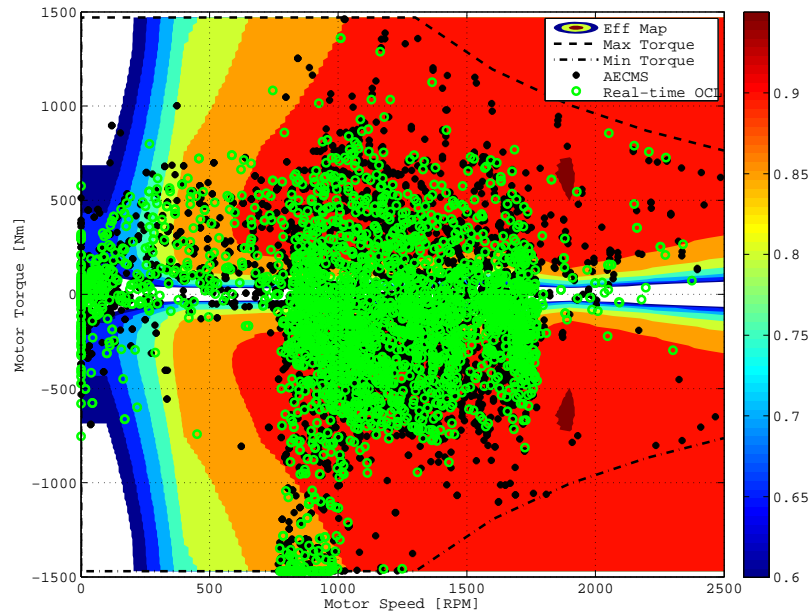


Figure 5.32: Electric motor operating points (Combination-2)

wider range of operation. The electric motor operation of the two strategies is very similar except for a few maximum torque points.

## 5.3 Conclusion

The different energy management strategies proposed in the dissertation have been implemented using a forward vehicle simulator. Several important performance metrics are defined and the strategies are evaluated using those metrics. Depending on realizability in a real vehicle, the strategies are classified into two groups, namely, non-realizable and realizable strategies. DP, ECMS and OCL are in the category of non-realizable strategy, while AECMS and real-time OCL are the realizable strategies. The performance metrics of the non-realizable strategies are compared with the DP solution and it can be seen that ECMS and OCL perform within 6% of the fuel consumption throughout any driving cycle. The amount of calibration effort necessary to implement ECMS and OCL are also quantified as *medium* because the calibration parameters must be calibrated for each driving cycle. The realizable strategies based on ECMS (AECMS) and OCL (real-time OCL) have been proposed and implemented using a forward vehicle simulator. The amount of calibration effort necessary to implement these strategies is *low* because the strategies are realtively insensitive to the calibration parameters and therefore can be easily implemented in a real vehicle. The performance metrics of the realizable strategies are evaluated over combined driving cycles to simulate the real world driving conditions. The most significant contribution of this chapter is the design and implementation of a real-time version of OCL developed and based on the stability and optimality framework formulated in Chapter 4. It is shown that the developed real-time OCL consumes around 1% less fuel than AECMS throughout the combined driving cycles.

# Chapter 6: Conclusion

In this dissertation, three main areas of energy management in HEVs are discussed: stability and optimality framework; design of realizable, stable and optimal energy management strategy; and, comparison of various non-realizable and realizable energy management strategies. The dissertation aims at designing energy management strategies for a pre-transmission parallel HEV. The pre-transmission parallel vehicle architecture and the simulation environment used to implement the strategies are developed in Chapter 2 and used throughout the dissertation to compare the strategies. The forward and backward vehicle simulator along with the Willans line model for engine fuel consumption rate and the battery SOC dynamics are proposed in this chapter.

The main contributions of Chapter 3 are the development and implementation of different energy management strategies such as DP, ECMS and AECMS for a pre-transmission parallel HEV. The energy management problem in a charge-sustaining HEV is formulated and several optimal control techniques are used to solve the problem. Because DP solves the problem backwards and provides the global optimal solution based on the sufficient conditions of optimality, it is a a benchmark solution for the rest of the dissertation. The DP algorithm is given the complete freedom of selecting the vehicle mode of operation and the torque/power split between engine and electric machine. The mode selection strategy used by DP is analyzed and simple rules to select the most appropriate mode of operation

are formulated. Though ECMS has been studied in the literature for a long time, the equivalence between ECMS and PMP is a relatively new result. The dissertation utilizes this equivalence between ECMS and PMP to design an ECMS based on the necessary conditions of optimality provided by PMP. The equivalence factor is written as a function of the co-state variable and the strategy has been implemented with a single calibration parameter. The reduction of the number of calibration parameters is significant because the amount of calibration effort necessary to implement the strategy in a real-vehicle is considerably decreased. The relationship between the equivalence factor and the battery SOC deviation from the reference at the end of the driving cycle is utilized to develop an adaptive strategy. Both the ECMS and AECMS proposed in this dissertation have been derived from the literature, while the application of the strategies in a backward vehicle simulator for a pre-transmission parallel HEV is a contribution to the literature. The implementation of DP algorithm available in the literature for a pre-transmission parallel HEV is an important contribution. The extraction of mode selection strategy from DP results for this particular vehicle architecture and the comparative analysis of the strategies are some of the other contributions of the chapter. The energy management strategies developed in this chapter are implemented and compared in Chapter 5 using a forward vehicle simulator.

Chapter 4 consists of several important contributions of the dissertation. The main contribution of this chapter is a new stability and optimality framework for designing an analytical energy management strategy. The proposed strategy is designed and developed for a charge sustaining pre-transmission parallel HEV, but the methodology is scalable to different vehicle architectures and component sizes. The chapter proves a series of theorems on solving the problem as a nonlinear optimal regulation problem with and without

disturbance rejection. The theorems are instrumental in developing a closed-form expression for the nonlinear state feedback based optimal control law. The resulting novel control law is proved optimal with respect to the fuel consumed over an infinite time horizon and guarantees local asymptotic stability of the origin. Although the optimality of the control law and asymptotic stability property of the origin are proved for an infinite time horizon, the results show the performance of the optimal control law when applied to a finite time driving cycle. The optimality ensures that minimum fuel is consumed and stability guarantees that battery SOC at the end of the driving cycle converges to $SOC_{ref}$. The optimal control law is implemented in a simplified backward simulator and its performance is compared with the global optimal solution from DP for several representative driving cycles such as Manhattan, WVU-Interstate, WVU-suburban and UDDS. The control law developed is a nonlinear state feedback based control law which depends on the vehicle architecture and parameters of the components (engine, electric machine and battery). The calibration parameter ($\mu$) must be tuned for each driving cycle using iterative shooting methods to guarantee optimality and stability. The strategy with the optimal $\mu^*$ for each driving cycle consumes within $4.5\%$ of the fuel consumed by DP and ensures that the SOC variation at the end of the driving cycle is less than $0.06\%$. Although the optimality and stability properties of the control law depend on the optimal value of the calibration parameter, because the strategy is reatively insensitive to the parameter, the closed-form control law developed is a signifcant contribution to the HEV energy management literature. The optimal control law shown here can also be easily implemented in a real vehicle because of its simplicity, and this is emphasized by implementing the strategy in a forward vehicle simulator.

In Chapter 5, the different energy management strategies proposed in the dissertation have been implemented using a forward vehicle simulator. Several important performance metrics are defined and the strategies are evaluated using those metrics. Depending on realizability in a real vehicle, the strategies are classified into two groups namely, non-realizable and realizable strategies. DP, ECMS and OCL are in the category of non-realizable strategies, while AECMS and real-time OCL are the realizable strategies. The performance metrics of the non-realizable strategies are compared with DP solution and it can be seen that ECMS and OCL perform within 6% of the fuel consumption and within 0.1% of $\Delta SOC$ at the end of any driving cycle. The amount of calibration effort necessary to implement ECMS and OCL are also quantified as *medium* because the calibration parameters must be calibrated for each driving cycle. The realizable strategies based on ECMS (AECMS) and OCL (real-time OCL) have been proposed and implemented using a forward vehicle simulator. The amount of calibration effort necessary to implement these strategies is *low* because the strategies are realtively insensitive to the calibration parameters and therefore can be easily implemented in a real vehicle. The performance metrics of the realizable strategies are evaluated over combined driving cycles to simulate real world driving conditions. The most significant contribution of this chapter is the design and implementation of a real-time version of OCL developed based on the stability and optimality framework formulated in Chapter 4. It is shown that the developed real-time OCL consumes approximately 2% less fuel than AECMS with about 1.5% battery SOC variation at the end of combined driving cycles.

Overall, the main contributions of this dissertation to the HEV energy management literature can be summarized as follows:

1. Formalization of a stability and optimality framework to analyze and design energy management strategies for charge-sustaining HEVs;

2. Design and development of a stable and optimal energy management strategy for a pre-transmission parallel HEV;

3. An analytical closed-form expression for the optimal control law has been developed and implemented;

4. Based on the framework, both non-realizable and realizable versions of the optimal control law with very less calibration effort have been proposed and implemented;

5. Implementation of DP, ECMS (based on PMP) and AECMS for pre-transmission parallel HEV;

6. Performance evaluation and comparison of different energy management strategies against the global optimal solution from DP.

## 6.1   Future work

This section of the chapter describes the future work that can be carried out based on the foundation developed by the dissertation.

### 6.1.1   Implementation of Real-time OCL

In the dissertation, the OCL is developed using the stability and optimality framework formulated in Chapter 4. This non-realizable strategy is modified to develop the real-time OCL which is a realizable strategy. The effectiveness of such a realizable strategy must be assessed using a hardware-in-the-loop set up. The performance of the strategy in the

presence of CAN bus communication and on-board memory, processor limitations is crucial for real time implementation. The strategy can then implemented in a real vehicle and compared against other realizable strategies. Because of the minimal number of calibration parameters and the ease of implementation, the strategy can give promising results.

## 6.1.2   Extension of OCL to other architectures

Throughout the dissertation, the energy management strategies have been designed and implemented for a pre-transmission parallel HEV. In Chapter 4, the OCL is developed for the vehicle which has a single degree of freedom between the engine and the electric motor. Because the stabilizing control law (4.42) decides the *optimal* engine power ($P_{ice}^*$), the optimal battery power ($P_{batt}^*$) is calculated from the drivability constraint imposed by the power requested at the wheels. In other HEV architectures (for example, series-parallel HEV [50]), there can be multiple degrees of freedom resulting from the stabilizing and optimizing control law. Thus for other architectures, the series of results proved in Chapter 4 must be re-formulated to account for a control input vector instead of a scalar control input.

## 6.1.3   Minimization of Engine Emissions and Battery Aging

The amount of emissions from the engine and the battery aging factor can also be included in the objective function to be minimized (equation 3.1) in the manner

$$\min_{u(t)} J_{new} = \int_{t_0}^{t_f} [\alpha_1 \dot{m}_f(\omega_{ice}, T_{ice}) + \alpha_2 \dot{m}_{CO,HC,NOx}(\omega_{ice}, T_{ice}) + \alpha_3 \dot{m}_{eqv,age}] dt, \quad (6.1)$$

where $\alpha_i, i = 1, 2, 3$, is the weighting factor corresponding to the different objectives, $J_{new}$ is the new objective function and $\dot{m}_{eqv,age}$ is the equivalent amount of fuel consumed corresponding to the aging of the battery, which can be thought as a function of the severity

factor of a battery [5]. The severity factor ($\sigma$) can be modeled as a function of battery SOC, temperature and its C-rate (rate of charge/discharge to/from the battery). The dependence of the severity factor on C-rate is based on the type of vehicle (HEV or PHEV) considered. For example, in a charge-sustaining HEV, the average battery C-rate is quite high (around $\pm 15C$) because of a smaller range of operation (0.5 to 0.8). In a PHEV, because the battery range of operation is quite large (0.2 to 0.9), the average battery C-rate is low (around $\pm 4C$). Hence the effect of battery C-rate on aging is minimal for a PHEV, unlike a HEV. The battery life estimation model using the severity factor [65, 66] is shown for PHEV applications. Since the severity factor depends on the battery temperature, a thermal model of the battery must be incorporated into the battery dynamics model shown in Section 2.2.1. Throughout the dissertation, the minimization has been performed with respect to the amount of fuel consumed and in order to include the emissions ([61]) and battery aging, the new objective function must be defined. The stability and optimality framework developed in Chapter 4 needs to re-formulated to minimize the new performance index. It can qualitatively observed from Fig. 5.23 and Fig. 5.28 that for the same amount of fuel consumed, the real-time OCL uses the battery very close to the $SOC_{ref}$ throughout the driving cycle. This tremendously reduces the stress on the battery life. The effect of the two strategies on battery aging can be quantitatively studied in detail by using the severity factor discussed above.

### 6.1.4   Extension of OCL to Plug-in HEVs

The stability and optimality framework and the OCL strategy developed in Chapter 4 can be applied to plug-in HEVs (PHEVs) with some modifications. In general, a PHEV essentially differs from a HEV in the fact that it uses a much larger range of battery SOC

(i.e., nominally from 0.2 to 0.9) because the battery energy can be replenished using the power grid. The range of battery SOC used is dependent on many factors such as driving cycle, energy management strategy, battery size, etc. Hence the battery SOC in a plug-in HEV is generally required to track a predefined profile throughout the driving cycle. The optimal trajectory to be tracked can either be an optimal SOC profile obtained from DP or a user-defined SOC profile. Because the energy management problem has been formulated using nonlinear optimal regulation theory, the objective of maintaining error in battery SOC/SOE to zero still holds true. Though the framework used to develop OCL must be re-formulated and the series of results needs to proposed and proved for OCL applied to PHEVs.

# Bibliography

[1] Q. Li, "Development and refinement af a hybrid electric vehicle simulator and its application in design space exploration," Master's thesis, The Ohio State University, 1998.

[2] G. Rizzoni, L. Guzzella, and B. M. Baumann, "Unified modeling of hybrid electric vehicle drivetrains," *IEEE/ASME Transactions on Mechatronics*, vol. 4, no. 3, pp. 246–257, September 1999.

[3] A. Brahma, Y. Guezennec, and G. Rizzoni, "Optimal energy management in series hybrid electric vehicles," *Proceedings of the 2000 American Control Conference*, vol. 1, no. 6, pp. 60–64, 2000.

[4] V. H. Johnson, K. B. Wipke, and D. J. Rausen, "HEV control strategy for real-time optimization of fuel economy and emissions," *SAE paper 2000-01-1543*, 2000.

[5] L. Serrao, S. Onori, A. Sciarretta, Y. Guezennec, and G. Rizzoni, "Optimal energy management of hybrid electric vehicles including battery aging," *Proceedings of the 2011 American Control Conference*, pp. 2125–2130, 2011.

[6] C. Lin, H. Peng, J. Grizzle, and J. Kang, "Power management strategy for a parallel hybrid electric truck," *IEEE Transactions on Control Systems Technology*, vol. 11, no. 6, pp. 839–849, 2003.

[7] C. Lin, H. Peng, J. Grizzle, J. Liu, and M. Busdiecker, "Control system development for an advanced-technology medium-duty hybrid electric truck," *SAE Paper 03TB-45*, 2003.

[8] M. Koot, J. Kessels, B. de Jager, W. Heemels, P. van den Bosch, and M. Steinbuch, "Energy management strategies for vehicular electric power systems," *IEEE Transactions on Vehicular Technology*, vol. 54, no. 3, pp. 771–782, 2005.

[9] Y. Zhu, Y. Chen, G. Tian, H. Wu, and Q. Chen, "A four-step method to design an energy management strategy for hybrid vehicles," *Proceedings of the 2004 American Control Conference*, vol. 1, 2004.

[10] S. Delprat, J. Lauber, T. Guerra, and J. Rimaux, "Control of a parallel hybrid power-train: optimal control," *IEEE Transactions on Vehicular Technology*, vol. 53, no. 3, pp. 872–881, 2004.

[11] M. Anatone, R. Cipollone, and A. Sciarretta, "Control-oriented modeling and fuel optimal control of a series hybrid bus," *SAE paper 2005-01-1163*, 2005.

[12] R. Cipollone and A. Sciarretta, "Analysis of the potential performance of a combined hybrid vehicle with optimal supervisory control," *Proceedings of the 2006 IEEE International Conference on Control Applications*, pp. 2802–2807, 2006.

[13] L. Serrao and G. Rizzoni, "Optimal control of power split for a hybrid electric refuse vehicle," *Proceedings of the 2008 American Control Conference*, pp. 4498 –4503, june 2008.

[14] N. Kim, S. Cha, and H. Peng, "Optimal control of hybrid electric vehicles based on pontryagin's minimum principle," *IEEE Transactions on Control Systems Technology*, vol. 19, no. 5, pp. 1279 –1287, September 2011.

[15] G. Paganelli, "Conception et commande dune chane de traction optimise pour vhicule hybride parallle thermique et lectrique," Ph.D. dissertation, Laboratoire dAutomatique et de Mcanique Industrielles et Humaines, Univ. Valenciennes, Valenciennes, France, 1999.

[16] L. Serrao, S. Onori, and G. Rizzoni, "ECMS as a realization of Pontryagin's minimum principle for HEV control," *Proceedings of the 2009 conference on American Control Conference*, pp. 3964–3969, 2009.

[17] L. Serrao, "A comparative analysis of energy management strategies for hybrid electric vehicles," Ph.D. dissertation, The Ohio State University, 2009.

[18] M. Hopka, A. Brahma, S. Dilmi, G. Ercole, C. Hubert, S. Huseman, H. Kim, G. Paganelli, M. Tateno, Y. Guezennec, G. Rizzoni, and G. Washington, "The 2000 ohio state university futuretruck," The Ohio State University, Tech. Rep., 2000.

[19] G. Paganelli, G. Ercole, A. Brahma, Y. Guezennec, and G. Rizzoni, "General supervisory control policy for the energy optimization of charge-sustaining hybrid electric vehicles," *JSAE Review*, vol. 22, no. 4, pp. 511–518, 2001.

[20] G. Paganelli, T. Guerra, S. Delprat, J. Santin, M. Delhom, and E. Combes, "Simulation and assessment of power control strategies for a parallel hybrid car," *Proceedings of the Institution of Mechanical Engineers, Part D: Journal of Automobile Engineering*, vol. 214, no. 7, pp. 705–717, 2000.

[21] K. Koprubasi, "Modeling and control of a hybrid-electric vehicle for drivability and fuel economy improvements," Ph.D. dissertation, The Ohio State University, 2008.

[22] E. J. Schacht, "Design and development of the ecocar vehicle and the vehicle controls providing efficiency and drivability," Master's thesis, The Ohio State University, 2011.

[23] C. Musardo, G. Rizzoni, Y. Guezennec, and B. Staccia, "A-ECMS: An adaptive algorithm for hybrid electric vehicle energy management," *European Journal of Control*, vol. 11, no. 4-5, pp. 509–524, 2005.

[24] C. Musardo and B. Staccia, "Energy management strategies for hybrid electric vehicles," Master's thesis, Politecnico di Milano, 2003.

[25] B. Gu and G. Rizzoni, "An adaptive algorithm for hybrid electric vehicle energy management based on driving pattern recognition," *Proceedings of the 2006 ASME Conference of International Mechanical Engineering Congress and Exposition*, vol. 2006, no. 47683, pp. 249–258, 2006.

[26] S. Onori, L. Serrao, and G. Rizzoni, "Adaptive equivalent consumption minimization strategy for hybrid electric vehicles," *Proceedings of the 2010 ASME Dynamic Systems and Control Conference*, vol. 2010, no. 44175, pp. 499–505, 2010.

[27] A. Chasse, A. Sciarretta, and J. Chauvin, "Online optimal control of a parallel hybrid with costate adaptation rule," *Proceedings of the 6th IFAC Symposium Advances in Automotive Control (AAC 2010)*, 2010.

[28] J. Kessels, M. Koot, P. van den Bosch, and D. Kok, "Online energy management for hybrid electric vehicles," *IEEE Transactions on Vehicular Technology*, vol. 57, no. 6, pp. 3428 –3440, November 2008.

[29] N. Jalil, N. Kheir, and M. Salman, "A rule-based energy management strategy for a series hybrid vehicle," *Proceedings of the 1997 American Control Conference*, vol. 1, pp. 689–693, June 1997.

[30] X. He, M. Parten, and T. Maxwell, "Energy management strategies for a hybrid electric vehicle," *Proceedings of the 2005 IEEE Vehicle Power and Propulsion Conference*, pp. 536–540, 2005.

[31] T. Hofman, M. Steinbuch, R. van Druten, and A. Serrarens, "Rule-based energy management strategies for hybrid vehicles," *International Journal of Electric and Hybrid Vehicles*, vol. 1, no. 1, pp. 71–94, 2007.

[32] P. Pisu and G. Rizzoni, "A comparative study of supervisory control strategies for hybrid electric vehicles," *IEEE Transactions on Control Systems Technology*, vol. 15, no. 3, pp. 506–518, 2007.

[33] D. Bianchi, L. Rolando, L. Serrao, S. Onori, G. Rizzoni, N. Al-Khayat, T.-M. Hsieh, and P. Kang, "A rule-based strategy for a series/parallel hybrid electric vehicle: An

approach based on dynamic programming," *Proceedings of the 2010 ASME Dynamic Systems and Control Conference*, vol. 1, no. 44175, pp. 507–514, September 2010. [Online]. Available: http://link.aip.org/link/abstract/ASMECP/v2010/i44175/p507/s1

[34] M. Back, M. Simons, F. Kirschbaum, and V. Krebs, "Predictive control of drivetrains," *Proceedings of the IFAC 15th Triennial World Congress*, 2002.

[35] M. West, C. Bingham, and N. Schofield, "Predictive control for energy management in all/more electric vehicles with multiple energy storage units," *Proceedings of the IEEE International Electric Machines and Drives Conference (IEMDC '03)*, vol. 1, 2003.

[36] R. Beck, F. Richert, A. Bollig, D. Abel, S. Saenger, K. Neil, T. Scholt, and K. Noreikat, "Model predictive control of a parallel hybrid vehicle drivetrain," *Proceedings of the 44th IEEE Conference on Decision and Control, 2005 and 2005 European Control Conference (CDC-ECC'05)*, pp. 2670–2675, 2005.

[37] D. De Vito, A. Miotti, and R. Scattolini, "Power flow management with predictive capabilities for a hybrid fuel cell vehicle," *Proceedings of the 5th IFAC Symposium on Advances in Automotive Control*, 2007.

[38] B. Sampathnarayanan, L. Serrao, S. Onori, G. Rizzoni, and S. Yurkovich, "Model predictive control as an energy management strategy for hybrid electric vehicles," *Proceedings of the 2009 ASME Dynamic Systems and Control Conference*, vol. 2009, no. 48937, pp. 249–256, 2009. [Online]. Available: http://link.aip.org/link/abstract/ASMECP/v2009/i48937/p249/s1

[39] I. Kolmanovsky, I. Siverguina, and B. Lygoe, "Optimization of powertrain operating policy for feasibility assessment and calibration: stochastic dynamic programming approach," *Proceedings of the 2002 American Control Conference*, vol. 2, pp. 1425–1430, 2002.

[40] C. Lin, H. Peng, and J. Grizzle, "A stochastic control strategy for hybrid electric vehicles," *Proceedings of the 2004 American Control Conference*, vol. 5, pp. 4710–4715, July 2004.

[41] C. Lin, M. Kim, H. Peng, and J. Grizzle, "System-level model and stochastic optimal control for a pem fuel cell hybrid vehicle," *Journal of Dynamic Systems, Measurement, and Control*, vol. 128, p. 878, 2006.

[42] L. Johannesson, M. Asbogard, and B. Egardt, "Assessing the potential of predictive control for hybrid vehicle powertrains using stochastic dynamic programming," *Proceedings of the 2005 IEEE Conference on Intelligent Transportation Systems*, pp. 366–371, 2005.

[43] W. Li, G. Xu, H. Tong, and Y. Xu, "Design of optimal, robust energy management strategy for a parallel hev," *Proceedings of the 2007 IEEE International Conference on Robotics and Biomimetics*, pp. 1894–1899, 2007.

[44] E. D. Tate, J. W. Grizzle, and H. Peng, "Shortest path stochastic control for hybrid electric vehicles," *International Journal of Robust and Nonlinear Control*, vol. 18, no. 14, pp. 1409–1429, 2008. [Online]. Available: http://dx.doi.org/10.1002/rnc.1288

[45] R. Bass and R. Webber, "Optimal nonlinear feedback control derived from quartic and higher-order performance criteria," *IEEE Transactions on Automatic Control*, vol. 11, no. 3, pp. 448 – 454, July 1966.

[46] D. L. Lukes, "Optimal regulation of nonlinear dynamical systems," *SIAM Journal on Control*, vol. 7, no. 1, pp. 75–100, 1969. [Online]. Available: http://link.aip.org/link/?SJC/7/75/1

[47] A. P. Willemstein, "Optimal regulation of nonlinear dynamical systems on a finite interval," *SIAM Journal on Control and Optimization*, vol. 15, no. 6, pp. 1050–1069, 1977. [Online]. Available: http://link.aip.org/link/?SJC/15/1050/1

[48] D. S. Bernstein, "Nonquadratic cost and nonlinear feedback control," *International Journal of Robust and Nonlinear Control*, vol. 3, pp. 211–229, 1993. [Online]. Available: http://dx.doi.org/10.1002/rnc.4590030303

[49] W. Haddad and V. Chellaboina, *Nonlinear Dynamical Systems and Control: A Lyapunov-Based Approach*. Princeton University Press, 2008. [Online]. Available: http://books.google.com/books?id=bUQN6Ph7YEIC

[50] J. M. Miller, *Propulsion Systems for Hybrid Vehicles*. London (UK): The Institution of Electrical Engineers, 2003.

[51] L. Guzzella and A. Sciarretta, *Vehicle Propulsion Systems: Introduction to Modeling and Optimization*. Springer, 2007.

[52] K. Bailey and B. Powell, "A hybrid electric vehicle powertrain dynamic model," *Proceedings of the 1995 American Control Conference*, vol. 3, pp. 1677–1682, June 1995.

[53] B. Powell, K. Bailey, and S. Cikanek, "Dynamic modeling and control of hybrid electric vehicle powertrain systems," *IEEE Control Systems*, vol. 18, no. 5, pp. 17 –33, October 1998.

[54] K. Butler, M. Ehsani, and P. Kamath, "A Matlab-based modeling and simulation package for electric and hybrid electric vehicle design," *IEEE Transactions on Vehicular Technology*, vol. 48, no. 6, pp. 1770 –1778, November 1999.

[55] K. Wipke, M. Cuddy, and S. Burch, "ADVISOR 2.1: A user-friendly advanced powertrain simulation using a combined backward/forward approach," *IEEE Transactions on Vehicular Technology*, vol. 48, no. 6, pp. 1751 –1761, November 1999.

[56] X. He and J. Hodgson, "Modeling and simulation for hybrid electric vehicles. I. Modeling," *IEEE Transactions on Intelligent Transportation Systems*, vol. 3, no. 4, pp. 235 – 243, December 2002.

[57] ——, "Modeling and simulation for hybrid electric vehicles. II. Simulation," *IEEE Transactions on Intelligent Transportation Systems*, vol. 3, no. 4, pp. 244 – 251, December 2002.

[58] A. Sciarretta and L. Guzzella, "Control of hybrid electric vehicles," *IEEE Control Systems Magazine*, pp. 60–70, April 2007.

[59] Y. Hu, S. Yurkovich, Y. Guezennec, and B. J. Yurkovich, "A technique for dynamic battery model identification in automotive applications using linear parameter varying structures," *Control Engineering Practice*, vol. 17, no. 10, pp. 1190 – 1201, June 2009. [Online]. Available: http://dx.doi.org/10.1016/j.conengprac.2009.05.002

[60] O. Sundstrom and L. Guzzella, "A generic dynamic programming Matlab function," *Proceedings of the 2009 IEEE Control Applications(CCA) and Intelligent Control(ISIC) Conference*, pp. 1625 –1630, July 2009.

[61] C. Musardo, B. Staccia, S. Midlam-Mohler, Y. Guezennec, and G. Rizzoni, "Supervisory control for nox reduction of an HEV with a mixed-mode HCCI/CIDI engine," *Proceedings of the 2005 American Control Conference*, vol. 6, pp. 3877–3881, 2005.

[62] R. Bellman, *Dynamic Programming*. New York: Courier Dover Publications, 2003.

[63] D. Bertsekas, *Dynamic Programming and Optimal Control*. Belmont, MA: Athena Scientific, 1995.

[64] L. Pontryagin, V. G. Boltyanskii, R. V. Gamkrelidze, and E. F. Mishchenko, *The Mathematical Theory of Optimal Processes*. NY: Wiley, 1962.

[65] P. Spagnol, S. Onori, N. Madella, Y. Guezennec, and J. Neal, "Aging and characterization of li-ion batteries in a hev application for lifetime estimation," *Proceedings of the 6th IFAC Symposium Advances in Automotive Control (AAC 2010)*, 2010.

[66] S. Onori, P. Spagnol, V. Marano, Y. Guezennec, and G. Rizzoni, "A life estimation method for lithium-ion batteries in plug-in hybrid electric vehicles applications," *International Journal of Power Electronics*, vol. 4, no. 3, pp. 302–309, 2011.